Elements of phenomenology of dark energy

Louis Perenon

AIX-MARSEILLE UNIVERSITÉ

ECOLE DOCTORALE 352

CENTRE DE PHYSIQUE THEORIQUE / UMR 7332

Thèse présentée pour obtenir le grade universitaire de docteur

Discipline: Physique et Sciences de la Matière
Spécialité: Astrophysique et Cosmologie

Louis PERENON

Elements of phenomenology of dark energy

Soutenue le 24/10/2017 devant le jury composé de:

Alessandra SILVESTRI	U. Leiden	Rapporteur
Álvaro DE LA CRUZ-DOMBRIZ	U. Cape Town	Rapporteur
Pierre TAXIL	CPT, U. Aix-Marseille	Examinateur
Anne Ealet	CPPM	Examinateur
Filippo VERNIZZI	CEA Saclay	Examinateur
Patrick VALAGEAS	CEA Saclay	Examinateur
Christian MARINONI	CPT, U. Aix-Marseille	Directeur de thèse

ABSTRACT

A little over a hundred years ago a revolution in modern physics occurred. The description of spacetime provided by General Relativity changed the way physics describes our universe. The Newtonian gravity force is promoted to a gravitational field paving spacetime and links intimately the energy content of the universe with its geometry. Mass curves spacetime which, in turn, dictates how bodies move in relation to one another. The foundation provided by General Relativity has allowed cosmologists to establish a well defined cosmological paradigm. Its large scale time evolution is understood to be the direct consequence of the type of energy it contains while the lumpiness of the large-scale structures we observe today, such as galaxies and clusters of galaxies, is the result of gravitational instabilities developing on the evolving frame. The increasing precision of several cosmological probes enabled the possibility of encoding our theoretical and observational knowledge within a standard model of cosmology; the ΛCDM paradigm. This model was able to account for the recent discovery that the expansion of the universe is accelerating; a milestone of modern cosmology. In the ΛCDM picture, the universe is constituted today for the major part by Cold Dark Matter along with the Cosmological Constant Λ that drives cosmic acceleration. However, this standard model is not fully complete and further breakthroughs in modern physics can be expected within this century. These will arise from an accurate description of high energy scales of gravity through a quantum theory of gravity —extremely small lengths— or through a new description of gravity at low energy scales —on cosmological distances. Such breakthroughs are essentially motivated on two grounds: using the Cosmological Constant introduces theoretical issues in a quantum field theory description and tentative observational evidences suggests our large scale description of the universe should be refined. Therefore, we devote the first chapter of this thesis to an overview of today's cosmological paradigm; starting from its founding principles, up to its shortcomings.

Finding alternatives to the standard model is of crucial importance for two reasons. On the one hand, a general theory providing a universal description of all the stages the universe has gone through, and of all physical interactions it contains, still evades our grasp. On the other hand, the second reason is more closely related to the subject of the thesis. A given cosmological model can indeed be tested against many observational probes so as to gauge its viability. However, the soundness and the precision of a viable model can only be assessed once it is compared to another model. This is why, the ΛCDM model stands as the most faithful model; describing most of the universe's evolution according to the observations gathered up to now. This is also why one has to explore alternatives to the standard model. An incredible amount of alternative theories have been put forward and most of them are based on the addition of degrees of freedom to the standard picture given by General Relativity. These additional freedoms can manifest in the form of a new energy component of the universe —the dark energy picture— or through fundamental modifications of the gravitational interaction —the modified gravity landscape. Such a profusion of research material, as much on the observational side as on the theoretical, has substantially increased our understanding of the universe. However, this is also at the expense of our efficiency in doing so, as it is rather cumbersome to study theories one by one and confront each theoretical proposal to observations. Aiming to study or create common formulations, enabling the description of large classes of alternative theories within the same framework, is an efficient path to overcoming this obstacle. This is the reason why, in chapter 2, after reviewing some alternative models

to ΛCDM, we will focus on presenting a promising unifying framework: the effective field theory of dark energy. This approach to modified gravity has established a common formalism virtually describing all alternative theories which add a single extra scalar degree of freedom to Einstein's equation. A large class of these models fall under Horndeski theories.

The increasing amount of theoretical knowledge, and the growing amount of data, is also a cry for phenomenological studies. Future surveys such as EUCLID, SKA, WFIRST and DESI, to name but a few, will provide ever more precise constraints on deviations from the standard model. In light of this, understanding the phenomenology behind alternative theories, extracting and testing observables which would characterise measurable deviations from standard gravity are thus a crucial step cosmological studies must go through today. Therefore, we consider the effective field theory of dark energy and attempt to provide answers to the following three guiding questions: *What is the cosmological portrait of gravity that emerges in Horndeski theories ? Are there any universal behaviours and, if yes, where do they stand with respect to the standard model ? Can we identify observables that will, in the future, enable us to discriminate between theories ?* To do so, in chapter 3, we show how one can parametrise the effective field theory of dark energy framework in order to extract predictions on a set of large-scale structure observables and how the effective field theory of dark energy framework can embed early modifications of gravity in Horndeski theories. Following this, we adopt a Monte Carlo procedure to explore Horndeski models, paying a significant attention to the viability of the models we obtain. This procedure enables us to identify some definite and less definite observational features Horndeski theories yield. This corresponds, for the major part, to what was explained in [1]. In the second half of chapter 3, we use the Monte Carlo approach to further synthesise the previous conclusions, and more, into an observable diagnostic. The goal of this diagnostic is to assess how Horndeski theories could be strongly disfavoured in an observable space given where future measurements will point. This corresponds to the results developed in [2].

The effective field theory of dark energy framework having allowed the exploration of the phenomenology of a large number of dark energy and modified gravity models we provide a review of the results it has produced in chapter 4. The goal of this final is twofold. It allows us to give a presentation of the landscape this framework can be applied to. In particular, we show the novel predictions it has brought up, the constraints that were derived with observations, but also how information on modified gravity can be extracted in an astrophysical context. We also discuss further theoretical an numerical developments without forgetting the caveats the effective field theory of dark energy presents. This chapter also has the purpose of discussing the results presented in chapter 3 with respect to other studies, and suggest paths needing to be explored in the future.

RÉSUMÉ EN FRANÇAIS

Un peu plus d'une centaine d'années en arrière, une révolution de la physique moderne s'est produite. La description de l'espace-temps fournie par la Relativité Générale a changé la façon dont la physique décrit notre univers. La force gravitationnelle newtonienne est remplacée par un champ gravitationnel, pavant l'espace-espace, qui relie le contenu énergétique de l'univers à sa géométrie de façon intrinsèque. L'espace-temps, courbé par les objets massifs, dicte comment les corps se meuvent les uns par rapport aux autres. La Relativité Générale a permis aux cosmologistes d'établir un paradigme cosmologique bien défini. L'évolution homogène, spatiale et temporelle, de l'univers à grande échelle est la conséquence directe du type d'énergie qu'il contient et la croissances des grandes structures que nous observons aujourd'hui, comme les galaxies et amas de galaxies, est le résultat d'instabilités gravitationnelles qui se développent dans l'univers en expansion. La précision croissante de plusieurs sondes cosmologiques a permis d'englober les connaissances théoriques et observationnelles dans un modèle standard de la cosmologie: le paradigme ΛCDM. Ce modèle fournit notamment un cadre simple pour expliquer la découverte récente que notre univers est entré il y à peu de temps dans une phase d'expansion accéléré: un jalon de la cosmologie moderne. S. Perlmutter, B.P. Schmidt et A.G. Riess ont reçu le prix Nobel en 2011 pour cette découverte effectuée en 1998. Dans le paradigme ΛCDM, l'univers est constitué aujourd'hui en majorité de matière noire froide (CDM) et d'énergie noire, décrite par la constante cosmologique, qui produit l'accélération cosmique. Cependant, ce modèle standard n'est pas entièrement complet et d'autres avancées dans la physique moderne peuvent être attendues au cours de ce siècle. Celles-ci pourront notamment découler d'une description précise de la gravité aux régimes d'énergie très élevée — échelles de distance extrêmement petites — grâce à une théorie quantique de la gravité ou à travers une nouvelle description de la gravité à faible énergie — sur les distances cosmologiques. Celles-ci sont essentiellement motivées par deux raisons: l'utilisation de la constante cosmologique introduit des problèmes théoriques dans une description de la théorie des champs quantiques et certaines tension naissantes suggèrent que notre description à grande échelle de l'univers doit être affinée. Le travail développé dans cette thèse s'insère dans ce contexte.

Dans le premier chapitre de ce manuscrit nous donnons un aperçu du modèle standard de la cosmologie; en partant de ses principes fondateurs jusqu'à ses faiblesses. L'évolution de l'univers à grande échelle, *i.e.* sa trame de fond, est caractérisée par les equations de Friedmann, et, elle est ainsi comprise comme étant la conséquence directe du type d'énergie qu'elle contient. Ces equations (voir (20)) pionnières de la cosmologie moderne relient l'évolution du paramètre de Hubble et sa dérivée, une mesure de la vitesse et de l'accélération de l'expansion de l'univers, au contenu énergétique de l'univers. Les composantes énergétiques sont modélisées par leur pression et leur densités dans une approche fluide. Ces grandeurs sont reliées par une équation d'état qui change suivant la nature de la composante considérée (voir Tableau 1). La modélisation de la formation des structures dans l'univers est faite grâce à la théorie des perturbations cosmologiques. Dans cette dernière, la formation des structures suit le paradigme de l'instabilité gravitationnelle, un scénario ascendant, où les petites perturbations s'effondrent avant les plus grandes à mesure que l'univers évolue. En somme, la description contemporaine de notre univers se visualise bien par l'analogie des fourmis se déplaçant sur un ballon qui gonfle. Le ballon symbolise la trame de fond

de l'univers qui s'étend alors que les fourmis rendent compte des grandes structures qui évoluent sur cette trame de fond.

Dans ce chapitre nous présentons aussi les sondes observationnelles, c'est à dire les moyens et techniques observationnelles, qui permettent de mettre en évidence le caractère accéléré de l'expansion de l'univers, telles que les supernovæ et le fond diffus cosmologique (CMB) pour ne citer que quelques exemples. Le phénomène d'accélération cosmique peut sembler contre-intuitif *a priori* en raison de la nature attractive de la gravité. Ce fait est maintenant corroboré par de nombreuses combinaisons de sondes. La composante énergétique qui le produit est la contribution majeure au budget énergétique total de l'univers à l'heure actuelle ($\sim 70\%$). Cependant, au sein du modèle standard de la cosmologie ΛCDM, des tensions entre les sondes cosmologiques peuvent être identifiées. Il est donc aujourd'hui nécessaire de comprendre si ces tensions sont dues à des erreurs systématiques de mesures ou la conséquence de nouveaux processus physiques encore inexpliqués. Sur le plan théorique, le modèle standard n'est pas encore capable d'apporter une description unifiée des époques jeunes et tardives de l'univers. De surcroit, décrire l'accélération cosmique avec la constante cosmologique produit des problèmes théoriques. Cette description semble être difficile à justifier sur le plan physique et donne lieu à un problème de naturalité ("naturalness") en raison de son instabilité au niveau des corrections quantiques.

Ainsi, trouver des alternatives au modèle standard revêt une importance cruciale et cela, en particulier, pour deux raisons. Une théorie générale fournissant une description universelle de toutes les époques de l'univers et de toutes les interactions physiques qu'il contient échappe encore à notre compréhension. La deuxième raison, plus étroitement liée au sujet de cette thèse, est la suivante. Un modèle cosmologique donné peut effectivement être testé contre de nombreuses observations afin d'établir sa viabilité. Cependant, la robustesse et la précision d'un modèle viable ne peuvent être évaluées qu'une fois comparées à un autre modèle. C'est ainsi que le modèle ΛCDM se présente comme le plus fidèle aujourd'hui en décrivant la majeure partie de l'évolution de l'univers selon les observations recueillies jusqu'à maintenant. C'est aussi pourquoi il faut explorer des alternatives au modèle standard pour palier ses faiblesses. Une quantité importante de théories alternatives ont été proposées et la plupart d'entre elles sont basées sur l'ajout de degrés de liberté à la Relativité Générale. Ces libertés supplémentaires peuvent se manifester sous la forme d'une nouvelle composante énergétique de l'univers —le paysage de l'énergie sombre— ou par des modifications fondamentales de l'interaction gravitationnelle — le royaume de la gravité modifiée. Dans le deuxième chapitre, nous présentons certains modèles alternatifs, en particulier, ceux qui relèvent des théories tenseur-scalaire où un seul degré de liberté scalaire est ajouté. Les théories les plus générales de ce type sont les théories de Horndeski.

Une telle profusion de matériel de recherche, tant sur le plan observationnel que sur le plan théorique, a considérablement amélioré notre compréhension de l'univers. Cependant, cela se fait également aujourd'hui au détriment de notre efficacité, car il devient trop fastidieux d'étudier les théories une par une et de confronter chaque proposition aux observations. Viser à étudier ou créer des formulations communes, permettant la description de grandes classes de théories alternatives dans le même cadre, est un moyen efficace de surmonter cet obstacle. C'est la raison pour laquelle, dans ce deuxième chapitre, nous présentons aussi un cadre unificateur très prometteur: la théorie effective de champ de l'énergie noire (EFT of DE). Cette approche de la gravité modifiée établi un formalisme commun décrivant pratiquement toutes les théories alternatives qui ajoutent un seul degré de liberté scalaire supplémentaire à l'équation d'Einstein. L'efficacité de ce formalisme découle du lien fondamental qu'il a avec les théories tenseur-scalaires. Les fonctions de couplage de l'action de l'EFT of DE paramétrisent ces théories en termes de fonctions structurelles qui

évoluent dans le temps et elles apparaissent naturellement dans l'expression des observables cosmologiques. Cela conduit à une comparaison simple des prédictions théoriques d'une vaste gamme de modèles de gravitation modifiée aux observations, comme nous le voyons dans le reste de cette thèse. De plus, un point important d'en l'EFT of DE est que la présence d'un champ scalaire est la conséquence inévitable de la brisure spontanée de la symétrie des difféomorphismes temporels. Néanmoins, cette description présente aussi des inconvénients. Étant une description linéaire, elle ne peut décrire des régimes non linéaires tels que les mécanismes d'écrantages que tout modèle de gravitation modifiée doit manifester pour être en accord avec les contraintes locales imposées par la gravité standard. Aussi, cette formulation est faite dans la jauge unitaire qui ne fournie pas une description covariante des théories, mais elle a l'avantage de classer les opérateurs dans l'ordre des perturbations. Toutefois, la description covariante de la théorie peut être retrouvée grâce au mécanisme de Stückelberg qui consiste à forcer une transformation de coordonnées temporelles où le champ de Goldstone est réintroduit. Il est aussi intéressant de souligner que le traitement des brisures spontanées de symétrie va au-delà de la cosmologie ou de la physique des particules. Par exemple, certains des auteurs qui ont développé l'EFT of DE ont appliqué cette méthode en physique de la matière condensée. Cela a permis la description des états de la matière "framids" et la prédiction de nouveaux états hypothétiques.

La quantité croissante de connaissances théoriques et la quantité croissante de données sont également un appel pour des études phénoménologiques. Les futurs satellites et télescopes tels que EUCLID, SKA, WFIRST et DESI, pour n'en citer que quelques-uns, fourniront des contraintes encore plus précises sur les écarts possibles par rapport au modèle standard. À la lumière de cela, la compréhension de la phénoménologie derrière les théories alternatives, l'extraction et le test d'observables qui caractériseraient des écarts mesurables par rapport à la gravité standard sont donc une étape cruciale de la cosmologie contemporaine. Par conséquent, dans le troisième chapitre de cette thèse, nous considérons l'EFT of DE et tentons de répondre aux trois questions directrices suivantes: *Quel est le portrait cosmologique de la gravité qui émerge des théories de Horndeski? Existe-t-il des comportements universels et, le cas échéant, où se situent-ils par rapport au modèle standard? Peut-on identifier des observables qui, à l'avenir, nous permettront de discriminer entre les théories?* Pour ce faire, nous montrons dans un premier temps comment paramétrer l'EFT of DE afin d'extraire des prédictions sur un ensemble d'observables caractérisant les structures à grande échelle. En particulier, nous nous concentrons sur des observable clefs pour la détection de la gravité modifiée tels que la constante effective de Newton, le paramètre de deflexion de la lumière et le taux de croissance des grandes structures. Dans un deuxième temps, nous proposons des modèles qui permettent de prendre en compte des modifications de gravité précoces dans l'évolution de l'univers afin de généraliser la modélisation de l'énergie sombre dans l'EFT of DE :

- "LDE" : les modifications de gravité disparaissent dans le passé.
- "EDE" : en plus du scénario LDE, le tenseur énergie-impulsion de l'énergie sombre peut être non négligeable dans le passé.
- "EMG" : en plus du scénario EDE, les fonctions de couplages peuvent être non négligeables dans le passé.

Nous adoptons une procédure de Monte Carlo pour explorer nos modèles de Horndeski. Nous choisissons une paramétrisation générale des fonctions de couplage et nous générons de façon aléatoire leurs paramètres (voir section 3.1.5). Nous accordons une attention très particulière à la viabilité

des modèles que nous obtenons. En effet, un modèle viable ne peut présenter des instabilités, telle que celles de Laplace ou celles reliées à des degrés de liberté fantômes ("ghosts"). Nous prenons aussi en compte des critères de sélection physiques, c'est à dire, n'autorisant pas les perturbations à se déplacer à une vitesse supérieure à celle de la lumière. Nous générons ainsi une dizaine de milliers de modèles viables et étudions leurs prédictions. Cette procédure nous permet d'identifier des prédictions bien définies sur les observables que les théories de Horndeski produisent (voir Figures de 16 à 22 et les discussions correspondantes). Ces résultats correspondent, pour la plupart, à ceux présentés dans [1]. Les théories de Horndeski ont effectivement une liberté fonctionnelle très vaste mais ce travail montre que l'utilisation de critères de sélection physiques permettent l'obtention de prédictions bornées et bien définies. Dans la deuxième moitié de ce troisième chapitre, nous utilisons l'approche de Monte Carlo pour synthétiser davantage les conclusions précédentes en établissant un "diagnostic observationel" des théories de Horndeski dans la formulation de l'EFT of DE. Le but de ce diagnostic est d'évaluer comment les théories de Horndeski pourraient être fortement favorisées ou exclues dans un espace d'observable selon les directions dans lesquelles pointeront les mesures des futures expériences. Cela correspond aux résultats développés dans [2]. Le diagnostic est résumé efficacement dans la Figure 28. En parcourant l'évolution temporelle, depuis les premières époques (un redshift de $z = 100$) jusqu'à aujourd'hui, des observables fondamentales tels que la constante effective de Newton μ, le paramètre de glissement gravitationnel η, le paramètre de deflexion de la lumière Σ et la fonction du taux de croissance linéaire des grandes structures $f\sigma_8$, nous avons constaté que les extensions à la Relativité Générale du type Horndeski peuvent être exclues si l'une des conditions suivantes s'applique (voir Figure 28, panneau de gauche):

- Les observables μ et Σ ont un signe opposé pour $z > 1,5$.
- $\mu < 1$ à $z = 0$.

Les sous-classes spécifiques de ces théories dans lesquelles les effets de gravitation modifiée sont limités aux temps tardifs ou non peuvent être discriminées lorsque des données au redshifts $z > 1,5$ seront disponibles dans le futur. En effet, nous trouvons que (voir Figure 28, panneau de droite):

- LDE sera exclu si $f\sigma_8 < (f\sigma_8)_{\Lambda CDM}$ à $z > 1,5$.
- EDE sera exclu si $f\sigma_8 > (f\sigma_8)_{\Lambda CDM}$ à $z > 1,5$ ou $f\sigma_8 > (f\sigma_8)_{\Lambda CDM}$ et $\Sigma > 1$ à $z > 1,5$.

Nous montrons aussi que ces résultats sont insensibles à un paramètre de l'équation d'état de l'énergie sombre constant dans la plage raisonnable $\bar{w} \in [-1.1, -0.9]$. Nous avons également trouvé que le diagnostic ne perd pas en prévisibilité lorsque des exigences de viabilité progressivement moins contraignantes sont imposées, notamment sur la vitesse de propagation des modes scalaires et tenseurs.

De plus, les mesures des amplitudes $f\sigma_8$ faibles, par rapport à la valeur extrapolée de Planck, fournies par les expériences à bas redshift semblent être quasi systématiques, en particulier dans les analyses où l'évolution de la trame de fond de l'univers est découplée du secteur des perturbations (voir [3–6] par exemple) et les théories linéaires de Horndeski semblent suivre la tendance. Ce travail montre que les théories linéaires de Horndeski aideraient à lever la tension connue sur le paramètre $\sigma_{8,0}$.

À la lumière de ce chapitre, il reste encore beaucoup à accomplir et un certain nombre d'améliorations seraient les bienvenues. Nous nous sommes concentrés sur des échelles beaucoup plus petites que

l'horizon de Hubble. Au fur et à mesure que les données s'améliorent à des échelles plus importantes, notre analyse devrait être étendue pour inclure les possibles effets dépendants de l'échelle provenant des termes de masse du champ scalaire qui sont de l'ordre de Hubble. Enfin, il serait utile d'étudier à quel point nos conclusions sont stables à l'inclusion de scénarios plus généraux tels que les théories GLPV ou lorsque des couplages conformes-disformes de la matière à la gravité sont considérés comme dans [7].

L'EFT of DE ayant permis l'exploration de la phénoménologie d'un grand nombre de modèle d'énergie sombre et de théories de gravité modifiée, nous fournissons une revue des résultats qu'elle a produits dans le chapitre final de la thèse. L'objectif de ce dernier est double. Cela nous permet de donner une présentation du paysage auquel le cadre EFT of DE peut être appliqué. En particulier, nous montrons les nouvelles prédictions qu'il a soulevées, les contraintes qui ont été dérivées avec les observations, mais aussi la façon dont l'information sur la gravité modifiée peut être extraite dans un contexte astrophysique. Nous discutons également d'autres développements théoriques et numériques sans oublier ses mises en garde. Ce chapitre a également pour but de discuter des résultats présentés au troisième chapitre par rapport à d'autres études et de suggérer des chemins à explorer à l'avenir.

En somme, l'EFT de DE est une description linéaire des théories de gravitation modifiée, donc elle ne peut capturer toute la phénoménologie de ces théories. Par exemple, la dynamique à petites échelles n'est pas décrite comme les mécanismes d'écrantage. Cependant, déjà au niveau linéaire, beaucoup a été accompli mais beaucoup reste encore à faire. Nous voyons que l'EFT of DE est un outil puissant pour explorer les scénarios de gravitation modifiée grâce à sa simplicité dans le calcul des observables et la paramétrisation des écarts à la gravité standard en termes de fonctions de couplage. Cela a permis l'obtention de caractéristiques universelles et de nouvelles prédictions observables dans la vaste gamme de théories tenseur-scalaire que sont les théories Horndeski et GLPV. Elle a également permis de contraindre les écarts par rapport au modèle standard avec les données. Le cadre EFT of DE ne définit pas une théorie spécifique en termes de variables laissant aux observations de contraindre leurs amplitudes, mais l'EFT of DE se paramétrise elle-même en terme de fonctions structurelles du temps, les dites fonctions de couplage. On peut ainsi interpréter les observations directement dans l'espace des théories et non dans le cadre d'un seul paradigme. Cependant, il y a un prix à payer. Ce prix est que la forme fonctionnelle des fonctions de couplage est inconnue. Les observations généralement ne disposent pas d'un pouvoir suffisant pour fixer des fonctions continues du temps, elles fixent des nombres. Avec les futures expérience et la quantité croissantes de données, les études qui incluent l'analyse des composantes principales ("PCA"), comme nous le voyons pour un cas particulier dans ce chapitre, sont un moyen prometteur de surmonter cette barrière. Jusqu'à présent, ce problème est manœuvré en ayant recourt à des modélisations phénoménologiques, c'est-à-dire en comprimant l'information inconnue contenue dans les fonctions structurelles en un ensemble fini de coefficients grâce à une forme paramétrique, comme nous l'avons fait dans le troisième chapitre. L'étape subtile consiste alors à concevoir une paramétrisation suffisamment souple et universelle pour permettre d'explorer la plus grande partie de l'espace des phases des théories stables et pouvoir toujours être suffisamment contraint par les observations.

La principale mise en garde dans l'EFT of DE est en effet la paramétrisation des fonctions de couplage. Par exemple, comme nous le voyons au troisième chapitre, nous avons besoin d'une expansion jusqu'à l'ordre 3 des fonctions de couplage pour capturer toutes les caractéristiques possible des observables. Cela implique qu'un modèle Horndeski, dans cette configuration, aurait

12 paramètres en plus des paramètres cosmologiques standards. Aujourd'hui, cela semble trop coûteux numériquement pour effectuer des méthodes du type Monte Carlo Chaine de Markov de façon raisonnable. C'est pourquoi la généralité et l'efficacité des paramétrisations ont été explorées dans la littérature afin de trouver le meilleur compromis. Dans [8, 9], les auteurs montrent que choisir les fonctions de couplage évoluant proportionnellement à la densité d'énergie de l'énergie sombre s'avère trop réducteur. Par conséquent, les approximations simplifiées des fonctions de couplage pourraient même manquer les signatures de gravitation modifiée. Heureusement, l'auteur dans [10] montre que les observables ne sont pas extrêmement sensibles aux courtes variations temporelle. Par conséquent, les paramétrages lisses sont en général suffisants pour décrire correctement l'espace des théories. Notamment, il est montré que l'utilisation de deux paramètres, un d'amplitude et un indice de puissance, pour chaque fonction de couplage est préférée sur des modèles plus complexes pour 86 % de l'espace des théories. Néanmoins, les auteurs dans [11] soulignent que les prévisions sur les paramètres EFT peuvent être considérablement affectées par le modèle pour l'évolution du temps des fonctions de couplage. Par conséquent, il semble maintenant crucial de mettre en œuvre des prévisions pour les mesures futures dans un paramétrage plus performant des couplages.

En conclusion, l'exploration de la phénoménologie des modèles d'énergie sombre est une vaste entreprise. L'étude présentée dans ce manuscript n'est qu'un grain de sable dans un large seau. Dans cette thèse, nous avons exploré une grande classe de théorie tenseur-scalaire; les théories de Horndeski. Ces dernières sont une possibilité dans une large gamme de théories de gravité modifiée. Nous pouvons regarder le diagramme en Figure 3 de [12], par exemple, pour se rendre compte à quel point le domaine des théories de la gravité modifiée est vaste. Néanmoins, les théories de Horndeski sont un cheminement crucial à explorer. Ils intègrent pratiquement toutes les théories qui ajoutent un degré de liberté scalaire en plus de la Relativité Générale. Par conséquent, en étudiant ces théories, nous explorons une des modifications les plus simples et physiquement motivées de la gravité: on ajoute un champ scalaire. Nous le savons maintenant, au moins un champ scalaire existe dans la nature: le champ de Higgs. De ce fait, nous pouvons s'interroger sur la possibilité qu'un autre champ scalaire provoque l'accélération cosmique. En outre, adopter une modification de la gravité simple est cruciale pour au moins une autre raison; ils fournissent des modèles mathématiquement sains et justifiés physiquement pour fournir un point de comparaison avec le modèle standard ΛCDM.

Le modèle standard contient certaines lacune, nous l'avons vu. Que ces dernières soit théoriques ou observationnelles, des améliorations doivent être explorées. Cela pourrait amener à des méthodes plus précises pour produire des données, ou révéler de la nouvelle physique devant être expliquée au-delà du modèle standard. L'exploration des écarts dans les sondes cosmologiques, et donc des processus physiques sous-jacents spécifiques, est incontournable pour évaluer les directions à suivre dans le future pour la complétion du modèle standard. À cet égard, de nombreux modèles alternatifs expliquant l'accélération cosmique ont été suggérés et la tâche d'évaluer la viabilité de chaque théorie, grâce aux observations, est une entreprise ardue. Par conséquent, des cadres unificateurs ont été construits pour donner la possibilité de tester plusieurs théories à la fois contre les observations. Nous nous sommes concentrés sur l'un d'entre eux: la théorie effective de champ de l'énergie sombre. Ce cadre nous a permis de tenter de répondre aux questions directrices présentées dans l'introduction de cette thèse. Nous avons montré que, malgré la grande liberté fonctionnelle des théories de Horndeski, l'application des exigences de viabilité mathématique et physique conduit à l'obtention de prédictions bornées sur les observables de la structure à grande échelle et ΛCDM se situe souvent à la frontière. Notamment, nous nous sommes concentrés sur

des observables tels que: la constante efficace de Newton, le paramètre de deflexion de la lumière et la fonction de croissance des grandes structures; des observables clés pour détecter des écarts par rapport au modèle standard. Nous avons procédé grâce à une approche de Monte Carlo pour générer des modèles viables dans la classe Horndeski et explorer les prédictions qu'elle produit. Cette approche nous a permis de décrire un diagnostic observable des théories de Horndeski qui contribuera à exclure ces théories compte tenu des mesures futures. Nous avons également accordé la possibilité aux théories de Horndeski dans le cadre de l'EFT of DE pour tenir compte des modifications précoces de la gravité.

Á ce jour, je travail en partie sur une étude dans laquelle nous contraignons les théories de Horndeski et GLPV dans l'EFT of DE avec des observations où une attention particulière est accordée aux contraintes astrophysiques. Nous avons montré que de nombreuses contraintes d'observation ont déjà été obtenues sur les théories et les sous-classes de Horndeski, grâce à l'EFT of DE. Bien que ces contraintes ne favorisent pas particulièrement les théories linéaires de Horndeski sur ΛCDM à ce stade, nous avons montré que la description de ces théories doit être améliorée dans ce cadre afin de s'assurer que l'on capture toute la phénoménologie, et cela, pour une évaluation approfondie en vue des expériences futures. Nous avons discuté de plusieurs chemins à suivre. Nous sommes au début de cette époque très excitante qu'est la cosmologie de précision et les prochaines années donneront lieu à une grande quantité de données observationnelles de haute précision. Il est donc primordial de préparer les outils théoriques, phénoménologiques et numériques pour analyser correctement toutes les informations dont nous aurons besoin pour améliorer la pertinence de notre paradigme cosmologique.

ACKNOWLEDGEMENTS

I wish to give many thanks to my PhD supervisor Christian Marinoni for giving me the opportunity to live this PhD adventure along with his oversight and the freedom he has given me. I would also like to thank the Centre de Physique Théorique, its administration and its IT staff for allowing me to do this PhD in the best environment possible. I thank my fellow post-doc friends warmly; I shared an office with Jose Beltràn Jiménez, Valentina Salvatelli and Stéphane Ilić who gave me precious help and support throughout my PhD. I am deeply grateful to my collaborators, Federico Piazza and Julien Bel, for their precious advice on the work I did during these 3 years. I am more than grateful to my family for looking after me, while most of this manuscript was written, due to a badly broken leg. I also thank in particular my mother and my sister for having a look at most of the English in this thesis. I must finish by thanking my friends, notably for providing the beers when they were most needed; a non-negligible aspect of a PhD student's life indeed.

CONTENTS

1

THE MODERN COSMOLOGICAL PARADIGM

Modern cosmology emerged once the mathematical tools and the physical interpretation behind the description of space-time and the gravitational force were revolutionised by A. Einstein. We give an overview of this in section 1.1. General Relativity, GR henceforth, leads to a description of the universe schematically divided into two parts. This is well illustrated by the analogy of ants moving on a balloon being filled with air. The smooth and homogeneous background evolution is symbolised by the inflating balloon, whereas the perturbations, the galaxies and clusters of galaxies, are symbolised by the ants walking on the balloon. The fundamental equations describing both parts will be respectively discussed in section 1.2 and 1.3. Then, in section 1.4, we shall see how cosmological probes allows one to constrain the fundamental description of the universe. Finally, having thus explored the theory and the observations at the base of the modern description of universe, we will be able to dress the picture given by the standard model of cosmology in section 1.5, but also give some issues remaining to be solved in section 1.5.4.

GENERAL RELATIVITY IN A NUTSHELL

Explaining the attraction between two massive bodies with a long range unknown force bothered many physicists and Newton himself. GR overcame this conceptual issue by showing the attractive gravitational force to be the result of bodies moving in a space-time that is curved by their masses. The development of GR by Einstein is generally attributed to the year 1915, with the publishing of his four famous papers [13–16], and consolidated in 1916 with his review [17]. Today, GR is understood to be the unique Lorentz invariant theory describing a local massless spin 2 field in 4 dimensions. To obtain such a clear definition required several decades of work, let us in this section briefly overview the construction of GR and some of its important definitions and principles.

The starting point is the need to complete Special Relativity [18], SR hereafter, to include acceleration. The revolutionary view of space-time it introduced was not enough, it described only motions in inertial frames. Einstein wanted to be able to describe the dynamics of accelerating bodies and frames universally. For instance, acceleration was the key ingredient in solving the apparent twin paradox. Let us imagine two twins, one remains on earth, one journeys into deep space thanks to a space-ship travelling almost as fast as the speed of light, and returns. On the one hand, in the frame of the earth, the dilation of time implies that the travelling twin will return having aged less than the stationary twin. On the other hand, taking the frame of the space ship, the twin inside the latter is stationary and the moving twin is the one on earth. In this scheme, once the twins are reunited on earth, the twin that stayed on earth should be younger due to time dilation. These two views are completely symmetrical, whether the stationary twin is the one considered in the ship or on earth, yet they give the opposite outcome. What is wrong ? This remains a paradox in SR but is broken when considering acceleration. The twin in the ship undergoes one acceleration during the lift off and one deceleration during the landing. This breaks the symmetry of the problem and the correct outcome is the travelling twin coming back less aged.

Equivalence principles

The lift "gedanken" (thought) experiment is possibly the one that shows best how Einstein was led to formulate GR. Einstein thought that an observer standing in a falling lift would feel exactly as if floating in a space-ship in deep space, and vice versa, an observer standing on earth would feel the same as if in a space-ship accelerating at $\|\vec{g}\|$. With this thought experience, Einstein understood the deep link matter and space-time display. This led him to postulate that a unifying theory needed to be *covariant*, in other words that the general theory of gravity should be invariant under general coordinate transformations. This equivalence found in the lift experiment is formulated through the *equivalence principals*.

According to Newton's second law of motion $\vec{F} = m\,\vec{a}$, a body of mass m will undergo an acceleration $\vec{a}$ under the force $\vec{F}$. Equivalently, this relation tells us that a body needs a force $\vec{F}$ to be put in motion, mediated by the acceleration $\vec{a}$, with the proportionality factor its mass m. One thus feels the idea of *inertia* arising, *i.e.* this mass m is the physical quantity that dictates the ability of a body to be put in motion. The *inertial mass* is thus the ratio of the norm of a force over the norm of an acceleration. Aside of this, in the context of gravitation, a long range force, one should define the *gravitational mass* as the ratio of the norm of the gravitational force over the norm of the gravitational acceleration. Now, if a body is in *free fall*, that is to say the motion of a body where gravity is the sole force acting on it, in a gravitational field of acceleration $\vec{g}$, one has $\vec{F} = m_i\,\vec{a} = m_g\,\vec{g}$, and thus $\vec{a} = \frac{m_g}{m_i}\,\vec{g}$. When one does such an exercise, one automatically sets the latter mass ratio to one, *i.e.* $m_g = m_i$.

The deeper meaning in this simplification is that all bodies fall in the same way: free fall is *universal*. This simplification is conceptually not trivial and has puzzled physicists for centuries. From J. Philoponus in the 6$^{\text{th}}$ century to Galileo and more recently Eötvös in 1889, B. Dicke in 1964 [19], no deference between m_i and m_g were found. Up to the point that the Eötvös parameter, the difference in the free fall of two objects of different mass,

$$\eta_{1,2} = \frac{1}{2}\frac{\left(\frac{m_i}{m_g}\right)_1 - \left(\frac{m_i}{m_g}\right)_2}{\left(\frac{m_i}{m_g}\right)_1 + \left(\frac{m_i}{m_g}\right)_2}\,, \tag{1}$$

has been constrained recently to be $\eta_{1,2} < 10^{-13}$ from the free fall of beryllium-aluminium and beryllium-titanium test body pairs in [20]. The quest for measuring a difference still runs, the satellite MICROSCOPE [21] launched in 2016 should be able to measure this parameter with a precision of 10^{-18}.

This tight constrain between m_i and m_g falls under the *Weak Equivalence Principle* (WEP) which implies the impossibility to distinguish between the effects of a gravitational field from those of an uniformly accelerated frame (recall Einstein's lift thought experiment) and thus that free fall is universal. According to Einstein, the WEP should not only be valid for free falling test-particles but also for any experiment. Thereby, the *Einstein Equivalence Principle* (EEP) adds on top of the WEP [22] that the outcome of any local non-gravitational test experiment is independent of the velocity of the free falling apparatus, and of where and when in the universe it is performed. A local non gravitational experiment corresponds to a small sized experiment performed in a freely falling laboratory. In the WEP and EEP, gravitational interactions are excluded. To include them a stronger version exists, the *Strong Equivalence Principal* (SEP). The SEP states [23] that the WEP is valid also for massive gravitating bodies and that in all freely falling frames the laws of SR, independent of velocity and position, are recovered locally and up to tidal gravitational forces.

The main consequence of the EEP is that gravitational interactions must depend on space-time curvature. This imposes any metric theory of gravity to satisfy the following properties [22, 24] :

i) Space-time is a manifold endowed with a metric ($g_{\mu\nu}$).

ii) The world lines of test bodies on such a manifold correspond to the geodesics of the metric, *i.e.* the shortest path between two points.

iii) All non gravitational laws of physics in local freely falling frames (Local Lorentz frames) are governed by SR.

The last statement has an important implication: for a body in free fall, it will be always possible to find a reference frame in which the body is in a rectilinear uniform motion, the *local inertial reference frame*. Therefore, assuming $m_i = m_g$, in such a frame the proper acceleration of a test body will be

$$\frac{d^2x^\mu}{d\tau^2} = 0\,, \tag{2}$$

with $\tau = \int ds/c$ the proper time of the body. The idea of Einstein was for the laws of physics to be valid in any frame and thus including gravitation, they needed to be written in the form of tensors under general coordinate transformations ($d\tilde{x}^\alpha = (\partial\tilde{x}^\alpha/\partial x^\mu)dx^\alpha$)[1]. For example, a rank 2 tensor must transform as

$$g_{\mu\nu} = \frac{\partial\tilde{x}^\alpha}{\partial\tilde{x}^\mu}\frac{\partial x^\beta}{\partial x^\nu}\tilde{g}_{\alpha\beta}\,. \tag{3}$$

From this, for (2) to be valid in any frames it needed to be complemented into

$$\frac{d^2\tilde{x}^\mu}{d\tau^2} + \Gamma^\mu_{\alpha\beta}\frac{d\tilde{x}^\alpha}{d\tau}\frac{d\tilde{x}^\beta}{d\tau} = 0\,. \tag{4}$$

This is the *geodesic equation* which enables one to find the shortest path between two points on the manifold. $\Gamma^\mu_{\alpha\beta}$ is the *connection*, thus the quantity enabling the parallel transport of a vector along a geodesic. One must use the non-metricty tensor to express the connection in terms of the metric, vanishing in GR, one has $\nabla^\mu g_{\alpha\beta} = 0$. ∇^μ is the covariant derivative, *i.e.* the extension of derivatives to curved space-time, defined for a tensor as

$$\begin{aligned}\nabla_\alpha T^{\mu_1\cdots\mu_p}{}_{\nu_1\cdots\nu_q} = \partial_\alpha T^{\mu_1\cdots\mu_p}{}_{\nu_1\cdots\nu_q} - \Gamma^\lambda_{\alpha\nu_1}T^{\mu_1\cdots\mu_p}{}_{\lambda\nu_2\cdots\nu_q} - \cdots - \Gamma^\lambda_{\alpha\nu_q}T^{\mu_1\cdots\mu_p}{}_{\nu_1\cdots\nu_{q-1}\lambda}\\ + \Gamma^{\mu_1}_{\alpha\lambda}T^{\lambda\mu_2\cdots\mu_p}{}_{\nu_1\cdots\nu_q} + \cdots + \Gamma^{\mu_p}_{\alpha\lambda}T^{\mu_1\cdots\mu_{p-1}\lambda}{}_{\nu_1\cdots\nu_q}\,.\end{aligned} \tag{5}$$

This leads to the expression of the connection of GR, the Levi-Civita connection which is expressed in terms of the Christoffel symbols[2]

$$\Gamma^\mu_{\alpha\beta} = \frac{1}{2}g^{\mu\nu}\left(g_{\alpha\nu,\beta} + g_{\beta\nu,\alpha} - g_{\alpha\beta,\nu}\right). \tag{6}$$

The display of $g_{\mu\nu}$ and $\Gamma^\mu_{\alpha\beta}$ in the equations of GR clearly highlights the geometrisation of a physical theory, a revolution in 1915. From this geometric formulation, one obtains that every quantities defined from the connection can be written in terms of the metric. In addition, GR is torsion free that is to say the anti-symmetric part of the connection vanishes ($\Gamma^\mu_{[\alpha\beta]} = 0$). Also, any structures are defined on what is called a *pseudo-Riemaniann* manifold, Riemannian means a differentiable manifold and the pseudo comes from the fact that the metric is not positive definite.

1 A convention used throughout this thesis is following. We adopt the Einstein summation, indices are summed when they are repeated above and below, *e.g.* $u_\mu u^\mu = u_0u^0 + u_1u^1 + u_2u^2 + u_3u^3$, Greek indices span from 0 to 3 and Latin indices span from 1 to 3.

2 The derivative symbols will be sometimes omitted for clarity thanks to the convention $\partial_\mu(\cdot) = (\cdot)_{,\mu}$ and $\nabla_\mu(\cdot) = (\cdot)_{;\mu}$

Einstein's field equation

Let us now overview how Einstein obtained his field equation. He adopted a heuristic approach. He knew that in the *weak field limit*, *i.e.* low space-time curvature and low energies, he had to recover Newton's dynamics for gravitating bodies such as the field equation for the Newtonian potential Φ,

$$\Delta\Phi = 4\pi G\rho\,, \tag{7}$$

where $\Delta = \delta^{ij}\partial_i\partial_j$, ρ the energy density at play and G Newton's constant. This equation links a second order differential operator acting on a potential with a measure of the mass distribution, thus a dynamical equation. To insure general covariance, both the left and right hand side of the new equation needed to be upgraded to tensors. For the later, the general relativistic extension to ρ is the *energy momentum tensor* $T_{\mu\nu}$. Using the metric directly for the former was to no avail, for $\Delta g_{\mu\nu}$ does not transform as a tensor under general coordinate transformations. On the other hand, the Riemann tensor, which measures to what extent the metric tensor is not locally isometric to that of Euclidean space,

$$R^{\mu}{}_{\nu\sigma\rho} = \partial_\sigma\Gamma^{\mu}_{\nu\rho} - \partial_\rho\Gamma^{\mu}_{\nu\sigma} + \Gamma^{\kappa}_{\nu\rho}\Gamma^{\mu}_{\kappa\sigma} - \Gamma^{\kappa}_{\nu\sigma}\Gamma^{\mu}_{\kappa\rho}\,, \tag{8}$$

yields too many indices. This is how Einstein first proposed, the Ricci tensor, a contraction of the Riemann tensor $R_{\mu\nu} = R^{\rho}{}_{\mu\nu\rho}$ as a candidate,

$$R_{\mu\nu} = \frac{8\pi G}{c^4}T_{\mu\nu}\,, \tag{9}$$

where c is the speed of light. However, further investigation revealed that this could not be a suitable candidate since $\nabla^\mu R_{\mu\nu} = \nabla_\nu R/2$ implied the conservation of energy was not satisfied. This, led Einstein to correct his equation to

$$G_{\mu\nu} = \frac{8\pi G}{c^4}T_{\mu\nu}\,, \tag{10}$$

where the Einstein tensor yields,

$$G_{\mu\nu} = R_{\mu\nu} - \frac{1}{2}Rg_{\mu\nu}\,, \tag{11}$$

with the Ricci scalar being $R = R^{\mu}{}_{\mu} = g^{\mu\nu}R_{\mu\nu}$, $g^{\mu\nu}$ the inverse of the metric defined as $g^{\mu\alpha}g_{\alpha\nu} = \delta^{\mu}{}_{\nu}$ and $\delta^{\mu}{}_{\nu} = \mathrm{diag}(1,1,1,1)$ is the Kronecker symbol. We will use the $(-,+,+,+)$ signature for the metric throughout this thesis. The Einstein tensor was proved much later, by J. Lovelock in 1971 [25], to be the only divergence-free rank 2 tensor containing up to second partial derivatives of the metric on a 4 dimensional differentiable manifold.

Soon after the publication of Einstein's articles on GR, D. Hilbert showed a more direct way to obtain Einstein's field equation from the variational principle. The action of GR was found,

$$S = \frac{c^4}{16\pi G}\int d^4x\sqrt{-g}R + S_{\mathrm{m}}(g_{\mu\nu},\psi)\,, \tag{12}$$

where the first integral is now called the Einstein-Hilbert term and S_{m} is the action for the matter fields, ψ, that gravitate, in other words matter that couple to the metric. Indeed, taking the variation of the action with respect to the inverse metric (12) yields the Einstein field equation (10) where the energy momentum tensor is obtained by

$$T_{\mu\nu} = -\frac{2}{\sqrt{-g}}\frac{\delta S_{\mathrm{m}}}{\delta g^{\mu\nu}}\,. \tag{13}$$

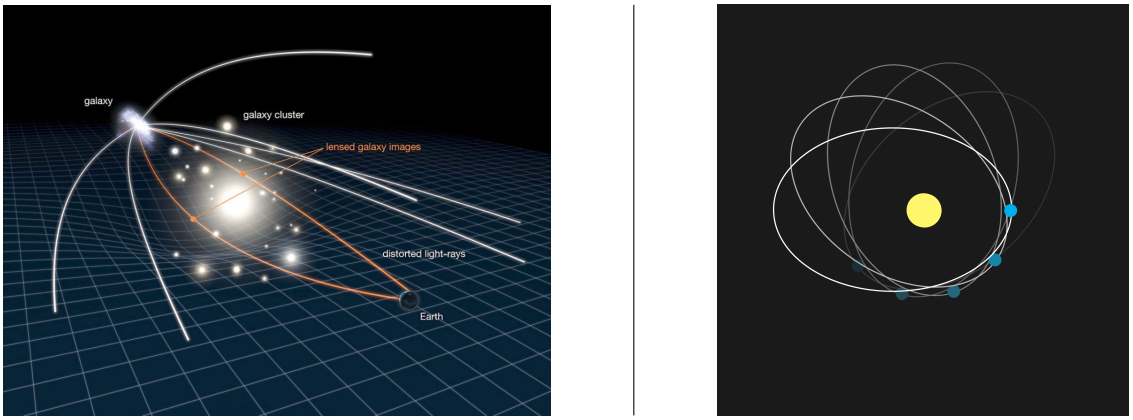

Figure 1: *Left*: Pictorial representation of gravitational lensing. CREDITS: NASA/ESA, http://www.cfhtlens.org/public/what-gravitational-lensing. *Right*: Representation of a perihelion precession.

Furthermore, in virtue of the *Bianchy identities* obtained by permuting ν, κ and η in

$$\nabla_\eta R_{\lambda\mu\nu\kappa} + \nabla_\kappa R_{\lambda\mu\eta\nu} + \nabla_\nu R_{\lambda\mu\kappa\eta} = 0\,, \tag{14}$$

on can shown that

$$\nabla^\mu T_{\mu\nu} = 0\,. \tag{15}$$

which is the generalisation of energy-momentum conservation with gravity. The Einstein field equation (10) shows the intimate link between the geometry of space-time and the energy components it supports, in J. Wheeler's words:

"Spacetime tells matter how to move; matter tells space-time how to curve".

Gravitation is the result of the curvature of space-time.

Achievements and short comings

Gravitational Lensing

One of the early achievements of GR is the correct computation of the deflection of light by massive objects, *i.e.* the *gravitational lensing of light*, as shown in Figure 1 (left panel). Einstein was the first to compute it correctly [26]. Einstein and GR thus became famous in 1919, when A. Eddington and his collaborators measured the change in the position of stars during a solar eclipse [27] which revealed GR to be consistent with their measurements. Einstein had performed a previous computation in 1911 that contained a factor 2 error due to the use of a wrong metric which he corrected later in 1915.

Mercury's perihelion precession

Newtonian gravity predicts that a body gravitating another one undergoes a fixed ellipsoidal orbit. However, it was pointed out by U. Le Verrier in 1859[3] that Mercury's orbit displayed precession,

3 U. Le Verrier (1859), "Lettre de M. Le Verrier à M. Faye sur la théorie de Mercure et sur le mouvement du périhélie de cette planète (Lettre from M. Le Verrier to M. Faye on the theory of Mercury and the motion of its perihelion)", Comptes rendus hebdomadaires des séances de l'Académie des sciences (Paris), vol. 49 (1859), pp.379–383.

that is to say the orbit rotated in time, as shown in Figure 1 (right panel). Einstein showed in [17] that GR predicted the correct precession angle which constituted another great proof of his theory.

Historically, the prediction of gravitational lensing and Mercury's precession are probably the most spectacular experimental confirmation of GR. Over the years more tests of GR have been done. GR is very tested experimentally in the solar system and in astrophysical contexts through the *Post-Newtonian Formalism* [22].

Static universes

We have seen some clear successes of GR. However, in the early years after its publication it led to some less satisfactory concepts. For instance, Einstein held strongly to the notion of a static universe for a long time. The Einstein universe [28] was infinite in time but spatially closed, a cylinder universe. It required the famous *Cosmological Constant* fixed to $\Lambda = 4\pi G\rho_{\mathrm{m}}$, to make the universe static by counter balancing the attractive matter density (ρ_{m}). To leave no free parameters, the curvature radius of the universe was fixed to $\Lambda^{-1/2}$. However, this universe did not resolve Olber's paradox "Why is the night sky so dark?", *i.e.* if the universe is infinite and static one should end up seeing a star in every corner of the sky and thus a bright night sky. This is indeed solved when an expanding universe is considered. The Einstein universe also suffered a more drastic issue, instability: an over-density (under-density) in matter collapses (expands).

Another competing model at that time was the de Sitter universe [29], a static universe with either positive or negative spatial curvature, where the matter in the universe is completely negligible with respect to the cosmological constant. This universe has grown important in cosmology especially for the description of *inflation*, an early accelerated expansion phase of the universe (see section 1.5.4.2), since it can be interpreted as a flat universe with an exponential expansion.

It is quite interesting to see that indeed physics is sometime a game of power. Probably due to the growing fame of Einstein, the ideas of a static universe held strong for some years over the works of A. Friedmann in 1922 and 1924 [30, 31] and G. Lemaître in 1927 [32] on expanding universes. The situation changed in the 1930s when E. Hubble published his results about the *flight of galaxies* (see section 1.2). This led Einstein to drop the cosmological constant and to abandon his idea of a static universe.

Let us finish by mentioning that GR works extremely well in all the regimes in which it has been tested [22, 26]. Nevertheless, despite numerous success, it must still be seen as an effective filed theory valid in a certain regime. One knows that GR lacks a UV-completion, that is to say a description of high energies such as a quantum description.

THE SMOOTH UNIVERSE

It is A. Friedmann, in 1922 [30], who found the most general solution of Einstein's fields equation for a uniform distribution of matter and energy. Thanks to this he was able to predict and model accurately the dynamical nature of the universe. This was confirmed seven years later by E. Hubble when he revealed the phenomenon of the "flight of galaxies" [33] guided by the evidence provided by B. Slipher, 10 years before, who showed that the light from nebulae were strongly red-shifted [34]. Today, the description of the universe inserts itself into the *cosmological principle* which provides a universal picture of the universe.

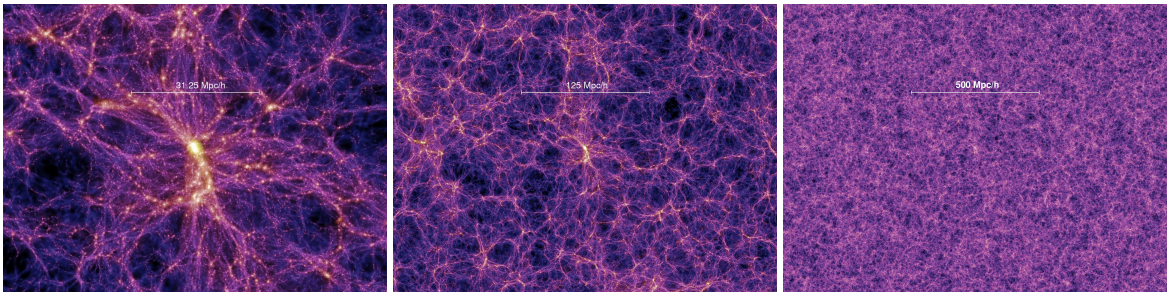

Figure 2: Images of the universe at different scales reconstructed from the Millennium Simulation [41], CREDITS: http://wwwmpa.mpa-garching.mpg.de/millennium/.

Cosmological principle

Nowadays, the universe is believed to be fairly identical everywhere on average. This means that if one looks at different large scale patches of the universe, one should not be able to spot characteristic differences between them but should rather be struck by their mutual resemblance. This fact is set under the *Cosmological Principle*, sometimes known as the Copernican principle. In a more mathematical approach, it is based on two properties that a manifold can exhibit:

i) *Isotropy*: Space looks the same in any direction for an observer at a specific point in space. This is described by the rotational invariance of the spatial part of the metric, *i.e.* the three spatial directions are Killing vectors of the metric.

ii) *Homogeneity*: The metric is the same throughout space.

On the one hand, the scale of homogeneity is still under debate among cosmologists. While the images constructed from the Millennium Simulation (see Figure 2) would lead us to set the scale of homogeneity at about ~ 200 Mpc/h, some evidences of very large structures in the universe exists, such as the Sloan Great Wall (423 Mpc) [35] or the Hercules–Corona Borealis Great Wall (2000-3000 Mpc) [36] for example. This could limit the use of the cosmological principle in certain cases. On the other hand, isotropy remains a strong principle still today [37]. It started to be well motivated with the discovery of the *Cosmic Microwave Background*, CMB henceforth, in 1964 by A. Penzias and R. Wilson [38] and first predicted in 1948 by R. Alpher and R. Herman [39]. The CMB is a relic radiation of the early universe, more details will be given in section 1.4.1.2. The scale of isotropy can be deduced from the distribution of galaxies. It has been estimated to be ~ 150 Mpc/h [40].

Friedmann equations

Friedmann's equations determine the evolution of the background of the universe, that is to say the evolution of the scale factor a and the amplitude of the spacial curvature, as a function of the density ρ and pressure p of the energy content of the universe in a perfect fluid description. To obtain the Friedmann equations, one must use the Friedman-Lemaître-Robertson-Walker (FLRW)

line element, that is the most general metric on a pseudo-Riemannian manifold with maximal symmetry on constant-time hyper-surfaces[4],

$$ds^2 = -dt^2 + a^2(t)\left(\frac{dr^2}{1-kr^2} + r^2\left(d\theta^2 + sin^2(\theta)d\phi^2\right)\right), \tag{16}$$

where k is a constant characterising the intrinsic curvature of space,

$$k = \begin{cases} +1 & \text{for a closed spherical universe} \\ 0 & \text{for an open flat universe} \\ -1 & \text{for an open hyperbolic universe} \end{cases} \tag{17}$$

and the energy momentum tensor of perfect fluids,

$$T_{\mu\nu} = \sum_i T^i_{\mu\nu} = \sum_i \Big((\rho_i + p_i)u_\mu u_\nu - g_{\mu\nu}p_i\Big), \tag{18}$$

with ρ_i and p_i respectively the energy density and pressure of the energy component of index i. This index corresponds to the form of energy content one can consider (baryonic matter, dark matter, radiation etc.). u_μ is the normalised velocity 4-vector defined as $u^\mu = dx^\mu/\sqrt{-ds^2}$ and so $u^\mu = (1, \vec{0})$. Using the FLRW line element (16) and the energy momentum tensor (18) in Einstein's field equation augmented with the cosmological constant

$$R_{\mu\nu} - \frac{1}{2}R\, g_{\mu\nu} + \Lambda g_{\mu\nu} = 8\pi G\, T_{\mu\nu}\,, \tag{19}$$

leads to the Friedmann equations

$$\left(\frac{\dot{a}}{a}\right)^2 = H^2 = \frac{8\pi G}{3}\sum_i \rho_i - \frac{k}{a^2} + \frac{\Lambda}{3}\,, \tag{20}$$

$$\frac{\ddot{a}}{a} = \dot{H} + H^2 = -\frac{4\pi G}{3}\sum_i \left(\rho_i + 3p_i\right) + \frac{\Lambda}{3}\,, \tag{21}$$

where the dot corresponds to derivatives with respect to cosmic time, *i.e.* the time measured by a clock at rest with respect to the expanding universe and $t = 0$ is set at the Big-Bang. We have also introduced the quantity $H = \frac{\dot{a}}{a}$ often called the Hubble parameter or Hubble rate, which characterizes the rate of expansion of the universe. ρ_i and p_i can be at most a function of time in order to satisfy the cosmological principle. It is important to understand that these two equations, the basis of modern cosmology, mean that the kinematic nature of the universe, expansion and acceleration, is fully described by its energy content through density and pressure. As a matter of fact, perfect fluids have their pressure and density linked by the equation of state

$$p_i = w_i\, \rho_i\,, \tag{22}$$

where each fluid composing the universe has a specific equation of state parameter w_i given in Table 1. Computing the conservation of the energy momentum tensor leads to the conservation of energy or continuity equation,

$$\dot{\rho}_i + 3H(1 + w_i)\rho_i = 0\,, \tag{23}$$

4 We will adopt the system of natural units for most of this thesis. It is defined by setting the reduced Planck constant, the Boltzmann constant and the speed of light to unity, *i.e.* $h/(2\pi) = k_B = c = 1$. This implies that all physical units are expressed in terms of energy as $[E] = [M] = [T]^{-1} = [L]^{-1}$.

Fluid component	Index	w_i
Pressure-less non relativistic matter (dust, galaxies, dark matter)	m	≈ 0
Relativistic particles (radiation)	r	$1/3$
Intrinsic spatial curvature	k	$-1/3$
Cosmological constant	Λ	-1
Dark energy or modified gravity	de	$< -1/3$

Table 1: Equation of state parameter of the common energy components contained in the universe.

which once integrated yields,

$$\rho_i = \rho_{i,0}\left(\frac{a_0}{a}\right)^{3(1+w_i)}, \tag{24}$$

where $\rho_{i,0}$ and a_0 are respectively today's value of the energy density considered and of the scale factor[5]. The first Friedmann equation can be rewritten in a purely energetic and dimensionless form, allowing straightforward physical interpretation:

$$\Omega_{\rm m}(t) + \Omega_{\rm r}(t) + \Omega_\Lambda(t) = 1 + \Omega_k(t)\,. \tag{25}$$

where on the left hand side

$$\Omega_i(t) = \frac{8\pi G}{3H(t)^2}\rho_i(t)\,, \tag{26}$$

are generally dubbed the (reduced) *density parameters*, in other words the cosmological parameters that characterize the proportion of the different forms of energy in the universe. To do so, we have used the definition of the critical energy density,

$$\rho_c = \frac{3H^2}{8\pi G}\,, \tag{27}$$

which is defined so that the spatial geometry is flat in a non accelerating universe. The matter content of the universe regroups standard matter, dubbed *baryons* in cosmology ($\Omega_{\rm b}$), and dark matter ($\Omega_{\rm dm}$) since both components are generally modelled to be pressure-less ($w_{\rm m} \approx 0$). This way, one has

$$\Omega_{\rm m} = \Omega_{\rm b} + \Omega_{\rm dm}\,. \tag{28}$$

The total amount of matter today is dominated by dark matter, DM thereafter, as $\Omega_{\rm dm,0} \approx 0.25$ against $\Omega_{\rm m,0} \approx 0.05$. Whereas the total energy content of the universe is dominated today by the component responsible for cosmic acceleration ($\Omega_{\Lambda,0} \approx 0.7$). Radiation, on the other hand, is completely negligible today ($\Omega_{\rm r,0} \ll 1\%$). We will discuss further the current constraints on these cosmological parameters in section 1.5.2. The term on the right hand side of (25) is defined as

$$\Omega_k(t) = \frac{-k}{a(t)^2H^2(t)}\rho_i\,, \tag{29}$$

and enables the link between the spatial curvature of the universe with its energy content. Depending on the sign of Ω_k the geometry of the universe changes as the pictorial representation in Figure 3 (right panel) shows. It is quite astonishing to see the expansion history can be characterised by such simple parameters and, depending on their values, the history and fate of the universe can change drastically (see Figure 3 (left panel)). Nevertheless, the universe is measured currently to be very close to spatial flatness ($\Omega_{k,0} < 1\%$) (see section 1.5.2).

5 An index 0 will indicate a quantity evaluated at present time throughout this thesis with the exception of tensor components.

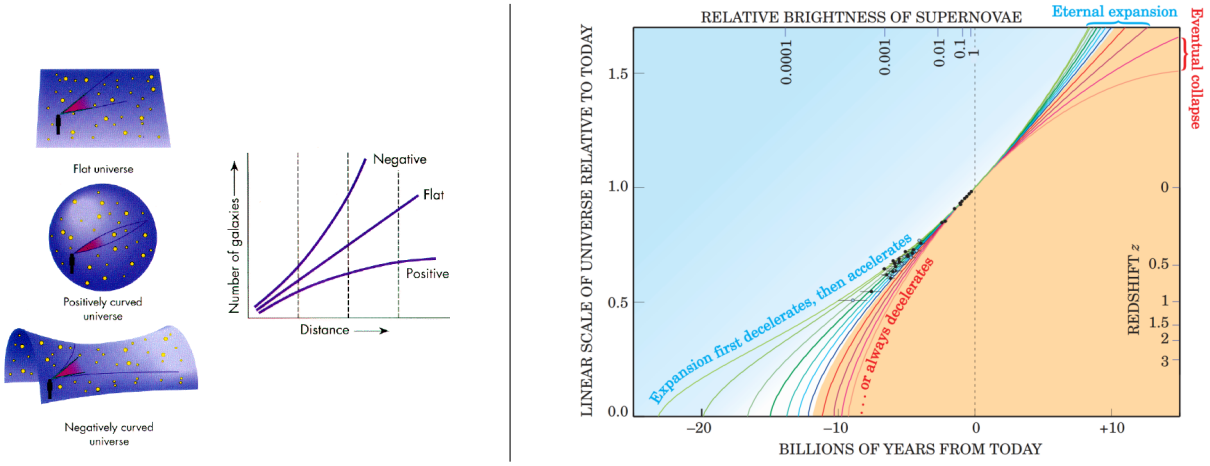

Figure 3: *Left*: Pictorial representation of the number of galaxies seen by an observer as a function of the distance in the universe depending on the curvature of space. CREDITS: http://abyss.uoregon.edu. *Right*: The fate of the universe for different cosmological models. The curves assume ρ_Λ ranging from 0.95 ρ_c (top curve) down to 0.4 ρ_c. CREDITS : http://www-supernova.lbl.gov/PhysicsTodayArticle.pdf.

The scale factor, however, is not a quantity one can observe and constrain directly. The fundamental observable of cosmology is the redshift:

$$z = \frac{\lambda_r - \lambda_e}{\lambda_e}\,, \tag{30}$$

where λ_e is the wave length of the emitted photon and λ_r is the wave length of the photon measured by the observer. The redshift is linked to the scale factor by

$$1 + z = \frac{a_0}{a}\,. \tag{31}$$

The shift of galaxy spectra to the red (redshift), which increases with the distance from the galaxy to the observer is the phenomenon that allowed Hubble to highlight the expansion of the universe. He characterised it thanks to the relation,

$$v = H_0\, d\,. \tag{32}$$

This fundamental relation, the Hubble law, links the recession velocity v of galaxies at a distance d from the observer with the constant of proportionality the Hubble constant H_0. The latter is constrained to be about $\approx 70\,\mathrm{k\,s^{-1}\,Mpc^{-1}}$ (see section 1.5.2). The redshift evolution of the Hubble rate can naturally be linked to the density parameters using the first Friedmann equation and (24),

$$H^2 = H_0^2 \left(\Omega_{\mathrm{r},0}\,(1+z)^4 + \Omega_{\mathrm{m},0}\,(1+z)^3 + \Omega_{k,0}\,(1+z)^2 + \Omega_{\mathrm{de},0}\, e^{\int w_{\mathrm{de}}(z)\,dz}\right), \tag{33}$$

which fully defines the background expansion of the universe. A dimension-less Hubble parameter is often also defined as

$$h = \frac{H_0}{100\,\mathrm{k\,s^{-1}\,Mpc^{-1}}}\,. \tag{34}$$

In this expression, the relevant unit to characterise distances in cosmology has appeared, the megaparsec (Mpc). This unit is probably impossible to be grasped by human standards as $1\,\mathrm{Mpc} \approx 3.26 \times 10^6$ ly $\approx 3{,}09 \times 10^{22}$ m. Nonetheless, let us keep in mind that the typical size of a galaxy is ~ 10 kpc, of a cluster of galaxies is ~ 1 Mpc, of super clusters 100 Mpc and of the observables universe today, c/H_0 with $H_0 \approx 70\,\mathrm{k\,s^{-1}\,Mpc^{-1}}$ is ~ 4000 Mpc.

Distances in cosmology

We have mentioned units to measure distances. The meter has been defined, since 1983, to be the distance light travels in 1/299792458 seconds. However, one must now ask the question: how does one define a distance in an expanding universe with non-euclidean geometry? Since we are dealing with distances, we will reintroduce c in the equations in this section for clarity.

In the FLRW universe, it is useful to redefine the metric by setting $r = \sin\chi$ ($k = 1$), $r = \chi$ ($k = 0$) and $r = \sinh\chi$ ($k = -1$) which leads to

$$ds^2 = -c^2dt^2 + a^2(t)\left[d\chi^2 + s_k^2(\chi)\left(d\theta^2 + \sin^2(\theta)d\phi^2\right)\right], \tag{35}$$

where

$$s_k(\chi) = \begin{cases} \sin\chi & \text{for } k = +1 \\ \chi & \text{for } k = 0 \\ \sinh\chi & \text{for } k = -1 \end{cases} \tag{36}$$

with χ the comoving interval defined by

$$\chi(z) = \frac{c}{a_0}\int_0^z \frac{dz}{H(z)}. \tag{37}$$

Comoving distance

Physically, the comoving distance is the distance between two objects in which cosmic expansion has been factored out, hence this distance does not depend on time. For instance, light travelling along the direction χ satisfies $ds^2 = -c^2dt^2 + a^2(t)d\chi^2 = 0$. From this, in a flat universe ($\Omega_k = 0$), light emitted at a time $t = t_e$, with $\chi = \chi_e$ and a redshift z will reach an observer at time $t = 0$, with $\chi = 0$ and $z = 0$, thus the comoving distance d_C is computed as

$$d_C = \int_0^{\chi_e} d\chi = -c\int_{t_0}^{t_e} \frac{dt}{a(t)} = c\int_0^z \frac{d\tilde{z}}{H(\tilde{z})}, \tag{38}$$

where we have set $a_0 = 1$ for simplicity, which is the case for a flat universe. As expected, this distance depends on the "cosmology" through $H(z)$. For very close objects, one can approximate

$$d_C \approx \frac{c}{H_0}z, \text{ for } z \ll 1. \tag{39}$$

Then, using the definition of the recession velocity with redshift, $v = zc$, we retrieve the Hubble law (32), $v \approx H_0 d_C$.

Luminosity distance

Theoretically, the comoving distance is very useful, however, it is not directly measurable. Flux on the other hand is an observable and is expected to follow the relation

$$f = \frac{L}{4\pi d_L^2}, \tag{40}$$

in curved space-time where d_L is the luminosity distance and L the luminosity. Note that the latter needs to be normalised cautiously. Taking $z = 0$, the flux is related to the observed luminosity by

$f = L_0/S_0$ where $S_0 = 4\pi s_k^2(\chi)$ is the area of a sphere of radius $s_k(\chi)$ at $z = 0$. From this one can derive

$$d_L^2 = s_k^2(\chi)\frac{L}{L_0}\,. \tag{41}$$

Luminosity is an amount of energy delivered during an interval of time. Therefore, a source that emits an energy of $\Delta E_e = L\Delta t_e$ during the time interval Δt_e will be observed as an energy $\Delta E_0 = L\Delta t_0$ during an interval Δt_0. Recalling that $\lambda \propto t$, we have $\Delta t_0/\Delta t_e = \lambda_0/\lambda_e = 1+z$, and $E \propto t^{-1}$ we have $\Delta E_e/\Delta E_0 = \lambda_0/\lambda_e = 1+z$. Therefore

$$\frac{L}{L_0} = \frac{\Delta E_e}{\Delta E_0}\,\frac{\Delta t_e}{\Delta t_0} = (1+z)^2\,, \tag{42}$$

from which we deduce the expression

$$d_L = s_k(\chi)(1+z)\,, \tag{43}$$

and for $z \ll 1$ one has $d_L \approx d_C$.

Angular diameter distance

The last distance one can consider in cosmology is the *angular diameter distance*. It is defined in such a way that the small angle approximation still holds in curved space,

$$d_A = \frac{\Delta l}{\Delta\theta}\,, \tag{44}$$

where $\Delta\theta$ is the angle of an object of physical size Δl orthogonal to the line of sight as seen by the observer. Taking the observed object to lie on the surface of a sphere of radius $s_k(\chi)$ and redshift z, the physical size Δl at a time $t = t_e$ must be

$$\Delta l = a(t_e)\,s_k(\chi)\,\Delta\theta = \frac{s_k(\chi)}{1+z}\Delta\theta\,, \tag{45}$$

which leads to define

$$d_A = \frac{d_L}{(1+z)^2}\,. \tag{46}$$

This is valid for any metric as long as the flux is conserved.

THE PERTURBED UNIVERSE

Now that we have seen the general equations ruling the background evolution of the universe, let us move on to the description of its perturbed sector, *i.e.* the behaviour and evolution of the large-scale structures (LSS) of the universe such as galaxies, clusters of galaxies and super clusters. The seeds of in-homogeneities in the universe are believed to arise from quantum fluctuations in the primordial universe. The evolution of these in-homogeneities is modelled classically in modern cosmology by *cosmological perturbation theory*.

Linear perturbation theory

In the gravitational instability paradigm, the formation of structures is understood to occur in a hierarchical way, that is to say with small-scale perturbations collapsing before large-scale perturbations. This is a *bottom-up* scenario. Solving Einstein equations requires a perturbative approach,

i.e. by slightly perturbing the quantities and studying their evolution on the smooth background. To do so, the metric is perturbed as

$$g_{\mu\nu} = \bar{g}_{\mu\nu} + \delta g_{\mu\nu} \tag{47}$$

where the quantity with a bar corresponds to the background value and the one preceded by δ is the perturbation on that background. The perturbed Einstein equation yields

$$\delta G_{\mu\nu} = 8\pi G\, \delta T_{\mu\nu}\,. \tag{48}$$

A thorough derivation of the full perturbation theory is something very involved (see for example [42, 43] for detailed derivations). For the pedagogical purposes of this thesis, we are going to obtain the linearised Einstein equations and stress-energy conservation, *i.e.* only expressions containing up to first order perturbations. For this, we consider a simplified case where only scalar perturbations without anisotropic stress, hence only non vanishing diagonal terms, are considered. The perturbed FLRW line element in the *conformal Newtonian gauge* (also called *longitudinal gauge*) reduces thus to

$$ds^2 = a^2(\eta)\big[-(1+2\Phi)d\eta^2 + (1-2\Psi)\delta^{ij}dx_i dx_j\big]\,, \tag{49}$$

where conformal time is defined as $\eta = \int_0^t \frac{d\tilde{t}}{a(\tilde{t})}$, Φ is the Newtonian potential and Ψ the curvature potential. (49) is a choice of gauge therefore all the following results will be derived in this specific gauge.

Fluid perturbations

Let us now compute the perturbed energy momentum tensor of a perfect fluid. For this, one perturbs the quantities it contains as

$$\rho(\vec{x},\eta) = \bar{\rho}(\eta) + \delta\rho(\vec{x},\eta)\,, \tag{50}$$

$$p(\vec{x},\eta) = \bar{p}(\eta) + \delta p(\vec{x},\eta)\,, \tag{51}$$

$$u^\mu(\vec{x},\eta) = \bar{u}^\mu(\eta) + \delta u^\mu(\vec{x},\eta)\,. \tag{52}$$

The reason we are able to make such a decomposition is thanks to the cosmological principle. Homogeneity allows to set $\bar{\rho} = \bar{\rho}(\eta)$ and $\bar{p} = \bar{p}(\eta)$ while isotropy allows us to consider the fluid component at rest, therefore for a comoving observer $u^\mu = (u^0, 0, 0, 0)$. Note that $\Phi(\vec{x},\eta)$ and $\Psi(\vec{x},\eta)$ are already the scalar perturbations in the line element (49). Perturbing (18) produces

$$\delta T^\mu{}_\nu = (\delta\rho + \delta p)\bar{u}^\mu\bar{u}_\nu + (\bar{\rho}+\bar{p})(\bar{u}_\nu\delta u^\mu + \bar{u}^\mu\delta u_\nu) - \delta p\,\delta^\mu_\nu\,. \tag{53}$$

Now we must compute the perturbation of the velocity 4-vector in terms of the metric. Since it is normalised, we have $g_{\mu\nu}u^\mu u^\nu = g^{\mu\nu}u_\mu u_\nu = -1$, hence

$$\delta g_{\mu\nu}\bar{u}^\mu\bar{u}^\nu + 2\bar{u}_\mu\delta u^\mu = 0\,. \tag{54}$$

Given that in the conformal Newtonian gauge we have $\bar{u}^\mu = (a^{-1}, \vec{0})$ and $\bar{u}_\mu = (a, \vec{0})$, we deduce

$$u^\mu = a^{-1}(1-\Phi, v^i)\,, \tag{55}$$

$$u_\mu = a(-1-\Phi, v^i)\,, \tag{56}$$

where $v^i = dx^i/d\eta$ is the coordinate velocity often dubbed *peculiar velocity* with respect to the expanding background. It is customary to define the *velocity divergence*,

$$\theta = \nabla_i v^i\,, \tag{57}$$

and the dimensionless *density contrast*,

$$\delta = \frac{\rho - \bar{\rho}}{\bar{\rho}} = \frac{\delta\rho}{\bar{\rho}} \,. \tag{58}$$

The initial state of fluctuations are modelled as a random field with mean $\langle\delta\rangle = 0$. Therefore, the density contrast increases in time, that is to say, initial over-densities grow whereas under-densities decay. Note that in the standard picture of inflation (see section 1.5.4.2), the initial fluctuation field is predicted to be Gaussian.

In the fluid description, as much as one defines an equation of state $p = w\rho$ in the background sector, one defines the propagation speed of scalar (adiabatic) perturbations as

$$c_s^2 = \frac{\delta p}{\delta\rho} \,, \tag{59}$$

which is of important physical relevance as we will see later. From all the above, we can write down the components of the perturbed energy momentum tensor,

$$\delta T^0{}_0 = -\delta\rho = -\bar{\rho}\,\delta \,, \tag{60}$$
$$\delta T^0{}_i = -\delta T^i{}_0 = (\bar{\rho} + \bar{p})v_i = (1+w)\bar{\rho}\,v_i \,, \tag{61}$$
$$\delta T^i{}_j = \delta p\,\delta^i_j = \bar{\rho}\,c_s^2\,\delta\,\delta^i_j \,. \tag{62}$$

Linearised Einstein equations

Now that we have expressed all the components of the perturbed energy momentum tensor, we need to compute the perturbation of the Einstein tensor. Perturbing (11) at first order yields

$$\delta G_{\mu\nu} = \delta R_{\mu\nu} - \frac{1}{2}R\,\delta g_{\mu\nu} - \frac{1}{2}g_{\mu\nu}\delta R \,, \tag{63}$$

where

$$\delta R_{\mu\nu} = \delta\Gamma^\alpha_{\mu\nu,\alpha} - \delta\Gamma^\alpha_{\mu\alpha,\nu} + \delta\Gamma^\alpha_{\mu\nu}\Gamma^\beta_{\alpha\beta} + \Gamma^\alpha_{\mu\nu}\delta\Gamma^\beta_{\alpha\beta} - \delta\Gamma^\alpha_{\mu\beta}\Gamma^\beta_{\alpha\nu} - \Gamma^\alpha_{\mu\beta}\delta\Gamma^\beta_{\alpha\nu} \,, \tag{64}$$
$$\delta\Gamma^\mu_{\alpha\beta} = \frac{1}{2}\delta g^{\mu\nu}\big(g_{\alpha\nu,\beta} + g_{\beta\nu,\alpha} - g_{\alpha\beta,\nu}\big) + \frac{1}{2}g^{\mu\nu}\big(\delta g_{\alpha\nu,\beta} + \delta g_{\beta\nu,\alpha} - \delta g_{\alpha\beta,\nu}\big) \,, \tag{65}$$
$$\delta R = \delta g_{\mu\nu}R^{\mu\nu} + g^{\mu\nu}\delta R_{\mu\nu} \,. \tag{66}$$

From this, we deduce the components of the perturbed Einstein tensor $\delta G^\mu{}_\nu = \delta^{\mu\alpha}G_{\alpha\nu} + g^{\mu\alpha}\delta G_{\mu\nu}$,

$$\delta G^0{}_0 = -2a^{-2}\Delta\Psi + 6a^{-2}H(\Psi' + \mathscr{H}\Phi) \,, \tag{67}$$
$$\delta G^0{}_i = -\delta G^i{}_0 = -2a^{-2}\nabla_i(\Psi' + \mathscr{H}\Phi) \,, \tag{68}$$
$$\delta G^i{}_j = a^{-2}\big[2\Psi'' + \Delta(\Phi - \Psi) + \mathscr{H}(2\Phi' + 4\Psi') + (4\mathscr{H}' + 2\mathscr{H}^2)\Phi\big]\delta^i_j + a^{-2}\nabla^i\nabla_j(\Psi - \Phi) \,, \tag{69}$$

where $\mathscr{H} = aH$ is the conformal Hubble rate and $'$ is a derivative with respect to conformal time. Now using the previously obtained components of the perturbed energy momentum tensor, we can write down the linearised Einstein equations for a fluid i. It proves useful to decompose them into

- ◇ **the 00 equation** :

$$-\Delta\Psi + 3\mathscr{H}(\Psi' + \mathscr{H}\Phi) = 4\pi G a^2\bar{\rho}_i\delta_i \,, \tag{70}$$

Note that the zero-th order contribution would have given the first Friedmann equation.

◇ **the 0i equation** :

$$\nabla(\Psi' + \mathscr{H}\Phi) = -4\pi G a^2 (1+w_i)\bar{\rho}_i \vec{v}\,, \tag{71}$$

◇ **the ij trace-part equation** :

$$\Psi'' + \mathscr{H}(\Phi' + 2\Psi') + (2\mathscr{H}' + \mathscr{H}^2)\Phi + \frac{1}{3}\Delta(\Phi - \Psi) = 4\pi G a^2 \bar{\rho}_i\, c_{s,i}^2\, \delta_i\,, \tag{72}$$

where we have used that the trace of the Kronecker symbol is equal to 3. Note that the zero-th order contribution would have given the second Friedmann equation.

◇ **the ij trace-less equation** :

$$\Phi - \Psi = 0\,, \tag{73}$$

If we had considered anisotropic stress we would not have obtained $\Phi = \Psi$.

Note that in the case of multiple fluids one would have to sum each components, for example $\bar{\rho}_i\delta_i$ becomes $\bar{\rho}_{\rm m}\delta_{\rm m} + \bar{\rho}_{\rm r}\delta_{\rm r}$ for matter and radiation. Another set of useful equations, although not independent from the linearised Einstein equations, can be derived from the perturbed energy conservation condition. Perturbing the latter produces

$$\delta T^{\mu}{}_{\nu;\mu} = \delta T^{\mu}{}_{\nu,\mu} - \delta\Gamma^{\alpha}_{\nu\beta} T^{\beta}{}_{\alpha} - \Gamma^{\alpha}_{\nu\beta}\delta T^{\beta}{}_{\alpha} + \delta\Gamma^{\alpha}_{\beta\alpha} T^{\beta}{}_{\nu} + \Gamma^{\alpha}_{\beta\alpha} T^{\beta}{}_{\nu} = 0\,, \tag{74}$$

from which one can deduce for a fluid i

- The $\nu = 0$ equation is the relativistic version of the *continuity equation*,

$$\delta_i' + 3\mathscr{H}(c_{s,i}^2 - w_i)\delta_i + (1+w_i)(\theta_i - 3\dot{\Psi}) = 0\,. \tag{75}$$

Note that the zero-th order contribution would have given the continuity equation $\bar{\rho}_i' + 3\mathscr{H}(1+w_i)\bar{\rho}_i = 0$. Equation (75) describes the evolution of density perturbations. The second term is a friction term (Hubble friction) and the last is the source term. We see that decreasing potential wells but also converging peculiar velocities contribute to the collapse of perturbations. In the Newtonian limit $w_i \ll 1$ and thus without the relativistic correction $\dot{\Psi}$, one recovers the usual continuity equation $\delta_i' + \theta_i = 0$.

- The $\nu = i$ equation is the relativistic version of the *Euler equation*,

$$\theta_i' + \left(\mathscr{H}(1-3w_i) + \frac{w_i'}{1+w_i}\right)\theta_i + \Delta\left(\frac{c_{s,i}^2}{1+w_i}\delta_i + \Phi\right) = 0\,. \tag{76}$$

This highlights that peculiar accelerations are sourced by gravity ($\Delta\Phi$) and pressure gradients ($c_{s,i}^2\Delta\delta_i$). One recovers the standard Euler equation $\theta_i' + \mathscr{H}\theta_i + \Delta(c_{s,i}^2\,\delta_i + \Phi) = 0$ in the Newtonian limit.

The perturbation variables $\Phi(\vec{x},\eta)$, $\Psi(\vec{x},\eta)$, $\delta(\vec{x},\eta)$ and $\theta(\vec{x},\eta)$ are stochastic fields. One can thus assume them to be the sum of plane waves $e^{i\vec{k}\cdot\vec{r}}$. There is no mode mixing and each plane wave obeys the same equation with different $\vec{k}$ since we are considering the linearised equations. Therefore, the linearity of the equations also allows us to drop $e^{i\vec{k}\cdot\vec{r}}$. Combining equations (70), (71) and (73) in Fourier space leads to the relativistic Poisson equation,

$$-k^2\Phi = 4\pi G a^2 \bar{\rho}_i \left(\delta_i + 3\mathscr{H}(1+w_i)\frac{\theta_i}{k^2}\right), \tag{77}$$

and combining (70), (72) and (73), one obtains the equation for the evolution of the Newtonian potential,

$$\Phi'' + 3\mathscr{H}\left(1 + c_{s,i}^2\right)\Phi' + \left(2\mathscr{H}' + \mathscr{H}^2\left(1 + 3\,c_{s,i}^2\right) + k^2 c_{s,i}^2\right)\Phi = 0\,. \tag{78}$$

Now, let us discuss some important limits on the scales we consider.

Super-horizon scales

Thermodynamics tells us that entropy is conserved in equilibrium. The universe containing far more photons than baryons, the entropy of the universe is dominated by the one of the photon bath in equilibrium. Therefore, any non-equilibrium processes that create entropy are negligible. This way, the expansion of the universe is considered to be *adiabatic*. Most models of the early universe predict initial fluctuations to be adiabatic. Adiabatic perturbations can be seen as their local state being the same as the background but with a small time shift. This describes the picture of a universe where small portions are slightly ahead or behind in its evolution. Such perturbations have $c_s^2 \approx w$.

On scales much larger than the Horizon, we can use the simplification $k \ll \mathscr{H}$. Using also $\mathscr{H}' = -\frac{1}{2}(1+3w)\mathscr{H}^2$, the equation (78) reduces to

$$\Phi'' + 3\mathscr{H}\left(1+w\right)\Phi' = 0\,. \tag{79}$$

This equation has two solutions, a decaying and a constant mode. Introducing the latter, which is the cosmologically interesting one, into (70) and using the first Friedmann equation, yields

$$\delta \approx -2\Phi = const.\,, \tag{80}$$

which implies that the perturbations are *frozen* on super Hubble scales as long as we have $c_s^2 \approx w$, which is true for both matter and radiation dominated epochs.

Sub-horizon scales

For the purpose of studying structure formation, let us now consider scales much smaller than the Horizon ($k \gg \mathscr{H}$) and non-relativistic matter ($w_\mathrm{m} \approx 0$ and $c_{s,\mathrm{m}}^2 \ll 1$). In this configuration, the Poisson equation (77) reduces to

$$-k^2\Phi = 4\pi G a^2 \bar{\rho}_\mathrm{m}\,\delta_\mathrm{m} = \frac{3}{2}\mathscr{H}^2\Omega_\mathrm{m}\delta_\mathrm{m}\,, \tag{81}$$

which, when used into (76), produces

$$\delta_\mathrm{m}'' + \mathscr{H}\delta_\mathrm{m}' + \left(c_{s,\mathrm{m}}^2 k^2 - \frac{3}{2}\mathscr{H}^2\right)\delta_\mathrm{m} = 0\,. \tag{82}$$

If $\mathscr{H} = 0$, the latter equation produces a standard wave equation. Furthermore, equation (82) implies that a perturbation will grow if and only if

$$c_{s,\mathrm{m}}^2 k^2 - \frac{3}{2}\mathscr{H}^2 < 0\,. \tag{83}$$

Considering the wave length of a perturbation is $\lambda = 2\pi\frac{a}{k}$, the perturbation will grow only if

$$\lambda_\mathrm{m} > c_{s,\mathrm{m}}\sqrt{\frac{\pi}{G\rho_\mathrm{m}}} \equiv \lambda_J\,. \tag{84}$$

Therefore, wave modes shorter than the Jeans length λ_J will undergo damped oscillations whereas larger ones will grow in time according to

$$\delta_\mathrm{m}'' + \mathscr{H}\delta_\mathrm{m}' - \frac{3}{2}\mathscr{H}^2\,\delta_\mathrm{m} = 0\,. \tag{85}$$

Cold dark matter (CDM) displays low velocity dispersion and an almost vanishing sound speed, the Jeans length is thus small. On the contrary, radiation has a large velocity dispersion, $c_{s,\mathrm{r}} = c/\sqrt{3}$, which leads to disabling any growth on scales smaller than the Hubble scale. For baryons, $c_{s,\mathrm{b}} = c_{s,\mathrm{r}}$ when they are coupled to photons in the early universe. After decoupling, the sound speed of baryons drops rapidly and they become trapped into the CDM gravitational potential wells. That is to say, that inside the Hubble scale, matter perturbations grow according to (85). The latter, when solved in the matter dominated era, leads to the solutions

$$\delta_{m,+} \propto a \propto t^{2/3}\,, \qquad \text{(growing mode)} \tag{86}$$

$$\delta_{m,-} \propto a^{-3/2} \propto t^{-1}\,, \qquad \text{(decaying mode).} \tag{87}$$

Using the growing mode solution in the Poisson equation (81) tells us that $\Phi = const.$ during the matter dominated epoch. Therefore, galaxies can form, clusters can grow, however, the *sine qua non* condition is to include dark matter in the universe.

Statistics of the LSS

The study of structure formation requires us to contrast observations, namely the grained nature of the universe described by discrete statistics (galaxies, clusters of galaxies etc.), with cosmological perturbation theory described by continuous processes (stochastic fields). Cosmology faces a statistical problem due to its nature, although it is possible to look back in time by looking far away, it is not possible to study many realizations of the same process to make statistics accurate, indeed "we have only one universe".

A good way to overcome this issue, is to study statistics on the scales of the perturbations, thanks to the quantity called the matter power spectrum

$$P_{\mathrm{m}}(k,t) = \frac{2\pi^2}{k^3}\langle \delta_{\mathrm{m}}(k,t)\delta^*_{\mathrm{m}}(k,t)\rangle\,.$$

The power spectrum is a measure of the average squared amplitude of the Fourier mode k of a given cosmological perturbation. Being sensitive to the cosmological parameters such as the amount of dark matter and baryons in the universe but also to the evolution of matter density perturbations, it is a powerful probe for cosmology. One can use Boltzmann codes to compute the power spectrum of a given model such as the Code for Anisotropies in the Microwave Background (CAMB) [44] or the Cosmic Linear Anisotropy Solving System (CLASS) [45].

The 2-point correlation function, hereafter simply called correlation function, is another statistical tool of the LSS. It is defined, and linked to the matter power spectrum, as

$$\xi(\vec{r},t) = \langle \delta_{\mathrm{m}}(\vec{x},t)\delta_{\mathrm{m}}(\vec{x}+\vec{r},t)\rangle = \frac{1}{(2\pi)^3}\int d^3k\, P_{\mathrm{m}}(k,t)e^{i\vec{k}\cdot\vec{x}}\,. \tag{88}$$

This statistical tool is thus very useful since it measures the amount of correlation between an over-density (resp. under-density) at a point with an over-density (resp. under-density) at another point separated by $\vec{r}$.

Another statistical tool to characterize the matter density field and the structure formation is the *filtered variance* or *root mean square (rms) of matter fluctuations*,

$$\sigma^2_R(t) = \int_0^{+\infty} \frac{k^3}{2\pi^2} P_{\mathrm{m}}(k,t)\hat{W}^2(kR)d\ln k\,, \tag{89}$$

where $\hat{W}(kR) = \frac{3j_1(kR)}{kR} = 3\frac{kRcos(kR)-sin(kR)}{(kR)^3}$ is the Fourier transform of the Top-Hat filter window function (a low pass filter). The filtered variance characterizes the density fluctuations of the matter density field over a filtering scale R.

The power spectrum is fully characterised by its shape and normalisation. Its normalisation is commonly made thanks to the rms of matter fluctuations at $8\,h^{-1}$Mpc, σ_8. This particular choice comes from the fact that the first galaxy redshift survey [46] showed that the rms of galaxy counts was around unity in spheres of $8\,h^{-1}$Mpc. The σ_8 quantity is dependent on redshift, from (89) we see that it has the same dependence as $\delta_{\rm m}$, and it is generally computed as $\sigma_8(z) = \sigma_{8,0}\,\delta_{\rm m}(z)/\delta_{\rm m}(z=0)$ where $\sigma_{8,0}$ is its present day value. The quantity commonly used to characterise the growth of structure is the *growth function* $f\sigma_8$; we will see why in section 1.4.2.3. It is the product of $\sigma_8(z)$ with the *growth rate* $f = d\ln\delta_{\rm m}/d\ln a$.

PROBES OF COSMOLOGY

Let us summarise in this section the main probes of cosmology. We focus in particular on how the discovery of cosmic acceleration was made historically and how it is now comforted by other measurements obtained thanks to complementary probes. It is important to see that observations of this phenomenon can be made by probing the background and perturbation sector, and combining such probes provides efficient tools to constrain the cosmological model.

Classical probes

Supernovae

Supernovae (SN) are stellar explosions of extreme intensity such that a supernova occurring in a galaxy would outshine the galaxies for a short period of time and a supernova occurring in the Milky Way could be seen with the naked eye. The first written record of a SN dates back to 185 AD (SN 185) in the *book of the Later Han* by a Chinese astronomer. J. Kepler used SN 1604, the latest to be observed in the Milky way with the naked eye, to go against the picture in which the universe beyond the planets is immutable, that is, the Aristotelian view of the cosmos; the dominating view at this epoch. The first classification of SN and their name "new star" are due to Lundmark who released a list of 60 suspected SN in 1921. Today SN are divided into two main classes, type II present hydrogen during the explosion whereas type I do not. Then, within the latter class, the presence (type Ia) of silicon during the explosion and the absence (type Ib and Ic). The thermonuclear supernovae (SNIa) are the ones of most interest for cosmology. They come as the end result of the agitated life of a *binary system* where the companions have different masses. The star with the lowest mass will evolve more rapidly. Once it has consumed all its hydrogen, it will start collapsing and reheating. At about 10^8K the Helium is fused into carbon and oxygen and any hydrogen left is ejected. The carbon-oxygen core contracts until the equilibrium between the Fermi electron degeneracy pressure and gravity has been reached. If the star before its collapse was above the Chandrasekhar limit [47], it will collapse into a *neutron star* or a *black-hole*. Otherwise the star will become a white dwarf. The white dwarf is a curious type of body since the heavier it is, the smaller it is. In the binary system configuration, the white dwarf increases its mass by accreting matter from its companion that by then has become a red giant. Once the white dwarf reaches the Chandraskhar limit, the high temperatures, and thus the high fusion reaction rate, will ignite a thermonuclear flame —the *carbon detonation*— which causes the supernova.

The point of interest for cosmologists is that the underlying mechanisms of the supernovae are universal and all supernovae lead to an absolute magnitude of about

$$M \approx 19.5 \tag{90}$$

at maximum light. Therefore, they were first said to be *standard candles* [48]. The slight deviations, of about ± 1.5 for a SNIa, arise from the variations in the composition of the core of the white dwarf. However, the luminosity of the SNIa has been shown to be correlated to the decay of its light curve over the 15 days after the maximum light. Therefore, SNIa if not strictly standard candles are at least *standardisable candles* [49]. In addition, supernovae are the brightest of all astrophysical events and display a characteristic silicon absorption peak in their light spectra making them incredibly useful distance indicators. To make this a probe of the cosmological model, one has to make use of the cosmological distances derived in section 1.2.3. One must use the luminosity distance d_L to define the *distance modulus*

$$\mu = m - M = 5 \log_{10}\left(\frac{d_L}{1\,\text{Mpc}}\right) + 25\,, \tag{91}$$

where m is the *apparent magnitude* of a light source and M its absolute magnitude. Therefore, by knowing the absolute magnitude (90) and measuring the apparent magnitude, the SNIa can thus be used to constrain cosmological parameters as depicted in Figure 4. Indeed, the use of the distance modulus with the measurements of SNIa is how the discovery of cosmic acceleration by S. Perlmutter [50], B.P. Schmidt et A.G. Riess [51] in 1998 (Nobel Prize 2011), was made thanks to a sample of 42 and 60 SNIa respectively. They showed that the universe today was composed with $\Omega_\text{m} \sim 0.3$ and $\Omega_\Lambda \sim 0.7$. In conslusion, when using SNIa in cosmology one measures distances, hence they are probes of the background evolution of the universe.

Cosmic Microwave Background

The CMB is the observable relic of the early universe. This relic radiation was first predicted in 1948 by R. Alpher and R. Herman [39] and first measured by A. Penzias and R. Wilson in 1964 [38]. The CMB was emitted at the recombination epoch around 380 000 years after the big bang when electrons and protons started to form hydrogen atoms. The observations of the CMB revealed the presence of a plasma with a homogeneous temperature, as shown in Figure 5. The slight temperature deviations are at the origin of the cosmological structures observed today. The release of the CMB is the result of the cooling of the primordial universe. The *recombination epoch* where electrons and protons merged into neutral hydrogen started when the universe had a temperature of about $T \sim 4000$ K, that is, when the number density of photons with energies above the ionization energy of hydrogen (13.6 eV) dropped below the baryon density. At $T \sim 3000$K, *decoupling* took place, all hydrogen atoms had formed and there were no more free electrons to absorb thermal radiation; the universe became transparent. The photons acquired an infinite mean free path and the set of points where these photons started travelling freely in the universe, seen from an observer on earth, is called the *last scattering surface*.

These photons are the CMB photons we measure today to have an almost perfect thermal black body spectrum at a temperature of about 2.72 K with anisotropies of the order of 10^{-5}. The CMB is sensitive to peculiar velocities, density fluctuations and the gravitational potentials. To confront CMB observations with the prediction of the temperature anisotropies from a cosmological model, one usually decomposes the temperature anisotropy field, *i.e* the dimensionless deviations from

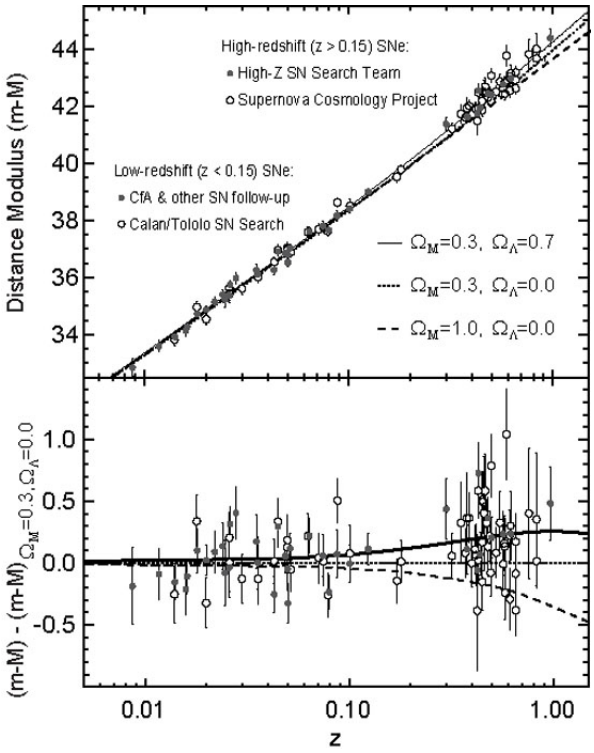

Figure 4: The distance modulus of measured SNIa and predicted by 3 models with different $\Omega_{m,0}$ and Ω_Λ as a function of redshift are shown. The lower panel corresponds to the residuals with respect to the $\Omega_{m,0} = 0.3$ and $\Omega_\Lambda = 0.0$ model. CREDITS : https://ned.ipac.caltech.edu/level5/March08/Frieman/Frieman3.html, figure adapted from [52, 53] based on [50, 51].

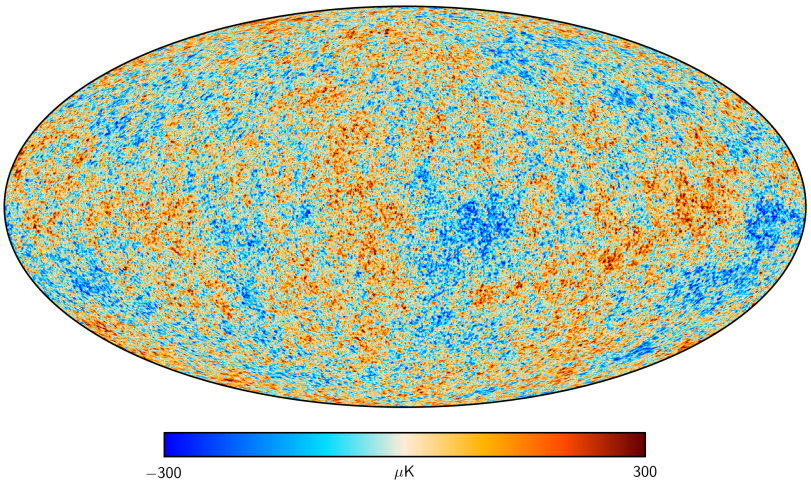

Figure 5: The cosmic microwave background where the color scale corresponds to the temperature anisotropies. CREDITS : Planck satellite, 2015, SMICA pipeline, https://www.cosmos.esa.int/web/planck .

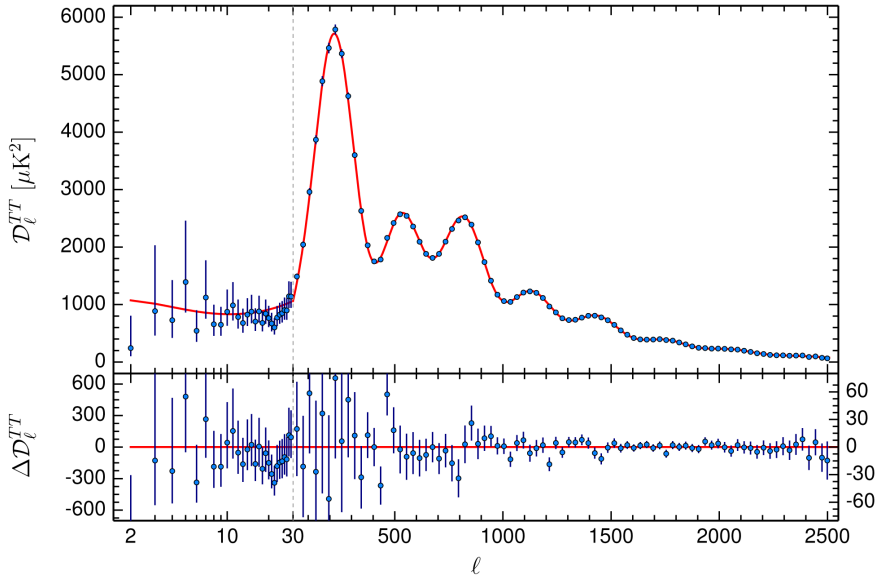

Figure 6: The temperature power spectrum measured from Planck [54]. The error bars show the $\pm 1\sigma$ uncertainties. The best fit base ΛCDM model is shown in red and residuals with respect to this model are shown in the lower panel.

the perfect black body temperature in a direction given by the unit vector $\vec{n}$, in spherical harmonics Y_{lm} as

$$\Theta(\vec{r},\eta) = \sum_{l=1}^{\infty} \sum_{m=-l}^{l} a_{lm}(\vec{r},\eta) Y_{lm}(\vec{n}) \,, \tag{92}$$

where the coefficients a_{lm} are taken to be statistically independent. Therefore, they have a zero mean value but a non vanishing variance. That is the quantity generally of interest to cosmologists, *i.e* the angular power spectrum

$$C_l = \frac{1}{2l+1} \sum_m \langle\, |a_{lm}|^2 \rangle \,, \tag{93}$$

where l is the multipole moment and is related to the measured angle θ by $\theta = \pi/l$. The C_l spectrum can be related to the temperature field in Fourier space by

$$C_l = \frac{2}{\pi} \int_0^\infty dk\, k^2 |\Theta_l(k)|^2 \,. \tag{94}$$

Like the matter power spectrum, the angular power spectrum contains crucial information about the cosmological model. An example of the measured angular power spectrum taken from the Planck collaboration [54] is shown in Figure 6. One can see for instance its main features, the several acoustics peaks, the relics of the baryonic acoustic oscillations phenomenon (see the following section). The amplitude of such peaks depends on $\Omega_{\rm m}$ and Ω_b whereas their position depends on Ω_k.

Deriving the complete formula for the temperature or the polarisation power spectrum requires numerical treatment for it involves solving Einstein and Boltzmann equations for the several coupled fluid components. Nevertheless, schematically speaking, the temperature anisotropies can be decomposed as [23]

$$\Theta = \Theta|_{LS} + \Theta|_{ISW} + \Theta|_{SEC} \,, \tag{95}$$

where the first term characterises all the effects coming from the last scattering surface, whereas the last two terms encompass effects related to the fact that we measure the CMB today. The second term corresponds to the *integrated Sachs Wolfe effect* (ISW). This effect corresponds to the gravitational red-shift the photons undergo when passing through deep potential wells during their travel from the last scattering surface to the CMB detector. The contribution of the ISW to the angular power spectrum corresponds to the integral of the time variation of the gravitational potentials

$$\Theta|_{ISW} = \int \left(\Phi' + \Psi'\right) d\eta \,. \tag{96}$$

Being sensitive to the time variations of the gravitational potentials, the ISW is thereby a useful probe to constrain the time evolution of dark energy, DE hereafter. However, unfortunately, it takes place at low multipoles in the angular power spectrum, that is where the data is the most affected by cosmic variance, making statistical inference less precise. The last term of (95) corresponds to second order effects such as the weak lensing of the CMB and others. The CMB is in some sense a "multi-probe" since it probes the background sector for $l \gtrsim 30$ thanks to the amplitude and position of the peak, whereas for $l \lesssim 30$ the perturbation sector is probed through the ISW effect. Measuring the lensing of the CMB is also a probe of the perturbation sector.

Baryonic acoustic oscillations

An important feature contained in the power spectrum and the angular power spectrum are baryonic acoustic oscillations (BAO). They are due to the competition between gravity and pressure forces, as gravity tries to compress the baryon-photon fluid, radiation pressure resists resulting in acoustic oscillations. Perturbations, over-densities and over-pressures, are dominated by photons and baryons as they are coupled together. Hence overpressure tries to equalize with its surrounding resulting in an expanding sound wave moving at its speed of sound (approximately 2/3 of the speed of light). After decoupling the photons are no longer interacting with the baryonic matter thus they diffuse away. This releases the pressure on the system, leaving shells of baryonic matter at fixed radius which then collapse under the gravity forces mainly due to DM. We see here that when the baryonic matter content of the universe grows at the expense of DM, namely $\Omega_{\rm b}$ grows and $\Omega_{\rm dm}$ decreases, the amplitude of the BAO increases. Indeed, the pressure effects of the baryonic matter coupled to light are more and more present. It produces a *standard ruler* for cosmology. The sound waves which travelled in the baryon-photon plasma before decoupling define a length scale, the *sound horizon*, which is computed as

$$r_s = \int_0^{t_{dec}} c_s \, dt \,, \tag{97}$$

where the sound speed $c_s = 1/\left(3\left(1+R_s\right)\right)$ with the baryon-to-photon density $R_s = 3\rho_{\rm b}/(4\rho_\gamma)$. This sound horizon r_s represents the average separation at which one expects to find an excess of pairs of galaxies. Therefore, measuring such a scale in a galaxy survey enables one to infer constraints on the cosmological parameters. BAO leading to a measure of distances is thus another probe of the background evolution of the universe.

Combination

The constraining power of probes often becomes higher when they can be combined since, generally, observations probing different physical processes lead to different degeneracies on the physical parameters they measure. The combination of SNIa, CMB and BAO shown in Figure 7 is one

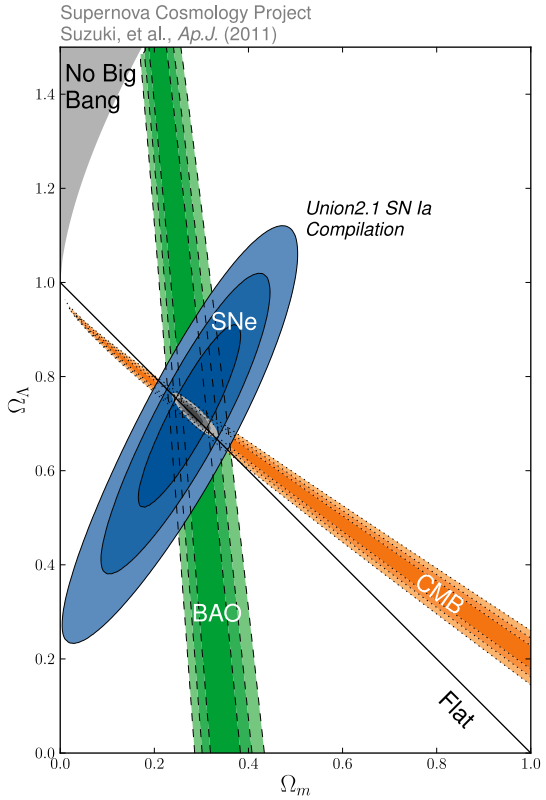

Figure 7: Plot of Ω_Λ versus $\Omega_{m,0}$ where SNIa, CMB and BAO constraints are shown. CREDITS : Supernova Cosmology Project [55].

example. The release of this contour plot was a great achievement in the understanding of the universe, as three probes constraining different physical processes converged to show the universe was not, in fact, matter dominated but contained $\Omega_{m,0} \sim 0.3$ and $\Omega_\Lambda \sim 0.7$ at the percentage level precision.

Complementary probes

Cluster counts

Dense regions of the universe are lit-up by countless galaxies. These dense regions are generally regrouped into clusters of galaxies, *i.e.* galaxies that are gravitationally bound together. Clusters shine both at optical wavelengths and at X-ray wavelengths thanks to the hot gas in their core (see Figure 8). It is generally more interesting to observe clusters in their X-ray emission to avoid optical pollution.

A lower amount of dark matter in the universe would result in observing fewer clusters today, whereas a lower amount of DE would lead to having more massive clusters today. Therefore, counting the number of clusters of a given mass in a given volume leads to a probe of matter and of DE once a model is assumed. For instance, the cluster abundance follows

$$\frac{dN(z)}{dzd\Omega} = \frac{c}{H(z)} d_A^2 (1+z)^2 \times \int_0^\infty dM f(M) \frac{dn(M,z)}{dM}, \tag{98}$$

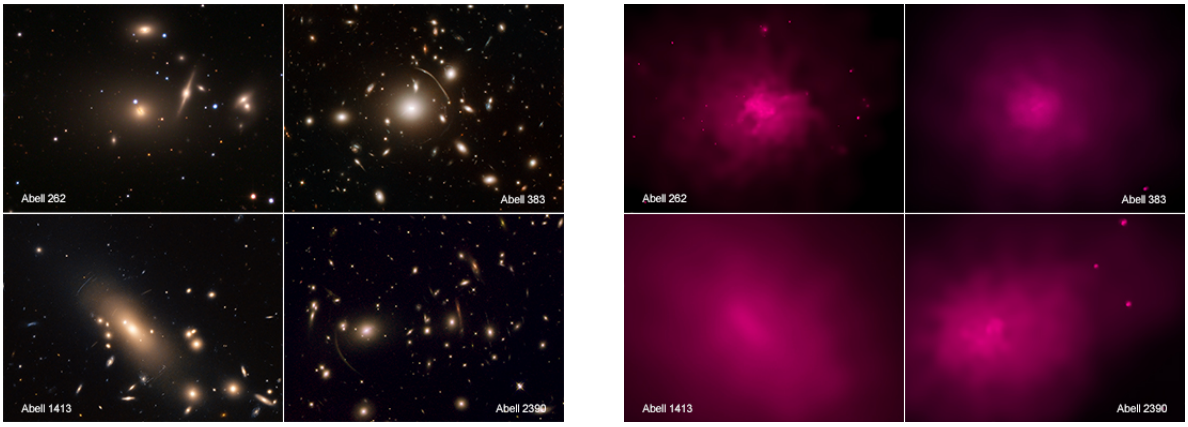

Figure 8: Images of clusters from Chandra X-ray Observatory launched in 2017 seen in the optical (*Left*) and X-ray (*Right*) wavelengths. CREDITS : http://chandra.harvard.edu/photo/2017/clusters/

where the first term on the right hand side is a geometric term and the second is a growth of structure term. Notably, the number objects with a mass between M and $M+dM$ can be given by Press-Schechter-like theory [56]

$$N(M)dM = \frac{1}{\sqrt{\pi}}\left(1+\frac{n_s}{3}\right)\frac{\bar{\rho}_{\rm m}}{M^2}\left(\frac{M}{M_c}\right)^{\frac{3+n_s}{6}}\exp\left(-\left(\frac{M}{M_c}\right)^{\frac{3+n_s}{3}}\right)dM \tag{99}$$

where M_c is the critical mass above which structures form and n_s is the scalar spectrum power-law index which quantifies the tilt of the primordial power spectrum. Let us note that in the same philosophy, counting *voids*, regions where the density is much lower than the average density, is therefore also a probe of DE [57].

Weak lensing

Gravitational lensing can be split into two categories, *strong lensing* and *weak lensing*. The former corresponds to the light being strongly bent by a punctual massive body. This leads to having clear lensing patterns around the lens, such as *Einstein's rings* (see Figure 9 (left panel)). On the other hand, the latter corresponds to an overall statistical effect. As the name suggests, weak lensing is described in the weak field limit and corresponds to the sum of all the deviations of light induced by the potentials of the surrounding massive bodies. Weak lensing provides a measure of masses without any prior knowledge of the composition or dynamics of the probed objects. The first analysis of the weak lensing of a cluster was carried out in 1990 by J. Tyson and collaborators [58] where they detected a coherent alignment of the *ellipticities* of galaxies, *i.e.* galaxy shapes, behind a cluster.

Weak lensing is an involved topic (see [59, 60] for recent reviews) where several categories can be found. For instance, one differentiates between *galaxy-galaxy lensing* [61] and *cosmic shear* [62]. The former corresponds to a punctual object lensing surrounding galaxies whereas the latter corresponds to the observation of alignment patterns of objects behind LSS. Let us summarize here, for pedagogical purposes, some important steps in weak lensing computations.

The true position of an object $\theta_{\rm true}$ is related to its deflected position $\theta_{\rm defl}$ by

$$\theta_{\rm true} = \theta_{\rm defl} - \frac{r_{ol}}{r_{ls}}\delta\vec{\theta}\,, \tag{100}$$

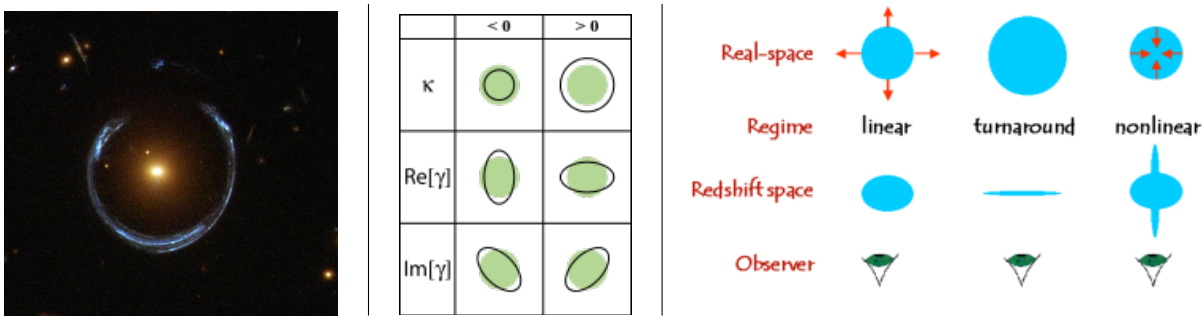

Figure 9: *Left*: Example of an Einstein ring (LRG 3-757). CREDITS : ESA/Hubble & NASA. *Middle*: Representation of the effects of convergence and shear on a circular source. CREDITS : https://en.wikipedia.org/wiki/Gravitational_lensing_formalism. *Right*: Representation of the effects induced by redshift space distortions.

where r_{ol} and r_{ls} are respectively the distance from the observer to the lens and the distance from the lens to the source. $\delta\vec{\theta}$ is the deflection angle which is related to the gravitational potentials along the line of sight by

$$\delta\vec{\theta} = -\nabla_\perp\big(\Phi+\Psi\big)d\eta\,. \tag{101}$$

This quantity will be indeed sensitive to an abnormal relation between the gravitational potentials and thus interesting to probe modification of gravity also. In practise, what is generally extracted from imaging surveys is the inverse magnification matrix

$$\mathbf{M}^{-1} = \frac{\partial\vec{\theta}_{\rm true}}{\partial\vec{\theta}_{\rm defl}} = \mathbf{I} + \int_0^{z_S} \frac{r_{ol}\,r_{ls}}{r_{os}}\,\nabla_\perp\nabla_\perp\big(\Phi+\Psi\big)\,\frac{d\eta}{dz}\,dz\,. \tag{102}$$

which, in the small deflections limit, is often parametrised as

$$\mathbf{M} = \begin{pmatrix} 1-\kappa-{\rm Re}[\gamma] & -{\rm Im}[\gamma] \\ -{\rm Im}[\gamma] & 1-\kappa+{\rm Re}[\gamma] \end{pmatrix} \tag{103}$$

where κ is the *convergence* and γ is the *shear parameter*. These parameters encode how the ellipticities are distorted by the gravitational potentials as shown in Figure 9 (middle panel).

Given that weak lensing allows one to make a map of the matter distribution of patches of the sky it can thus be used to constrain the matter power spectrum. Therefore, it produces a powerful probe of the cosmological parameters thus the cosmological model. Let us finish by stating however that weak lensing studies are not an easy task since they require wide and deep surveys and good quality images. Indeed, detecting very faint lensing correlations requires to average over a high density of background objects.

Redshift space distortions and $f\sigma_8$

When extracting measurements from galaxy surveys there are two important issues to have under control: *galaxy biasing* and *redshift space distortions* (RSD). Observations probe visible matter, stars, galaxies, clusters of galaxies and, unfortunately, visible matter is not a perfect tracer of the distribution of dark matter. Therefore, establishing the distribution of visible matter, baryons, will allow one to predict the distribution of dark matter only once a galaxy biasing model has been taken into account. Moreover, it happens that galaxies and clusters of galaxies have large proper

motions relative to the comoving frame. Therefore, any conversion from redshift space to real space will be affected, distorted, by these peculiar velocities.

Peculiar velocities produce two distortion effects. In the linear regime, on large scales ($\gtrsim 20\,\mathrm{h}^{-1}\mathrm{Mpc}$), the dominating distortion effect is due to the matter perturbations falling towards high density peaks in a coherent flow. Distributions of galaxies appear *squashed* along the line of sight (see Figure 9 (right panel)). This is the so-called Kaiser effect [63]. In the non-linear regime, on small scales ($\sim 1\,\mathrm{h}^{-1}\mathrm{Mpc}$), the dominating distortion is due to the randomness of the peculiar velocities. The center of the distribution of galaxies appears elongated along the line of sight, the so-called *fingers of god* effect [64] (see Figure 9 (right panel)).

Let us sketch the computation that relates the power spectrum in real and redshift space considering the Kaiser effect. The position of the source in redsift space $\vec{s}$ is related to that of real space $\vec{r}$ by

$$\vec{s} = \left(1 + \frac{v_\parallel(r) - v_\parallel(0)}{Hr}\right)\vec{r}\,, \tag{104}$$

where $v_\parallel(r) = \vec{v}\cdot\vec{r}/r$ is the comoving peculiar velocity component along the line of sight, $v_\parallel(0)$ is the one of the observer with respect to the source and $r = \|\vec{r}\|$. This leads to expressing the galaxy density contrast $\delta_{g,s}$ in redshift space with the one of real space $\delta_{g,r}$ by

$$\delta_{g,s} = \delta_{g,r} - 2\frac{\Delta v_\parallel(r)}{Hr} - \frac{1}{H}\frac{dv_\parallel}{dr}\,, \tag{105}$$

where $\Delta v_\parallel(r) = v_\parallel(r) - v_\parallel(0)$. The simplest modelling of galaxy biasing is to assume that the galaxy density contrast in real space is equal to the one of matter up to a linear bias factor [65]. In Fourier space it yields

$$\delta_{g,r} = b\,\delta_\mathrm{m}\,. \tag{106}$$

The expression of peculiar velocities for a coherent flow given from cosmological perturbation theory depends the galaxy contrast as

$$\vec{v} = iHf\delta_\mathrm{m}\frac{\vec{k}}{k^2} = iH\frac{f}{b}\delta_{g,r}\frac{\vec{k}}{k^2}\,, \tag{107}$$

with f the growth rate. Using (105) and (107) in the case of surveys spanning small angles, one obtains after some computations [63]

$$P_{g,s}(k,\mu) = P_{g,r}(k)\left(1 + 2\frac{f}{b}\mu^2 + \frac{f^2}{b^2}\mu^4\right), \tag{108}$$

where $\mu = \vec{k}\cdot\vec{r}/(kr)$ is the cosine of the angle between a given mode $\vec{k}$ and the line of sight. On can thus observe the key consequence of RSD: the isotropic matter power spectrum in real space becomes anisotropic in redshift space. From this, since b and f are positive values, one can grasp the effect of the coherent in fall: the power spectrum in redshift space will appear boosted or suppressed depending on μ, *i.e* maximum along the line of sight ($\mu = 1/(kr)$) and minimum perpendicular to the line of sight ($\mu = 0$).

An interesting step to extract a characteristic measurement for cosmology is as follows. Schematically, the relation (106) implies that the galaxy power spectrum can be decomposed as $P_{g,s} = b^2\sigma_8^2\tilde{P}_\mathrm{m}$ with $\tilde{P}_\mathrm{m}$ being the matter power spectrum normalised at high redshifts and σ_8 the root mean square of matter perturbations characterising the time evolution of the matter perturbations. Hence, one can write

$$P_{g,s}(k,\mu) = \tilde{P}_\mathrm{m}(k)\left((b\sigma_8)^2 + \frac{2}{3}(b\sigma_8)(f\sigma_8)\mu^2 + \frac{1}{5}(f\sigma_8)^2\mu^4\right). \tag{109}$$

This way, one can extract from a fitting process the RSD parameter $f\sigma_8$. This growth function is an archetypal probe of the perturbed sector of the universe as it can be predicted theoretically (see section 1.3.2).

Future experiments

Let us present some key future experiments which will provide data for studies around the DE phenomenon.

- **Euclid** : The Euclid satellite [66–68] is an ESA mission in preparation. It should be launched after 2020. It will probe the distance-redshift relation and the evolution of LSS by measuring the redshift and the shape of billions of galaxies and clusters over 15 000 square degrees of the extragalactic sky, up to a redshift of 2. These measurements will be made mainly thanks to weak lensing and galaxy clustering. The scientists in charge of the mission also hope to expand the mission to measure supernovae in the future.
- **SKA** : The Square Kilometre Array is a multi radio telescope project which should be built in Australia and South Africa starting in 2018. SKA will be sensitive to the 21cm emission line of hydrogen allowing the mapping of billions of galaxies at high redshifts and at the borders of the observable universe. SKA's aims will lead to more results on the DE phenomenon thanks to BAO and RSD measurements [69–72]. SKA has also the goal to study the epoch of re-ionization and cosmic magnetic fields.
- **WFIRST** : The Wide Field Infrared Survey Telescope [73] is a NASA observatory scheduled to be launched after 2020. It has been designed to study DE but also for the detection of exoplanets for example. The goal of the telescope is to probe the universe through infrared wavelengths which are blocked to ground telescopes by the atmosphere.
- **DESI** : The Dark Energy Spectroscopic Instrument [74] is a spectrograph that should be installed on the Mayall 4-meter telescope at Kitt Peak National Observatory (USA) in 2018. It is scheduled to obtain the spectra and the redshift of 18 million emission-line galaxies, 4 million luminous red galaxies and 3 million quasi-stellar objects. The measurements to constrain DE will be made thanks to BAO and RSD. It also has the goal to measure the sum of neutrino masses and signatures from inflation.

THE STANDARD MODEL OF COSMOLOGY ΛCDM

The Λ-cold dark matter, ΛCDM henceforth, model emerged in the late 1990s and is considered to be the standard model of cosmology today, sometimes also dubbed the concordance model. In this model, the dominating components are the cosmological constant Λ and cold dark matter (CDM). In ΛCDM, geometry and kinematics are driven by the energy content of the universe and GR with a cosmological constant is assumed to be the theory of gravity. Today, Λ its the simplest and most faithful way to model cosmic acceleration according to observations. It was used notably by Perlmutter, B.P. Schmidt and A.G. Riess [50, 51] in 1998 when fitting the distance modulus curves of SNIa (see section 1.4.1.1). It also predicts the abundances in the universe of hydrogen, deuterium, helium, lithium, *i.e. big-bang nucleosynthesis* (BBN), and the existence and the structure of the CMB, both in very good agreement with observations [54]. Let us briefly review here some expressions the cosmological constant yields, the current constraints on the cosmological parameters characterising this model and some existing observational discrepancies.

Cosmic acceleration with Λ

The action of the standard model corresponds to GR augmented with the cosmological constant as

$$S = \frac{1}{16\pi G}\int d^4x\sqrt{-g}\left(R - 2\Lambda\right) + S_{\rm m}(g_{\mu\nu},\psi)\,, \tag{110}$$

which yields the Einstein equation (19) and the Friedmann equations (20). Today, probes and combinations of probes we have discussed in the previous section lead to a measurement of the value of the cosmological constant of

$$\Lambda_{obs} \approx 4\times 10^{-54}\mathrm{m}^{-2}\,. \tag{111}$$

This gives rise to a puzzle for theoreticians who now need to explain to what this extremely small number corresponds[6]. The cosmological constant is much smaller than the size of a proton squared $\sim 10^{-30}\mathrm{m}^2$. Such a small quantity should be explained thanks to a quantum theory perspective. One could rightfully switch the side of the cosmological constant in the Einstein equation (19) leading to another interpretation. The cosmological constant can then be seen as an effective perfect fluid with the energy momentum tensor

$$T^{\Lambda}_{\mu\nu} = \rho_\Lambda u_\mu u_\nu + p_\Lambda(u_\mu u_\nu - g_{\mu\nu}) = \frac{\Lambda}{8\pi G_{\rm N}} g_{\mu\nu}\,, \tag{112}$$

with pressure and density defined as

$$\rho_\Lambda = -p_\Lambda = \frac{\Lambda}{8\pi G_{\rm N}}\,, \tag{113}$$

and thus giving rise to a repulsive force and a constant equation of state parameter $w_\Lambda = -1$. Nowadays, the cosmological constant is studied in the context of *vacuum energy*. However, computing the zero mode quantum fluctuations corrections to it leads to some issues as we will see in section 1.5.4.4.

Current constrains

The cosmological parameters characterising ΛCDM can all be constrained by the CMB power spectra and this to an astonishing percentage level precision. The most precise measurements on the CMB are due to the Planck satellite, launched in May 2009 and operated by the European Space Agency (ESA) in strong collaboration with the National Aeronautics and Space Administration (NASA). Table 2 shows the most recent constraints from this satellite on the cosmological parameters. It is important to note that already within the CMB, considering combinations of its different spectra helps reducing the errors bars (their acronyms are defined in the caption of Table 2).

More specific surveys are generally sensitive to a single or a few parameters, and operating combinations between surveys can significantly increase the precision, as we have already seen in section 1.4.1.4. The spatial curvature of the universe is another example. Considering CMB measurements only, spatial curvature has been constrained to $\Omega_{k,0} = -0.040^{+0.038}_{-0.041}$ (at 95% confidence

6 Note that the cosmological constant has the units of an inverse area. It is now known in black hole physics that the entropy of a black hole is proportional to the surface of its horizon [75]. This has made the study of surfaces carrying fundamental degrees of freedom a hot topic in theoretical physics in the recent years, see for example the *holographic principle* [76, 77]. Therefore, some physicists investigate whether the entropy, the horizon of the universe and Λ could all be related. These ideas are speculative at the moment but could lead to interesting developments in the future.

Parameter	Planck TT+lowP	Planck TT,TE,EE+lowP	Planck TT,TE,EE+SIMlow
$\Omega_{\mathrm{b},0}h^2$	0.02222 ± 0.00023	0.02225 ± 0.00016	0.02218 ± 0.00015
$\Omega_{\mathrm{c},0}h^2$	0.1197 ± 0.0022	0.1198 ± 0.0015	0.1205 ± 0.0014
τ	0.078 ± 0.019	0.079 ± 0.017	0.0596 ± 0.0089
$\ln(10^{10}A_\mathrm{s})$	3.089 ± 0.036	3.094 ± 0.034	3.056 ± 0.018
n_s	0.9655 ± 0.0062	0.9645 ± 0.0049	0.9619 ± 0.0045
H_0	67.31 ± 0.96	67.27 ± 0.66	66.93 ± 0.62
$\Omega_{\mathrm{m},0}$	0.315 ± 0.013	0.3156 ± 0.0091	0.3202 ± 0.0087
$\sigma_{8,0}$	0.829 ± 0.014	0.831 ± 0.013	0.8174 ± 0.0081

Table 2: Constraints on some of the parameters characterising the base ΛCDM cosmology computed from the baselines of Planck likelihoods from [54] (left and middle column) and [78] (right column). The errors displayed correspond to the 68% limits. The acronyms TT, TE, EE and lowP respectively stand for temperature (autocorrelation) power spectrum, the cross correlation between the temperature and E-mode power spectrum, the E-mode (autocorrelation) power spectrum and the low multipole part of polarisation power spectrum. SIMlow corresponds to the new low-multipole likelihood based on simulations introduced in [78]. The cosmological parameters in this table that we have not discussed so far are the following: τ is the Thomson scattering optical depth from reionisation. A_s is the normalisation of the primordial power spectrum.

level from Planck TT,TE,EE+lowP [54]). This implies a 2σ detection of positive spatial curvature. Nevertheless, considering on top of this the lensing of the power spectrum and BAO measurements shifts back the constraint and significantly increases the precision to [54]

$$\Omega_{k,0} = 0.000 \pm 0.005\,. \tag{114}$$

The universe today is thus measured to be very close to spatial flatness. Therefore, it is often set to be flat for simplicity.

On the other hand, the base ΛCDM model needs to be extended to include neutrinos so as to produce a faithful description of the universe. Taking neutrinos into account, the CMB produces the constraints depicted in Table 3. These constraints are well in agreement with the standard model of particle physics. Indeed, they are found to be very light as the sum of the neutrino masses Σm_ν is measured to be below the eV scale and the effective number of neutrino-like relativistic degrees of freedom N_eff is measured to be close to 3.

As for the amount of relativistic radiation today, a simple estimation consists in using the constraint on the matter-radiation equality redshift $z_\mathrm{eq} \approx 3371 \pm 23$ [54]. Then, equating the matter and radiation energy densities at this redshift yields $\Omega_{\mathrm{m},0}(1+z_\mathrm{eq})^3 = \Omega_{\mathrm{r},0}(1+z_\mathrm{eq})^4$, thus $\Omega_{\mathrm{r},0} \sim 10^{-5}$. Radiation is thereby a completely negligible component in the total energy budget of the universe today.

To finish the discussion on the constraints on the cosmological parameters, let us consider the equation of state of DE. Considering an extension of the ΛCDM model where a constant DE equation of state parameter w_de is free, the CMB alone favours slightly more negative than -1 values as shown in Table 3. However, a combination of Planck TT,TE,EE+lowP with BAO, SNIa, a probe of H_0, and lensing of the power spectrum shifts back the constraint to the true ΛCDM value $w_\mathrm{de} = -1$, at 95% confidence level it yields [54]

$$w_\mathrm{de} = -1.019^{+0.075}_{-0.080}\,. \tag{115}$$

Parameter	Planck TT,TE,EE+lowP	Planck TT,TE,EE+SIMlow
Σm_ν [eV]	< 0.492	< 0.340
$N_{\rm eff}$	$2.99^{+0.41}_{-0.39}$	$2.91^{+0.39}_{-0.37}$
w_D	$-1.55^{+0.58}_{-0.48}$	$-1.59^{+0.58}_{-0.46}$

Table 3: Constraints on some of the 1-parameter extensions to the base ΛCDM model from [54] (left column) and [78] (right column). The errors displayed correspond to the 95% limits.

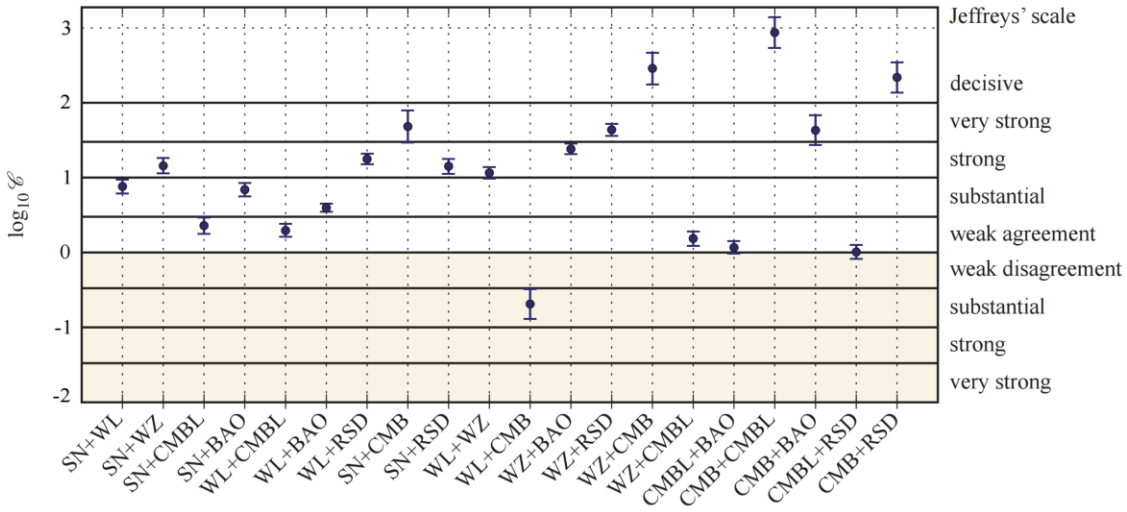

Figure 10: Figure 1 in [79] where the results of the concordance test between cosmological data sets are summarised.

Observational discrepancies

From the previous, one sees that the standard model of cosmology ΛCDM is well constrained and produces strong agreements with observations. However, when going into more details and considering more specific surveys, it seems to produce some observational tensions which could be tentative evidence for physics beyond the standard model. Yet, such tensions must be taken with care, since they could arise from a lack of control of delicate systematic errors or could also be very well due to a failure of the standard model. The consistency betweens pairs of cosmological surveys has been tested in [79]. The author used Bayesian inference to assess quantitatively whether there is concordance between different datasets when the ΛCDM model is considered. This study reveals there is good agreement in general between most of the up-to-date and major datasets in cosmology. The net exception is the discordance between CMB and weak-lensing measurements (see Figure 10). Let us now discuss more specific measurements that produce tensions within the standard model.

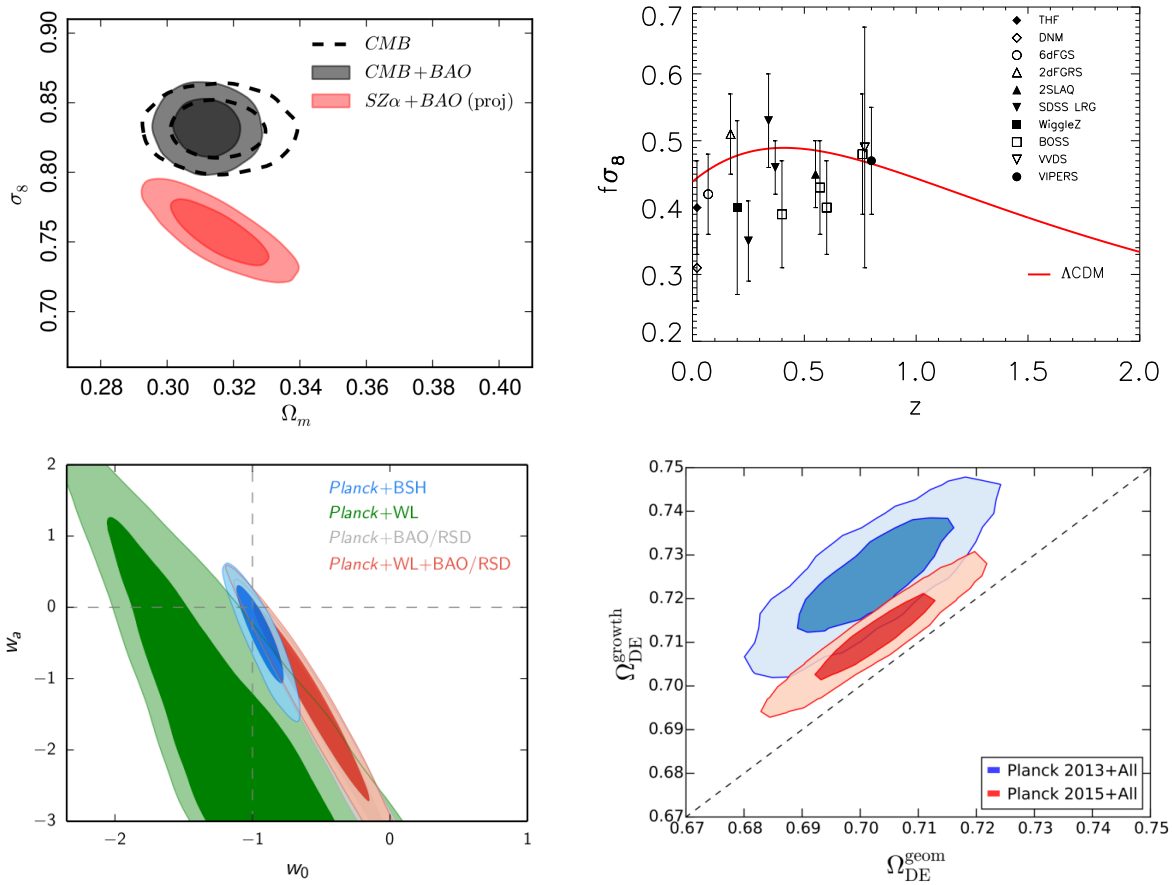

Figure 11: *Top left*: Figure 4 of [80]. Likelihood contours for ($\sigma_{8,0}$, $\Omega_{m,0}$) for CMB, BAO and SZ (Sunyaev-Zeldovich) cluster counts data . *Top right*: Redshift evolution of $f\sigma_8$ predicted by the Planck ΛCDM best fit and compared to data, the error bars represent their 1σ standard deviation. *Bottom left*: Figure 28 of [54]. Likelihood contours for the CPL parametrisation $w(a) = w_0 + w_a(1-a)$ [81, 82] for various data combinations. The acronym BSH stands for BAO+SNIa+H_0. *Bottom right*: Figure 2 of [5]. Constrains on Ω_{de} when the background and perturbation sector contributions are split using the probes of Table 4.

The Hubble constant

Probably the most intriguing tension, at least because of its statistical significance, concerns measurements of the Hubble constant H_0. The most resent release of the Planck collaboration [78] gives $H_0 = 66.93 \pm 0.62\,\mathrm{k\,s^{-1}\,Mpc^{-1}}$ at 68% confidence level (c.l.) under the assumption of a ΛCDM model. This result is in tension at more than 3σ with the measurement of the Hubble Space Telescope (HST) of $73.24 \pm 1.74\,\mathrm{k\,s^{-1}\,Mpc^{-1}}$ at 68% c.l. [83]. Another independent measurement, although less precise, seems also to give a higher Hubble constant, the strong lensing survey H0LiCOW has recently measured [84] $H_0 = 71.9^{+2.4}_{-3.0}\,\mathrm{k\,s^{-1}\,Mpc^{-1}}$ at 68% c.l.. Furthermore, authors in [85] have shown the observation of 580 SNIa of the Union 2.1 compilation [86] to be compatible with ΛCDM at 2σ c.l., whereas the results obtained with measurements of $H(z)$ compiled in [87] with H_0 of [83] not to be. Interestingly, the tension between the HST and Planck measurements can be alleviated when considering a coupled quintessence model (see section 2.1.3.1).

Cosmological Probe	Measurement	Geometry	Growth
CMB	high-l (TT, TE and EE power spectra)	✓	
CMB	low-l (TT, TE and EE power spectra)		✓
CMB	$40 \leqslant l \leqslant 400$ lensing power spectrum		✓
SNIa	d_l	✓	
BAO	D_V/r_s, d_A/r_s and $c/(Hr_s)$	✓	
Clusters	$\Omega_{\rm m}^{\beta}\sigma_8$		✓
RSD	$f\sigma_8$		✓

Table 4: Probes considered in the analysis carried out in [5] (Table 1 therein). The geometrical or growth nature of the probes is also highlighted.

Root mean square of matter perturbations

A tension with measurements of $\sigma_{8,0}$ also exists. The CMB tends to prefer higher values than local measurements. Figure 11 (top left quadrant) shows that the Sunyaev-Zeldovich cluster counts from the Planck satellite favour lower values as compared to that constrained by the CMB. This can also be grasped with the naked eye, ΛCDM seems to slightly over estimate $f\sigma_8$ measurements as depicted in Figure 11 (top left quadrant). Moreover, Planck CMB measurements are in tension with surveys of cosmic shear (weak lensing) such as CFHTLens [88] and KiDS-450 [89]. The most striking example is when considering the clustering parameter $S_8 = \sigma_8\sqrt{\Omega_{\rm m}/0.3}$ where a 2.3σ tension between the measurement of KiDS-450 and Planck [89] arises. Interestingly, the tension within $\sigma_{8,0}$ can be relieved by DE models (see for instance [4]).

Lensing

There has been some debate about the parameter $A_{\rm L}$ which controls the amount of gravitational lensing in small scale anisotropies [90]. The most recent measurement of this parameter by Planck [78] $A_{\rm L} = 1.15^{+0.13}_{-0.12}$ at 95% c.l is more than 2σ away from unity which is the base ΛCDM value. In addition, for weak lensing, the bottom left quadrant of Figure 11 shows that the combination of Planck CMB data and weak lensing puts ΛCDM ($w_0 = -1$, $w_a = 0$) 2σ away. However, the tension is alleviated once measurements of BAO and RSD are considered. This is one manifestation of the discordance between CMB and weak lensing measurements mentioned previously.

High-l's and low-l's in the CMB

Some studies split the various power spectra into their high-multipole (high-l) part ($l \geqslant 1000$) and low-multipole (low-l) ($l \leqslant 1000$) to test the self-consistency of CMB measurements [91, 92]. These types of studies reveal interestingly that some parameters are not always self consistent in between their constraints obtained thanks to the high-l and low-l part. Sometimes, some parameters can have either the low or high-l value in tension with the measurements from another survey. For instance, authors in [92] show that the Planck high-l prediction $H_0 = 64.1 \pm 1.7\,{\rm k\,s^{-1}\,Mpc^{-1}}$ is in 3σ tension with the value $73.0 \pm 2.4\,{\rm k\,s^{-1}\,Mpc^{-1}}$ from [93]. This tension is even worse (5σ) considering the 2016 measurement of $H_0 = 73.24 \pm 1.74\,{\rm k\,s^{-1}\,Mpc^{-1}}$ [83]. On the other hand, the low-l value $H_0 = 69.7 \pm 1.7\,{\rm k\,s^{-1}\,Mpc^{-1}}$ is consistent within 2σ. The authors claim however that the existing discrepancy between the Planck and South Pole Telescope (SPT) high-l CMB spectra renders the

interpretation of this tension, among others, as evidence for physics beyond the standard model ΛCDM to be disfavoured.

Parameter splitting

The idea of splitting probes can be pushed further. Authors in [5] have pursued an analysis where some parameters of the ΛCDM model were split also into their background (geometry, kinematics) contribution and perturbation sector (dynamics, growth) contribution. This was achieved by considering that the probes, displayed in Table 4, could constrain one contribution or the other. For instance, a part of the analysis in [5] constituted in constraining the standard set of parameters for a flat ΛCDM model

$$\{H_0, A_s, n_s, \tau, w_{\rm de}, \Omega_b h^2, \Omega_{\rm cdm}^{\rm geom} h^2, \Omega_{\rm cdm}^{\rm growth} h^2\}\,, \tag{116}$$

where $\Omega_{\rm cdm}$ was split. The results displayed in the bottom right of Figure 11 show that data seem to favour a larger amount of DE when considering growth of structures than when considering the background evolution. This is interesting since modified gravity models often produce smaller values of σ_8 today with respect to ΛCDM by lowering the amount of dark matter over DE for instance. One should note that $\Omega_{\rm m}$ or $\Omega_{\rm de}$ are intrinsically linked and degenerate with σ_8, indeed schematically more matter induces more clustering.

Theoretical shortcomings

From the previous sections, one sees that modern cosmology is endowed with the well based standard model ΛCDM despite some observational discrepancies. Yet, within or beyond the standard model, some crucial questions remain to be answered by cosmology. In this section, we shall review some of the issues actively explored in cosmology by giving a sketch of the overall history of the universe.

Planck era

The birth or the origin of the universe is not yet understood clearly. Commonly it is modelled as a Big-Bang, an initial time where the universe was infinitely small and its energy density infinitely high. Some alternative views put forward cyclic and bouncing universes. Nevertheless, the common paradigm agrees with the fact that the universe in its premises was in a special epoch, the *Planck era*, where energies were of the order of the Planck scale,

$$M_{\rm pl} = \sqrt{\frac{hc}{16\pi^2 G}} \approx 2.4 \times 10^{18}\ \text{GeV}\,, \tag{117}$$

and any classical description fails. The need to consider a quantum description of gravity followed by grand unification theory (GUT), where electroweak (EW) and strong interactions are regrouped arises. In brief, the standard picture of the universe tells us that right after this era the universe grew at an exponential rate, *inflation*. The expansion induced the universe to cool down, which enabled the fundamental forces to reveal themselves little by little until BBN started to create light atoms. After this primordial universe where radiation was the dominating component, the universe went into a period of matter domination where LSS emerged. Today, the universe has entered into another period of cosmic acceleration.

Primordial universe

The epoch that followed the Planck era also bears intriguing facts. A model that describes the physics of such an epoch must be able to solve several problems. The *horizon problem*, stated in 1968 by C. Misner [94], consists in understanding how the universe can be homogeneous and isotropic on large-scales when such scales cannot be causally connected due to the finite speed of light. For instance, the tiny deviations in the CMB imply that it is thermalised, however the large patches forming it are not in causal connection. Another issue one must consider is the *flatness problem*. The universe has been measured to be very close to spatially flat today and $\Omega_k \propto a^{-2}$ implies the early universe was even flatter in its premises by many orders of magnitude. This appears as a *fine-tuning*, since a flat universe corresponds to a point in the parameter space ($\Omega_k = 0$) as compared to closed ($\Omega_k < 0$) or hyperbolic ($\Omega_k > 0$) spatial geometries, which needs to be explained. There is another problem broached sometimes, but somewhat more controversial, the *monopole problem*. Many GUT theories predict the creation of *topological defects* and the magnetic monopole is one of them. This monopole has never been detected and this could be explained by an early period that extremely diluted the universe. Some cosmologists do not think this to be an issue since these topological defects are already hypothetical, in M. Rees words[7],

"Skeptics about exotic physics might not be hugely impressed by a theoretical argument to explain the absence of particles that are themselves only hypothetical. Preventive medicine can readily seem 100 percent effective against a disease that doesn't exist!"

The first model which solved these problems was proposed by A. Guth in 1980 [95]. The idea is that the universe must have gone through a period of extremely rapid expansion in its early times such that its content was substantially stretched and diluted. This period is called *inflation*. In models of inflation, the universe underwent an exponential expansion which lasted from 10^{-36} seconds after the Big Bang to around 10^{-32}s, and the temperature dropped by 5 orders of magnitude or so, depending on the inflationary model. Note that to solve the problems mentioned above the universe needs to increase its size by at least $N > 50$ e-foldings (depending on the inflationary model). For example, during inflation the physical wavelength ($a\lambda$ with $a \propto t^n$ with $n > 1$) grows faster than the Hubble horizon ($H \propto t$) and therefore the former is pushed outside of the latter. This leads to regions originally causally connected to be no longer after inflation, which solves the horizon problem. The space-time of inflation is quasi de Sitter, the universe must be very close to it, but not quite, for inflation to end. That is also why the primordial power spectrum is *almost* scale invariant.

The most simple model of inflation contains a scalar field, the *inflaton*. Its potential energy drives the exponential expansion of the universe, and to do so it must dominate over its kinetic energy. That is why an almost flat potential is generally required to lead to a sufficient amount of inflation. The inflation ends when its *slow-roll* parameters, measures of the slope of the potential, grow to unity. The temperature returns to the temperature of the universe before inflation thanks to the *re-heating* process, where the large potential energy of the scalar field decays into the standard model particles. The universe then enters into the *radiation dominated era*. Many different types of inflationary models exists today, some with one scalar field but different potentials or some with several scalar fields (see [96–98] for details). Alternative models to inflation also exist such as *Bouncing cosmologies* [99, 100]. In these models, the universe is not born in an initial singularity but rather at the end of the contracting phase of the previous universe, the *Big-Bounce*. *Conformal field theories* also attempt to provide a description of the early universe [101]. It is interesting to

7 Rees, Martin. (1998). Before the Beginning (New York: Basic Books)

note that in the realm of quantum gravity, in general, String theories predict inflation whereas loop-quantum gravity predicts big-bounces.

Let us mention here that the primordial universe ends schematically when BBN starts. It took place once the quantum chromodynamics (QCD) transition and nuclear fusion happened, themselves following the EW transition which occurred after inflation. The physics behind BBN is very important for cosmology as it is a probe for fundamental physics. The key point is that certain elements contained in the universe today could not have been produced or not sufficiently by stellar processes, thus these elements must come from BBN. Comparing such abundances today leads to constraints on parameters, to mention but a few, the Hubble rate and the value of the Newton constant at BBN.

Dark matter

Once atoms of heavier and heavier mass had formed, the universe entered the *matter dominated era*. Matter started to collapse where it was over-dense, the seeds being quantum fluctuations present before inflation. However, the consideration of baryonic matter as the only matter content of the universe does not allow a correct prediction of today's amplitude and density of large-scale structures. To overcome this issue, cosmologists resorted to add a new form of matter to the cosmological model: dark matter. This form of matter was thus named for it does not seem to interact through electromagnetic or through strong interactions but only with baryonic matter through gravity and maybe through the weak interaction. The first indirect observation of the DM phenomenon was made through the observation of the abnormal peculiar velocities of galaxies in the Coma cluster, by Zwicky in 1933 [102]. In the gravitational instability paradigm, DM would have created important inhomogeneities by gravitational collapse. Once baryonic matter was decoupled from photons, DM played a catalysing role in the evolution of cosmological perturbation, allowing the fast growth of aggregates of baryonic matter into today's cosmological structures as we have discussed previously. Neutrinos play also a role in the formation of structures by slowing it slightly due to their large mean free path.

The DM phenomenon is now quite well understood and modelled from the cosmological point of view indeed. However, it still remains a puzzle for particle physics to understand its nature and its constitution. Nowadays, DM is understood to be cold, in opposition to earlier theories of hot dark matter, in the sense that particles of DM are assumed to have a velocity distribution much lower than the speed of light. The quest to detect the first DM particles is very active. Detection techniques are numerous, they can be done by direct or indirect methods and in particle accelerators or via astrophysical processes (see [103] for a review on particle dark matter). The number one candidate for DM particles are *weakly interacting massive particles* (WIMPS) which are supposed to interact very weakly through the weak interaction. Another candidate is *axions*, light particles introduced to solve the strong charge-parity problem: why QCD does not seem to break the charge-parity symmetry on the contrary to the EW interaction. On the astrophysical point of view, the cold dark matter description still contains difficulties. For instance, it fails to explain the *missing satellites problem* [104], *i.e.* the fact that n-body simulations predict more dwarf galaxies around galaxies of the type of the Milky Way than what we observe. Another issue is the *cupsy halo problem* [105] where CDM simulations produce density distributions of dark matter halos much more peaked with respect to observations.

Issues with the cosmological constant

Modelling late time acceleration with the cosmological constant produces some theoretical drawbacks, for example, the *fine-tuning problem*. In order to illustrate this issue, let us consider a scalar field ϕ with the following action

$$S_\phi = \int d^4x \sqrt{-g}\Big[\frac{1}{2}\phi^{,\mu}\phi_{,\mu} - V(\phi)\Big] . \tag{118}$$

The first term in the squared brackets corresponds to the kinetic energy of the scalar field and the second to its potential energy. The energy momentum tensor can be deduced from (118) and yields

$$T_{\mu\nu} = \phi_{,\mu}\phi_{,\nu} - g_{\mu\nu}\Big[\frac{1}{2}\phi^{,\mu}\phi_{,\mu} + V(\phi)\Big] \tag{119}$$

The vacuum state corresponds to the minimum energy state. Therefore, one needs to consider a set-up where the kinetic energy is null and the field is at the minimum of its potential. This implies

$$\langle T_{\mu\nu}\rangle = -V(\phi_{\rm min})\, g_{\mu\nu} , \tag{120}$$

from which we must define $\rho_{\rm vac} = V(\phi_{\rm min})$ to stick to the definition of the energy momentum tensor of a field placed in the vacuum state [106]

$$\langle 0|T_{\mu\nu}|0\rangle = -\rho_{\rm vac}\, g_{\mu\nu} . \tag{121}$$

Note that $\rho_{\rm vac}$ has actually two contributions, the classical one coming from the value of the potential at its minimum (118) and a quantum one which comes from the zero point fluctuations of the ground state.

The fact that vacuum energy should gravitate was first proposed by W. Nernst in 1914[8] in the context of the electromagnetic field. Experimentally, it has been shown to exist thanks to the Casimir effect in 1947. Casimir experiments measure the difference of vacuum energy in between two different configurations. However, the physical interpretation of this effect is subject to controversy for it can also be explained by the relativistic Vander Waals forces between the two metal plates rather than by using the zero-point energies of the vacuum state [107]. Nevertheless, let us state that vacuum fluctuations being a form of energy and according to GR they should gravitate. Therefore, a consistent expression of Einstein's equation once quantum field theory is considered sums up to [106]

$$R_{\mu\nu} - \frac{1}{2}R\, g_{\mu\nu} + \Lambda_{_B} g_{\mu\nu} = 8\pi G\left(T^{\rm matter}_{\mu\nu} + \langle T_{\mu\nu}\rangle\right), \tag{122}$$

where the cosmological constant appearing is the one in the action (110) and is simply a new parameter of the theory, *i.e.* the *bare* cosmological constant. Now, for (122) to be equivalent to that of the standard model of cosmology ΛCDM (19), it must be cast into

$$R_{\mu\nu} - \frac{1}{2}R\, g_{\mu\nu} + \Lambda_{\rm eff} g_{\mu\nu} = 8\pi G\, T^{\rm matter}_{\mu\nu} , \tag{123}$$

where

$$\Lambda_{\rm eff} = \Lambda_{_B} + 8\pi G\, \rho_{\rm vac} . \tag{124}$$

The effective cosmological constant $\Lambda_{\rm eff}$ is the observed one, thus the one constrained by cosmological tests as in (111).

8 W. Nernst, "Über einen Versuch von quantentheoretischen Betrachtungen zur Annahme stetiger Energieänderungen zurückzukehren", Verhandlungen der Deutschen Physikalischen Gesellschaft, 4, p. 83 (1914).

A simple estimation of $\rho_{\rm vac}$ often found in literature is of the following form. Considering a field of mass m, momentum q and frequency w, its zero-point energy will be given by $E = w/2 = \sqrt{q^2+m^2}/2$. Then integrating over all the zero-point energies up to a cut off scale $q_{max} >> m$ yields

$$\rho_{\rm vac} = \frac{1}{2}\int_0^{q_{max}} \frac{d^3q}{(2\pi)^3}\sqrt{q^2+m^2} \approx \frac{q_{\rm max}^4}{16\pi^2}\,. \tag{125}$$

The strong coupling scale of gravity is the Planck scale, it is thus the natural cut-off scale and $q_{\rm max}$ should thus be taken to be $M_{\rm pl}$. This gives the vacuum energy density equal to

$$\rho_{\rm vac} \sim 10^{74}\,{\rm GeV}^4\,. \tag{126}$$

On the other hand, from the observed value of the cosmological constant one can also estimate

$$\rho_\Lambda \approx \frac{\Lambda_{obs} M_{\rm pl}^2}{8\pi} \sim 10^{-47}\,{\rm GeV}^4\,, \tag{127}$$

leading to a discrepancy between observed and predicted value of $\rho_{\rm vac}$ of 121 orders of magnitude when taking the Planck cut off, and does not decrease relevantly when taking other cut-off's such as EW or QCD. The conclusion is then that the term Λ_B in (124) needs to be extremely fine tuned for (124) to be valid since $\rho_{\rm vac}$ is huge in comparison to the observed value $\Lambda_{\rm eff}$. This is what is dubbed the *cosmological constant problem* or *fine-tuning problem*.

Another issue affiliated to the cosmological constant is the *coincidence problem*. This issue is however somewhat more controversial than the previous one [108]. It represents the fact that the energy density linked to the cosmological constant is of the same order of magnitude than that of matter today

$$\rho_\Lambda \sim \rho_{\rm m}(z=0)\,. \tag{128}$$

This can be considered quite curious since matter and the cosmological constant do not scale the same way with redshift at all. Therefore having them of the same order today seems to be a strange coincidence and maybe a fine tuning which should be explained. To be precise, the coincidence happened at

$$z_{coinc.} = \left(\frac{\Omega_{\Lambda,0}}{1-\Omega_{\Lambda,0}}\right)^{1/3} - 1 \approx 0.3\,. \tag{129}$$

This leads us to ask our selves why the universe started accelerating only recently and not some time in the past or in the future. Our knowledge of structure formation tells us that if cosmic acceleration started too early, no LSS or even stars and planets would have had the time to form before the universe got ripped apart by the repulsive force induced by the cosmological constant.

CONCLUSION

In this chapter, we have seen that General Relativity provides the means to study the evolution of the background and the perturbations of the universe. The background evolution is characterised by the Friedmann equations which link the Hubble rate to the energy content of the universe. The modelling of the formation of structures in the universe is made thanks to cosmological perturbation theory. The general picture of structure formation follows the gravitational instability paradigm, a bottom-up scenario, where small perturbations collapse before large ones as the universe evolves. We have given a review of the basic of linear perturbation theory. Let us note that, however, more complex and refined descriptions can be achieved. For instance, in standard perturbation theory [109] one can consider higher order perturbations for a more accurate description.

One can also considered the recent description from the *effective field theory of large-scale structures* [110] proposed to push the scale at which an analytical modelling of the power spectrum is possible further towards non linear scales. Numerically, for example, CAMB can compute the non-linear power spectrum thanks to the non-linear clustering Halofit model [111, 112].

We have also discussed the astonishing fact that observations show the universe to be in an accelerated expansion phase today. This can be counter intuitive at first due to the attractive nature of gravity. This fact is now supported by many combinations of probes. The energy component responsible for it is the major contribution to the total energy budget of the universe at present time ($\sim 70\%$). In fact, our knowledge and the modelling of the universe are symbolised today through the standard model of cosmology ΛCDM. However, on the observational side, tensions in between cosmological probes can be spotted. They may very well be due to either systematic errors or new physics. On the theoretical side, the standard model lacks the important completion which would allow a unifying description of the very early and later epochs of the universe. In the late epochs, also, describing cosmic acceleration with the cosmological constant produces theoretical issues. That is why, in the next chapter, we will discuss alternative ways to describe the late-time expansion history of the universe.

2

DARK ENERGY AND MODIFIED GRAVITY

Dark energy models and modified gravity theories are actively explored today. The former explains cosmic acceleration thanks to a new form of energy while the latter by modifying the equations of GR, *i.e.* the gravitational interaction, at a fundamental level. Schematically speaking, dark energy could be seen as modifying the fluid components ρ_i and p_i in the Friedmann equation,

$$\frac{\ddot{a}}{a} \propto G \times \sum_i \left(\rho_i + 3p_i\right), \tag{130}$$

whereas modified gravity could be seen as modification of the gravitational constant G. However, given the profound equivalence between the geometry and the energy content of the universe arising from Einstein's equation (10), the distinction between dark energy and modified gravity could usually be understood as a semantic concern, physically one often induces the other. We will often use one or the other term blindly in the rest of this thesis. Note, however, that a distinction could be made in principle, for example, *quintessence* models do not yield an abnormal relation between the gravitational potentials ($\Phi = \Psi$) whereas *scalar-tensor theories* do, thus the former could be called a dark energy model and the latter modified gravity. We will give an overview of such models in section 2.1.

Finding viable alternative models to ΛCDM does not come without hurdles. Driving cosmic acceleration requires a theory to produce notable effects on cosmological scales, *i.e* exhibit infrared modifications of GR. However, local tests of gravity limit stringently any deviations from GR on astrophysical scales. This produces the need for modified gravity theories to incorporate *screening mechanisms*. We will discuss how some of these processes emerge naturally in the context of scalar tensor theories in section 2.2. Moreover, the research around cosmic acceleration has created an incredible amount of dark energy models. It thus seems important to manufacture frameworks where many theories can be tested on the same grounds. The goal is then to create a "meta-formalism" where its parameters can be constrained by observations, and deducing constraints on a specific theory should come straightforwardly from the mapping of the theory to the unifying framework. This seems indeed more efficient than having to constrain each theory one by one. We will end this chapter by presenting one promising framework to do so, the *effective field theory of dark energy*.

ALTERNATIVE THEORIES TO ΛCDM

Many alternatives to the standard model exists. Let us state here that well before the standard model of cosmology was established, straight after the first publications on GR, physicists were already exploring modifications of the latter. Notably, in 1919, one of the first modified gravity, MG henceforth, theory was born: Einstein-Cartan gravity[1]. The idea in this theory is that the intrinsic spin of fermions produces torsion, *i.e.* the Levi-Civita connection is no longer symmetric. This theory has not been ruled out by observations and is still popular nowadays. It produces

1 Élie Cartan. "Sur une généralisation de la notion de courbure de Riemann et les espaces à torsion." C. R. Acad. Sci. (Paris) 174, 593–595 (1922). "Sur les variétés à connexion affine et la théorie de la relativité généralisée." Part I: Ann. Éc. Norm. 40, 325–412 (1923) and ibid. 41, 1–25 (1924); Part II: ibid. 42, 17–88 (1925).

interesting phenomenology such as replacing the Big-Bang by a Big-Bounce, and black holes by worm-holes. For the purposes of this thesis, we will discuss mostly theories which add a single scalar degree of freedom to the Einstein-Hilbert action.

Quintessence

One of the first model suggested to solve the issues of the cosmological constant used an additional scalar field. It originated in the late 1980s [113, 114] and is now dubbed *quintessence* [115]. The name quintessence harkens back to the ancient Greek thought in which space beyond the Earth was filled with a fifth element called aether.

The quintessence field couples to all the other components in the universe through gravity. This extra scalar field ϕ is dynamical, *i.e* it varies across time, and fluctuates, *i.e* varies in space, in opposition to the cosmological constant. The gravitational action of quintessence is of the form

$$S_{\rm g} = \int d^4x\sqrt{-g}\Big[\frac{1}{16\pi G}R + \mathscr{L}_\phi\Big]\,, \tag{131}$$

where

$$\mathscr{L}_\phi = -\frac{1}{2}g^{\mu\nu}\phi_{,\mu}\phi_{,\nu} - V(\phi)\,, \tag{132}$$

is the Lagrangian density of the quintessence field, $g^{\mu\nu}\partial_\mu\phi\partial_\nu\phi$ its canonical kinetic energy and $V(\phi)$ its potential energy density. Let us note that this action is almost like the one of the inflaton, although the fundamental difference is that, in the context of DE, one must also consider matter. Therefore, the total action is $S = S_{\rm g} + S_{\rm m}$. The scalar field has an effective mass defined as

$$m_\phi = \sqrt{V_{,\phi\phi}}\Big|_{\phi_{\rm min}}\,, \tag{133}$$

where $V_{,\phi\phi} = d^2V/d\phi^2$ and the associated energy momentum tensor is the one defined in (119). Alike the cosmological constant, it can be associated to a perfect fluid where its pressure and density must be

$$p_\phi = \frac{1}{2}\dot\phi^2 - V(\phi)\,, \tag{134}$$

$$\rho_\phi = \frac{1}{2}\dot\phi^2 + V(\phi)\,, \tag{135}$$

and equation of state is thus

$$w_\phi = \frac{p_\phi}{\rho_\phi} = \frac{\dot\phi^2 - 2V(\phi)}{\dot\phi^2 + 2V(\phi)}\,. \tag{136}$$

In the case of a flat FLRW universe, varying the action (131) with respect to the metric produces the Friedmann equations,

$$H^2 = \frac{8\pi G}{3}\Big[\frac{1}{2}\dot\phi^2 + V(\Phi) + \rho_{\rm m}\Big]\,, \tag{137}$$

$$\dot H = -\frac{8\pi G}{2}\Big[\dot\phi^2 + \rho_{\rm m} + p_{\rm m}\Big]\,, \tag{138}$$

and varying it with respect to ϕ yields the evolution equation for the scalar field, *i.e*. its equation of motion

$$\ddot\phi + 3H\dot\phi + V_{,\phi} = 0\,. \tag{139}$$

The behaviour of the quintessence field is regulated by its potential $V(\phi)$. For instance, matter domination ($\rho_m >> \rho_\phi$) is insured by a steep potential $\dot{\phi}^2 >> V(\phi)$. In opposition, cosmic acceleration requires $\dot{H} + H^2 > 0$ which implies from the Friedmann equations that $w_\phi < -1/3$, hence a shallow potential $\dot{\phi}^2 < V(\phi)$. This is the slow-roll condition as in analogy with inflation. Many models have been proposed [115–117] according to the potential chosen (see [118] for a recent review) and they are now generally classified into two categories: *freezing* and *thawing* models [119]. In the former, the quintessence field rolls down its potential as long as $H > m_\phi$ and eventually "freezes" once cosmic acceleration kicks in. Typical potentials for freezing models are

$$V(\phi) = m^{4+n}\phi^{-n} \quad (n > 0)\,, \tag{140}$$

$$V(\phi) = m^{4+n}\phi^{-n} e^{\alpha \frac{\phi^2}{M_{\rm pl}^2}}\,, \tag{141}$$

where m corresponds to a mass scale. These potentials do not have a minimum and this is why the field rolls down slowly towards infinity and eventually "freezes".

On the contrary, in thawing models, the Hubble friction term ($H\dot{\phi}$) in (139) "freezes" the field at early times with $w_\phi \approx -1$, until $H < m_\phi$ when it starts to evolve and drive cosmic acceleration. Typical representatives of such models are

$$V(\phi) = V_0 + m^{4-n}\phi^n \quad (n > 0)\,, \tag{142}$$

$$V(\phi) = m^4 \cos^2(\phi/f)\,. \tag{143}$$

One particularity of these models is that the potential energy of the quintessence field can drop below zero in the future implying the collapse of the universe.

Freezing quintessence models exhibit a *tracker behaviour* [120]. At early times, the field has a density slightly less than radiation but "tracks" its evolution until matter-radiation equality. It then starts to have the behaviour of DE ($w_\phi \approx -1$) and produces cosmic acceleration. Such a tracker solution relieves the coincidence problem and has also been argued to partly solve the fine-tuning problem [117]. The freedom for tracking solutions is restricted however. The reduced density attributed to the field $\Omega_\phi = \frac{8\pi G}{3H^2}\rho_\phi$ is constrained stringently by early time physics such as BBN and CMB. It must be less than 1% from the Planck satellite measurements [80].

For the quintessence field to be able to drive cosmic acceleration, its effective mass must be of the order of Hubble

$$m_\phi \sim H_0 \sim 10^{-33}\,\text{eV}\,, \tag{144}$$

which is extremely small. Indeed, the least massive particle of the standard model of particle physics is the neutrino with a mass of the order of the eV. Therefore, quintessence provides the means to drive cosmic acceleration should vacuum energy vanish or be subdominant, and the means to describe the evolution of perturbations. However, to do so, it shifts the fine tuning issue of the cosmological constant to a fine tuning of the potential of the scalar field [121]. This is why, a step further for a more convenient modelling of DE is to study scalar field models where cosmic acceleration is not driven by the potential term.

k-essence

It has been shown in [122, 123], based on earlier studies [124, 125], that cosmic acceleration can be produced without a fine-tuned potential. This is the goal of theories where the kinetic term

accounts for cosmic acceleration, the so-called *k-essence*, short for kinetic-quintessence. In this case, the action for the scalar field is of the form

$$S_\phi = \frac{1}{16\pi G}\int d^4x\sqrt{-g}\,p(\phi,X)\,, \tag{145}$$

where $X = \phi^{,\mu}\phi_{,\mu}/2$ is the canonical kinetic energy density. The derived momentum tensor of the k-essence field is

$$T^\phi_{\mu\nu} = p_{,X}\phi_{,\mu}\phi_{,\nu} + p(\phi,X)g_{\mu\nu}\,, \tag{146}$$

with the energy density and pressure defined as

$$\rho_\phi = 2Xp_{,X} - p(\phi,X)\,, \tag{147}$$

$$p_\phi = p(\phi,X)\,. \tag{148}$$

The equation of motion of the k-essence field is more involved than for quintessence

$$\left[p_{,X}g^{\mu\nu} + p_{,XX}\phi^{;\mu}\phi^{;\nu}\right]\phi_{;\nu\mu} + 2Xp_{,\phi X} - p_{,\phi} = 0\,. \tag{149}$$

One example of k-essence is the *ghost condensate* proposed in [126] where the Lagrangian density is taken to be

$$p(\phi,X) = -X + \frac{X^2}{m^4}\,. \tag{150}$$

We have seen in section 1.5.2 that observations constrain today's value of equation of state of DE $w_{\rm de}$ closely to -1, however, $w_{\rm de} \lesssim -1$ is not excluded. Producing such an equation of state requires a negative kinetic term which is generally plagued with a ghost instability, *i.e* energy density unbounded from below (see section 2.3.3). Here, the addition of the quadratic term X^2 insures the safe crossing of the phantom barrier $w_{\rm de} = -1$. Other examples of k-essence models have been proposed in the context of string theories and brane models, such as the *tachyon model* [127] and *Dirac-Born-Infeld theories* [128].

k-essence models can also exhibit tracking solutions as for quintessence and drive acceleration with $w_\phi \approx -1$. They are thus viable alternatives to the cosmological constant provided the time evolution of w_ϕ they produce remains consistent with future measurements.

f(R) theories

Another path explored in parallel to the inclusion of a scalar field is to modify the Einstein-Hilbert directly. If it is promoted to a function of the Ricci scalar, one enters the realm of f(R) theories. These theories became popular in 1980, when A. Starobinsky showed that adding an R^2 term produced an action with an asymptotic de Sitter solution on a homogeneous background [129]; thus a suitable model for inflation. Then, with the discovery of the cosmic acceleration, f(R) theories have been studied widely in the context of DE and many models have been proposed (see [130] for a modern review). The generic action of f(R) theory is

$$S = \frac{1}{16\pi G}\int d^4x\sqrt{-g}\,f(R) + S_{\rm m}(g_{\mu\nu},\psi)\,, \tag{151}$$

which, once varied with respect to the metric, yields the field equation

$$f_{,R}R_{\mu\nu} - \frac{1}{2}f\,g_{\mu\nu} - \nabla_\mu\nabla_\nu f_{,R} + \Box f_{,R}\,g_{\mu\nu} = 8\pi G T_{\mu\nu}\,, \tag{152}$$

with $f = f(R)$, $f_{,R} = df/dR$ and $T_{\mu\nu}$ the energy momentum tensor of matter and radiation. Replacing the Ricci scalar by a function of itself has substantial consequences. For instance, taking the trace of (152) gives

$$3\Box f_{,R} + f_{,R}R - 2f = 8\pi G T\,, \tag{153}$$

where T is the trace of the energy momentum tensor. This equation is dynamical, a wave equation, on the contrary to the case of GR; $R = 8\pi G T$. It shows that $f_{,R}$ corresponds to a propagating degree of freedom: the *scalaron* [129]. The tensor equation (152) yields for a flat FLRW universe with non-relativistic pressure-less matter and radiation the "modified Friedmann equations"

$$3f_{,R}H^2 = 8\pi G\big(\rho_{\rm m} + \rho_{\rm r}\big) + \frac{1}{2}\big(f_{,R}R - f\big) - 3H\dot{f}_{,R}\,, \tag{154}$$

$$-2f_{,R}\dot{H} = 8\pi G\big(\rho_{\rm m} + \frac{4}{3}\rho_{\rm r}\big) - H\dot{f}_{,R} + \ddot{f}_{,R}\,. \tag{155}$$

Throughout the previous computations, setting $f(R) = R - 2\Lambda$ would produce the standard model equations. The equations (154) and (155) are not solvable analytically. The Ricci scalar of flat FLRW metric ($R = 6(2H^2 + \dot{H})$) makes these equations fourth order non-linear coupled differential equations. Nevertheless, note that once the system is solved, it is always possible to construct by identification an effective DE component which satisfies the standard continuity equation $\dot{\rho}_{\rm de} + 3H(\rho_{\rm de} + p_{\rm de}) = 0$. This enables a more straightforward understanding of the behaviour of f(R) theories and an easier comparison with observations.

The evolution of matter perturbation can be seen as being ruled by a time and scale dependent effective Newton constant $G_{\rm eff}$. Indeed, taking the perturbed FLRW line element (16), the Poisson equation for f(R) theories in the large scale limit can be cast into

$$-k^2\Phi = 4\pi G_{\rm eff}\, a^2 \delta\rho_{\rm m}\,, \tag{156}$$

where

$$G_{\rm eff} = \frac{1}{8\pi f_{,R}}\,\frac{1 + 4m\frac{k^2}{a^2R}}{1 + 3m\frac{k^2}{a^2R}}\,, \tag{157}$$

with the mass term $m = (Rf_{,RR})/f_{,R}$.

f(R) theories can be written in terms of a scalar field. To do so, one must perform the conformal transformation

$$g_{\mu\nu} \to \tilde{g}_{\mu\nu} = \Omega^2 g_{\mu\nu}\,, \tag{158}$$

with the conformal factor $\Omega^2 = f_{,R}$. Then, making the identifications

$$\phi = \sqrt{\frac{3}{16\pi G}}\ln f_{,R}\,, \tag{159}$$

$$V(\phi) = \frac{Rf_{,R} - f}{16\pi G f_{,R}^2}\,, \tag{160}$$

allows one to rewrite the action (151) in the form

$$\tilde{S}_\phi = \int d^4x\sqrt{-\tilde{g}}\Big[\frac{1}{16\pi G}\tilde{R} - \frac{1}{2}\tilde{g}^{\mu\nu}\phi_{;\mu}\phi_{;\nu} - V(\phi)\Big] + S_{\rm m}\Big(e^{-\sqrt{\frac{16\pi G}{3}}\phi}\,\tilde{g}_{\mu\nu}, \psi\Big)\,. \tag{161}$$

The action (151) is written in the *Jordan frame*, the frame in which the gravitational Lagrangian is modified with respect to GR and the matter Lagrangian remains the same as in the standard

model. It is the physical frame, that is to say, the one where the energy momentum tensor of matter is covariantly conserved, in which test-particles follow geodesics of the metric and in which experiments are performed, thus, the frame of most direct physical interpretation [131]. In opposition, the action (161) is written in the *Einstein frame*, where no coupling to curvature (here the Ricci scalar R) can be seen but where a coupling has appeared in the matter sector: $\exp\left(-\sqrt{16\pi G/3}\,\phi\right)$. Indeed, the metric $\tilde{g}_{\mu\nu}$, to which the matter fields ψ couple, is itself coupled to the scalaron through the conformal factor. The Einstein frame is the frame where one obtains the field equation in the form of Einstein field equation as opposed to (152). In fact, from (161) one sees that f(R) theories are equivalent to the so called *coupled quintessence* models with a fixed coupling ($Q = -\sqrt{(4\pi G)/3}$) between the scalaron and matter fields (see the next section).

Over the years of exploration of these models, it has been shown (see [132] and references included) that f(R) theories must fulfil a number of analytical conditions in order to produce viable models :

- $f_{,R} > 0$ for $R \geqslant R_0$ to avoid anti-gravity, R_0 being the Ricci scalar evaluated at present time.
- $f_{,RR} > 0$ for $R \geqslant R_0$ for the compatibility with local gravity tests, to make sure the matter dominated era occurs and for the stability of cosmological perturbations.
- $f(R)$ must asymptote to $R - 2\Lambda$ for $R \gg R_0$ for the compatibility with local gravity tests and to make sure the matter dominated era occurs.
- $0 < \frac{Rf_{,RR}}{f_{,R}} < 1$ at $\frac{Rf_{,R}}{f} = 2$ for the stability of the late-time *de Sitter attractor*, *i.e* the future phase where DE will be fully dominant.

The Hu and Sawicki model [133]

$$f(R) = R - \mu R_c \frac{\left(\frac{R}{R_c}\right)^{2n}}{\left(\frac{R}{R_c}\right)^{2n} + 1}, \tag{162}$$

and the Starobinsky model [134]

$$f(R) = R - \mu R_c \left[1 - \left(1 + \frac{R^2}{R_c^2}\right)^{-n}\right], \tag{163}$$

where $n, \mu, R_c > 0$, are two substantially studied models passing the previous conditions. To fulfil these condition, f(R) theories must in general have more than one free parameter indeed. In such phenomenological models there are no theoretical prescriptions that allows one to predict the order of magnitude of the free parameters. It thus seems that the fine tuning of the cosmological constant is replaced by the tuning of more parameters. The observational constrains on f(R) theories (see for example [135–139]) lead towards having viable models being almost observationally indistinguishable from ΛCDM.

Interacting dark energy models

Models where DE and DM interact, *i.e.* are coupled through an additional interaction aside of gravity, are dubbed *interacting dark energy* models. They present an interesting alternative to the cosmological constant problems. The first of these models, *coupled quintessence*, was proposed by Wetterich in 1994 [140]. Today more complicated scenarios have been studied (see for instance [141, 142]). The idea of coupled quintessence is that the general action of the theory

$$S = S_{\rm EH} + S_\phi + S_{\rm m} + S_{\rm int} \tag{164}$$

has an interacting term $S_{\rm int}$ beyond the Einstein-Hilbert term $S_{\rm EH}$, matter term $S_{\rm m}$ and quintessence S_ϕ (131). It is customary to parametrise this interaction directly from the "non-conservation" of the matter and DE energy momentum tensor by

$$\nabla^\mu T^\phi_{\mu\nu} = -Q T^m \nabla_\nu \phi \,, \tag{165}$$
$$\nabla^\mu T^m_{\mu\nu} = +Q T^m \nabla_\nu \phi \,, \tag{166}$$

where $T^m \approx \rho_{\rm m}$ is the trace of the matter energy momentum tensor and the coupling Q symbolises the interaction rate. In a FLRW metric, one obtains the continuity equations

$$\dot\rho_\phi + 3H\rho_\phi(1+w_\phi) = -Q\rho_{\rm m}\dot\phi \,, \tag{167}$$
$$\dot\rho_{\rm m} + 3H\rho_{\rm m} = +Q\rho_{\rm m}\dot\phi \,, \tag{168}$$
$$\dot\rho_{\rm r} + 4H\rho_{\rm r} = 0 \,. \tag{169}$$

The last equation was expected to be equal to zero since the trace of the energy momentum tensor of photons vanishes $T^r = g^{\mu\nu}T^r_{\mu\nu} = \rho_{\rm r} - 3p_{\rm r} = 0$. The scalar field equation yields

$$\ddot\phi + 3H\dot\phi + V_{,\phi} = -Q\rho_{\rm m} \,. \tag{170}$$

From the previous 4 equations, we observe Q to regulate the evolution of all the fluids components in the model. Assuming $\dot\phi > 0$, $Q > 0$ leads to the conversion of energy from DE to DM and $Q < 0$ the opposite. Interestingly, it has been shown in [143] that a weakly negative coupling relieves the tension we have mentioned concerning the HST measurements (section 1.5.3). CMB observations have also constrained $Q \lesssim 0.1$ [144]. Should future measurements constrain Q to be negative, a sound description of the universe would emerge: DM converts itself into DE as time goes on. Depending on ones leanings, this could seem a comforting and natural description of the evolution of the universe since we observe $\Omega_{\rm de}$ to grow over $\Omega_{\rm m}$.

The DGP braneworld

The Dvali-Gabadadze-Porrati (DGP) [145] braneworld model does not require a DE component nor a cosmological constant to produce cosmic expansion (see [146] for a review). In this extradimensional model, our 3+1 dimensional spacetime, dubbed the *brane*, is embedded in a 4+1 dimensional Minkowsky space time, the *bulk*. The idea of extra dimensions within a gravitational theory has been studied since the last century. Today, compact extra dimensions are an important component of string theories. Also, the idea of "diluting" the cosmological constant in extra-dimensions was proposed more than thirty years ago in [147].

Let us look briefly into the DGP model. Taking $x^A = (x^\mu, x^5)$ to be the coordinates of the bulk space time and $\tilde g_{AB}$ its metric, the induced metric on the brane is defined as $g_{\mu\nu} = x^A_{,\mu}x^B_{,\nu}\tilde g_{AB}$. We will write the quantities of the bulk with a tilde and for the brane without. From this, the DGP action takes the form

$$S = \frac{M_{\rm pl}^2}{2}\int d^4x\sqrt{-g}\left(R + \mathcal{L}_{\rm m}\right) + \frac{\tilde M_{\rm Pl}^3}{2}\int d^5x\sqrt{-\tilde g}\,\tilde R \,, \tag{171}$$

where matter is only included in the brane and thus the sole component coupled to the bulk metric is gravity. The idea of this model is that gravity dilutes itself at large distances in the bulk. In fact, gravity resembles that of GR up to the characteristic length scale defined by

$$r_c = \frac{M_{\rm pl}^2}{\tilde M_{\rm Pl}^3} \,, \tag{172}$$

and above which gravity starts "leaking" into the bulk. Notably, it was shown in [146] that in the weak field limit one has

$$\Phi(r) \sim -\frac{\tilde{G}m}{r^2}, \qquad r \gg r_c\,, \tag{173}$$

$$\Phi(r) \sim -\frac{Gm}{r}, \qquad r \ll r_c\,, \tag{174}$$

where $\tilde{G} \propto \tilde{M}_{\rm Pl}^{-3}$. This is a type of Vainshtein screening (see section 2.2) as below the r_c scale GR is preserved .

Recent studies [6] have shown this model to be almost excluded by LSS data. Also, a decoupling mechanism must be invoked to explain the smallness of $\tilde{M}_{\rm Pl}$. Indeed, one needs $r_c \sim H_0^{-1}$ for the DGP model to produce cosmic acceleration which implies $\tilde{M}_{\rm Pl} \sim 100$ MeV, which seems un-natural since one expects quantum gravity effects taking place in the bulk at this scale to have some effects in the brane. Therefore, this raises more unknowns as to what is the decoupling mechanism in the bulk which prevents us from observing these effects. It was also shown that the self-accelerating solution, *i.e* the solution which produces cosmic acceleration through genuine modifications of gravity rather than from a negative pressure component, unfortunately introduces a ghost mode [148]. Therefore, DGP models seem to have a hard time producing viable alternatives to ΛCDM.

Scalar tensor theories

Brand-Dicke theory

The Brans-Dicke theory of gravity, or Jordan-Brans-Dicke theory, is one of the first scalar-tensor theory. The characteristic of these theories stems from having the extra scalar field coupled to a curvature term in the action. In 1961, R. Dicke and C. Brans released their theory [149] based on earlier work of P. Jordan[2]. Their goal was to modify GR in order for it to include Mach's principle. It was much later shown given the discovery of cosmic acceleration, that minimal changes to the original Brans-Dicke theory allowed for it to produce cosmic acceleration [150]. The action of the theory is

$$S = \frac{1}{16\pi}\int d^4x\sqrt{-g}\Big(\phi R - \frac{\omega_{BD}}{\phi}\nabla_\mu\phi\nabla^\mu\phi\Big) + S_{\rm m}(g_{\mu\nu},\psi)\,, \tag{175}$$

where ω_{BD} is the Brans-Dicke parameter; the parameter quantifying the extra freedom of the theory. A potential term $-V(\phi)$ is sometimes added in the action. The action is written in the Jordan frame and one can see a *non-minimal coupling* has appeared, that is, a curvature term (here the Ricci scalar R) multiplied by a function of the scalar field (here simply ϕ). Another characteristic to see in this action is the replacement of the Newton constant with $1/\phi$. Varying (175) with respect to the scalar field yields the evolution equation

$$\Box\phi - \frac{\nabla_\mu\phi\nabla^\mu\phi}{2\phi} + \frac{\phi}{2\omega_{BD}}R = 0\,, \tag{176}$$

and varying it with respect to the metric $g_{\mu\nu}$ produces the field equation

$$R_{\mu\nu} - \frac{1}{2}R\,g_{\mu\nu} - \frac{1}{\phi}\big(\nabla_\mu\nabla_\nu\phi - \Box\phi g_{\mu\nu}\big) - \frac{\omega_{BD}}{\phi^2}\big(\nabla_\mu\phi\nabla^\mu\phi - \frac{1}{2}g_{\mu\nu}\nabla_\alpha\phi\nabla^\alpha\phi\big) = \frac{8\pi}{\phi}T_{\mu\nu}\,. \tag{177}$$

2 J. Jordan, "Schwerkraft und Weltall", Vieweg (Braunschweig): Projective Relativity (1955)

Combining the equations (176) and (177) one obtains the wave equation for the scalar degree of freedom

$$\Box\phi = \frac{8\pi}{3+2\omega_{BD}}\rho_{\rm m}\,. \tag{178}$$

From this, one can see that the matter distribution sources the scalar field which itself contributes to the curvature through (177). The tensor equation (177) and the evolution equation of the scalar field (176) in a FLRW space time produce a system of 3 coupled differential equations for a and ϕ

$$\left(\frac{\dot a}{a}\right)^2 + \frac{\dot a}{a}\frac{\dot\phi}{\phi} - \frac{\omega_{BD}}{6}\left(\frac{\dot\phi}{\phi}\right)^2 + \frac{k}{a^2} = \frac{8\pi}{3\phi}\sum_i \rho_i\,, \tag{179}$$

$$\frac{\ddot a}{a} + \frac{1}{2}\frac{\ddot\phi}{\phi} + \frac{1}{2}\frac{\dot a}{a}\frac{\dot\phi}{\phi} + \frac{\omega_{BD}}{3}\left(\frac{\dot\phi}{\phi}\right)^2 = -\frac{4\pi}{3\phi}\sum_i\left(\rho_i + 3p_i\right), \tag{180}$$

$$\frac{\ddot\phi}{\phi} + 3\frac{\dot a}{a}\frac{\dot\phi}{\phi} = \frac{1}{3+2\omega_{BD}}\frac{8\pi}{\phi}\sum_i\left(\rho_i - 3p_i\right). \tag{181}$$

The standard Friedmann equations are recovered for $\omega_{BD}\to\infty$ and $\phi\to 1/G$. As for f(R) theories and many MG theories, Brans-Dicke theories also produce an effective Newton constant

$$G_{\rm eff} = \frac{4+2\omega_{BD}}{3+2w}\frac{1}{\phi}\,. \tag{182}$$

In fact, Brans-Dicke theories augmented with a potential include f(R) theories for

$$\omega_{BD} = 0\,, \tag{183}$$

$$\phi = f(R)\,, \tag{184}$$

$$V(\phi) = \frac{1}{16\pi G}\left(Rf_{,R} - f\right). \tag{185}$$

Brans-Dicke theory has been tested observationally and the Brans-Dicke parameter ω_{BD} is best constrained by local gravity tests. The most recent Cassini-Huygens measurements lead to $\omega_{BD} > 4\times 10^4$ at 2σ using the post-Newtonian approach [151]. This theory has not been ruled out so far and remains a viable alternative to the standard model.

The Brans-Dicke action can be generalised to that of the basic action for scalar-tensor theories:

$$S_\phi = \frac{1}{16\pi G}\int d^4x\sqrt{-g}\left[A(\phi,R) + B(\phi)g^{\mu\nu}\phi_{,\mu}\phi_{,\nu}\right], \tag{186}$$

and one can see immediately it includes the models we have discussed previously thanks to the mapping,

- ΛCDM : $A(\phi,R) = R - 2\Lambda$ and $B(\phi) = 0$.
- Quintessence : $A(\phi,R) = R - V(\phi)$ and $B(\phi) = 1/2$.
- f(R) theories : $A(\phi,R) = f(R)$ and $B(\phi) = 0$.
- Brans-Dicke theory : $A(\phi,R) = \frac{G}{\phi}R$ and $B(\phi) = \frac{G}{\phi}\omega_{BD}$.

Galileon theories

Galileon theories were first proposed in [152] as a generalisation of the 4-dimensional brane action of the DGP model. It is a scalar tensor theory, where the modifications to gravity are induced by the Galileon scalar field ϕ. The four dimensional brane action of the DGP model is invariant under the (Galilean) *shift symmetry*

$$\phi \to \phi + b + v_\mu x^\mu \,, \tag{187}$$

where b and v_μ are constants. This symmetry is inherited from the 5-dimensional Poincaré invariance of the DGP bulk action [153]. Lagrangians preserving the shift symmetry can avoid the ghost in the self-accelerating branch the DGP model was plagued with. Exactly 5 Lagrangians exists and they produce second order equations of motions in a 4-dimensional Minkowski spacetime. They constitute the action of Galileon theories

$$S = \int d^4x\sqrt{-g}\Big(\frac{R}{16\pi G} - \sum_{i=1}^{5} c_i \mathscr{L}_i\Big) + S_{\rm m}(g_{\mu\nu}, \psi) \,, \tag{188}$$

where the c_i are the dimensionless free parameters of the theory and

$$\mathscr{L}_1 = m^3\phi \,, \tag{189}$$

$$\mathscr{L}_2 = \phi_{,\mu}\phi^{,\mu} \,, \tag{190}$$

$$\mathscr{L}_3 = m^{-3}\phi_{,\mu}\phi^{,\mu}\Box\phi \,, \tag{191}$$

$$\mathscr{L}_4 = m^{-6}\phi_{,\mu}\phi^{,\mu}\Big((\Box\phi)^2 - \phi_{,\alpha\beta}\phi^{,\alpha\beta} - \frac{1}{4}R\,\phi_{,\mu}\phi^{,\mu}\Big) \,, \tag{192}$$

$$\mathscr{L}_5 = m^{-9}\phi_{,\mu}\phi^{,\mu}\Big((\Box\phi)^3 - 3\,\phi_{,\alpha\beta}\phi^{,\alpha\beta}\Box\phi + 2\,\phi_{,\mu\alpha}\,\phi^{,\alpha}{}_{,\beta}\,\phi^{,\beta\mu} - 6\,\phi_{,\alpha}\,\phi^{,\alpha\mu}\,\phi^{,\nu}G_{\mu\nu}\Big) \,, \tag{193}$$

where the mass must be $m \sim \left(M_{\rm pl}H_0^2\right)^{1/3} \sim 10^{-17}$ GeV in order to drive cosmic acceleration. Usually, c_1 is set to zero in order for the latter to be driven by the kinetic terms rather than a potential; hence avoiding the quintessence fine tuning issue. The non linear couplings between the derivatives of the field and R or $G_{\mu\nu}$ will change the way matter affects the geometry of the universe with respect to GR. Such effects will be screened in high curvature regimes thanks to the Vainshtein mechanism (see section 2.2). The Galileon action when generalized to curved space falls under the class of Horndeski theories, and these non linear couplings break the shift symmetry. Galileon models have been constrained observationally and yield a suitable alternative to the cosmological constant, however, they are not necessarily favoured over ΛCDM by data [154].

Horndeski theories

Up to what complexity can one generalise scalar-tensor theories? It was shown by R. Woodard [155] that on a 4-d manifold, a non-degenerate Lagrangian containing time derivatives higher than first will produce Ostrogradsky instabilities. Therefore, equations of motion can be at most second order in time derivatives. This has therefore been argued to be the reason why differential equations of higher order than two do not appear in the description of any physical phenomenon [156].

In the context of gravity, *Horndeski theories* are the most general 4-dimensional scalar-tensor theories keeping the field equations of motion at most second order directly. These theories were first proposed by G. Horndeski [157] and were recently revived by [158] as *generalised Galileons*. Horndeski theories are described by the action

$$S = \int d^4x\sqrt{-g}\sum_{i=2}^{5}\mathscr{L}_i + S_{\rm m}(g_{\mu\nu}, \psi) \,, \tag{194}$$

where the Lagrangians L_i are

$$\mathscr{L}_2 = G_2(\phi, X)\,, \tag{195}$$

$$\mathscr{L}_3 = G_3(\phi, X)\Box\phi\,, \tag{196}$$

$$\mathscr{L}_4 = G_4(\phi, X)R - 2G_{4,X}\left[(\Box\phi)^2 - \phi_{;\mu\nu}\phi^{;\mu\nu}\right], \tag{197}$$

$$\mathscr{L}_5 = G_5(\phi, X)G_{\mu\nu}\phi^{;\mu\nu} + \frac{1}{3}G_{5,X}\left[(\Box\phi)^3 - 3(\Box\phi)\phi_{;\mu\nu}\phi^{;\mu\nu} + 2\phi_{;\mu\alpha}\phi^{;\alpha}{}_{;\beta}\phi^{;\beta\mu}\right], \tag{198}$$

with G_i ($i = 2,3,4,5$) functions of the scalar field ϕ and its canonical kinetic energy $X = -\nabla^\mu\phi\nabla_\mu\phi/2$, the partial derivatives $G_{i,X} = \partial G_i/\partial X$, and $G_{\mu\nu}$ the Einstein tensor. The term $G_2(\phi, X)$ is the k-essence term, $-G_3(\phi, X)\Box\phi$ is the cubic Galileon term, $G_4(\phi, X)$ is the generalisation of the Einstein-Hilbert term, and $G_5(\phi, X)G_{\mu\nu}\phi^{;\mu\nu}$ is the non-minimal derivative coupling to Einstein's tensor. Horndeski theories thereby regroup most of the theories we have discussed, and more, thanks to the mapping:

- ΛCDM : $G_4 = \frac{1}{16\pi G}\big(R - 2\Lambda\big)$, $G_2 = G_3 = G_5 = 0$.
- Quintessence : $G_2 = -X - V(\phi)$, $G_4 = \frac{1}{16\pi G}$, $G_3 = G_5 = 0$.
- f(R) theories : $G_2 = \frac{1}{16\pi G}\big(Rf_{,R} - f\big)$, $G_4 = \frac{f_{,R}}{16\pi G}$, $G_3 = G_5 = 0$.
- Brans-Dicke theory : $G_2 = -\frac{\omega_{BD}X}{16\pi\phi}$, $G_4 = \frac{1}{16\pi}\phi$, $G_3 = G_5 = 0$.
- Kinetic Braiding gravity [159] : $G_2 = G_2(\phi, X)$, $G_3 = G_3(\phi, X)$, $G_4 = G_4(\phi)$, $G_5 = 0$.
- Galileon gravity [152] : $G_2 = c_2X$, $G_3 = c_3m^{-3}X$, $G_4 = \frac{1}{16\pi G} + c_4m^{-6}X^2$, $G_5 = c_5m^{-9}X^2$.

We will study Horndeski theories more in depth in their effective field theory formulation in the following sections and chapters.

GLPV theories

The hint of having healthy theories beyond that of Horndeski arose from the effective field theory of dark energy construction (see section 2.3). The first covariant formulation of *Beyond Horndeski* theories or *GLPV* theories, was first proposed in [160] (see also [161] for early studies in this direction). The action of such theories contains additional terms in $\mathscr{L}_4$ and $\mathscr{L}_5$ with respect to that of Horndeski :

$$\begin{aligned} L_4^\phi \equiv\ & G_4(\phi, X)\,{}^{(4)}R - 2G_{4,X}(\phi, X)(\Box\phi^2 - \phi^{;\mu\nu}\phi_{;\mu\nu}) \\ & + F_4(\phi, X)\epsilon^{\mu\nu\rho}{}_\sigma\,\epsilon^{\mu'\nu'\rho'\sigma}\phi_\mu\phi_{\mu'}\phi_{\nu\nu'}\phi_{\rho\rho'}\,, \end{aligned} \tag{199}$$

$$\begin{aligned} L_5^\phi \equiv\ & G_5(\phi, X)\,{}^{(4)}G_{\mu\nu}\phi^{;\mu\nu} + \frac{1}{3}G_{5,X}(\phi, X)(\Box\phi^3 - 3\Box\phi\,\phi_{\mu\nu}\phi^{\mu\nu} + 2\phi_{\mu\nu}\phi^{\mu\sigma}\phi^\nu{}_\sigma) \\ & + F_5(\phi, X)\epsilon^{\mu\nu\rho\sigma}\epsilon^{\mu'\nu'\rho'\sigma'}\phi_\mu\phi_{\mu'}\phi_{\nu\nu'}\phi_{\rho\rho'}\phi_{\sigma\sigma'}\,, \end{aligned} \tag{200}$$

where $\epsilon_{\mu\nu\rho\sigma}$ is the totally antisymmetric Levi-Civita tensor. One recovers Horndeski theories by setting $F_4(\phi, X) = F_5(\phi, X) = 0$.

Horndeski and Beyond Horndeski theories are degenerate theories. In mathematical terms, the transformation to phase space variables is not invertible, which can also be seen as the vanishing of the determinant of the corresponding Hessian matrix. This implies there are less degrees

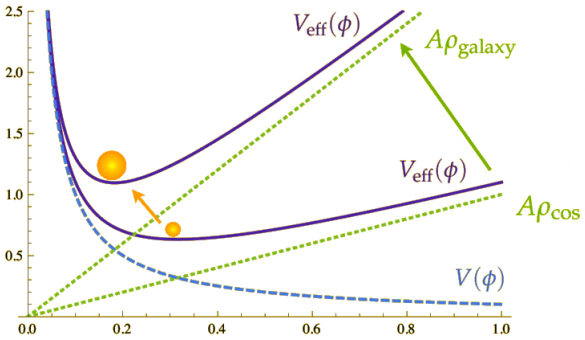

Figure 12: Representation of the potential and effective potential for the chameleon screening mechanism for two set ups : high density (galaxy, clusters, etc.) and low density (cosmos). Courtesy of J. Beltràn Jiménez.

of freedom than originally expected. In Horndeski theories, the equations of motions are second order (in time derivatives) directly, although one would naively expect to have 4th order equations from a Lagrangian with second derivatives. In GLPV theories, the equations of motions are third order. However, since the determinant of the Hessian vanishes, the extra constraints reduces the equations to second order. This is why GLPV theories yield in appearance third order equations of motions but produce a single scalar degree of freedom propagating with a healthy second order equation. An interesting phenomenological difference between Horndeski and GLPV theories is the fact that, in the latter, the scalar field affects the sound speed of matter perturbations even if it is minimally coupled to the metric.

SCREENING MECHANISMS

Infrared modifications of gravity induce a fifth force from the introduction of new degrees of freedom, however, this new force has never been detected experimentally. Therefore, in order to recover GR on small scales and in high density environments, MG theories must contain screening mechanisms which, schematically speaking, make the fifth force "hide" itself in such environments. These mechanisms are provided by the non-linearities of the theory and can be classified in three families. Let us consider a Lagrangian for a scalar field perturbed as $\phi = \bar{\phi} + \delta\phi$ with the non-linear terms

$$\mathscr{L}_\phi = \frac{1}{2} Z(\bar{\phi}) \partial_\mu \delta\phi \partial^\mu \delta\phi - \frac{1}{2} m^2(\bar{\phi}) \delta\phi^2 + g(\bar{\phi}) \delta\phi \delta\rho_{\rm m} \,. \tag{201}$$

The term $Z(\phi_0)$ would yield the *Vainshtein* [162], *K-mouflage* [163] and *Kinetic* [164] screening mechanisms, the function $m^2(\phi_0)$ would yield the *chameleon* [165] and $g(\phi_0)$ the *symmetron* [166] and *dilaton* [167] mechanism. Let us now go through the guiding principles behind some of these mechanisms key for the observational viability of MG theories.

Chameleon

The chameleon is the screening mechanism that can take place in f(R) theories for example. In this mechanism, the central quantity is the Compton wavelength of the scalar field; the inverse of its effective mass. This effective mass depends on the density of the scalar field's environment. In practice, in galaxies or clusters the density is high, the effective mass of the scalar field increases

and the fifth force can be suppressed with respect to the Newtonian force. On the contrary, the average matter density is very low on cosmological scales and thus the effective mass of the scalar field is small; the scalar field transmits a fifth force.

To be more practical, let us consider the f(R) action in the Einstein frame

$$S_\phi = \int d^4x\sqrt{-g}\Big[\frac{1}{16\pi G}R - \frac{1}{2}\phi^{;\mu}\phi_{;\mu} - V(\phi)\Big] + S_{\rm m}\big[A^2(\phi)g_{\mu\nu},\psi\big)\,, \tag{202}$$

where we have introduced a conformal and universal (same for all matter species) coupling $A^2(\phi)$ between the chameleon scalar field ϕ and the matter fields ψ. Varying this action with respect to ϕ produces the equation of motion in the Einstein frame

$$\delta\phi = V_{,\phi} - A_{,\phi}\rho_{\rm m}\,, \tag{203}$$

where we have considered a non relativistic, pressure-less source $\rho_{\rm m}$. One can then deduce that the scalar field will be influenced by the matter source through the effective potential

$$V_{\rm eff} = V(\phi) + A(\phi)\rho_{\rm m}\,. \tag{204}$$

Provided $V(\phi)$ and $A(\phi)$ are chosen wisely so that the effective potential develops a minimum, the mass of the chameleon field is then

$$m^2_{\rm min} = V_{,\phi\phi}(\phi_{\rm min}) + A_{,\phi\phi}(\phi_{\rm min})\rho_{\rm m}\,. \tag{205}$$

Figure 12 highlights well how the previous two equations behave in a high and low density set up. Indeed, one can see that while the potential is unaffected, the effective potential becomes deeper in a dense region as in a cluster of galaxies and thus the mass of the chameleon field increases, whereas in a low density environment, that is, on cosmological scales, the effective potential is shallower and the mass lighter.

Vainshtein

The Vainshtein mechanism is found in Horndeski theories, massive gravity [168], braneworld models such as DGP and de-gravitation theories [169]. This mechanism relies on the fact that derivative couplings of a scalar field become large near massive objects. The non-linearities of the scalar field increase its kinetic energy which weakens its interaction with matter.

Let us take the example of a cubic Galileon Lagrangian

$$\mathscr{L}_\pi = -3(\partial\pi)^2 - \frac{1}{\Lambda_s^3}\Box\pi(\partial\pi)^2 - \frac{\pi}{M_{\rm pl}}\rho_{\rm m}\,, \tag{206}$$

where $(\partial\pi)^2$ is short for $\partial^\mu\pi\partial_\mu\pi$ and $\Lambda_s \sim \sqrt{L^{-2}M_{\rm pl}}$ is the strong coupling scale of Galileon theories. Provided they drive cosmic acceleration, one has $L \sim H_0$, hence $\Lambda_s \sim (1000\ {\rm km})^{-1}$. Screening will occur when $|(\partial\pi)^2| > \Lambda_s^3$. Let us be slightly more precise and sketch the procedure described in [170]. Varying the action (206) with respect to the scalar field π gives the equation of motion

$$3\Box\pi + \frac{1}{\Lambda_s^3}\Big((\Box\pi)^2 - \big(\partial_\mu\partial_\nu\pi\big)^2\Big) = \frac{1}{2M_{\rm pl}}\rho_{\rm m}\,. \tag{207}$$

In the case of a point source of mass M, the trace of the energy momentum tensor becomes $T = -M\delta^{(3)}(\vec{x})$ with $\delta^{(3)}$ the 3 dimensional Dirac delta and the equation (207) reduces to

$$\nabla\cdot\left(6\nabla\pi+\vec{r}\frac{4}{\Lambda_s^3}\frac{(\nabla\pi)^2}{r}\right)=\frac{M}{M_{\rm pl}}\delta^{(3)}(\vec{x})\,, \tag{208}$$

for a spherically-symmetric static configuration [171]. Integrating the latter equation over a sphere centred around the point source yields

$$6\nabla\pi+\frac{4}{\Lambda_s^3}\frac{(\nabla\pi)^2}{r}=\frac{M}{4\pi r^2 M_{\rm pl}}\,. \tag{209}$$

This equation can be solved analytically and gives

$$\nabla\pi=\pm\frac{\Lambda_s^3}{r}\left(\sqrt{9r^4+4r_V^3 r}-3r^2\right) \tag{210}$$

where we have introduced the characteristic scale for the mechanism, the *Vainshtein radius*

$$r_v=\left(2GML^2\right)^{\frac{1}{3}}\,. \tag{211}$$

The "-" solution produces unstable perturbations [172]. Considering the "+", one can split the solution into two asymptotic regimes

- On large scales $r\gg r_V$, one has $\nabla\pi(r\gg r_V)\approx\frac{1}{3}\frac{GM}{r^2}$, and since a force is $F\approx|\nabla\pi|$, one obtains the ratio of the scalar (fifth) force F_π to the standard gravity force F_g

$$\frac{F_\pi}{F_g}\approx\frac{1}{3}\,. \tag{212}$$

- On small scales $r\ll r_V$, one has $\nabla\pi(r\ll r_V)\approx\frac{1}{\sqrt{r}}$, and therefore the field is screened, its strength is much lower than standard gravity

$$\frac{F_\pi}{F_g}\approx\left(\frac{r}{r_V}\right)^{\frac{3}{2}}\,. \tag{213}$$

The key signature of the Vainshtein mechanism is therefore the new scale it introduces defined by the Vainshtein radius. It indicates the transition scale between the regions where non linearities of the scalar field become dominant or negligible with respect to standard gravity. The region around the radius sets the difference between the screened region, where the field is weakly coupled to matter, with the un-screened region where the field is strongly coupled to matter (see Figure 13).

THE EFFECTIVE FIELD THEORY OF DARK ENERGY

In section 2.1, we have focused on models that incorporate an extra scalar degree of freedom to the Einstein-Hilbert action. Such models are numerous and one is tempted to ask whether a way to describe all these theories at a fundamental level and in a common framework exists. This unifying description should be able to grant the user the possibility to study and test many models against observations at once. A promising way to achieve this goal is to use *effective field theory*. Effective field theory is a description of the low energy scales of a more fundamental theory. For example, GR is an effective field theory of a quantum gravity theory. The advantage of using an

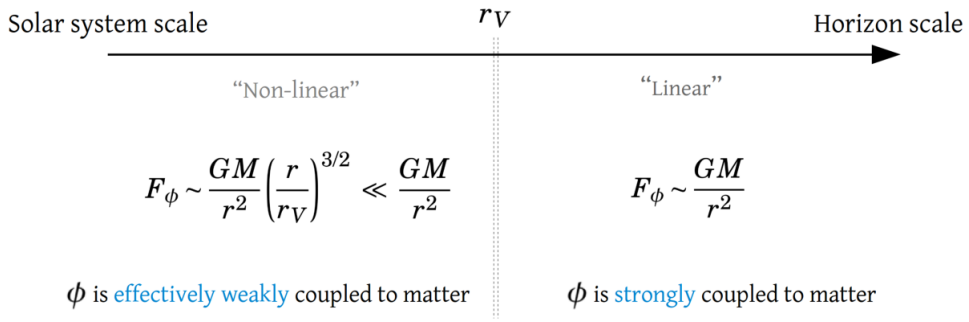

Figure 13: Schematic diagram of the evolution of the screening strength depending on the scale.

effective field theory is that one only deals with the degrees of freedom associated with the low energy part of the theory, thus integrating out higher energy scales sometimes irrelevant for the problem at hand.

In the context of attempting an explanation of cosmic acceleration thanks to either DE of MG, one is generally concerned by the cosmological evolution of the universe. The expansion of the universe is a low energy process, indeed the energy scale associated to DE, $m_{\rm de}$, can be estimated from the first Friedmann equation as

$$H^2 = \frac{m_{\rm de}^4}{M_{\rm pl}^2} \to m_{\rm de} = \sqrt{M_{\rm pl} H_0} \sim 1\,\text{meV}\,. \tag{214}$$

Short scale and high energy interactions (> 1 eV) are often not relevant when comparing DE models to cosmological observations; hence (214) places DE as a suitable ground for an effective field theory description. This has been proposed in the recent years: the *effective field theory of dark energy*, EFT of DE hereafter.

Generalities

Before going through the construction of the action of the EFT of DE, let us see how it came about and on what fundamental principles it is based on.

Development of the EFT of DE

Scalar fields are not used exclusively to model late-time cosmic acceleration. Their use is required to break de Sitter invariance in inflation for example. A common description of single scalar field inflationary models is the *Effective Field Theory of Inflation*. It has been initiated in [173] and systematically developed in [174]. This is the seed of the description of DE with an EFT framework. The key point used to produce such unifying description is to apply an effective field theory construction to cosmological perturbations directly. They are treated as the Goldstone boson of spontaneously broken time-translations as we will see in the next section. Such a description was then used to describe quintessence [175] and later extended to include Horndeski and GLPV theories in [176–178] and [179, 180]. The EFT of DE is a description up to linear level as we will see further on, thereby, it does not include non-linearities such as the ones producing screening mechanisms. Nonetheless, at linear level, the EFT of DE can virtually describe all DE or MG theories which include a single scalar degree of freedom in addition to standard gravity. Therefore, it describes Horndeski and GLPV theories. It has also been recently used to describe Hořava-Lifshitz

gravity [181, 182]. There exist another formulation of the EFT action established in [183]. We will present it in chapter 4 . Many theoretical studies have been maid thanks to the EFT of DE [184–191] and many phenomenological results have been obtained; we will give an overview of them in the final chapter of this thesis. The EFT of DE has also been extended to include interacting DE [7] or kinetic matter mixing [192], mildly-non linear scales [193], two scalar field scalar field (DE and DM) [194], K-mouflage [195], and higher-order scalar-tensor theories [196]. For the purpose of this thesis we concentrate on the EFT of DE in its "original" non extended form. Let us understand now on what it is based on and how it is constructed.

Spontaneous symmetry breaking in cosmology

Where does one find spontaneous symmetry breaking in a cosmological context? Let us better understand this concept first by taking an example in the standard model of particle physics. EW theory has its SU(2) × U(1) gauge symmetry broken spontaneously into a diagonal U(1) by the Higgs mechanism. The Goldstone bosons[3] created by the spontaneously broken symmetry can be absorbed in the longitudinal degrees of freedom of the vector boson $W_{\pm}$ and Z in the *unitary gauge*. Gauge invariance is lost in this set-up to the benefit of dealing directly with the observable low-energy degrees of freedom of the theory, *i.e*. one Higgs particle and three massive vector bosons.

For our concerns, GR stands as a gauge theory from its invariance under general coordinate transformations. The metric field plays the role of the gauge field sector. In the case of Minkowski or de Sitter spacetimes, time translations are a global symmetry as they contain a time-like killing vector. One can say that time translations are broken by any spacetimes that do not bear such a killing vector. For example, inflation is quasi-de Sitter due to the almost scale invariant primordial power spectrum and the need to exit the accelerating phase at some point. Therefore, inflation is said to *spontaneously* break time translations and this must be accompanied by a Goldstone excitation. The Goldstone excitation comes about upon the application of the Stückleberg mechanism (see section 2.3.2.3). This implies that the presence of a scalar field is simply the inevitable consequence of the broken time translations; the root of an effective field theory of cosmological perturbations [178]. In summary, a FLRW background that is neither Minkowski nor de Sitter must yield a propagating scalar degree of freedom. These scalar fluctuations are the *adiabatic perturbations* in the case of Inflation. It is a little more subtle for DE because one needs to involve matter fields. This complications is bypassed by applying the EFT construction only to the gravitational sector, thereby assuming the WEP to be valid and thus considering the matter fields to couple universally to the metric through the standard covariant matter action $S_{\rm m}(g_{\mu\nu}, \psi)$. This amounts to consider the existence of a *Jordan metric*. Note that it would possible, although more complicated, to consider different matter sectors coupled to different metrics.

Construction of the action

Let us sketch how the action of the EFT of DE is constructed starting by defining the unitary gauge. We follow the presentation given in [176–178] using the redefinition of the coupling function proposed in [197].

3 A boson is a particle with an integer spin and therefore it follows Bose-Einstein statistics as opposed to a fermion (half-integer spin which follows Fermi-Dirac statistics).

Unitary gauge

The unitary gauge was first introduced in the context of the EW spontaneous symmetry breaking by S. Weinberg in 1971 [198]. In cosmology, it was used for cosmological perturbation theory by H. Kodama and M. Sasaki in 1984 [199], under the name of *velocity orthogonal gauge*. A definition of the unitary gauge is in short:

The unitary gauge is the choice of the basis in which the Goldstone boson components of a field responsible for the spontaneous symmetry breaking vanish.

For DE or inflation, the unitary gauge is constructed as follows. In a perturbed FLRW universe, the scalar field is decomposed as

$$\phi(t,\vec{x}) = \bar{\phi}(t) + \delta\phi(t,\vec{x}). \tag{215}$$

Choosing the time coordinate to be function of ϕ such that $\delta\phi = 0$ simplifies further equation (215). This way ϕ defines a preferred time slicing ($\phi = const.$); constant time hypersurfaces coincide with constant scalar field hypersurfaces. Seeing this in a fluid language implies that the velocity of the scalar field is orthogonal to the constant time hypersurfaces, *i.e.* the velocity orthogonal gauge. Doing so, the action will not bear the scalar field, it is in some sense "eaten" by the metric. Therefore, one forgets about ϕ and builds the action thanks to the unit vector n_μ perpendicular to the time slicing. This vector yields in the unitary gauge

$$n_\mu = -\frac{\partial_\mu\phi}{\sqrt{-(\partial_\mu\phi)^2}} \to -\frac{\delta^0_\mu}{\sqrt{-g^{00}}}\,. \tag{216}$$

This way, for example, the quintessence term transform as

$$-\frac{1}{2}(\partial\phi)^2 - V(\phi) \to -\frac{1}{2}\dot{\bar{\phi}}^2 g^{00} - V(t)\,, \tag{217}$$

and the cubic Galileon term as

$$(\partial\phi)^2\Box\phi \to (2/3)(-g^{00})^{3/2}\dot{\bar{\phi}}^3 K \tag{218}$$

$$= -2\dot{\bar{\phi}}^2\left[\ddot{\bar{\phi}}\sqrt{-g^{00}} - H\dot{\bar{\phi}}\left((-g^{00})^{3/2} - 1\right)\right] + (2/3)\left[(-g^{00})^{3/2} - 1\right]\dot{\bar{\phi}}^3\delta K\,. \tag{219}$$

where δK is the perturbation of the trace of the extrinsic curvature tensor (see (220)). It follows from the unitary gauge construction that, along with 4-d covariant terms such as the Ricci scalar and any curvature invariants, any contractions of tensors with n_μ are allowed in the action, for instance, g^{00} and R^{00}. The complete set of operators in the action is found by also considering covariant derivatives of n_μ. Equivalently, one can use their projection orthogonal to the constant time hypersurfaces, that is, the extrinsic curvature tensor

$$K_{\mu\nu} = h_\mu{}^\sigma\nabla_\sigma n_\nu\,, \tag{220}$$

with the induced metric defined as $h_{\mu\nu} = g_{\mu\nu} + n_\mu n_\nu$ and $n^\sigma\nabla_\sigma n_\nu \propto h_\nu{}^\mu\partial_\mu g^{00}$. One must not forget that the coefficients in front of the operators in the action should be made time dependent since time translations are broken. In particular, as opposed to inflation, if one wants to keep matter minimally coupled to the Jordan frame metric, a free function of time must be allowed to multiply the Ricci scalar.

Despite loosing apparent covariance, using the unitary gauge leads to advantages. The operators in the action can be organized straightforwardly in the order of perturbations. Consequently, operators beyond the linear order do not affect the background evolution of the universe. Moreover, the way the action is expanded yields direct observable implications. For example, the cubic operators of the EFT of inflation are related to the observable three-point functions of the CMB.

EFT of DE action

The above considerations imply, in summary, that the action will contain

- four-dimensional diffeomorphism-invariant scalars multiplied in general by functions of time, *e.g.* the Ricci scalar and any curvature invariants.
- four-dimensional covariant tensors with free upper 0 indices and all spatial indices contracted, *e.g.* g^{00}, R^{00}, etc.
- three-dimensional objects living on the $t = const.$ hypersuface, *e.g.* the extrinsic curvature K^{ij} its trace K and the three dimensional curvatures terms ${}^{(3)}R$, ${}^{(3)}R_{ij}$, etc.

In total, the EFT of DE gravitational action [177] yields thus

$$\begin{aligned} S = \int d^4x\sqrt{-g}\frac{M^2(t)}{2}\Big[& R - \lambda(t) - \mathscr{C}(t)g^{00} + \mu_2^2(t)(\delta g^{00})^2 - \mu_3(t)\delta K\delta g^{00} \\ & - \epsilon_4(t)\Big(\delta K^2 - \delta K_{\mu\nu}\delta K^{\mu\nu}\Big) + \tilde{\epsilon}_4(t)\,{}^{(3)}R\,\delta g^{00} \\ & - \bar{\epsilon}_4^2(t)\delta K^2 + \bar{\epsilon}_5(t)\,{}^{(3)}R\,\delta K + \kappa(t)\,{}^{(3)}R^2 \\ & + ... \\ & + \mathscr{L}_{\rm m}(g_{\mu\nu},\psi)\Big] \end{aligned} \tag{221}$$

where (M^2, λ, $\mathscr{C}$, μ_2^2, μ_3, ϵ_4, $\tilde{\epsilon}_4$, $\bar{\epsilon}_4$,$\bar{\epsilon}_5$, κ) are the coupling functions, *i.e.* the structural functions of time that scale the evolution of the background and perturbations. The first line of (221) corresponds to the operators acting on the background. Including the second line yields the most general EFT action for single scalar field up to quadratic order in the Jordan frame, *i.e.* the GLPV action in the EFT framework. Horndeski theories are recovered by setting $\tilde{\epsilon}_4 = \epsilon_4$. These two lines encompass all the models depicted in Table 5. The third line includes operators that lead to higher order space derivatives. The ellipsis stand for higher order terms, for example those constructed with the Weyl tensor (see [176] for details). It proves useful to define the Brans-Dicke coupling (the EFT version of w_{BD}) as the time variation of the bare Planck mass M^2

$$\mu_1(t) = \frac{d\ln M^2(t)}{dt}\,. \tag{222}$$

The background functions $\mathscr{C}(t)$ and $\lambda(t)$ are not free function of the theory. They depend on the Hubble parameter $H(t)$, $\mu_1(t)$ and the matter content. We will give their expression in section 2.3.4.

Stüeckelberg mechanism

Given a Lagrangian in the unitary gauge, gauge invariance is restored upon application of the *Stückelberg "trick"*. In others words, the method to make the Goldstone excitation resulting from the spontaneously broken time translations appear in (221). To do so, one has to force back the broken gauge transformation on the fields in the Lagrangian by imposing the time coordinate transformation

$$t \to \tilde{t} = t + \pi(x^\mu)\,, \tag{223}$$

$$x^i \to \tilde{x}^i = x^i\,, \tag{224}$$

	μ_1	λ	$\mathscr{C}$	μ_2^2	μ_3	ϵ_4	$\tilde{\epsilon}_4$
ΛCDM	0	const.	0	0	0	0	0
Quintessence	0	✓	✓	0	0	0	0
k-essence	0	✓	✓	✓	0	0	0
Brans-Dicke	✓	✓	✓	0	0	0	0
$f(R)$	✓	✓	0	0	0	0	0
Kinetic braiding [159]	0	✓	✓	✓	✓	0	0
DGP	✓	✓	✓	✓	✓	0	0
$f(G)$ -Gauss-Bonnet [200]	✓	✓	✓	✓	✓	✓	0
Galileons	✓	✓	✓	✓	✓	✓	0
Horndeski	✓	✓	✓	✓	✓	✓	0
GLPV	✓	✓	✓	✓	✓	✓	✓

Table 5: Some of the explicit DE models and MG theories encompassed by the action (221).

where π is the Goldstone field. This induces time dependent functions in the action to transform as

$$f(t) \to f(t+\pi(x)) = f(t) + \dot{f}(t)\pi(x) + \dots , \tag{225}$$

while scalars do not. The latter holds also true for the volume element and the matter action, since we assume it to be covariant and universally coupled to the Jordan metric. The transformations of the quantities of interest for the EFT of DE are

$$M^2 \to M^2 + \mu_1 M^2 \pi + \frac{1}{2}(\dot{\mu}_1 + \mu_1^2) M^2 \pi^2 , \tag{226}$$

$$g^{00} \to g^{00} + 2g^{0\mu}\dot{\pi} + g^{\mu\nu}\partial_\mu\pi\partial_\nu\pi , \tag{227}$$

$$\delta K_{ij} \to \delta K_{ij} - \dot{H}\pi h_{ij} - \partial_i\partial_j\pi , \tag{228}$$

$$\delta K \to \delta K - 3\dot{H}\pi - \frac{1}{a^2}\partial^2\pi , \tag{229}$$

$${}^{(3)}R_{ij} \to {}^{(3)}R_{ij} + H(\partial_i\partial_j\pi + \delta_{ij}\partial^2\pi) , \tag{230}$$

$${}^{(3)}R \to {}^{(3)}R + \frac{4}{a^2}H\partial^2\pi . \tag{231}$$

Stability of theories

One of the advantages of the EFT of DE is its capability to give a straightforward assessment of the stability of a model. The severity of this problem depends on the type of instability encountered.

Toy model

In order to illustrate this, let us consider the quadratic action for one scalar degree of freedom π

$$L = \frac{1}{2}M^2(t)\left[\dot{\pi}^2 - c_s^2(t)|\nabla\pi|^2 - \frac{1}{2}m^2(t)\pi^2\right] , \tag{232}$$

where $M^2(t)$ is the running Planck mass of the theory, c_s^2 is the so-called propagation speed (which coincides with the actual propagation speed of π-waves of momentum larger than m^2) and m^2

is the mass of the scalar degree of freedom. This Lagrangian can present 3 different types of instabilities:

- *Tachyon instability*. This is the less severe instability and corresponds to having $m^2 < 0$. This is not a catastrophic instability since it signals the presence of exponentially growing modes as e^{mt}. The time scale of the instability is therefore set by m. If $m \ll H_0$, the time scale for the development of the instability is larger than the age of the universe and it would not manifest yet. Hence, a model can still be viable with tachyonic instabilities as long as the corresponding mass is sufficiently small.

- *Gradient/Laplacian instability*. This instability is more severe than the previous one. It corresponds to having $c_s^2 < 0$. Again, this signals the presence of exponentially growing modes of the form $e^{c_s k t}$. The difference with respect to the tachyon instability is that now the timescale is set by $c_s k$, which can be, in principle, arbitrarily large. Within an EFT framework we expect to have some cutoff k_{max} for the validity of the EFT so the shortest timescale on which the instability will develop is such a k_{max}. However, since the background must evolve on timescales $\eta_0 \ll k_{max}$, this means that the instability develops instantaneously as seen by the background evolution. Hence, these instabilities are fatal for the viability of the model.

- *Ghosts*. This instability corresponds to having $M^2 < 0$ and signals the presence of modes with negative kinetic energy. Having modes with negative kinetic energy means vacuum is unstable against processes involving the ghost modes and normal particles. This is another instability one cannot tolerate.

The EFT of DE case

The stability conditions in the case of the EFT of DE can be obtained thanks to the Arnowitt-Deser-Misner (ADM) formalism (see [177, 178] for instance) or, as we do here, by applying the Stückelberg trick to (221) and choosing the Newtonian gauge. The propagating scalar degree of freedom in the EFT of DE being a Stückelberg field, it has no mass and thus cannot develop tachyon instabilities. From now on, since we will explore the phenomenology of Horndeski theories in chapter 3, we restrict ourselves to the case $\epsilon_4 = \tilde{\epsilon}_4$. The action takes the form [177, 197]

$$S_\pi = \int a^3 M^2 \left[A\left(\mu_1, \mu_2^2, \mu_3, \epsilon_4\right) \dot{\pi}^2 \; - \; B\left(\mu_1, \mu_3, \epsilon_4\right) \frac{(\vec{\nabla}\pi)^2}{a^2} \right] , \tag{233}$$

where the other two stability conditions in the scalar sector, the ghost and gradient free condition, expressed in terms of the coupling functions are respectively given by

$$A \; = \; (\mathscr{C} + 2\mu_2^2)(1+\epsilon_4) + \frac{3}{4}(\mu_1 - \mu_3)^2 \geqslant 0 \tag{234}$$

$$B \; = \; (\mathscr{C} + \frac{\mathring{\mu}_3}{2} - \dot{H}\epsilon_4 + H\mathring{\epsilon}_4)(1+\epsilon_4) - (\mu_1 - \mu_3)\left(\frac{\mu_1 - \mu_3}{4(1+\epsilon_4)} - \mu_1 - \mathring{\epsilon}_4\right) \geqslant 0 \, . \tag{235}$$

We have defined with a circle some "generalized time derivatives"

$$\mathring{\mu}_3 \; \equiv \; \dot{\mu}_3 + \mu_1\mu_3 + H\mu_3 \, , \tag{236}$$

$$\mathring{\epsilon}_4 \; \equiv \; \dot{\epsilon}_4 + \mu_1\epsilon_4 + H\epsilon_4 \, . \tag{237}$$

The definition of sound speed of dark energy perturbations follows,

$$c_s^2 \; = \; \frac{B}{A} \, , \tag{238}$$

which is the propagation speed of the scalar degree of freedom. It is described, in the case of Horndeski and GLPV theories, by the dispersion relation $\omega^2 = c_s^2 k^2$, ω being the pulsation.

For the stability of tensor perturbations, one needs to study the propagation of tensor modes from the action (221). One must consider the spatial metric

$$h_{ij} = a^2(t) e^{2\zeta} \hat{h}_{ij} \,, \tag{239}$$

where $\det \hat{h} = 1$, $\hat{h}_{ij} = \delta_{ij} + \gamma_{ij} + \frac{1}{2}\gamma_{ik}\gamma_{kj}$, γ_{ij} is traceless and divergence-free, *i.e.* $\gamma_{ii} = \partial_i \gamma_{ij} = 0$. Then, since tensor and scalar modes are decoupled at the linear level, one can simply replace this metric into the action (221), producing

$$S_\gamma^{(2)} = \int d^4x a^3 \frac{M^2}{8} \left[(1+\epsilon_4)\dot{\gamma}_{ij}^2 - \frac{1}{a^2}(\partial_k \gamma_{ij})^2 \right] . \tag{240}$$

This implies the ghost and gradient free conditions for tensor modes to be respectively

$$c_T^2 = \frac{1}{1+\epsilon_4} \geq 0 \,, \tag{241}$$

$$M^2 \geq 0 \,. \tag{242}$$

Hence, on can observe that the propagation speed of tensor modes can be different from one in Horndeski and GLPV theories, *i.e.* $\epsilon_4 \neq 0$.

Background and equations of motion

The construction and the stability of the EFT of DE action having been addressed, we shall now move on to the structure it produces. We want to obtain the characteristic equations the action produces in order be able to compute observable predictions in the following chapters. First, we take the perfect-fluid assumption to obtain the background equations of motion and decompose the matter energy momentum tensor as

$$T^0{}_0 = -(\rho_\mathrm{m} + \delta\rho_\mathrm{m}) \,, \tag{243}$$

$$T^0{}_i = (\rho_\mathrm{m} + p_\mathrm{m})\partial_i v = -a^2 T^i{}_0 \,, \tag{244}$$

$$T^i{}_j = (p_\mathrm{m} + \delta p_\mathrm{m})\delta^i_j + \left(\partial^i \partial_j - \frac{1}{3}\delta^i_j \partial^2 \right) \sigma \,, \tag{245}$$

with ρ_m and p_m being respectively the background energy density and pressure of matter and $\delta\rho_\mathrm{m}$, δp_m their perturbations. v is the 3-velocity potential and σ is the scalar component of the anisotropic stress. Varying the first line of the action (221) with respect to the metric yields the background equations

$$\mathscr{C} = \frac{1}{2}\left(H\mu_1 - \dot{\mu}_1 - \mu_1^2 \right) - \dot{H} + \frac{k}{a^2} - \frac{1}{2M^2}(\rho_\mathrm{m} + p_\mathrm{m}) \,, \tag{246}$$

$$\lambda = \left(5H\mu_1 + \dot{\mu}_1 + \mu_1^2 \right) \dot{H} + 3H^2 + 2\frac{k}{a^2} - \frac{1}{2M^2}(\rho_\mathrm{m} - p_\mathrm{m}) \,, \tag{247}$$

where the Hubble rate $H(t)$ is free to be set by the user. From this, we see that the background equations $\mathscr{C}$ and Λ are linked to M^2, H and matter. At this point, one can see that the freedom of a Horndeski model is represented in the EFT of DE by one constant and five functions of time:

$$\left\{ \rho_{\mathrm{m},0},\, H(t),\, \mu_1(t),\, \mu_2^2(t),\, \mu_3(t),\, \epsilon_4(t) \right\} , \tag{248}$$

where the evolution of $\rho_{\rm m}$ will be provided by the definition of $H(t)$. As we will see in the next chapter, $\{\rho_{\rm m,0}, H(t)\}$ can be described by two constants when choosing $H(t)$ to be that of ΛCDM. At this point, let us continue with the structure of the background equations. Since we have considered the Jordan frame, test particles follow geodesics and the matter energy momentum tensor is conserved in the standard way

$$\dot{\rho}_{\rm m} + 3H(\rho_{\rm m} + p_{\rm m}) = 0\,. \tag{249}$$

On the contrary, the non-minimal coupling of the scalar field to gravity implies DE is not conserved. It proves useful to keep track of the fluid description by defining the fluid quantities thanks to the modified Friedmann equations

$$H^2 + \frac{k}{a^2} = \frac{1}{3M^2}(\rho_{\rm m} + \rho_{\rm de})\,, \tag{250}$$

$$\dot{H} - \frac{k}{a^2} = -\frac{1}{2M^2}(\rho_{\rm m} + \rho_{\rm de} + p_{\rm m} + p_{\rm de})\,. \tag{251}$$

Then, the "non-conservation" can be quantified by a continuity equation, using (250), (251) and (249) one obtains

$$\dot{\rho}_{\rm de} + 3H(\rho_{\rm de} + p_{\rm de}) = 3\mu_1 M^2\left(H^2 + \frac{k}{a^2}\right)\,. \tag{252}$$

The non conservation of DE is thus essentially regulated by the Brans-Dicke coupling μ_1.

Finally, using (250) and (251) in (246) and (247) allows the simplification

$$\mathscr{C} = \frac{1}{2}(H\mu_1 - \dot{\mu}_1 - \mu_1^2) + \frac{1}{2}(\rho_{\rm de} + p_{\rm de})\,, \tag{253}$$

$$\lambda = \frac{1}{2}(5H\mu_1 + \dot{\mu}_1 + \mu_1^2) + \frac{1}{2}(\rho_{\rm de} - p_{\rm de})\,. \tag{254}$$

One could equivalently define an effective $\rho_{\rm de}^{\rm eff}$ and $p_{\rm de}^{\rm eff}$

$$\rho_{\rm de} = \frac{M^2}{M_{\rm pl}^2}\rho_{\rm de}^{\rm eff} + \left(\frac{M^2}{M_{\rm pl}^2} - 1\right)\rho_{\rm m}\,, \tag{255}$$

$$p_{\rm de} = \frac{M^2}{M_{\rm pl}^2}p_{\rm de}^{\rm eff} + \left(\frac{M^2}{M_{\rm pl}^2} - 1\right)p_{\rm m}\,, \tag{256}$$

so as to recover a more standard form of Friedmann equations

$$H^2 + \frac{k}{a^2} = \frac{1}{3M_{\rm pl}^2}\left(\rho_{\rm m} + \rho_{\rm de}^{\rm eff}\right)\,, \tag{257}$$

$$\dot{H} - \frac{k}{a^2} = -\frac{1}{2M_{\rm pl}^2}\left(\rho_{\rm m} + \rho_{\rm de}^{\rm eff} + p_{\rm m} + p_{\rm de}^{\rm eff}\right)\,, \tag{258}$$

where the dependency on the non-minimal coupling M^2 has been hidden in the DE component.

Now, having all the equations characterising the background, let us obtain the equations of motions of the perturbations. To do so, one applies Stückelberg trick to the action (221) and considers the linearly perturbed FLRW metric with only scalar fluctuations,

$$ds^2 = -(1+2\Phi)dt^2 + 2\partial_i\alpha\, dt dx^i + a^2(t)\left[(1-2\Psi)\delta_{ij} + 2\chi_{ij}\right]dx^i dx^j\,, \tag{259}$$

where $\chi_{ij} \equiv (\partial_i\partial_j - \frac{1}{3}\delta_{ij}\partial^2)\beta$ is given in terms of the scalar perturbation β. Then one must vary (221) with respect to each scalar components and then fix $\alpha = \beta = 0$ in the derived equation to recover the Newtonian gauge. This procedure produces

◇ 00**-component** ($\delta S/\delta\Phi = 0$)**:**

$$M^2\left(\frac{k^2}{a^2}\left((\mu_1-\mu_3)\pi - 2\Psi(\epsilon_4+1)\right) + \Phi\left(2\mathscr{C} - 6H^2\epsilon_4 - 6H^2 - 6H\mu_1 + 6H\mu_3 + 4\mu_2^2\right) + \dot{\pi}\left(-2\mathscr{C} + 3H\mu_1 - 3H\mu_3 - 4\mu_2^2\right)\right.$$
$$\left. +3\pi\left(H\left(2\mathscr{C} - H\mu_1 + \mu_1^2 + \dot{\mu_1}\right) + \dot{H}\left(-2H\epsilon_4 - \mu_1 + \mu_3\right)\right) - 3\dot{\Psi}\left(2H\epsilon_4 + 2H + \mu_1 - \mu_3\right)\right) = \delta\rho_{\rm m} \tag{260}$$

◇ 0i**-component** ($\delta S/\delta\alpha = 0$)**:**

$$M^2\left(\pi\left(-2\mathscr{C} + H\mu_1 + 2\dot{H}\epsilon_4 - \mu_1^2 - \dot{\mu_1}\right) + \Phi\left(2H\epsilon_4 + 2H + \mu_1 - \mu_3\right) + \left(\mu_3 - \mu_1\right)\dot{\pi} + 2\dot{\Psi}(\epsilon_4+1)\right) = -(p_{\rm m}+\rho_{\rm m})v \tag{261}$$

◇ ij**-trace component** ($\delta S/\delta\Psi = 0$)**:**

$$M^2\left(\frac{k^2}{a^2}\left(-\frac{2}{3}\pi\left(\epsilon_4(H+\mu_1) + \mu_1 + \dot{\epsilon_4}\right) + \frac{2\Psi}{3} - \frac{2}{3}\Phi(\epsilon_4+1)\right)\right.$$
$$+\Phi\left(2\mathscr{C} + 6H^2\epsilon_4 + 6H^2 + 4H\mu_1 - 3H\mu_3 + 2H\mu_1\epsilon_4 + 2H\dot{\epsilon_4} + 2\dot{H}(\epsilon_4+2) + 2\mu_1^2 + 2\dot{\mu_1} + \dot{\mu_3} + \mu_1\mu_3\right)$$
$$+\pi\left(-2\mathscr{C}\mu_1 - 2\dot{\mathscr{C}} + 3H^2\mu_1 - 6\mathscr{C}H - 2H\mu_1^2 - 2H\dot{\mu_1} + \dot{H}\left(2\epsilon_4(3H+\mu_1) + \mu_1 + 2\dot{\epsilon_4}\right) + 2\epsilon_4\ddot{H} - \mu_1^3 - \ddot{\mu_1} - 3\dot{\mu_1}\mu_1\right)$$
$$+\dot{\pi}\left(-2\mathscr{C} - 2H\mu_1 + 3H\mu_3 + 2\dot{H}\epsilon_4 - 2\left(\mu_1^2 + \dot{\mu_1}\right) - \dot{\mu_3} - \mu_1\mu_3\right)$$
$$\left.+\dot{\Phi}\left(2H\epsilon_4 + 2H + \mu_1 - \mu_3\right) + 2\dot{\Psi}\left((\epsilon_4+1)(3H+\mu_1) + \dot{\epsilon_4}\right) + \left(\mu_3-\mu_1\right)\ddot{\pi} + 2(\epsilon_4+1)\ddot{\Psi}\right) = \delta p_{\rm m} \tag{262}$$

◇ ij**-traceless component** ($\delta S/\delta\beta = 0$)**:**

$$M^2\left(\pi\left(\epsilon_4(H+\mu_1) + \mu_1 + \dot{\epsilon_4}\right) - \Psi + \Phi(\epsilon_4+1)\right) = \sigma \tag{263}$$

Combining (260) and (261) produces the EFT of DE generalisation of the Poisson equation,

◇ **Generalised Poisson equation:**

$$M^2\left(\frac{k^2}{a^2}\left((\mu_1-\mu_3)\pi - 2\Psi(\epsilon_4+1)\right) - 2\dot{\pi}\left(\mathscr{C} + 2\mu_2^2\right) + \Phi\left(2\mathscr{C} - 3H\mu_1 + 3H\mu_3 + 4\mu_2^2\right) + 3\dot{H}\left(\mu_3-\mu_1\right)\pi + \left(3\mu_3 - 3\mu_1\right)\dot{\Psi}\right)$$
$$= \delta\rho_{\rm m} - 3H(p_{\rm m}+\rho_{\rm m})v \tag{264}$$

The full set of equations needed to capture all the modifications of gravity in the perturbed sector are indeed involved. However, as we will see in the next chapter, one can simplify these equations on certain scales thanks to the *quasi-static approximation*. This enables one to condense all the information in two observables: the effective Newton constant and the gravitational slip parameter.

CONCLUSION

We have seen that many alternative models to ΛCDM exist. A large class of which fall under the label of scalar-tensor theories where a single scalar degree of freedom is added to GR. The most general theories of this type were Horndeski theories until recently, when they were generalised to

GLPV theories. The achievement in this generalisation transpires from the third order equations of motion they yield and yet, the degree of freedom they produce propagates with a healthy second order equation. In the realm of DE and MG, scalar-tensor theories are only the "tip of the iceberg". We have not discussed, massive gravity and bi-gravity (see [168] for a detailed review) where a mass is given to the graviton, and many more (see for instance the summary diagram in Figure 3 of [12]). This profusion of theories calls for unifying descriptions. For instance, the parametrised post-Newtonian formalism [22] offers the possibility of efficiently confronting gravitational theories with solar system and astrophysical tests. It has notably shown how stringently gravity is constrained to be that of GR on small scales. The parametrised post-Friedmannian formalism [201] is a complementary tool of the parametrised post-Newtonian formalism. While the latter is valid in the weak field limit such that an expansion around the Minkowski metric is justified, the parametrised post-Friedmannian formalism is valid for any background space times provided the curvature perturbations are small.

In this chapter, however, we have concentrated on presenting another unifying framework: the effective field theory of dark energy. The reason for this stems from the fundamental link the EFT of DE has with scalar-tensor theories. The coupling functions of the action parametrise these theories in terms of structural functions of time which, in turn, appear naturally in the expression of observables. This leads to an easy comparison of theoretical predictions with observations, as we will see in the rest of this thesis. One profound revelation of the EFT of DE description is the presence of a scalar field arising as the inevitable consequence of the spontaneously broken time translations of spacetime. This description has its advantages and drawbacks. Being a linear description, it cannot describe non-linear regimes such as the screening mechanism we have discussed in section 2.2. Moreover, the unitary gauge description looses the apparent covariance of the theory, however, it has the benefit of classifying operators in order of perturbations. Nevertheless, the covariant description of the theory can be recovered thanks to the Stückelberg trick which consist in forcing a time coordinate transformation where the Goldstone field is reintroduced.

As a concluding remark of this chapter and before moving to observable predictions of the EFT of DE, it is interesting to point out that treating broken symmetries goes indeed beyond cosmology. For instance, some of the authors that developed the EFT of DE have applied the EFT method to condense matter physics [202]. This enabled the description of *framids*, a common description of matter states, and the prediction of new hypothetical states.

3

FEATURES IN LARGE SCALE STRUCTURE OBSERVABLES

In this chapter, we shall put the tools provided by the EFT of DE into practical use. The background motivation, as we have mentioned in the introduction of this thesis, is to give the means for MG theories to be efficiently diagnosed in perspective of future surveys. In the context of LSS observables, any deviations from ΛCDM will imply some atypical relation among the curvature perturbation Ψ, the Newtonian potential Φ and the matter density contrast $\delta_{\rm m}$. These effects can be encoded within time and scale modifications to the effective Newton's constant μ and to the gravitational slip parameter η [203]. The former quantity describes how fluctuations of the matter fields interact in the universe, while the latter encapsulates the non-standard relation between the Newtonian potential Φ (time-time part of the metric fluctuations) and the curvature potential Ψ (space-space part). One can derive a further parameter from μ and η, Σ, which is more relevant for lensing surveys [204, 205]. Σ relates the matter over-density with the lensing (or Weyl) potential $\Phi_+ = (\Phi + \Psi)/2$. We will consider the growth function $f\sigma_8$ which, as we have seen in section 1.4.2.3, can be optimally estimated from the analysis of RSD. This is another key quantity turning galaxy redshift surveys into gravity probes. Thanks to these set of observables of the LSS, which provide an efficient tool-kit to characterise modified gravity effects, we will try, in this chapter, to bring answers to the guiding questions mentioned in the introduction. We will also use this chapter to introduce a novel classification of dark energy scenarios we embed in linear Horndeski theories:

- *Late-time dark energy* **(LDE)**: This is the reference class of models, in which both the dark energy momentum tensor and the possible modifications of gravity (*i.e.* the non-minimal gravitational couplings) become negligible at early times.

- *Early dark energy* **(EDE)**: In these scenarios dark energy can contribute to the total energy momentum tensor even at early times, while non-minimal gravitational couplings are kept as a late-time phenomenon.

- *Early modified gravity* **(EMG)**: Linear Horndeski theories in their full generality. Not only does dark energy always contribute to the total energy momentum tensor, but modified gravity effects are also persistent at early times, during matter domination.

This chapter is organised as follows. We present first a practical guide to the EFT of DE for extracting observable predictions. Then, we discuss the definite and less definite predictions of linear Horndeski theories and sub classes we obtain. We use the term "linear" Horndeski since it is the part the EFT of DE describes. However, this is the regime of interest when considering LSS observables. Finally, we establish an observable diagnostic of linear Horndeski theories thanks to the correlations of the LSS observables.

EXPLORING DARK ENERGY MODELS

Extracting observable features of EFT models from the set equations of motions we derived in section 2.3.4 requires a number of additional steps. One must choose the background expansion history and compute the LSS observables thanks to their expressions with the EFT couplings — accurately parametrised— while bearing in mind stability imperatives. One possible direction to

follow is to use numerical codes that solves Boltzmann equations such as EFT-CAMB [206] and hi_class [207]. However, we pursue a complementary route in this chapter. We use a Monte Carlo generation of viable models to assess the statistical tendencies the EFT models produce.

Setting the background evolution history

The accelerated nature of the universe is not given by the EFT of DE per say but by the background expansion it is applied onto, dubbed the effective background. The advantage of this description is that one can directly set the background evolution to flat ΛCDM, as it is strongly suggested by observations, and concentrate on MG predictions on the perturbed sector. Doing so, we also follow the prescription used in the release of cosmological measurements. Generically, they are released in a ΛCDM background fiducial model, therefore, the sake of effective comparison leads us to chose ΛCDM for the background evolution as well. We set the background thusly

$$H^2(z) = H_0^2 \left[x_0 (1+z)^3 + (1-x_0)(1+z)^{3(1+\bar{w})} \right] , \tag{265}$$

where the reduce matter density of the background at present time, x_0, and the constant effective equation of state parameter, $\bar{w}$, are free parameters that we will set to Planck 2015 measurements [54] ($x_0 = 0.315$, $\bar{w} = -1$). We neglect the contribution of radiation, since our analysis is restricted to redshifts $z < 100$.

We use the fractional matter density of the background reference model calculated at any epoch, x, as our time variable. Its expression as a function of the redshift is

$$x = \frac{x_0}{x_0 + (1-x_0)(1+z)^{3\bar{w}}} . \tag{266}$$

This time variable proves useful for late-time cosmology for two reasons. It characterises the evolution of the universe by smoothly interpolating between $x = 1$, deep in the matter dominated era, and to its present value of x_0 as depicted in Figure 14. It has also the benefit of "zooming in" the late time epoch when the transition to DE domination takes place. This change of time variable implies a derivative with respect to cosmic time can be converted into one with respect to x as

$$\frac{d}{dt} = 3H\bar{w}x(1-x)\frac{d}{dx} . \tag{267}$$

Having specified the background geometry $H(z)$, we must express the functions $M^2(t)$ and $\mathscr{C}(t)$ accordingly. First of all, $M^2(t)$ and μ_1 are related by (222). By inverting the latter, we obtain

$$M^2(t) = \frac{M_{\rm pl}^2}{(1+\epsilon_4(x_0))^2} \exp\left(\int_{t_0}^{t} dt' \mu_1(t') \right), \tag{268}$$

where today's initial conditions have been set according to (281). One can equivalently parametrise either M^2 or μ_1, we choose μ_1 (see section 3.1.5). To fully determine the evolution equation for the background coupling [1] $\mathscr{C}$ given by (246), considering pressure-less matter, we still need to supply an expression of $\rho_{\rm m}$. There, $\rho_{\rm m}$ represents the *physical* energy density of non-relativistic matter. By "physical" we mean the quantity appearing in the energy momentum tensor. It scales as a^{-3} since we work in the Jordan frame. We can define the physical fractional energy density thusly

$$\Omega_{m,0} \equiv \frac{\rho_{\rm m}(t_0)}{3M_{\rm pl}^2 H_0^2} . \tag{269}$$

1 The background coupling function $\lambda(t)$ does not play a role in the LSS observables nor in the stability of theories

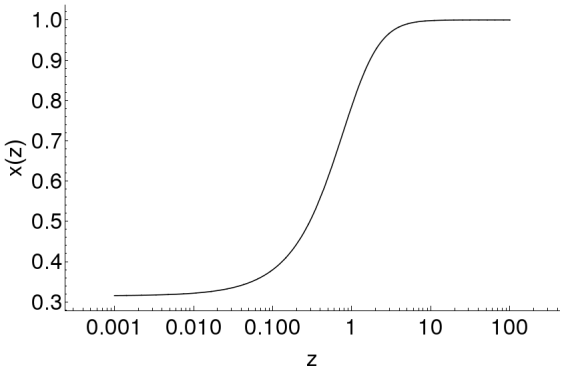

Figure 14: Plot of the function $x(z)$ form (266) with $x_0 = 0.315$ and $\bar{w} = -1$.

In principle, one could try to measure $\rho_{\rm m}(t_0)$ by directly weighing the total amount of baryons and DM, for instance within a Hubble volume. In parallel, the effective $\bar{\rho}_{\rm m}$ would arise from the effective description of (265) and would be measured by constraining the background with SNIa measurement for example. This implies that, in theories of MG, $\rho_{\rm m}$ and $\bar{\rho}_{\rm m}$ can be at most proportional [197]. The same goes for $\Omega_{m,0}$ and x_0, however, we set $\Omega_{m,0} = x_0$ for simplicity.

In conclusion, by setting the background evolution to that of a flat ΛCDM model, an EFT model is now described by

$$\left\{ x_0,\, \bar{w},\, \mu_1(t),\, \mu_2^2(t),\, \mu_3(t),\, \epsilon_4(t) \right\}. \tag{270}$$

These functions and constants are coordinates in the parameter space of the EFT models (see Figure 15). We shall now obtain the expressions of the LSS observables they produce.

Extracting observables

There is a range of scales on which extracting perturbation observables from MG theories is relatively straightforward: the window of comoving Fourier modes $k_{\rm sh} < k < k_{\rm nl}$. For momenta less than the non-linear scale, $k_{\rm nl} \simeq (10\,{\rm Mpc})^{-1}$, one can trust linear perturbation theory. For momenta well above the sound horizon scale $k_{\rm sh} \simeq aH/c_s$ (c_s being the speed of sound of DE fluctuations), one can neglect the time derivatives of the metric and scalar fluctuations in the linear equations of motions in front of k, the so called *quasi-static approximation* [208, 209]. In this regime, it is possible to compute algebraically the effective reduced Newton constant $G_{\rm eff}(t,k)$ and the gravitational slip parameter $\eta(t,k)$ of a given EFT of DE model [177]. The entire set of perturbation equations we presented in section 2.3 reduces, in the flat Newtonian gauge $ds^2 = -(1+2\Phi)dt^2 + a^2(1-2\Psi)\delta_{ij}dx^i dx^j$, to

$$-\frac{k^2}{a^2}\Phi = 4\pi G_{\rm eff}(t,k)\delta\rho_{\rm m}\,, \tag{271}$$

$$\eta(t,k) = \frac{\Psi}{\Phi}\,. \tag{272}$$

Moreover, in surveys of LSS, modes well inside the Hubble horizon are generally observed. One can thus ignore mass terms in the perturbation quantities π, Φ and Ψ, because they are naturally

of order Hubble if the scalar degree of freedom plays a relevant role in the acceleration of the universe, and are small compared to the gradient terms[2].

Effective gravitational coupling (μ)

In this set-up, the action (221) becomes for linear Horndeski theories

$$S = \int a M^2 \Big[(\vec{\nabla}\Psi)^2 - 2(1+\epsilon_4)\vec{\nabla}\Phi\vec{\nabla}\Psi - 2(\mu_1+\mathring{\epsilon}_4)\vec{\nabla}\Psi\vec{\nabla}\pi + (\mu_1-\mu_3)\vec{\nabla}\Phi\vec{\nabla}\pi - \left(\mathscr{C} + \frac{\mathring{\mu}_3}{2} - \dot{H}\epsilon_4 + H\mathring{\epsilon}_4\right)(\vec{\nabla}\pi)^2 \Big] - a^3\Phi\delta\rho_{\rm m}\,, \tag{273}$$

where $\delta\rho_{\rm m} = \rho_{\rm m}\delta_{\rm m}$ is the perturbation of the non-relativistic energy density, a dot means derivative w.r.t. proper time. We take first the variation of (273) with respect to the curvature potential Ψ to obtain the expression of $G_{\rm eff}$. It produces the algebraic relation

$$\Psi = (1+\epsilon_4)\Phi + (\mu_1+\mathring{\epsilon}_4)\pi \tag{274}$$

that, once substituted back into (273), yields

$$S = \int a M^2 \Big\{ -(1+\epsilon_4)^2(\vec{\nabla}\Phi)^2 + \left[\mu_1 - \mu_3 - 2(\mu_1+\mathring{\epsilon}_4)(1+\epsilon_4)\right]\vec{\nabla}\Phi\vec{\nabla}\pi - \left[\mathscr{C} + (\mu_1+\mathring{\epsilon}_4)^2 + \frac{\mathring{\mu}_3}{2} - \dot{H}\epsilon_4 + H\mathring{\epsilon}_4\right](\vec{\nabla}\pi)^2 \Big\} - a^3\Phi\rho_{\rm m}\delta_{\rm m}\,. \tag{275}$$

We can solve the coupled π-Φ system by taking the variation of (275) with respect to π, giving another algebraic relation

$$\left[2\mathscr{C} + 2(\mu_1+\mathring{\epsilon}_4)^2 + \mathring{\mu}_3 - 2\dot{H}\epsilon_4 + 2H\mathring{\epsilon}_4\right]\pi \;=\; \left[\mu_1 - \mu_3 - 2(\mu_1+\mathring{\epsilon}_4)(1+\epsilon_4)\right]\Phi\,. \tag{276}$$

By inserting the later into (275) and then varying the result w.r.t to Φ, we obtain, in Fourier space,

$$-\frac{k^2}{a^2}\Phi = 4\pi G_{\rm eff}(t)\rho_{\rm m}\delta_{\rm m}\,, \tag{277}$$

where

$$G_{\rm eff} \;=\; \frac{1}{8\pi M^2(1+\epsilon_4)^2}\,\frac{a_0}{b_0}\,. \tag{278}$$

with

$$\begin{aligned} a_0 &= 2\mathscr{C} + \mathring{\mu}_3 - 2\dot{H}\epsilon_4 + 2H\mathring{\epsilon}_4 + 2(\mu_1+\mathring{\epsilon}_4)^2\,,\\ b_0 &= 2\mathscr{C} + \mathring{\mu}_3 - 2\dot{H}\epsilon_4 + 2H\mathring{\epsilon}_4 + 2\frac{(\mu_1+\mathring{\epsilon}_4)(\mu_1-\mu_3)}{1+\epsilon_4} - \frac{(\mu_1-\mu_3)^2}{2(1+\epsilon_4)^2} = \frac{2B}{1+\epsilon_4}\,, \end{aligned} \tag{279}$$

with B being the gradient free stability condition (234). An alternative route one could have followed was to use the two algebraic relations in the generalised Poisson equation (264) directly.

Now, we need to specify the relation between $G_{\rm eff}$ and the Newton constant $G_{\rm N}$ —or, equivalently, the Planck mass $M_{\rm pl}$— to define appropriately the effective Newton constant, the ratio of the two. Powerful Solar System [211, 212] and astrophysical [213, 214] tests impose stringent limits on MG. As we have mentioned in section 2.2, realistic models must incorporate screening mechanisms that ensure convergence to GR on small scales and/or high-density environments. Such an

2 Note that we would not have been allowed to do so if we were exploring chameleon and $f(R)$ models, which phenomenologically require a mass for the scalar field much larger than H [210].

astrophysical effect is not encoded within the EFT of DE; the couplings in (273) depend only on time and not on space. A "temporal" or "cosmological" screening also exists which screens out MG effects at high redshifts [215]: even though the EFT formulation does not provide a microscopic description of how this comes about, it does effectively account for such a temporal effect via the time-dependent functions, μ_1, μ_2^2, μ_3 and ϵ_4. By inspection of action (275) we conclude that in a screened environment, the "bare" gravitational coupling M^{-2} gets simply addressed by a factor of $(1+\epsilon_4)^{-2}$. This is what we obtain in the Poisson equation (271) if we switch off the mixing term $\vec{\nabla}\Phi\vec{\nabla}\pi$. We thus define a *screened* gravitational coupling

$$G_{\rm sc}(t) \equiv \frac{1}{8\pi M^2(1+\epsilon_4)^2}\,, \tag{280}$$

valid only in (totally) screened environments. Since we live and perform experiments in a screened environment, the value of $G_{\rm cs}$ evaluated today must be the Newton constant measured by Cavendish experiments for example. Hence

$$G_{\rm N} \equiv \frac{1}{8\pi M_{\rm pl}^2} \simeq \frac{1}{8\pi M^2(x_0)(1+\epsilon_4(x_0))^2}\,. \tag{281}$$

In summary, beyond the "bare" mass M multiplying the Einstein Hilbert term in the unitary gauge action (221), we can define three gravitational couplings of interest:

i)

$$\mu_{\rm sc} = \frac{G_{\rm sc}}{G_{\rm N}} = \left(\frac{M(x_0)(1+\epsilon_4(x_0))}{M(1+\epsilon_4)}\right)^2 \tag{282}$$

is the gravitational coupling of two objects in the quasi-static approximation *when screening is effective*. In other words, it characterises the un-screenable MG effects introduced by the scalar field.

ii)

$$\mu_{\rm ff} = \frac{G_{\rm eff}}{G_{\rm sc}} = \frac{a_0}{b_0} = 1 + \frac{1+\epsilon_4}{B}\left[\frac{\mu_1-\mu_3}{1+\epsilon_4} - (\mu_1+\mathring{\epsilon}_4)\right]^2 \tag{283}$$

is the quantity characterising the strength of the fifth-force mediated by the scalar field. Physically, the scalar field contribution to the gravitational interaction must always be attractive, as expected from a (healthy) spin-0 field. This is indeed the case since $B \geqslant 0$ and $(1+\epsilon_4)^{-1} \geqslant 0$ for a healthy theory.

iii)

$$\mu = \frac{G_{\rm eff}}{G_{\rm N}} = \mu_{\rm sc} \times \mu_{\rm ff} \tag{284}$$

is the total gravitational coupling of two objects in the quasi-static approximation and in the linear regime, *i.e. when screening is not effective*. This is the quantity which is relevant on large (linear) cosmological scales.

Growth function ($f\sigma_8$)

The effective gravitational constant comes as part of the source term in the evolution of the linear density perturbations of matter $\delta_{\rm m}$:

$$\ddot{\delta}_{\rm m} + 2H\dot{\delta}_{\rm m} - 4\pi\mu G_{\rm N}\rho_{\rm m}\delta_{\rm m} = 0\,. \tag{285}$$

The $\delta_{\rm m}$ variable being difficult to observe, it would be preferable to characterise the growth of structures thanks to the growth function $f\sigma_8$ we have presented in section 1.4.2.3. The growth rate f, using $f = d\ln,\delta_{\rm m}/d\ln a$, can be obtained by converting (285) into

$$3\bar{w}(1-x)xf'(x) + f(x)^2 + \left[2 - \frac{3}{2}(\bar{w}(1-x)+1)\right] f(x) = \frac{3}{2}x\mu\,, \tag{286}$$

which approximates the true evolution of f in the Newtonian regime (below the Hubble scale) and well after the initial, radiation dominated phase of cosmic expansion. We compute the amplitude of $\sigma_8(x)$ in a given EFT model, by rescaling the Planck best fitting value $\sigma_{8,0}^{\rm Planck}$ as follows:

$$\sigma_8^{\rm EFT}(x) = \frac{D_+^{\rm EFT}(x)}{D_+^{\rm Planck}(x_0)}\sigma_{8,0}^{\rm Planck}\,, \tag{287}$$

where D_+ is the growing mode of linear matter density perturbations obtained by integrating the growth rate.

Gravitational slip parameter (η)

Having specified the effective gravitational constant μ, we must now provide an expression for the gravitational slip parameter η in order to fully describe all possible modifications of gravity. By inserting (276) into (274) we obtain

$$\eta = 1 - \frac{c_0}{a_0}\,, \tag{288}$$

with

$$c_0 = (\mu_1 + \mathring{\epsilon}_4)(\mu_1 + \mu_3 + 2\mathring{\epsilon}_4) - \epsilon_4(2\mathscr{C} + \mathring{\mu}_3 - 2\dot{H}\epsilon_4 + 2H\mathring{\epsilon}_4)\,. \tag{289}$$

Note that μ and η share the same term a_0.

Light deflection parameter (Σ)

In general, observations probing the gravitational potentials, such as weak lensing measurements, are not directly sensitive to the gravitational slip parameter but rather to the sum of the gravitational potentials $\Phi + \Psi$, as we have seen in section 1.4.2.2. Therefore, we chose to consider also the light deflection parameter Σ defined by $-\frac{k^2}{a^2}(\Phi+\Psi) = 8\pi\Sigma(t,k)G_{\rm N}\rho_{\rm m}\delta_{\rm m}$. In GR, as for η, it is equal to 1. In MG, it is not necessarily and it can be expressed straightforwardly as the combination of μ and η

$$\Sigma = \frac{\mu}{2}(1+\eta)\,. \tag{290}$$

This theoretical degeneracy between LSS observables will be instrumental in understanding specific predictions of linear Horndeski theories in section 3.3.1.

Embedding dark energy scenarios

One feature of freezing quintessence models we saw in section 2.1.1 is their tracking behaviour. As compared the standard model, the tracking solution, despite mimicking radiation, can allow a non negligible amount of DE in the past [216, 217]. An intuitive way to account for the early effects it produces is to directly parametrize the DE component $\Omega_{\rm de}$ [218] to yield *early dark energy* [219]. The background evolution is thereby supplemented with a DE component effective at early times, $\Omega_{\rm ede}$, and treated as a free parameter [220–223]. In this spirit, many types of parametrisations

have been introduced and tested [224, 225]. However, late observations [80] have put stringent bounds on $\Omega_{\rm ede}$ (less than 1%). As a consequence of these tight bounds, new paths have been studied. For example, the authors in [226] show how interacting early DE and DM can alleviate the coincidence problem. Authors in [227] have studyed early modifications of gravity effects on cosmological observables revealing that stronger coupling with matter arises.

Therefore, we would like for our EFT of DE description to be able to account for early modifications to GR. Since functional expression of the couplings is not imposed by the EFT of DE, one can change the asymptotic behaviours of the couplings to achieve this goal. Starting from the classical modelling of DE in the EFT formulation, we suggest, in the following, a novel classification of early DE models embedded in linear Horndeski theories. One particularity of these new models stems from the fact that they affect solely the perturbation sector. The background being fixed to that of ΛCDM, they evade the strong constraints on early modifications to the background.

Late-time dark energy (LDE)

A general consensus for modelling time dependent coupling functions of the DE sector is to require their switching off at early times in order to fulfil early tests such as BBN and CMB. An order zero parametrisation used commonly in literature (see for example [192, 197, 228–230]) is

$$\text{" coupling function}(t) = \bar{\Omega}_{\rm de}(t) \times \text{const. "}\,, \tag{291}$$

where $\bar{\Omega}_{\rm de}(t)$ is the background fractional DE density. Therefore, modifications of gravity are parametrized to follow the background evolution of the DE component. However, this is not sufficient. The full recovery of GR at early times requires an additional condition. In order to see that, one must substitute $\rho_{\rm m} = 3M_{\rm pl}^2 xH^2$, obtained from (269), into (246), hence

$$\frac{\mathscr{C}}{H^2} = \frac{1}{2}\left(\frac{\mu_1}{H} - \frac{\dot{\mu}_1}{H^2} - \frac{\mu_1^2}{H^2}\right) - \frac{\dot{H}}{H^2} - \frac{3}{2}\frac{M_{\rm pl}^2}{M^2}\,x\,. \tag{292}$$

Provided that $\mu_1/H \underset{x\to 1}{\to} 0$, (292) implies

$$\frac{\mathscr{C}}{H^2} \underset{x\to 1}{\to} \frac{3}{2} - \frac{3}{2}\frac{M_{\rm pl}^2}{M^2}\,, \tag{293}$$

thereby a cancellation between the last two terms on the RHS of (292) is necessary to obtain $\mathscr{C}/H^2 \underset{x\to 1}{\to} 0$, and in parallel $\lambda/H^2 \underset{x\to 1}{\to} const.$, so as to recover the standard model at early times. From (268), one can see the condition on $\mathscr{C}/H^2$ and λ/H^2 to be nothing else than asking a condition on M^2, *i.e.* $M^2 \underset{x\to 1}{\to} M_{\rm pl}^2$, thus requiring DE to be fully vanishing at high redshifts ($x \to 1$).

LDE is thus the minimal model, in which all effects of DE are confined to late times. Not only do non minimal couplings (μ_1, μ_2^2, μ_3, ϵ_4) go to zero at early times but M goes to $M_{\rm pl}$. In other words, the energy density of non relativistic particles $\rho_{\rm m}$ must saturate the Friedmann equations at early time. In summary,

$$\text{LDE} \left\{\frac{M^2}{M_{\rm pl}^2} \to 1\,,\, \frac{\mu_1}{H} \to 0\,,\, \frac{\mu_2^2}{H^2} \to 0\,,\, \frac{\mu_3}{H} \to 0\,,\, \epsilon_4 \to 0\right\}_{x\to 1}. \tag{294}$$

$x \to 1$	$M^2/M_{\rm pl}^2$	μ_1/H	$\mu_3/H, \epsilon_4$	μ	η	Σ	c_s
LDE	1	0	0	1	1	1	#
EDE	#	0	0	#	1	#	1
EMG	#	0	#	#	#	#	#

Table 6: Summary of the phenomenological effects of the different dark energy scenarios. The symbol # stands for a constant different from 0 and 1.

Early dark energy (EDE)

In light of the above, an immediate extension is to relax the condition on M^2 to explore early DE. The DE will contribute to the total energy momentum tensor even at early times, while, however, all non-minimal couplings vanish. As mentioned for quintessence models, the only way this is possible is thanks to a tracker behaviour, *i.e.* for DE to acquire the same physical equation of state as DM early on, so that it becomes indistinguishable from the latter as long as the background evolution is concerned. In summary,

$$\text{EDE} \left\{ \frac{M^2}{M_{\rm pl}^2} \to \text{const.}\,, \frac{\mu_1}{H} \to 0\,, \frac{\mu_2^2}{H^2} \to 0\,, \frac{\mu_3}{H} \to 0\,, \epsilon_4 \to 0 \right\}_{x\to 1}\,. \tag{295}$$

A caveat must be issued regarding the use we make of the adjective "early". Our study is oblivious of the radiation dominated epoch. Therefore "early" means for us always well after equivalence, at $z \simeq 100$, but well before the onset of acceleration, at $z \simeq 1$. Accordingly, the early non-standard scenarios we are considering evade Big-Bang Nucleosynthesis (BBN) constraints. In principle, since the background expansion is fixed to that of ΛCDM, the time at which neutrinos decouple and the neutron-proton fluid exits from equilibrium is not modified in our non-standard gravitational scenarios. However, the time elapsed from this epoch ($T \sim 0.8$ Mev) to that when BBN begins ($T \sim 0.1$ Mev), which regulates neutron decays and accounts for the final neutron-to-proton ratio available for nucleosynthesis, critically depends on the value of the Newton constant.

Early modified gravity (EMG)

The last extension is to allow for the asymptotic value of the non-minimal couplings at early times to be different from zero. However, the Brans-Dicke non-minimal coupling μ_1 needs a special attention due to its link with M^2; (268) implies for any asymptotic value of μ_1 different from zero M^2 would either tend to zero or plus infinity, corresponding to infinite or zero gravitational coupling respectively. We thus restrict to the cases when $\mu_1 \to 0$. In summary, EMG is the most general case,

$$\text{EMG} \left\{ \frac{M^2}{M_{\rm pl}^2} \to \text{const.}\,, \frac{\mu_1}{H} \to 0\,, \frac{\mu_2^2}{H^2} \to \text{const.}\,, \frac{\mu_3}{H} \to \text{const.}\,, \epsilon_4 \to \text{const.} \right\}_{x\to 1}\,. \tag{296}$$

Allowing modifications of gravity also deep in matter domination without altering the background evolution is the novelty of the scenarios EDE and EMG. Table 6 summarises the features of the three types of DE considered in this paper and highlights the effects they have on the asymptotic behaviour of some relevant quantities of the EFT of DE.

Viability of theories

We will require all our models to be free of instabilities according to section 2.3.3. Furthermore, along the arguments detailed in [231], we will generally not allow superluminal propagation speeds for either scalar or tensor modes. On top of these theoretical requirements, we should exclude models that are already ruled out by current observations. As for the choice of the background expansion rate, which we describe via the effective Hubble rate (265), we exploit current limits available in the perturbed sector of the universe. Notably, the local value of gravitational waves of EFT of DE models has been recently constrained leading to a bound on the value of $\epsilon_4(x_0) \sim 10^{-2}$ [232], hence we simply set its present value to 0 for simplicity. Also, the speed of tensor modes has been argued to be tightly constrained from below by the gravitational Cerenkov effect of cosmic rays, $1 - c_T < 2 \times 10^{-15}$[233]. However, the typical energy scale of the the emitted gravitons, $\sim 10^{10}$ GeV, is well above the expected limit of validity of an effective theory of DE. For instance, the cut-off scale of Galileon theories is $\Lambda_s \sim \sqrt{H_0^2 M_{\rm Pl}} \sim (1000 \text{ km})^{-1} \sim 10^{-12}$ eV (see section 2.2). In summary, we require our models to fulfil

Stability of the models,

$$A \geq 0 \qquad \text{ghost free (scalar)}, \tag{297}$$
$$B \geq 0 \qquad \text{gradient free (scalar)}, \tag{298}$$
$$M^2 > 0 \qquad \text{ghost free (tensor)}, \tag{299}$$
$$c_T^2 \geq 0 \qquad \text{gradient free (tensor)}, \tag{300}$$

Subluminal propagation speeds,

$$c_s^2 \leqslant 1 \qquad \text{scalar modes}, \tag{301}$$
$$c_T^2 \leqslant 1 \qquad \text{tensor modes}, \tag{302}$$

Observational requirement (compatibility with current constraints),

$$\epsilon_4(x = x_0) = 0\,. \tag{303}$$

The dependence of our conclusions on the requirement of sub-luminal propagation speeds will be assessed in Sec. 3.3.2.1.

As already discussed in section 3.1.3, the models we are considering are ineffective in describing cosmic evolution at such an early epoch as those where BBN could be used to constrain them. However, on the opposite end, *i.e.* today, Lunar ranging tests have put constraints on the variation of Newton's constant, at around $\dot{G_{\rm N}}/G_{\rm N} < 0.02 H_0$ (see [234] for a detailed review). Since we are not considering EFT operators beyond the linear level, it is difficult to predict how non-linearities would affect the definition of G_N for our models. It is however misleading to draw the conclusion that the coupling μ_1 or M^2 would end up being severely constrained. Indeed, variations in the Planck mass could still be relatively large, although appropriately counter-balanced by the specific time scaling of ϵ_4 (and so $\dot{c_T}$, see (281)). Accordingly, we do not consider the Lunar ranging constraint as an additional viability criteria. We simply note that linear Horndeski models passing this constraint would constitute a sub-sample of the whole set of healthy theories considered in this study.

Exploration protocol

We have the expressions of the LSS observables at our disposal, we have chosen the background history suggested by observations, we have defined the possible asymptotic behaviour coupling functions can have within linear Horndeski theories and we have defined the viability framework we focus on. In light of this, we must now parametrise acutely the coupling functions.

On the one hand, the cases of LDE and EDE require the switching off of the coupling functions deep in matter domination, therefore a $(1-x)$ factor is requested to follow the prescription of (291). Then, one must give enough flexibility to the coupling functions to access all the observable features of linear Horndeski theories. An intuitive guess is to call for a polynomial expansion in powers of $(x-x_0)$ for example. A posteriori tests have shown that an expansion up to $(x-x_0)^2$ is enough to cover all the rich phenomenology of our models. In summary, the coupling functions for LDE and EDE yield :

$$\mu_1(x) = H\ (1-x)\Big(p_{11}+p_{12}(x-x_0)+p_{13}(x-x_0)^2\Big)\,, \tag{304}$$

$$\mu_2^2(x) = H^2(1-x)\Big(p_{21}+p_{22}(x-x_0)+p_{23}(x-x_0)^2\Big)\,, \tag{305}$$

$$\mu_3(x) = H\ (1-x)\Big(p_{31}+p_{32}(x-x_0)+p_{33}(x-x_0)^2\Big)\,, \tag{306}$$

$$\epsilon_4(x) = \quad (1-x)\Big(\quad p_{42}(x-x_0)+p_{43}(x-x_0)^2\Big)\,. \tag{307}$$

According to the discussion in section 3.1.3, the LDE case requires a constraint on the expansion coefficients of μ_1. By using (268), the constraint

$$\frac{1-x_0}{6\bar{w}}\left[2p_{12}+p_{13}(1-3x_0)\right]-\frac{\ln x_0}{3\bar{w}}\left[p_{11}-x_0p_{12}+x_0^2p_{13}\right]=0 \tag{308}$$

must be imposed to enforce $M^2(x\to 1)\to M_{\rm pl}^2$. Note that there is no order 0 parameter for ϵ_4 given the observational bounds discussed in section 3.1.4.

On the other hand, the EMG case displays non vanishing coupling functions (except μ_1), hence the factor $(1-x)$ is left out :

$$\mu_1(x) = H\ (1-x)\Big(p_{11}+p_{12}(x-x_0)+p_{13}(x-x_0)^2\Big)\,, \tag{309}$$

$$\mu_2^2(x) = H^2\Big(p_{21}+p_{22}(x-x_0)+p_{23}(x-x_0)^2\Big)\,, \tag{310}$$

$$\mu_3(x) = H\ \Big(p_{31}+p_{32}(x-x_0)+p_{33}(x-x_0)^2\Big)\,, \tag{311}$$

$$\epsilon_4(x) = \quad \Big(\quad p_{42}(x-x_0)+p_{43}(x-x_0)^2\Big)\,. \tag{312}$$

To study the predictions of these DE scenarios, we explore the space of non-minimal couplings μ_1, μ_2^2, μ_3 and ϵ_4 that covers the entire set of Horndeski theories by a Monte Carlo procedure. We randomly generate the coefficients $p_{i,n}$. We reject the theories that do not pass the viability conditions of section 3.1.4 until we have produced 10^4 viable models. We find that dealing with the full parameter space, the chance of hitting a viable theory is much lower than 1%. In addition, we want the quasi-static approximation to have a large enough range of applicability, we therefore also impose $c_s > 0.1$, which allows us to cover the Fourier volume of the EUCLID mission [209]. We

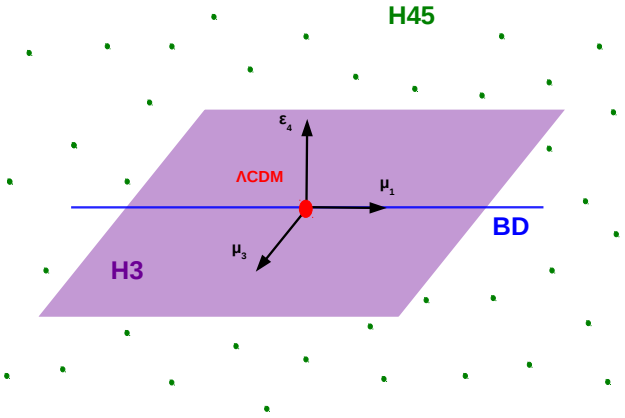

Figure 15: Pictorial representation of the space of theories spanned by the EFT coordinates μ_1, μ_3 and ϵ_4.

emphasize, however, that this is a very weak selection effect on our randomly generated models. There is no "natural unit" in the space of expansion coefficients, however, the coupling functions are expected to be of order 1. Therefore, we randomly generate the coefficients in the interval $p_{i,n} \in [-1, 1]$.

SIGNATURES FROM BRANS-DICKE TO HORNDESKI THEORIES

In this section, we analyse the time evolution of the LSS observables presented in section 3.1.2 generated from our Monte Carlo procedure. In particular, we want to see whether the predictions of linear Horndeski and sub classes follow bounded trends in the most restrictive set-up: LDE scenario, all viability conditions requested and $\mu_2^2 = 0$. The coupling μ_2^2 does not appear explicitly in the observables but plays a role in the ghost stability conditions only. Its function being a modulation of the sound speed; keeping it would broaden significantly the space of stable theories. Hence, we will set it to zero at first and assess its effect later in section 3.2.5.

In summary, we will restrict our exploration to EFT models with the background expansion set to ΛCDM exactly ($\bar{w} = -1$) and theories with the non-minimal coupling of Brans-Dicke (*BD*), μ_3 of the cubic galileon- and Horndeski-3 (*H3*), and ϵ_4 present in galileon-Horndeski 4 and 5 (*H45*) Lagrangians. They all correspond to coordinates in the space of theories as schematically shown in Figure 15.

Effective gravitational constant and its components

The redshift dependence of the effective Newton constant appears to be well bounded by our viability conditions. Indeed, Figure 16 shows that the μ of our large class of models have a similar evolution pattern over time. The universal behaviour of $\mu(x)$ is best captured by the following few features.

First, all the curves display a negative derivative at $x = 1$, which implies stronger gravitational attraction ($\mu \geq 1$) at early epochs ($z > 2$). This behaviour was proved analytically in [197] for a restricted set of models in which the expansion for the couplings is retained only at zero-th order. By inspection of Figure 16, we note the effect to be still there at any order in the expansion.

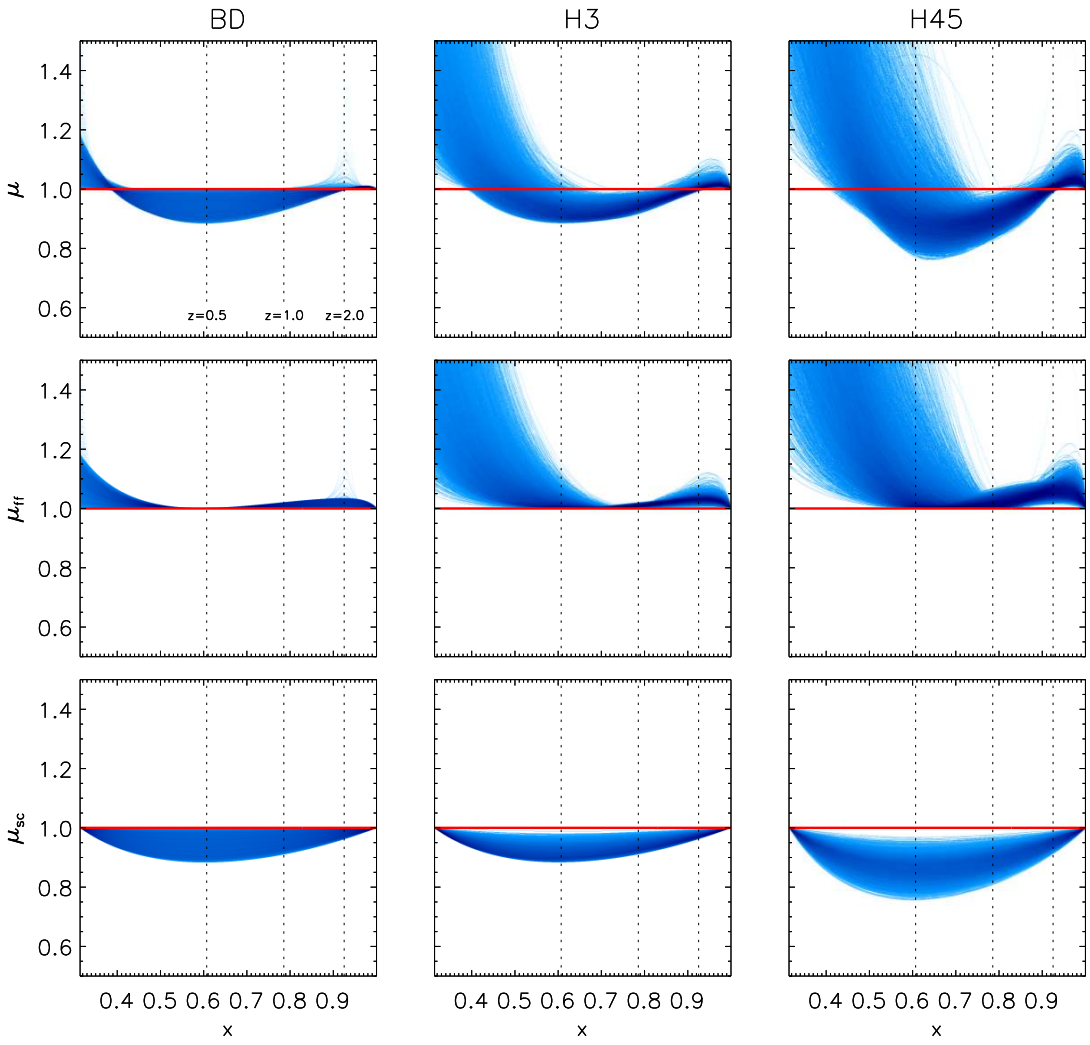

Figure 16: The behaviour of μ (top row) and its two separate contributions of (284) (middle and bottom row) as a function of the reduced matter density x is shown for a sample of 10^4 randomly generated viable models of *BD*, *H3* and *H45*. The shades of blue highlight the density of curves passing through a point. The dotted vertical lines identify, from left to right, the cosmic epochs $z = 0.5$, $z = 1$ and $z = 2$. The thick red line represents ΛCDM. Note that *H3* and *H45* do not seem to approach this limit in a continuous way. The point is that *BD*, *H3* and *H45* correspond to "subspaces" of progressively higher dimensions in the theory space (see Figure 15). ΛCDM represents a well-defined limit for all models, but the volume of stable theories for *H3* and *H45* asymptotically reduces to an "hyperplane" of lower dimensions in the vicinity of ΛCDM. As a result, the neighbourhood of ΛCDM is effectively a volume-zero subset in our randomly generated of models. Nonetheless, the Monte Carlo procedure does recover ΛCDM as a limiting case of *BD*.

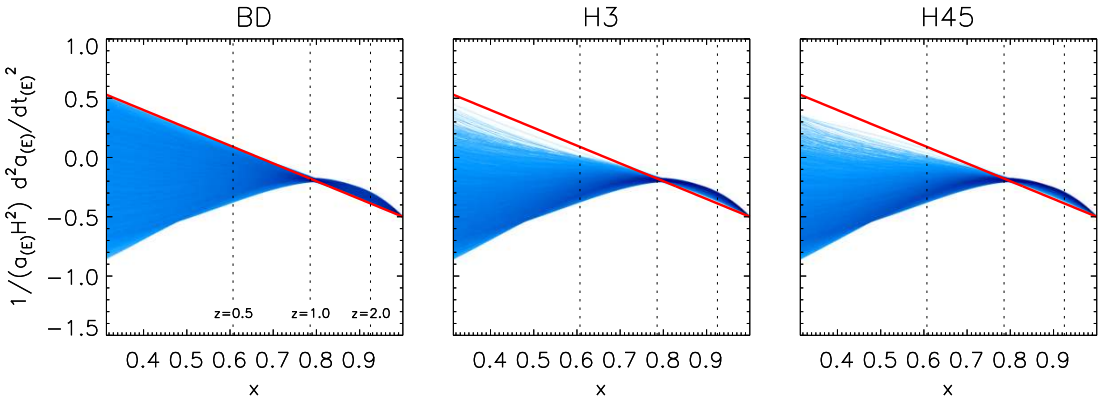

Figure 17: The behaviour of $d^2a_E/dt_E^2/(a_E H^2)$ as a function of the reduced matter density x is shown for the viable 10^4 EFT models. The ΛCDM predictions are shown in red.

The amplitude of the initial bump in $\mu(x)$ varies, with a few models displaying also conspicuous departures from the standard model. The width of the time interval over which this early stronger gravity period extends is quite model dependent. We find that this bump can be levelled out by going to the EDE and EMG cases.

Even more interesting is the fact that all the models consistently predict the amplitude of μ to be suppressed, $\mu \leq 1$ in the redshift range $0.5 \lesssim z \lesssim 1$ before turning stronger, once again, around the present epoch. The reason for the intermediate range suppression is that at those redshifts the dominant contribution to the total of μ is given by the screened gravitational coupling $\mu_{\rm sc}$. Viability conditions always make $\mu_{\rm sc} \leq 1$ during the whole evolution. The characteristic *S-shape* pattern shown in Figure 16 is clearly a feature common to all models.

Within covariant Galileon theories —a subclass of the models considered here— the same qualitative behaviour of μ was found (see *e.g* Ref. [235], Fig. 9, Ref. [236], Fig. 3), although the background evolution in that more constrained case is different from ΛCDM. Regarding the weaker gravitational attraction at intermediate redshifts, these results are in agreement with those in [237].

A way to make sense of why the effective gravitational constant is stronger/weaker than the corresponding standard model value at characteristic cosmic epochs, is to keep in mind its decomposition expressed in (284). Stability conditions (298) and (302) imply $\mu_{\rm ff} \geqslant 1$. Physically, this means that the scalar field contribution to the gravitational interaction is always attractive, as expected from a (healthy) spin-0 field. This circumstance is displayed in the second row of Figure 16. The behaviour of $\mu_{\rm sc}$ (see the last row of Fig. 16) also has a physical interpretation related to the viability of the models, although somewhat more subtle. First, note that the value of such a quantity today is unity by definition —as we have argued in section 3.1.2.1, $G_N \equiv G_{\rm sc}(t_0)$— while at early epochs ($x = 1$) it is given by the asymptotic value of M^2. On the other hand, the overall behaviour of $\mu_{\rm sc}$ as a function of time can be understood as a product of the two independent factors, M^{-2} and $(1+\epsilon_4)^{-2}$. The latter quantity is always lower than unity because tensor perturbations are assumed to propagate at subliminal speed (see (302)). Also M^{-2} decreases as a function of the redshift (i.e. backward in time) at around the present epoch. The physical reason is better understood

in the "Einstein frame"—the frame in which the metric is decoupled from the scalar—which for the background evolution simply reads as (see e.g. [176])

$$g^{(E)}_{\mu\nu} = \frac{M^2(t)}{M^2_{\rm pl}} g_{\mu\nu} \,. \tag{313}$$

A growth of M as a function of the redshift means less acceleration in the Einstein-frame, thus implying that the observed acceleration in the physical (Jordan) frame is due to a genuine MG effect (self-acceleration). Therefore, the third row of Figure 16 provides a rough estimate of the amount of self-acceleration for the various randomly generated models. Curves that deviate the most from ΛCDM represent models with strong self-acceleration, while the opposite cases represent models in which acceleration is essentially due to a negative pressure component in the energy momentum tensor.

To better quantifying the production of self-acceleration, let us to compare the amount of acceleration a theory produces in the Jordan and Einstein frames [238]. The scale factor and time derivative in both frames are related by (see section 5.2 of [176] for details):

$$a_E = \frac{M}{M_{\rm pl}} a \tag{314}$$

$$\frac{d}{dt_E} = \left(\frac{M}{M_{\rm pl}}\right)^{-1} \frac{d}{dt} \tag{315}$$

where we have denoted the quantities in the Einstein-frame with a subscript (E) and the Jordan frame quantities without a subscript. It is then straightforward to obtain the acceleration in the Einstein frame,

$$\frac{d^2 a_E}{dt_E^2} = \frac{a_E}{2} \left(\frac{M^2}{M^2_{\rm pl}}\right)^{-1} \left(2\frac{\ddot{a}}{a} + \mu_1 H + \dot{\mu}_1\right) , \tag{316}$$

where the dot means derivative w.r.t time in the Jordan frame. The term $\ddot{a}/a$ being the acceleration in the Jordan frame, hence that of ΛCDM, the production of self acceleration arises from M^2 and/or its log derivative μ_1. It is striking to see in Figure 17 that our models can produce a substantial amount of self-acceleration, for instance more than half of the curves have their $\ddot{a}_E$ changing sign for $z < 0.5$. In other words, the self acceleration produced is so strong that it is able to change the sign of the acceleration between the Jordan and Einstein frames, *i.e.* produce genuine modifications of gravity [210]. We must emphasise that theories exhibiting strong self-acceleration do not necessarily deviate substantially from ΛCDM in the LSS observables. We have conducted a test where only theories with $\ddot{a}_E < 0$ today were selected and the same phenomenology was obtained.

Growth of matter perturbations

The universal evolution of μ is expected from (286) to result in a characteristic growth history for the linear density fluctuations of matter. Figure 18 shows that the expectation of a pattern of stronger/weaker growth phases with respect to the prediction of ΛCDM is confirmed. Understandably, since f obeys the evolution equation (286) sourced effectively by $x\,\mu$, it responds to periods of stronger/weaker gravity with a time-lag. Moreover, as an integrated effect, f has a smaller spread compared to μ. The first thing worth highlighting is that essentially all MG models with the same expansion history of ΛCDM consistently predict that cosmic structures grow at a stronger pace, compared to ΛCDM, at all redshifts greater than $z \sim 2$. A second distinctive feature is that non-standard models of gravity are generally less effective in amplifying matter fluctuations during the

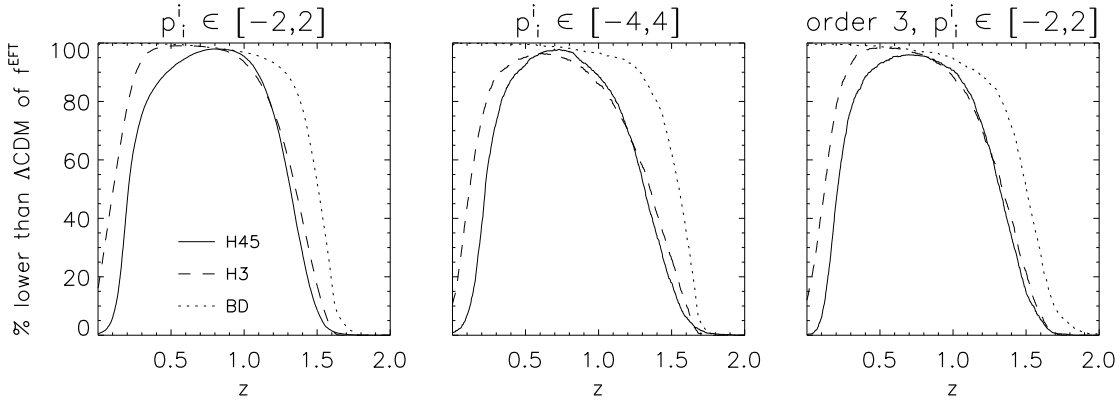

Figure 18: Percentage of randomly generated EFT models with growth rate f *lower* than that predicted by ΛCDM Planck-cosmology as a function of the redshift z. We have checked the robustness of our analysis by changing the interval of the randomly generated expansion coefficients (center) and by augmenting the order of the expansion (right).

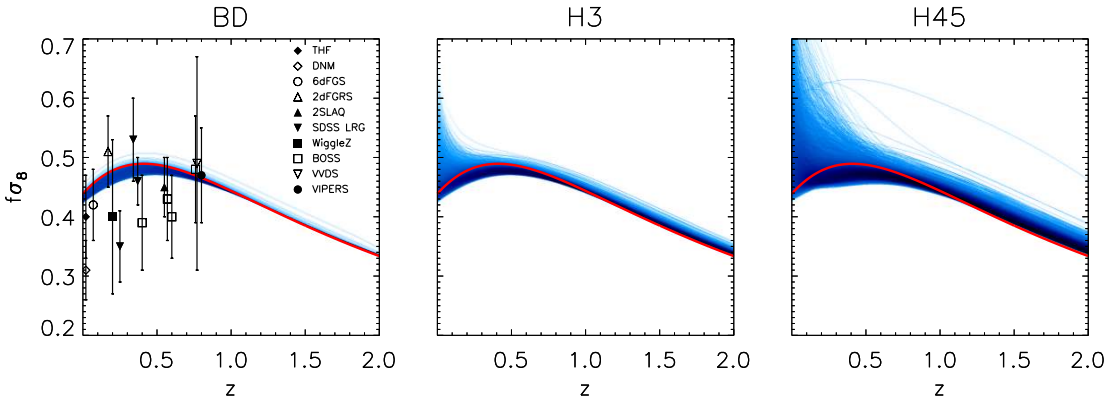

Figure 19: The redshift evolution of $f\sigma_8$ expected in 10^4 viable EFT models is shown and compared to data. The error bars represent 1σ standard deviation. The evolution predicted by the best Planck fit is shown in red.

intermediate epochs in which cosmic acceleration is observed, i.e. in the redshift range $0.5 \lesssim z \lesssim 1$. Figure 18 shows that 95% of the growth rates predicted in the *BD*, *H3* and *H45* classes of theories are weaker than expected in the standard ΛCDM scenario.

These predictions can be compared to observations. A collection of available measurements of the growth related quantity $f\sigma_8$ is presented in Figure 19 and compared to the most generic predictions of *BD*, *H3* and *H45* theories. The current errorbars are still large, therefore one should not read too much into these plots. Nonetheless, it is intriguing that the data suggest less growth than is predicted by ΛCDM. If this holds up in future surveys, it would be important to check that growth is *stronger* than ΛCDM at $z > 1$, as is predicted by the bulk of the models. In fact, recent observations at higher redshifts $z \sim 1.4$ [239], seem to be suggestive of an early epoch with an excess of growth with respect to ΛCDM ($f\sigma_8(z = 1.4) = 0.482 \pm 0.116$ at 1σ), although the error bar being too large it does not yet allow to draw any meaningful interpretations. However, it serves as an illustration that, if such values were to hold up, they would effectively confirm a definitive prediction of linear Horndeski theories.

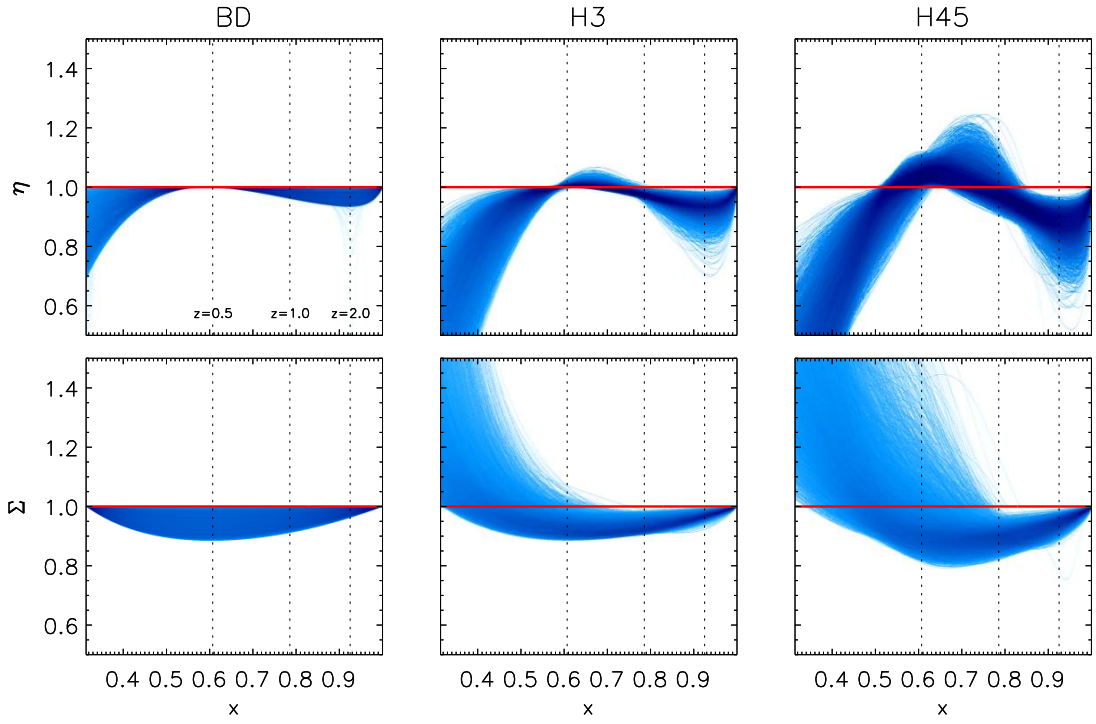

Figure 20: The amplitude of the gravitational slip η and lensing potential Σ as a function of x for 10^4 viable EFT models. The expected values of both these functions in a ΛCDM cosmology are shown in red. The vertical dotted lines correspond from left to right to $z = 0.5$, $z = 1$ and $z = 2$.

Gravitational slip and light deflection parameter

While the peculiar velocity of galaxies falling into the large scale overdensities of matter constrains the possible growth histories of cosmic structures, CMB and weak gravitational lensing provide complementary probe of gravity, notably they allow one to test whether the metric potentials Φ and Ψ are indeed equal, as predicted by GR in the absence of anisotropic stress, or differ as predicted by most non-standard models of gravity. For *BD*-like theories it is straightforward to show analytically that the amplitude of the curvature potential Ψ is never greater than the Newtonian potential Φ, that is, at any epoch, $\eta(t) \leq 1$. For this specific class of theories, the lensing potential reduces to $\Sigma = \mu_{\rm sc}$. From our earlier results (see Figure 20, right panels), we see that this observable cannot be larger than unity at any cosmic epoch, and must be equal to 1 (the ΛCDM value) at the present time.

When additional degrees of freedom are allowed (like in *H3* and/or *H45* models), we still find distinctive features in the evolution of η and Σ. Indeed, the slip parameter is always smaller than unity at any redshift except possibly in the window $0.5 \lesssim z \lesssim 1$, where relevant deviations from the ΛCDM expectations can be observed. Moreover, η is never larger than ~ 1.5 at any cosmic epoch. Similar to the case of *BD*-like theories, the lensing potential Σ is weaker than the standard model value at high redshifts ($z > 0.5$–1), but becomes stronger (greater then unity) in recent epochs. Indeed, virtually all *H3* and *H45* models predict an amplitude of Σ greater than 1 at the present time.

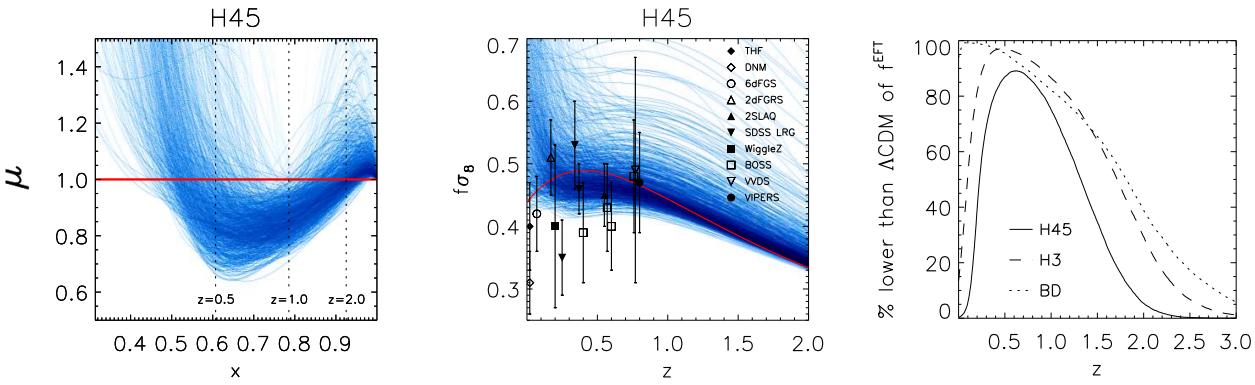

Figure 21: The plots displayed are computed in the w-parametrisation scheme. The evolution of $\mu(x)$ (left panel), $f\sigma_8(z)$ (middle panel) for a sample of 10^3 randomly generated models of viable *H45* theories is shown. The thick red line represents the prediction of ΛCDM. The percentage of 10^4 randomly generated models with growth rate f lower than that predicted by ΛCDM is shown in the right panel.

Different parametrisation scheme

Having seen the pattern of stronger/weaker gravity on predictions of the growth of structures to be mostly regulated by the bare Planck mass M^2, we should asses how these results are affected when the latter is parametrised differently. Authors in [197] have used a specific parametrisation of the Brans-Dicke non-minimal coupling $\mu_1(t)$, based on the "physical" equation of state parameter for DE $w_{\rm de} = p_{\rm de}/\rho_{\rm de}$. This is the equation of state parameter one obtains by matching (250) to that of ΛCDM. We dub this scheme "w-parametrisation" in opposition to the "μ-parametrisation" adopted in this chapter. This parametrisation provides a complementary way to solve the background/perturbation sector degeneracy in the action (273) so that the function $\mathscr{C}$ is no longer free but is directly linked to μ_1. A little bit of algebra is enough to show that μ_1 and the physical equation of state parameter $w_{\rm de}$ are related as follows (see [197] for details)

$$\mu_1(x) = \frac{3\bar{w}H(1-x)}{w-\bar{w}(1-x)}\left[w-\bar{w}+x(1-x)\frac{\bar{w}}{w}\frac{dw}{dx}\right]. \tag{317}$$

One can thus proceed by expanding in a polynomial series the function $w_{\rm de}$

$$w_{\rm de}(x) = \bar{w}\,\frac{1-x_0}{1-x_0(1+\epsilon_4(x_0))^2} + p_1^{(1)}(x-x_0) + p_1^{(2)}(x-x_0)^2\ , \tag{318}$$

instead of μ_1 as we have done in this chapter. The zero-th order term is obtained from the condition $x_0 = \Omega_{m,0}$ we fixed. We keep, however, the other couplings functions expanded as presented in section 3.1.5. We chose to randomly pick $p_1^{(i)} \in [-0.8, 0.8]$ (for $w_{\rm de}$) and $p_{2,3}^{(i)} \in [-2, 2]$ (for μ_3 and ϵ_4) in order for μ curves to have the same amplitude as in the μ-parametrisation. Figure 21 displays some of the results we obtain. The resemblance of μ to the one presented in Figure 16 confirms the robustness of our findings; the universal behaviour of μ (*S-shape*) is recovered no matter what parametrisation is used for μ_1. In addition, the fraction of models with lower/higher growth with respect to ΛCDM displays the same general scaling as a function of z. We find that $\sim 90\%$ of *H45* theories predict growth rates below the ΛCDM prediction in the redshift window $0.5 \lesssim z \lesssim 1$. The change of parametrisation implies a slight modification of the asymptotic behaviour of the coupling functions μ_1 and $\mathscr{C}/H^2$ at $x = 1$, more precisely a modification of the speed at which these

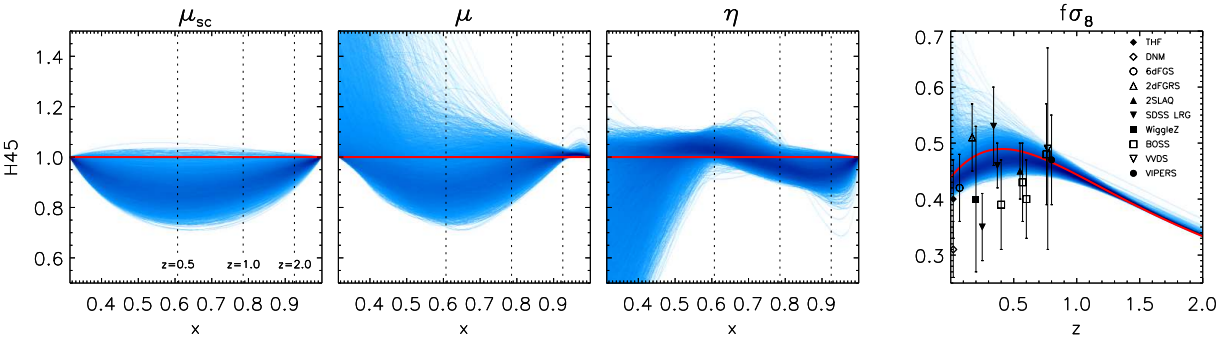

Figure 22: The amplitude of μ_{sc}, μ, η as a function of the reduced matter density x and $f\sigma_8$ as a function of the redshift z for 10^4 viable EFT models where μ_2^2 is switched on. The expected values of both these functions in a ΛCDM cosmology are shown in red. The vertical dotted lines correspond from left to right to $z = 0.5$, $z = 1$ and $z = 2$.

two functions go to zero during mater domination. This is well illustrated by the tail of the curves, the transition to the super-growth epoch is now shifted to higher redshifts ($z \sim 2.5$).

In summary, computing the coupling function μ_1 by a direct expansion as in (304) or computing it with w expanded as in (318), although producing different behaviours of the function μ_1, does not affect our general findings. This gives evidence of the independence of our results from the functional form that has been chosen for the couplings and, indirectly, from the choice of the time variable x. Indeed, it is not difficult to see that expanding in a different time variable is analogous to changing the functional form for the couplings. Therefore, from now on we stay with the "μ-parametrisation".

Gauging the effects of μ_2^2

Let us now allow for the μ_2^2 parameter to be turned on and be free to vary in the interval $[-1, 1]$ as the other couplings. Inspecting Figure 22 tells that μ_2^2, even though only affecting the sound speed, and more precisely the no-ghost stability condition (234), induces non-negligible back reactions on the LSS observables. As expected it significantly broadens the space of viable models. We understood from the previous sections that the period of weaker gravity in $\mu(x)$ at intermediate redshifts was induced by the μ_{sc} component. Figure 22 reveals that switching on μ_2^2 is the necessary condition for LDE models to exhibit $\mu_{sc} > 1$, and thus $M^2 < M_{pl}^2$, in a stable way. Therefore, it leads to a subset of models displaying $\mu > 1$ at intermediate redshifts, *i.e.* stronger gravity (and faster growth) and also deeper gravity potentials than the standard model. Since, under these conditions, light should bend more on average, it does not come as a surprise that models exhibiting $\mu > 1$ in $z \in [0.5, 1]$ also display $\eta > 0$, *i.e.* $\Phi > \Psi$ (or $\Sigma < 1$). Therefore, we conclude that the clear pattern of weaker/stronger growth is partially broken by $\mu_2^2 \neq 0$. It breaks down at low redshift, yet the feature of EFT models predicting more growth than ΛCDM at $z \gtrsim 1.5$ remains.

DIAGNOSTIC OF HORNDESKI THEORIES

From the previous, despite large functional freedom, Horndeski theories seem to produce definite time behaviours in their prediction, provided the viability of models is required. We should thus push the analysis further towards an observable diagnostic. Previous research has shown the

LDE :

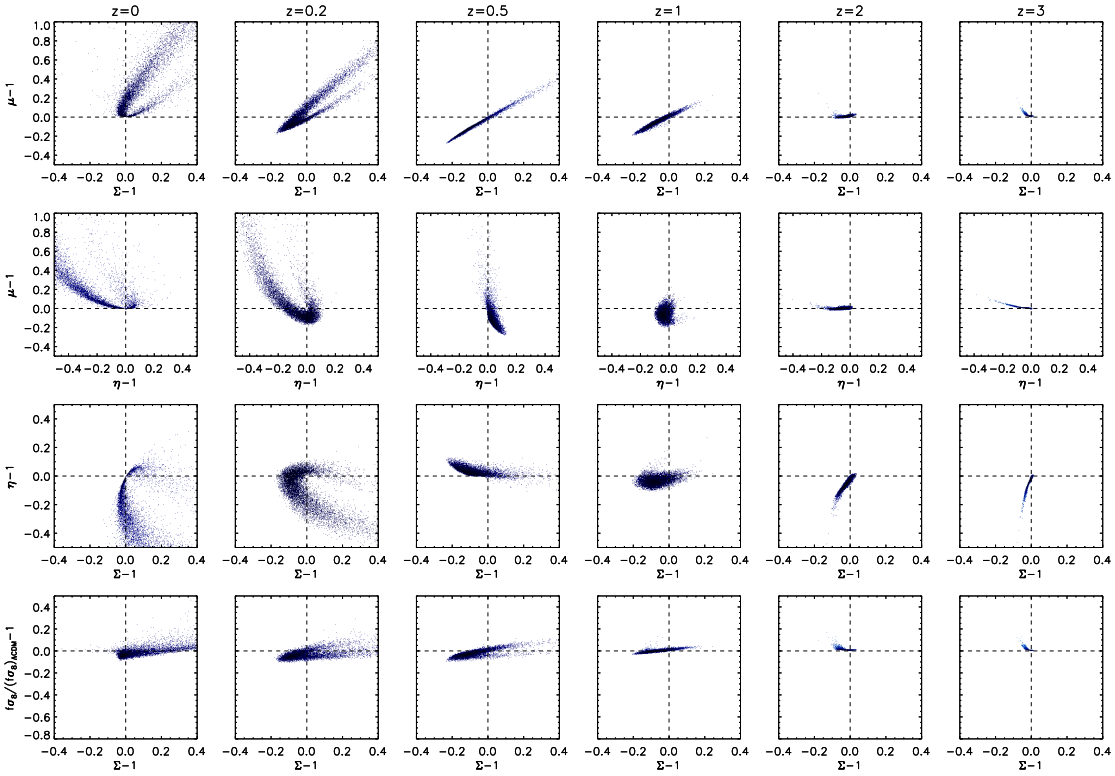

Figure 23: The correlations between μ, η, Σ and $f\sigma_8$ is displayed at several redshift epochs, from left to right $z = \{0,\ 0.2,\ 0.5,\ 1,\ 2,\ 3\}$, for the 10^4 viable EFT models in the LDE scenario. The ΛCDM prediction corresponds to the intersection of the two dashed lines. The gray/blue scale highlights the density of points.

correlations of the LSS observables to provide an effective tool to constrain MG (see for instance [80, 204, 205, 240]). Let us therefore see where do the predictions of linear Horndeski theories stand in these observable plane. We allow now μ_2^2 to vary as the other couplings and study the EDE and EMG scenario by using the Monte Carlo procedure.

Correlations as a diagnostic tool

Inspecting the first row of panels in Figure 23 shows that we recover two definite features: *(i)* the peculiar *S-shape* redshift evolution of the effective Newton constant $\mu(z)$ in LDE models. Notably, the subset of models displaying $\mu > 1$ in the interval $0.5 < z < 1$, have small size relative to the entire set of simulated models and are due to the coupling μ_2^2; *(ii)* the time evolution of μ affects strongly the growth of structures, as captured by the $f\sigma_8$ observable. Figure 23 shows that amplitude of $f\sigma_8$ expected in a ΛCDM model is always minimal if compared to linear Horndeski expectations for $z > 1.5$.

The remarkable tightness of the growth rate evolution of $f\sigma_8(z)$ also deserves a comment. Despite μ, η and Σ spanning, especially at low redshift, a large range of values, absolute deviations of $f\sigma_8$ from the ΛCDM prediction are never larger than 20% at all cosmic epochs investigated. The remarkably low theoretical dispersion, or equivalently, the poor sensitivity of $f\sigma_8$ to the variation of the Horndeski couplings is not, however, prejudicial from the observational side, for the purposes

of model identification. Indeed, it is also remarkable that no single model displays both $f\sigma_8 < 0$ and $\Sigma > 0$ for any $z > 1$. Measurements of $f\sigma_8$ from redshift surveys, when combined with lensing estimations of Σ, provide thus an interesting diagnostic tool: evidences of even a single data point lying in the top right quadrant of the $f\sigma_8 - \Sigma$ plane at redshift larger than 1 would definitely rule out LDE of the Horndeski type as a viable candidate for theoretical interpretation.

Among the features emerging from Figure 23 there is a strong positive correlation between μ and Σ at high redshifts, or, even more telling, the lack of theories predicting $\mu - 1$ and $\Sigma - 1$ of opposite sign as long as $z > 0.5$. When the behaviour of the gravitational slip parameter is closely scrutinized, the fact that both η and μ cannot be positive once $z > 1$ also stands out.

The question is now whether any violation of these features is a smoking gun of the failure of the LDE models only, or, more interestingly, if it can rule out even more general linear Horndeski scenarios. The classification scheme outlined in section 3.1.3 contains the possibility that DE is present early in the matter domination era, either in the energy momentum tensor (EDE) or also as early modified gravity (EMG). Figure 24 shows that the presence of modifications of GR at early times alters the values of LSS observables even in the late universe. Indeed, irrespectively of the specific scenario, viability conditions favour theories with μ smaller than 1 for $z > 0.5$. Despite the fact that we are now allowing initial values of M^2 different than $M_{\rm pl}^2$, the tendency of having $M^2 > M_{\rm pl}^2$ survives. On the other hand, the EMG scenario is the only possibility to produce a small subset of models with $\mu > 1$ at early times. This can be understood by looking at (284). Stability requirements impose $B \geqslant 0$ and $\epsilon_4 \geqslant -1$ ($c_T \geqslant 0$), and the quantity in squared brackets of (283) is by definition greater than or equal to 0. Therefore, allowing non vanishing ϵ_4 and μ_3 at $x = 1$ pushes up the value of μ at early times. The above expression shows that the value of μ at present time, $\mu(x_0)$, is always greater than or equal to unity whatever the DE scenario, a consequence of the expressions (282) and (283). Equation (282), as we recall, also illustrates the competition between the two major physical mechanism that contribute to the amplitude of the gravitational coupling, we recall : *(i)* the fifth force induced by the scalar field, which must always be attractive, hence larger than unity, for a massless spin 0 field (embodied by the term in squared brackets) and *(ii)* the possibility of realising weaker gravity through the $M^{-2}(1+\epsilon_4)^{-2}$ component, which, as pointed out in section 3.2.1, is related to the amount of self-acceleration a model produces.

The behaviour of μ at early times affects the $f\sigma_8$ observable at late epochs. For instance, the amplitude of $f\sigma_8$ predicted in EDE scenarios is lower than the standard ΛCDM value for $z > 0.5$, as opposed to LDE, for which models systematically flip over ΛCDM at $z \gtrsim 1.5$. Therefore, the ΛCDM growth history appears as an extremum on wide redshift intervals not only among the whole class of LDE models, but also when EDE scenarios are considered. Intriguingly, only EDE models manage to strongly suppress the amplitude of the linear growth function at present time. On the opposite, the only models allowing for a faster growth than ΛCDM (with $f\sigma_8$ more than 20% higher), are the EMG scenarios. This is not surprising for, as we said, it is the only set-up for which $\mu > 1$ at early times.

The asymptotic value of the gravitational slip parameter η at $x = 1$ is, by definition, 1 when the coupling functions μ_3 and ϵ_4 vanish. Therefore, only very mild differences arise between LDE and EDE at early times. On the contrary, the redshift dependence of η is significantly affected in the EMG case, since μ_3 and ϵ_4 are different from zero at all cosmic epochs. As far as the evolution of Σ is concerned, the amplitude calculated in LDE and EDE scenarios is always lower than ΛCDM for $z > 1.5$. Once more, the standard model appears as an extremal model. EMG is the only mechanism enabling Σ to be greater than unity also at high redshifts.

EDE :

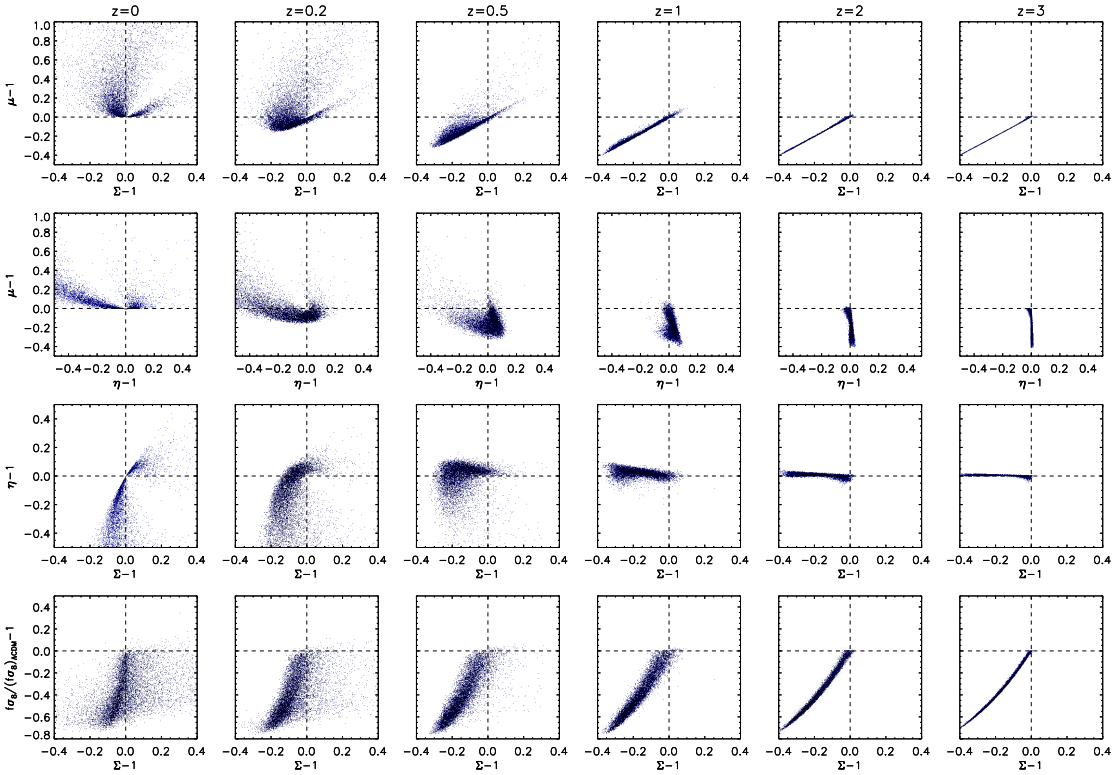

EMG :

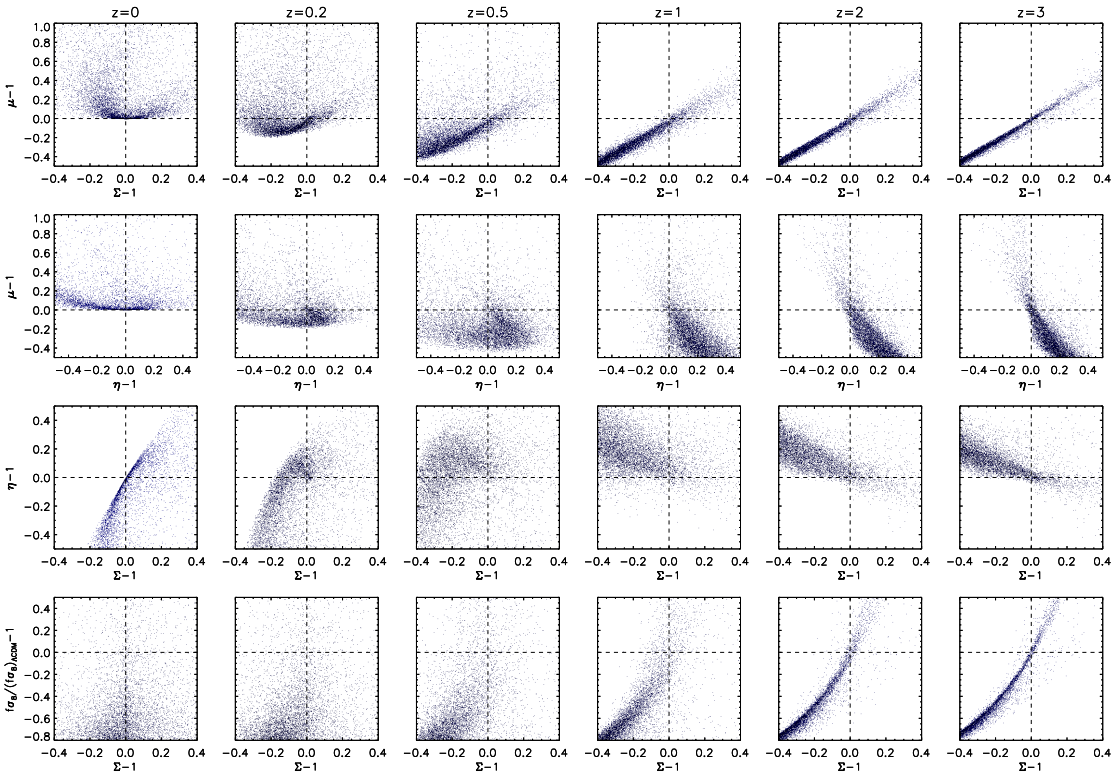

Figure 24: Same as in figure 23 but for 10^4 viable models in the EDE and EMG scenario.

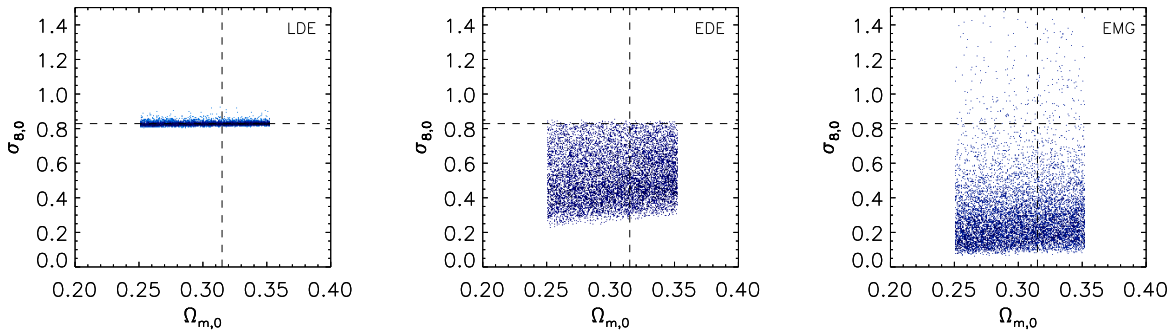

Figure 25: Present day value of σ_8 as a function of the fractional matter density today $\Omega_{m,0} = x_0$ of 10^4 EFT models. Here, the value of $\Omega_{m,0}$ per model is left as free parameter and is randomly generated, as are the coefficients of the coupling functions. The background has been set to a flat ΛCDM background. The intersection of the dashed lines corresponds to the Planck measurements [54].

The positive correlation marked between μ and Σ for $z > 1.5$ persists in EDE models as it did in LDE models. In fact, since

$$\mu - 1 = \left(\frac{2}{1+\eta}\right)(\Sigma - 1) - \frac{\eta - 1}{1+\eta}\,, \tag{319}$$

a $\sim 45^\circ$ correlation should be seen as long as η is close to unity. This stands out clearly, at high redshifts, for LDE and for EDE scenarios, as opposed to the EMG case which displays slightly more dispersion, for it exhibits larger values of η. Assuming a non-standard gravitational signal would be detected by future surveys, we can therefore tentatively conclude from comparing Figs. 23 and 24 that the linear Horndeski class of models would be ruled out by high redshift measurement if μ and Σ have different sign for $z > 1.5$. The same conclusion holds if future estimates should eventually converge on a local ($z = 0$) value of the effective Newton constant lower than unity, since $\mu_{\rm ff}(x_0) \geq 1$ and $\mu_{\rm sc}(x_0) = 1$ by definition. In addition, we observe a systematic increase in the scatter of the η values, first when considering the μ_2^2 parameter to not be zero at all times in the LDE case, and then when allowing more generic initial conditions such as in the EDE and EMG scenarios.

In much of the same way as the plane μ–Σ provides a diagnostic for the whole class of linear Horndeski models, the plane $f\sigma_8$–Σ allows us to tell apart linear Horndeski DE sub-classes. For example, if $f\sigma_8 > (f\sigma_8)_{\Lambda CDM}$ at $z > 1.5$, then EDE scenarios are ruled out. Similarly, LDE is not viable if both $f\sigma_8$ and Σ have smaller amplitude than predicted by ΛCDM for $z > 1.5$.

Identical conclusions follow from the analysis of the amplitude of the σ_8 observable alone. Figure 25 shows the present-day linear extrapolation $\sigma_{8,0}$, which we assume to be normalized by the Planck measurements at last scattering. Predictions closely reproduce the ΛCDM limit in all the LDE models. However, a local measurement of σ_8 showing large deviations from the ΛCDM extrapolation will be instrumental for disentangling EDE from EMG scenarios. The first would be definitely ruled out if observational evidences should indicate that $\sigma_{8,0} \gtrsim 0.9$. The EDE and EMG scenarios could thus be a way to release the $\sigma_{8,0}$ tension we discussed in section 1.5.3. We note that lower values of σ_8 are also found in the "kinetic matter mixing" model considered in [192].

In summary, we find the effects of early modification of GR to be conspicuous also at low redshift. Joint measurements of the η, Σ and $f\sigma_8$ observables would give strong indications as to the type of DE required for a faithful description of cosmological perturbations. Indeed, complementing an

analysis on the growth of structures with lensing observables increases substantially the discriminating power between models.

Consistency checks

Let us investigate under what changes the observable diagnostic depicted in the previous section might change. As a first test, we have checked whether the correlations we find are unchanged even if the coefficients are picked from Gaussian distributions centred around 0, the ΛCDM value, and with a standard deviation of 1. More interestingly, in the following we assess the impacts of relaxing some of the viability conditions, the propagation speeds, and the change of the background equations of state parameter $\bar{w}$.

Testing viability conditions

When dealing with the dark sector it is still, debated whether super-luminal propagation in a low-energy effective theory can be acceptable. We tend to see super-luminality as a serious pathology of a low-energy theory, following the reasoning in [231]. However, for the sake of generality, in Figure 26 we show the effects of relaxing the conditions on the propagation speeds of the scalar and the tensors modes.

It is worth noting that, in our formulation, a theory exhibiting $c_s > 1$ can always be tuned back to $c_s \leqslant 1$ by using the parameter μ_2^2. The latter, as we recall, does not enter the expressions of the LSS observables. Therefore, switching on μ_2^2 allows one to include linear Horndeski models with $c_s > 1$ but $\mu_2^2 = 0$, in some sense. This is well illustrated in Figure 26 since the predictions with the conditions S and the condition $S + c_s$ are virtually the same. One can rightfully conclude that the selection criterion $c_s < 1$ is useless once a non null μ_2^2 is considered.

On the other hand, by writing μ as

$$\mu = \left(\frac{c_T}{c_T(x_0)}\right)^4 \frac{M^2(x_0)}{M^2} \frac{a_0}{b_0}\,, \tag{320}$$

one already appreciates analytically how $c_T > 1$ strengthens gravity at high redshifts. This is highlighted by Figure 26, the correlation lines of in the μ–Σ or $f\sigma_8$–Σ planes are thinner once the $c_T \leqslant 1$ is implemented. The practical conclusion out of this analysis is if a data point was to be found at high redshifts in the top left corner of either the μ –Σ or $f\sigma_8$–Σ plane, only a linear Horndeski model with a $c_T > 1$ would be valid. More will be able to be said once c_T is tightly constrained at large redshifts by future measurements of the electromagnetic counter part of gravitational wave emitting events [241, 242].

Changing the background

Does the evolution of perturbed sector observables depend on the acceleration of the background metric? What we find is that setting $\bar{w} = -0.9$ does not change the diagnostic described in the previous section. We thus do not display plots to be concise. The effect of lowering the DE equation of state below $\bar{w} = -1$ is also very mild, but worth commenting. Crossing the $\bar{w} = -1$ means considering violations of the null energy condition. Such violation can be produced in a stable theory only by switching on the non-minimal gravitational couplings (see Figure 1 and 2 in [197]), and therefore in a region of the space of theories that is "far" from ΛCDM (where all couplings vanish). Nevertheless, the effects of MG are not significantly amplified as it can be seen by comparing

S :

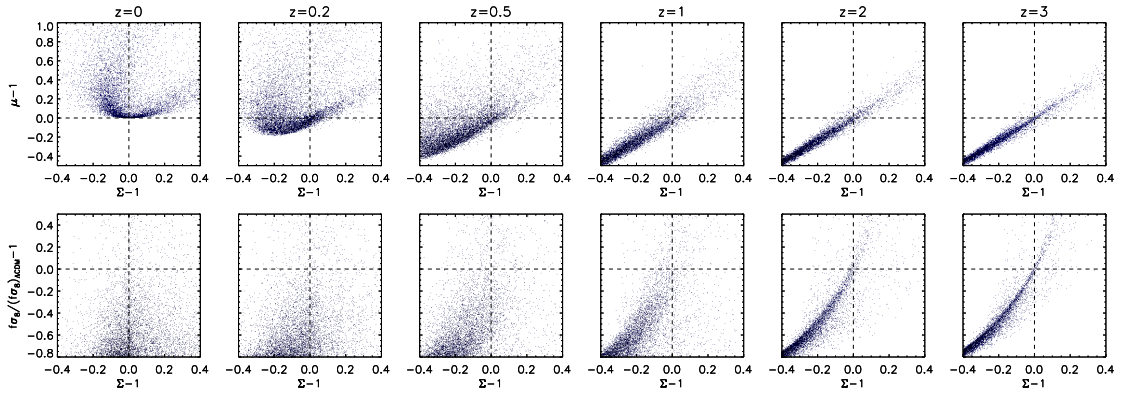

$S + c_s$:

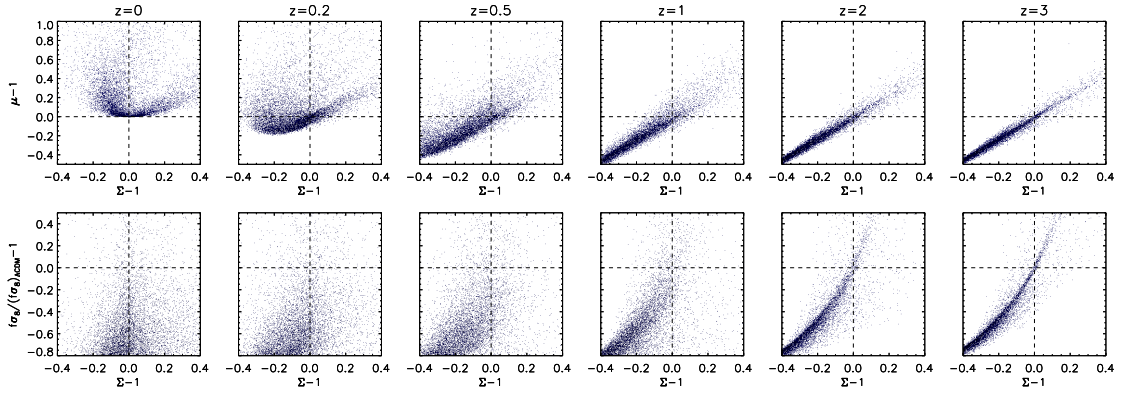

$S + c_T$:

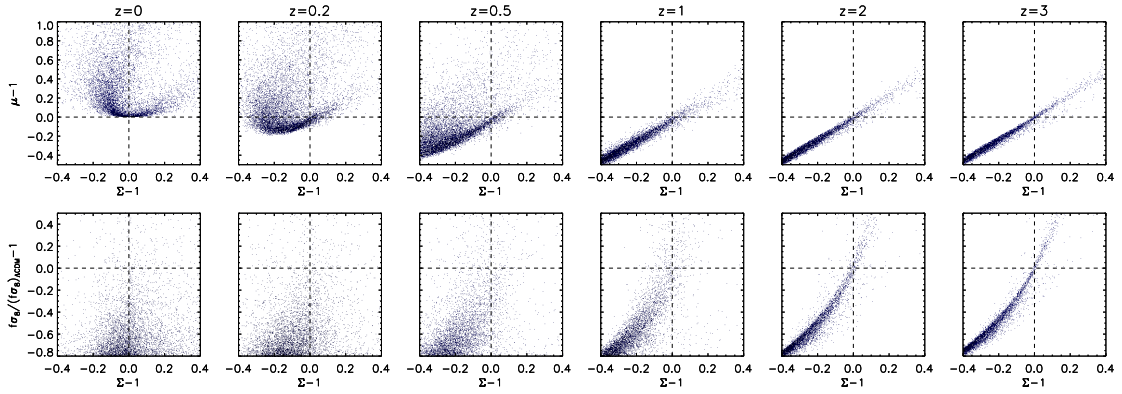

Figure 26: Correlations in the μ–Σ and $f\sigma_8$–Σ planes for 10^4 EMG models with the stability condition S (first two rows), the stability condition S and $c_s \leqslant 1$ (middle two rows) and the stability condition S and $c_T \leqslant 1$ (bottom two rows). The background evolution has been set to a flat ΛCDM. The ΛCDM prediction stands at the intersection of the two dashed lines.

LDE :

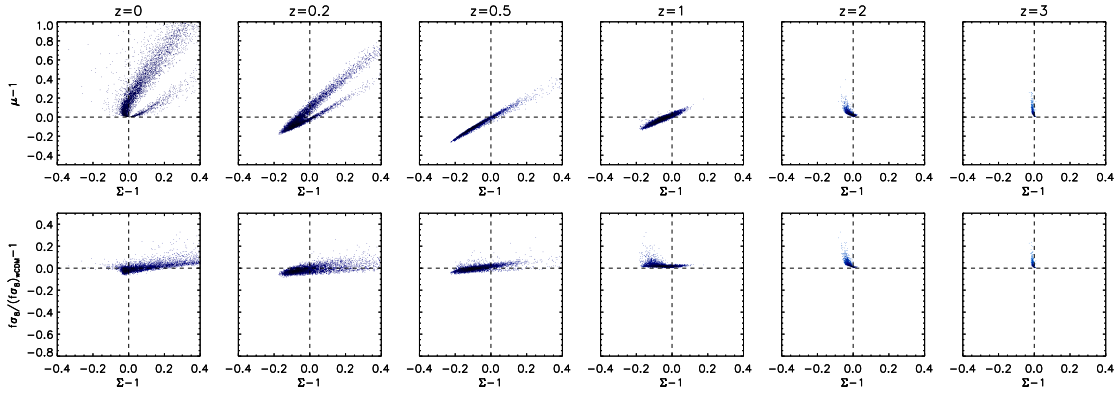

EMG :

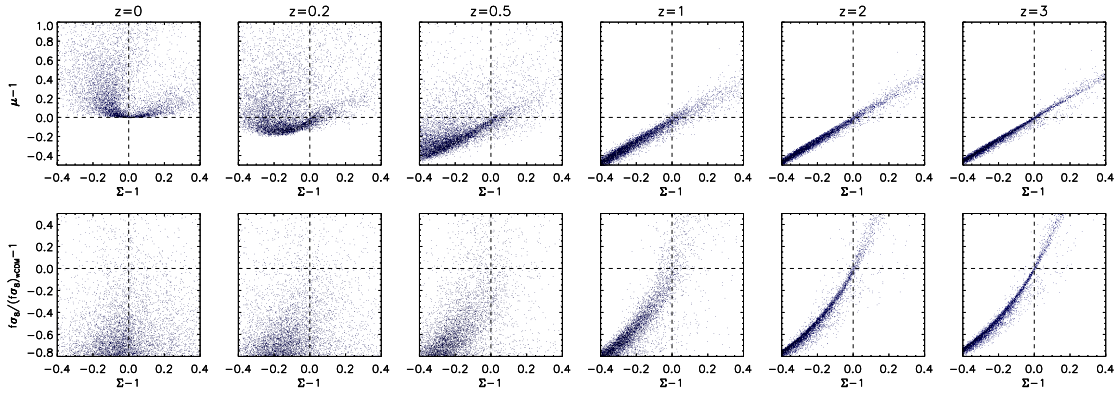

Figure 27: Correlations in the μ–Σ and $f\sigma_8$–Σ for 10^4 LDE models (top two rows) and 10^4 EMG models (bottom two rows) with the full viability conditions requested but the background *e.o.s* set to $\bar{w} = -1.1$. The $(w = -1.1)$CDM prediction corresponds to the crossing of the two dashed lines.

Figure 23 and 24 to Figure 27. The amplification effect is effectively compensated by the wide variations of the couplings and by the large volume in the theory space that we are considering, even in the $\bar{w} < -1$ case. In summary, we do not find distinctive definite features of LSS phenomenology characteristic to stable violations of the null energy condition.

CONCLUSION

In the first part of this chapter, we have seen that LSS observables in linear Horndeski theories can be economically described in terms of two constant parameters, $x_0, \bar{w}$, which control the evolution of the background metric, as well as four functions $\mu_1(t)$, $\mu_2^2(t)$, $\mu_3(t)$ and $\epsilon_4(t)$ which, being active in the perturbation sector, determine how matter fluctuations evolve in time at the linear level. Then we chose to scan the theory space by generating the expansion coefficients of the EFT functions in a Monte Carlo fashion and required the background expansion rate $H(z)$ to be that of a ΛCDM model.

This procedure has enabled us to show that under strict viability requirements, linear Horndeski theories do present bounded time trends for LSS observables and that the ΛCDM predictions often stands out as an extremal model. Pushing the analysis further, we have achieved an observable diagnostic of linear Horndeski theories. The EFT of DE also allowed us to investigate what Horn-

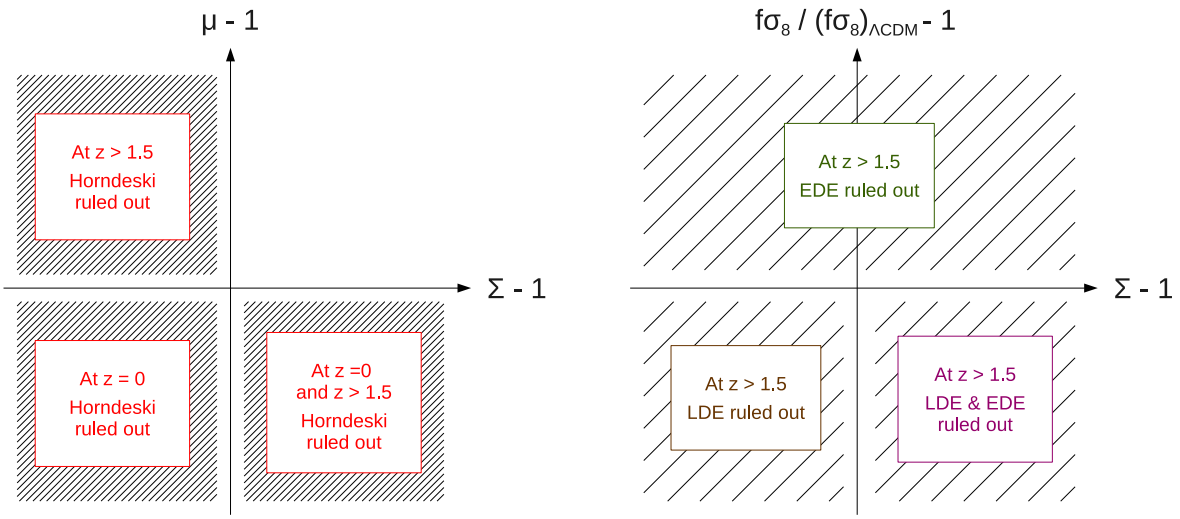

Figure 28: Schematic diagrams of the fundamental observable planes allowing to discard linear Horndeski theories (left diagram) and the type of DE embedded (right diagram).

deski theories "had to say" about early DE. The observable diagnostic and the answer to the latter question can be effectively summarized in Figure 28. By tracing the time evolution, from early epochs ($z = 100$) down to present day, of fundamental LSS observables such as the reduced effective Newton constant μ, the gravitational slip parameter η, the lensing parameter Σ and the linear growth function of LSS $f\sigma_8$ we have found that GR extensions contemplating an additional scalar degree of freedom with second order equations of motion can be definitely ruled out if one of the following conditions apply (Figure 28, left panel):

- The observables μ and Σ have an opposite sign for $z > 1.5$
- $\mu < 1$ at $z = 0$

Specific sub-classes of such theories in which the MG effects are limited to late times could be discriminated if data at redshift $z > 1.5$ eventually become available for both redshift and lensing surveys. Indeed, we find that above that critical redshift (Figure 28, right panel):

- LDE will be ruled out if $f\sigma_8 < (f\sigma_8)_{\Lambda CDM}$ at $z > 1.5$
- EDE will be ruled out if $f\sigma_8 > (f\sigma_8)_{\Lambda CDM}$ at $z > 1.5$ or $f\sigma_8 > (f\sigma_8)_{\Lambda CDM}$ and $\Sigma > 1$ at $z > 1.5$

These results are insensitive to the background DE $e.o.s$ parameter within the reasonable range $\bar{w} \in [-1.1, -0.9]$. We have also found the diagnostic not to lose predictability when progressively less constraining viability requirements are imposed.

Furthermore, measurements of low $f\sigma_8$ amplitudes,with respect to the Planck-extrapolated value, provided by local redshift surveys seem to be quasi systematic, especially in analyses where the background is decoupled from the perturbation sector (see [3–6] for instance) and linear Horndeski theories seem follow the trend. Recalling discussion on the $\sigma_{8,0}$ tension in section 1.5.3, one can clearly feel from our analysis that linear Horndeski theories would help in alleviating this tension.

In light of this chapter, there is still much to be accomplished and a number of improvements would be welcome. We have focused on scales much smaller than the Hubble radius. As data improves on larger scales, our analysis should be extended to include possible scale dependent effects coming

from mass terms of the scalar field that are of the order of Hubble. Lastly, it would be useful to study to which level our diagnostic plots are stable to the inclusions of more general scenarios such as GLPV theories or when conformal-disformal couplings of matter to gravity are considered [7].

4

PHENOMENOLOGY WITH THE EFFECTIVE FIELD THEORY OF DARK ENERGY

In this final chapter, we shall give a review of the phenomenological results obtained with the EFT of DE up till now. This literature review is thus meant to provide the state of the art of the EFT of DE field and we shall use it to contextualise the results obtained in the previous chapter when possible.

The straightforwardness of the EFT of DE for computing predictions and for singling out theoretically viable models has led to many studies and results. An important factor of the outreach of the EFT of DE stems from its inclusion into Einstein-Boltzmann codes. The first of which being EFTCAMB, an extension of CAMB (Code for Anisotropies in the Microwave Background) [44]. This code is based on the formulation of the EFT from [176]. The hi_class (Horndeski in the Cosmic Linear Anisotropy Solving System) [207] extension to CLASS (the Cosmic Linear Anisotropy Solving System) [45] and COOP (Cosmology Object Oriented Package) [243] also exist, both are based on the α-basis [183].

In this chapter we will first present the novel predictions unveiled thanks to the EFT of DE before concentrating on the observational constraints it has produced. Then, we will show how the EFT of DE has been used in astrophysical context. We finish by discussing further investigations and conclude by highlighting the caveats in the EFT of DE.

NOVEL PREDICTIONS

Let us start by presenting an alternative formulation of the EFT of DE that parametrises linear Horndeski and GLPV theories before entering a general discussion of the predictions obtained using the EFT of DE. The goal of this section is to highlight how the "user-friendly" parametrisation of observables, stability conditions and the straightforward numerical implementation of the MG theories provided by the EFT of DE has lead to a number of novel and specific predictions.

The α-basis

The alternative parametrisation of EFT of DE, we dub the α-basis as opposed to the μ-basis we have used in the previous chapters, was recently found in [183] and further developed in [244, 245]. It has substantially contributed the release of novel predictions and constraints. The α-basis has the benefit of attaching the evolution of coupling functions to clear physical effects. However, the theory-friendly view point is lost, subsets of Horndeski theories are described by more involved combinations of the coupling functions as compared to the μ basis. The quadratic action in the α-basis for GLPV theories is the most concise in the unitary gauge following the ADM decomposition. In this case, the line element yields

$$ds^2 = -N^2 dt^2 + h_{ij}(dx^i + N^i dt)(dx^i j + N^j dt) \tag{321}$$

where N^2 is the lapse, N^i is the shift, and the action yields [244]

$$\begin{aligned} S = \int d^4x \, \frac{M_*^2(t)}{2} \Big\{ & \delta_2 \Big[\sqrt{-g} \Big({}^{(4)}R - 6H^2 + 2\rho_{\rm m}/M_*^2 - \frac{2}{N}\big(2\dot{H} + (\rho_{\rm m} + p_{\rm m})/M_*^2\big)\Big)\Big] \\ & + 2H\alpha_M(t)\delta_2\big[\sqrt{h}(K - 2H)\big] + \alpha_T(t)\delta_2\big(\sqrt{h}\,{}^{(3)}R\big) \\ & + a^3H^2\alpha_K(t)\delta N^2 + 4a^3H\alpha_B(t)\delta N\delta K + a^3\alpha_H(t)\delta N\,{}^{(3)}R\Big\}\,, \end{aligned} \tag{322}$$

where δ_2 refers to taking the expansion at second order in perturbations, h is the determinant of the spatial metric h_{ij}. Similarly to the μ-basis, the time variation of Planck mass is quantified by the non minimal coupling

$$\alpha_M = \frac{1}{H}\frac{d\ln M_*^2}{d\ln t}\,. \tag{323}$$

A Horndeski model in the α-basis is thus described by 5 functions of time

$$\Big\{\rho_{\rm m,0},\, H(t),\, \alpha_M(t),\, \alpha_K(t),\, \alpha_B(t),\, \alpha_T(t)\Big\}\,, \tag{324}$$

where all the α coupling functions bear a distinct physical effect:

- α_M is the *running Planck mass rate*. It has contributions from the G_4 and G_5 functions of the Horndeski action (194).
- α_K is the *kineticity*. It measures the intrinsic dynamics of scalar field, *i.e.* that arising from its kinetic energy term. It bears contributions from all the G_i functions.
- α_B is the *braiding*. It quantifies the coupling between the scalar field and the metric, *i.e* their kinetic mixing. It regulates also the clustering of dark energy. It has contributions from the G_3, G_4 and G_5 functions.
- α_T is the *tensor speed excess*. It regulates the excess speed of gravitational waves as $\alpha_T = c_T^2 - 1$. It does not vanish in models where a non-linear derivative coupling of the scalar field to the metric is considered. It has contributions from the G_4 and G_5 functions.
- α_H is the *Beyond Horndeski coupling*. It quantifies "non-Horndeski-ities" and one recovers Horndeski theories by setting $\alpha_H = 0$.

The mapping to convert the α to the μ-basis is given by

$$M_* = M\sqrt{1+\epsilon_4}\,, \tag{325}$$

$$\alpha_M = \frac{\dot{\epsilon_4}}{H(1+\epsilon_4)} + \frac{\mu_1}{H}\,, \tag{326}$$

$$\alpha_K = \frac{2\mathscr{C} + 4\mu_2^2}{H^2(1+\epsilon_4)}\,, \tag{327}$$

$$\alpha_B = \frac{\mu_1 - \mu_3}{2H(1+\epsilon_4)}\,, \tag{328}$$

$$\alpha_T = -\frac{\epsilon_4}{1+\epsilon_4}\,, \tag{329}$$

$$\alpha_H = \tilde{\epsilon}_4 - \epsilon_4\,. \tag{330}$$

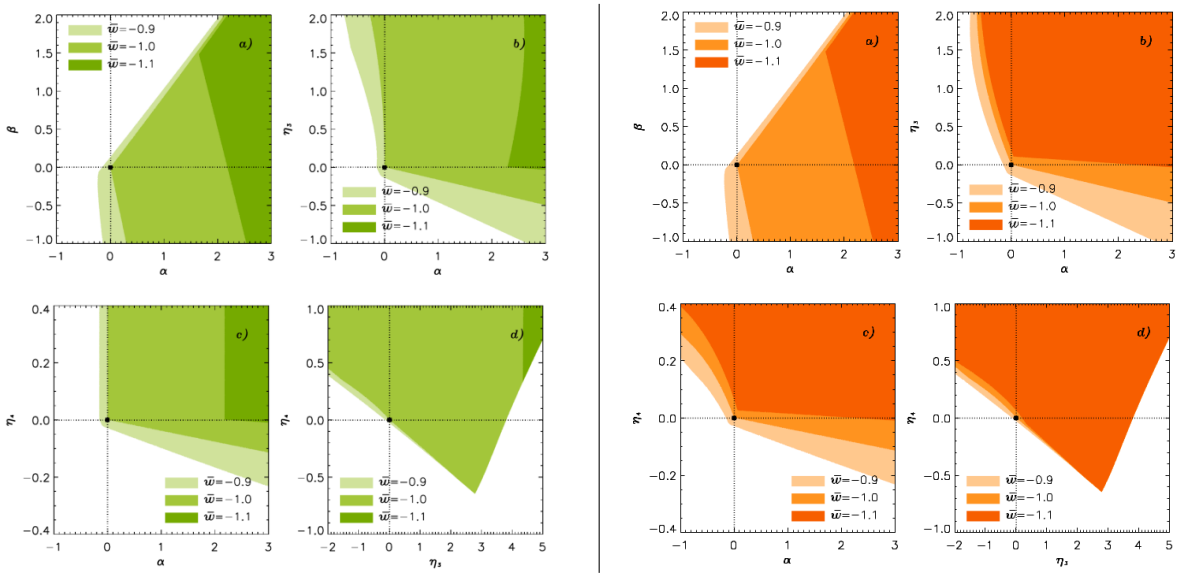

Figure 29: Figure 1 and 2 in [197]. The stability regions of the Linear Horndeski theories are shown. The results have been obtained in an order zero expansion of the coupling function μ_2^2, μ_3 and ϵ_4 (η_2, η_3 and η_4 are the coefficients respectively) while the coupling μ_1 is specifically parametrised with the parameters α and β (see [197] for details). The *left panel* displays the results for $\eta_2 = 0$ and *right panel* for $\eta_2 = 10^6$.

Impact of stability conditions

Having the stability conditions expressed in terms of the EFT coupling functions makes assessing whether a model is viable or not direct. In this respect, the first article in which the EFT of DE was used to obtain predictions focused, among others, on the impacts of stability conditions for several values of the background equation of state [197]. As showed in Figure 29, the stability conditions shrink the allowed space of EFT parameters up to the point where ΛCDM corresponds to a corner of the stability region. This picture highlights well the fact that ΛCDM corresponds to the EFT stability functions (A and B) being strictly equal to zero (see. section 2.3.3). In the realm of scalar tensor theories, ΛCDM stands at the border. More importantly, this analysis reveals the location in the parameter space of models within the linear Horndeski class which violate the null energy condition in a stable manner, *i.e.* super-accelerating models ($\bar{w} < -1$). The space of such models shrinks when the background equation of state decreases. In particular, the ΛCDM origin is no longer at the border of the space but well outside of it. This begs the conclusion that a non-minimal coupling must be switched on in order to have stable violations of the null-energy condition.

The results we have discussed in chapter 3 are a direct follow up to this study of the impact of stability conditions detailed above. The latter were shown to significantly cut the parameter space and to leave ΛCDM at the border. Therefore, looking for bounded trends on observables and comparing them to ΛCDM was the natural next step. We will see further on in this chapter that the stability conditions have been revealed to be useful strong priors when constraining models with data. In chapter 3, we do recover some of the features discussed in [197]. The shrinking of the stability space when going to $\bar{w} < -1$ transpires in our diagnostic for which, in this case, the spread of the models in the correlations shrinks. We also discussed how μ_2^2 had the effect of

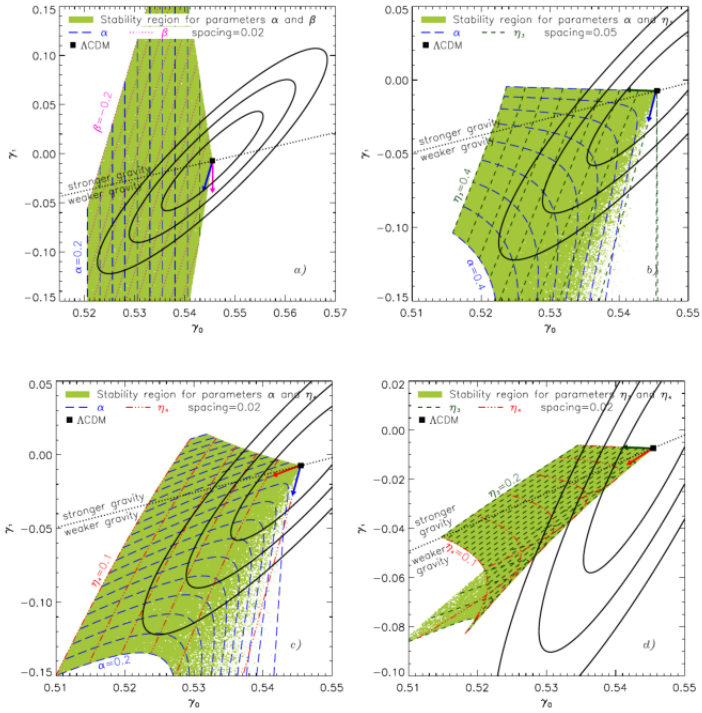

Figure 30: Figure in 3 [197]. Stable regions of Horndeski theories in the $\gamma_0 - \gamma_1$ plane from the EFT framework. The dotted line corresponds to the boundary between stronger and weaker gravity predictions with respect to ΛCDM. The 68%, 95% and 99% likelihood contours correspond to the constraints forecasted for a EUCLID-like survey.

broadening the space of stable models. This transpired for the major part on the behaviour of the M^2 component (in $\mu_{\rm sc}$), hence also on the low redshift predictions of $f\sigma_8$. The right panel of Figure 29 shows how the stability regions are broadened when μ_2^2 is switched on. In particular, although the parametrisation is not strictly the same as us and here μ_2^2 has a huge value today, one can see how μ_2^2 switched on allows: *(i)* to open the region for $\alpha < 0$ which coincides with enabling $\mu_{\rm sc} > 1$, while η_3 and η_4 are virtually unaffected which coincides with $\mu_{\rm ff}$ being unaffected; *(ii)* the $\bar{w} < -1$ case to crawl back on the stability space covered by the other two cases $\bar{w} = \{-1.0, -0.9\}$.

Growth history

A goal one is after when considering MG theories is predictions of lower growth at low redshift so as to palliate for the tension on the $\sigma_{8,0}$ measurements (see section 1.5.3). However, it is generally not expected of scalar-tensor theories to produce lower growth than that of ΛCDM since the fifth-force strengthens gravity by definition. The EFT of DE has contributed for the major part in showing it is not, in fact, always the case for linear Horndeski models. The likeliness of Horndeski theories to produce lower growth was shown first in [197] by considering the growth index parametrisation of the growth rate:

$$f = \Omega_{\rm m}^{\gamma_0 + \gamma_1 \ln(\Omega_{\rm m})} . \tag{331}$$

Considering a ΛCDM background evolution, authors have shown (see Figure 30) that, given stability conditions, the space of theories leading to weaker gravity in the $\gamma_0 - \gamma_1$ plane is much larger than that of stronger gravity. In other words, Horndeski theories are more likely to produce

models which exhibit weaker gravity than stronger as compared to ΛCDM. This fact was highlighted, in chapter 3, from the time evolution of the $f\sigma_8$ predictions, the correlations and also in the $(\sigma_{8,0}, \Omega_{m,0})$ plane (Figure 30). In is interesting to note also that in Figure 30 ΛCDM stands clearly at the corner of the accepted region in the $\gamma_0 - \gamma_1$ plane. This is not necessarily to be expected since it corresponds to an involved parametrisation of an observable and not directly to the stability conditions. This is what gave us the hint that we should search for an extremising behaviour of ΛCDM in $f\sigma_8$ predictions for Horndeski theories. We found it to exist, however, μ_2^2 is the key function modulating the redshift intervals on which ΛCDM is extremal.

The analytical prescriptions for Horndeski theories to display weaker gravity were explained first in [237]. The author showed that the two key quantities were c_T and $\Omega_{\rm m}$. This amounts to the same conclusions we have found from a different perspective through the behaviour of $\mu_{\rm sc}$. Indeed, c_T, *i.e.* α_T or ϵ_4 depending on the basis, is one the two quantities in $\mu_{\rm sc}$ (see (282)) and the other being M^2. The latter can be linked to $\Omega_{\rm m}$ as follows. When we set the background evolution of the EFT models to that of ΛCDM in section 3.1.1, it implies we are setting in fluid description

$$H^2 = \frac{1}{3M^2(t)}(\rho_{\rm m} + \rho_{\rm de}) = \frac{1}{3M_{\rm pl}^2}(\bar{\rho}_{\rm m} + \bar{\rho}_{\rm de}). \tag{332}$$

In the previous equation, $\bar{\rho}_{\rm m}$ and $\bar{\rho}_{\rm de}$ correspond to the effective background (ΛCDM) while $\rho_{\rm m}$ and $\rho_{\rm de}$ are the physical densities the model would exhibit in a fluid description. In fact, if one wants to stick with a fluid description of the model, equation (332) is the equation one should use to define $\rho_{\rm m}$ and $\rho_{\rm de}$ given a chosen effective background. Defining $\Omega_{\rm m} = \rho_{\rm m}/(\rho_{\rm m} + \rho_{\rm de})$, $\bar{\Omega}_{\rm m} \equiv x = \bar{\rho}_{\rm m}/(\bar{\rho}_{\rm m} + \bar{\rho}_{\rm de})$ and using $\rho_{\rm m} = \bar{\rho}_{\rm m}$ implies from (332)

$$\frac{x}{\Omega_{\rm m}} = \frac{M^2}{M_{\rm pl}^2}\,. \tag{333}$$

Therefore, the interpretation of weaker gravity in $\mu_{\rm sc} \propto M^{-2}(1+\epsilon)^{-2}$ induced by $M^2/M_{\rm pl}^2 > 1$ is equivalent to $\Omega_{\rm m} < x$. In summary, whether one thinks in terms of $\Omega_{\rm m}$'s or the bare Planck mass M^2, the important point is that Horndeski and GLPV theories naturally produce a fifth force, the scalar-matter coupling, but also produce intrinsic (un-screenable) modifications of the gravitational interaction, and it is the latter that is responsible for predictions of lower growth at low redshifts. The author in [237] has also shown that the extra freedom in GLPV theories makes them more compatible with redshift-space distortions measurements than Horndeski theories. This is indeed because GLPV theories have more freedom in general, in particular, it can be explained in the EFT of DE language since one can show for GLPV theories that

$$\mu_{\rm sc} = \frac{M_{\rm pl}^2}{M^2}\frac{c_T^2}{(1+\alpha_H)^2}\,, \tag{334}$$

thereby α_H gives an extra freedom on top of M^2 and c_T to modulate the stronger/weaker gravity pattern through $\mu_{\rm sc}$, hence fit RSD data in a even more flexible way as compared to Horndeski theories.

Observational signatures on cosmological spectra

Let us now move on to the effects the EFT parameters within the Horndeski class have been shown to produce on the angular power power spectrum, lensing spectrum and bi-spectrum. While the

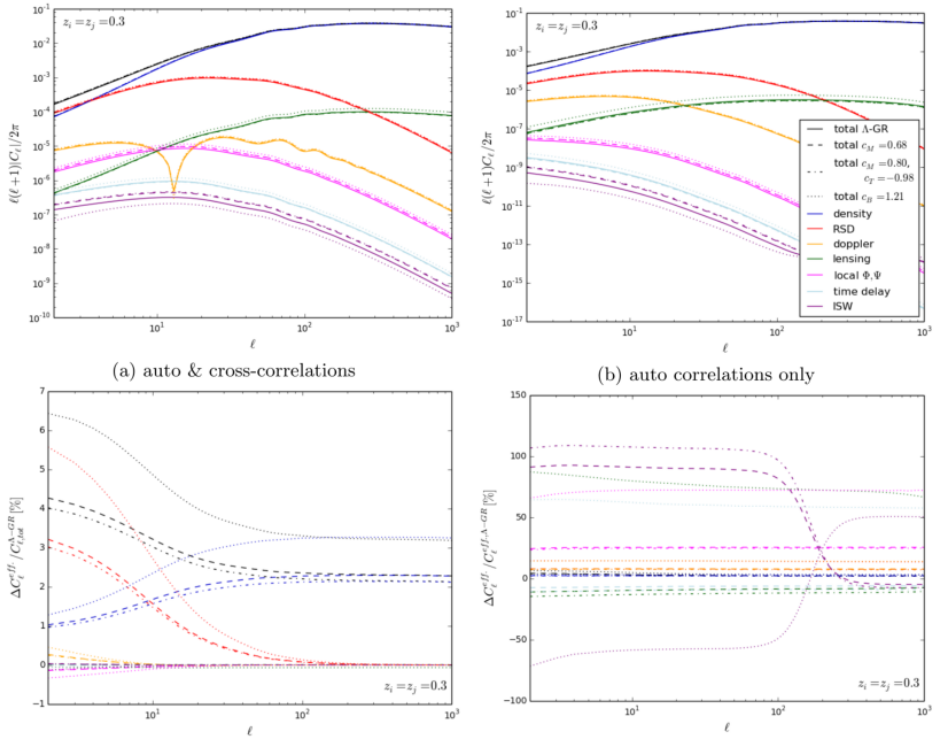

Figure 31: Figure 3 in [246]. Several relativistic contributing to the galaxy number count angular power spectrum are shown for the correlation of the redshift bin $z = 0.3$ with itself. ΛCDM and Galileon models with specific values of the EFT parameters are considered. The *top-left* panel displays the relativistic effects including their cross-correlation with density whereas the *top-right* panel shows the pure auto-correlation. The lower panels correspond to the relative difference of each cases with respect to ΛCDM.

hight and position of the acoustic peaks of the angular power spectrum should not be affected much by the EFT coupling functions since the former are essentially controlled by the energy densities, they will have a clear effect on low multipoles ($l \lesssim 20$) through the ISW effect (see also section 4.2.2). Such effects can be seen at larger multipoles ($l \lesssim 300$) on the lensing power spectra. Both effects have been illustrated in Figure 1 of [247], for instance.

Integrated quantities along the line of sight are indeed of paramount importance when considering MG power spectra. Authors in [246] have shown that Galileons models can produce up to $\mathcal{O}(1000\%)$ deviations from GR on the ISW effect, while they only yield $\mathcal{O}(10\%)$ deviations on $f\sigma_8$. The effects induced by these integrated quantities are especially dominant when considering correlations of galaxy number counts at different redshifts and can add-up to $\sim 50\%$ deviations in the total signal which could be observable with future surveys. This highlights the importance of considering epochs well before the DE domination because relativistic effects will show up on constraints at present time given their integrated nature. From this, we expect indeed our LDE Horndeski scenario to be constrained efficiently by CMB physics but, in particular, we expect the EDE and EMG versions to be stringently constrained by such integrated effects.

Authors in [246] take into account a series of relativistic effects playing a role in galaxy number counts and compare their respective contribution to ΛCDM and Galileon models (see Figure 31). It is interesting to note that, on the one hand, all the contributions of the relativistic effects de-

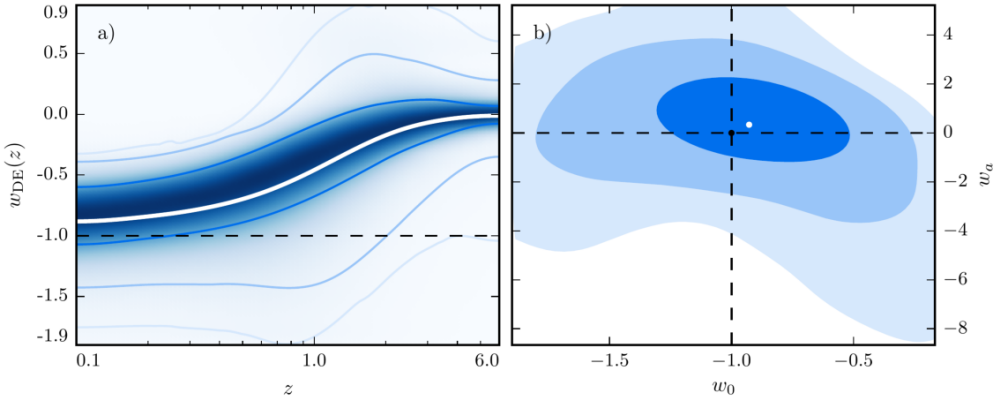

Figure 32: Figure 2 in [248]. *Left*: The probability density of the background $\bar{w}$. *Right*: The projection of the probability density in the w_0-w_a plane of the CPL parametrisation. The white lines/points correspond to the mean, the contours to the 68%, 95%, 99% c.l. intervals and the dotted lines to the ΛCDM predictions. The shades of blue in the left plot are an indicator of the probability density.

crease significantly when the multipole increases, *i.e* on smaller scales, whereas the contribution of the lensing convergence does not, and its variation over multipoles is mild in comparison. The relativistic effects are exclusively large-scale effects as compared to lensing. On the other hand, the galaxy number counts are mostly dominated by RSD while the ISW effect yields the smallest contribution (see upper panels). However, the latter is the contribution that gives the largest deviation with respect to ΛCDM as expected (see bottom right panel). Therefore, with the increasing precision of future surveys, considering such effects in numerical computations is becoming more and more important. Comparing the contributions of each relativistic effects rather that the total contribution on power spectra could give strong insight as to which deviations of gravity are favoured by data or not.

The effects of the couplings functions on the bispectrum have been studied in [230]. Authors have shown that having large deviations in the bispectrum kernel is incompatible without introducing large deviations in first-order quantities if the following naturalness condition is satisfied

$$|\alpha_4, \alpha_5| \lesssim |\alpha_M, \alpha_T| \lesssim \mathcal{O}(1)\,, \tag{335}$$

where α_4 and α_5 are the second order coupling functions in the perturbation expansion. Such a relation is expected to hold in realistic DE or MG models, *i.e*. in a healthy perturbation scheme the contribution of the $n^{\rm th}$ order is expected to be smaller than that of the $n^{\rm th}-1$ order. Authors show thus that in general it is unnatural in Horndeski theories to produce 10% (1%) deviations of the bispectrum introducing even larger ~ 30% (~ 5%) deviations in the linear growth rate. One simplifying conclusion derived out of this, is that the bispectrum kernel of Horndeski theories can be is approximated by that of ΛCDM when considering future observationally viable predictions.

Background evolution

Up till now, most analysis we have discussed consider the background to be that of ΛCDM. It is a reasonable choice since ΛCDM provides the most faithful model of the background evolution of the universe given observations, but, also because the analyses discussed focused on MG effects

induced on the perturbation sector. The freedom contained in Horndeski theories allows them to virtually produce any background depending on the form of the G_i functions. In the EFT formulation, this amounts to having no prior knowledge on how to parametrise $H(t)$. That is why one picks a parametric form that could either, be fixed according to ones taste, or constrained with data, depending on the analysis undertaken. However, using too specific parametric forms could bias the outcome as one is already selecting a branch of models at the level of the background. We have shown thanks to our diagnostic that predictions on LSS observables are very mildly affected by reasonable choice of a constant $\bar{w}$. Yet, a constant equation of state could be a strong assumption and in this era of precision cosmology more involved evolution of $\bar{w}$ must be thoroughly investigated.

In this respect, the analysis carried out in [248] goes further than assuming a constant or even parametric form of $\bar{w}$. Authors in [248] have investigated the type of background evolution Horndeski theories favour without assuming a parametric form of $\bar{w}$. They use principal component analysis in order to constrain the unknown evolution of the background equation of state $\bar{w}$. A theoretical prior covariance matrix for $\bar{w}$ is derived thanks to a Monte Carlo procedure and the application of physical viability conditions. Interestingly, it was shown that the prior favours a tracking behaviour as depicted in Figure 32. The authors map this evolution onto the Chevallier-Polarski-Linder (CPL) parametrisation $w = w_0 + w_a(1-a)$ [81, 82] (see the right panel of Figure 32). It is interesting to observe that since the contours on (w_0, w_a) are large this tracking behaviour could help lifting the tension between weak lensing CMB tension (see section 1.5.3 and the bottom left panel of Figure 11). However, we note that the mean of the curves stands slightly on the diagonally opposed quadrant of the weak lensing induced contours (see Figure 11). The authors also apply this analysis to quintessence models using the EFT of DE, and, as expected, a tracker behaviour is found but $w_0 < -1$ is excluded by stability. Indeed, as we have seen in section 2.1, one has to go at least to k-essence models to obtain a safe crossing of the phantom barrier $\bar{w} = -1$. In light of the above, one conclusion that begs is the need to asses the effects of a time evolving background equation of state on LSS observables in the context of Horndeski theories.

PARAMETER AND OBSERVABLE CONSTRAINTS

There are many key paths one can follow for the study of dark energy. We have discussed one of them: the exploration of the observable predictions a model produces. This leads to spotting characteristic, observational or theoretical, features the model yields and thus understanding better its phenomenology. Another crucial and complementary path is to constrain the deviations with respect to our concordance model thanks to observations. This is of paramount importance to distinguish between models viable or not and understanding what deviations from standard gravity are allowed observationally. The final goal is indeed to see whether observations or datasets favour MG over ΛCDM. Therefore, we shall now go through the constraints obtained with the EFT of DE.

Running Planck mass, linear EFT and f(R) models

The running Planck mass α_M at present time has been constrained in [243]. This participated in showing that combining CMB data and the H_0 prior from Riess *et al.* [93] favours at nearly 2σ a positive α_M as shown in Figure 33. However, only a slight preference remains when considering geometric probes. The author in [243] points also out that an increasing effective Planck mass ($M^2(t)$) suppresses the unlensed CMB power spectrum on low multipoles ($l \lesssim 30$) via the ISW effect,

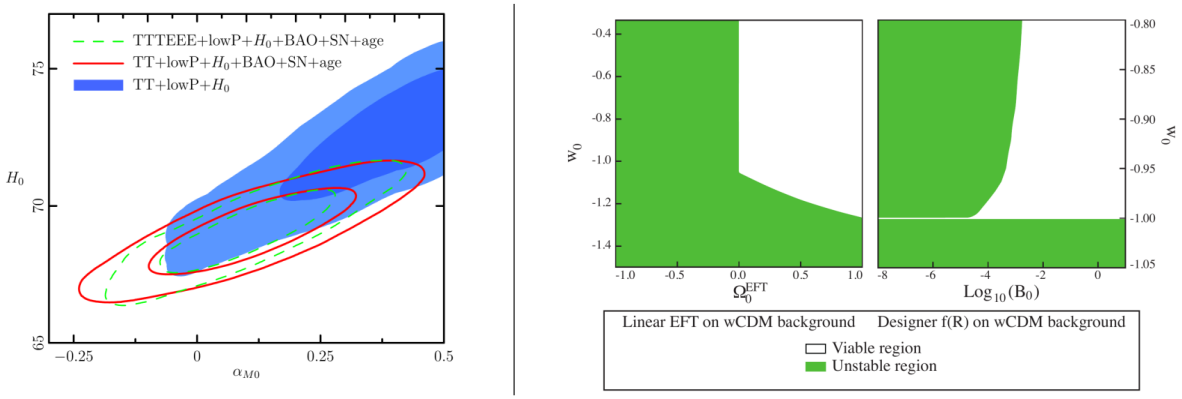

Figure 33: *Right*: Figure 3 in [243]. The marginalised constraints on H_0 and $\alpha_{M,0}$ are shown with several likelihoods and priors as depicted in the labels. The contours are the 68% and 95% c.l.. *Left*: Figure 1 in [249]. Stability regions in the linear EFT and f(R) designer model are shown.

but enhances the lensing power spectrum. This is indeed in agreement from what was found in [247]. We note that a positive value of α_M today, *i.e.* an increasing M^2, means μ_{sc} decreases back in time and thus favouring a period of weaker gravity at low redshifts, given the analysis presented in chapter 3.

Authors in [249], the first article on parameter constraints obtained thanks to the EFT formulation, consider a *linear EFT model*, *i.e.* where only the background EFT coupling functions $M^2(t)$, $C(t)$ and $\lambda(t)$ are switched on. In the parametrisation of EFTCAMB, the effective Planck mass is traded with a factor $1+\Omega$ such that:

$$\frac{M^2}{M_{\rm pl}^2}(t) = 1 + \Omega(t)\,. \tag{336}$$

In this analysis, the background is set to that of a wCDM background implying the $C(t)$, $\lambda(t)$ system is cast in terms of $\Omega(t)$. It is then parametrised as being proportional to the scale factor $\Omega = \Omega_0^{\rm EFT} a$. The EFT formulation also allowed the authors to consider f(R) gravity. In this analysis, the *designer* approach is used, that is, fixing the background evolution (here wCDM) and using the Friedmann equation to solve for $f(R)$. The f(R) model is parametrised by today's value of the Compton wavelength of the scalaron, B_0, in Hubble units

$$B = \frac{f_{RR}}{1+f_R}\frac{\mathcal{H}R'}{\mathcal{H}' - \mathcal{H}^2}\,, \tag{337}$$

where $'$ is a derivative with respect to conformal time.

This analysis allowed to show that the stability conditions (shown in Figure 33's right panel) can act as a strong prior in deriving constraints on the parameters contained in the EFT models. The constraints obtained are shown in Figure 34. For the designer f(R) model, it is interesting to note that the constraints obtained from the combination of probes are shown to be very strong on the present day value of the equation of state, $\bar{w}_0 \in (-1, -0.9997)$ at 95% c.l.. For the linear EFT models, the constraints obtained yield the bound $\Omega_0^{\rm EFT} < 0.061$ at 95% c.l. for the ΛCDM background and $\Omega_0^{\rm EFT} < 0.058$ for wCDM background.

The linear EFT and designer f(R) model have also been used in [250] to answer the question whether MG can reconcile the tension between CMB measurements and lensing, *i.e.* the A_L ten-

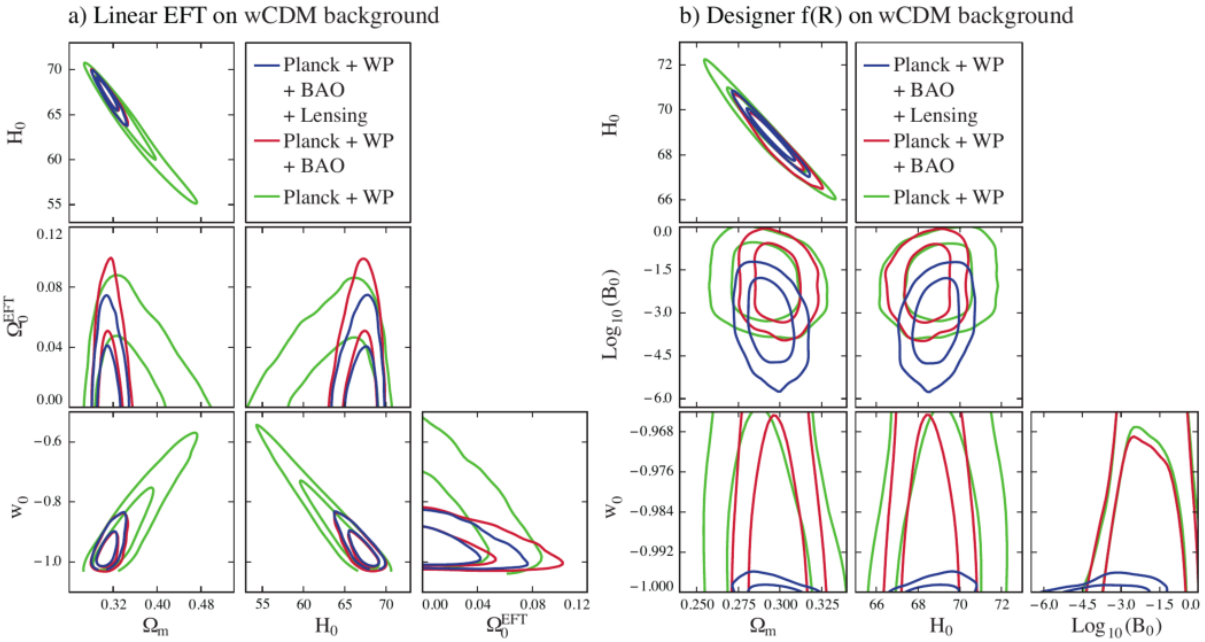

Figure 34: Figure 2 in [249]. The confidence regions on the parameters of the linear EFT and f(R) designer model are shown for several combination of observables. The acronym WP stands for WMAP low-polarisation.

sion. To look into this, authors choose to simulate CMB anisotropy and CMB lensing spectra assuming Planck 2015's best-fit values and the Planck blue book on beam and noise specifications. From this, models with an effective Newton constant stronger than $G_{\rm N}$ can have an modulating effect similar to that of A_L. Nevertheless, this induces higher values of $\sigma_{8,0}$ which in turn strengthens the tension with CFHTLenS measurements. It would therefore be interesting to see if switching on the other EFT parameters can solve this issue.

The f(R) Hu-Sawicki model (see section 2.1.3) has also been constrained with the EFT of DE [251]. Authors chose this model to present in detail the procedure needed for the full mapping of a specific model of MG into EFTCAMB. An interesting result, was that $\sigma_{8,0}$ and $|f_R^0|$ are degenerate but the WiggleZ galaxy number density counts favour a high value of both parameters while CMB and CFHTLenS measurements favour smaller values. All in all, WiggleZ data favour a non-vanishing value of the Hu-Sawicki model parameter, $\log_{10}(-f_R^0)$, which implies a large value of $\sigma_{8,0}$, CFHTLenS drags the estimate of $\log_{10}(-f_R^0)$ back to the ΛCDM limit. The scale dependence of the cosmological observables $f\sigma_8$ and E_G (another MG observable [252]) in Hu-Sawicki f(R) model are also shown and discussed.

Horndeski theories

Looking at how observables are expressed as a function of the EFT couplings can already give strong indications and constraints on the observable predictions of Horndeski theories. Indeed, with the knowledge of the structure of Horndeski theories, authors in [240] have derived a set of consistency conditions that allows one to rule out Horndeski theories or sub classes given where future measurements will lie. Let us summarise a few of their important findings. An important

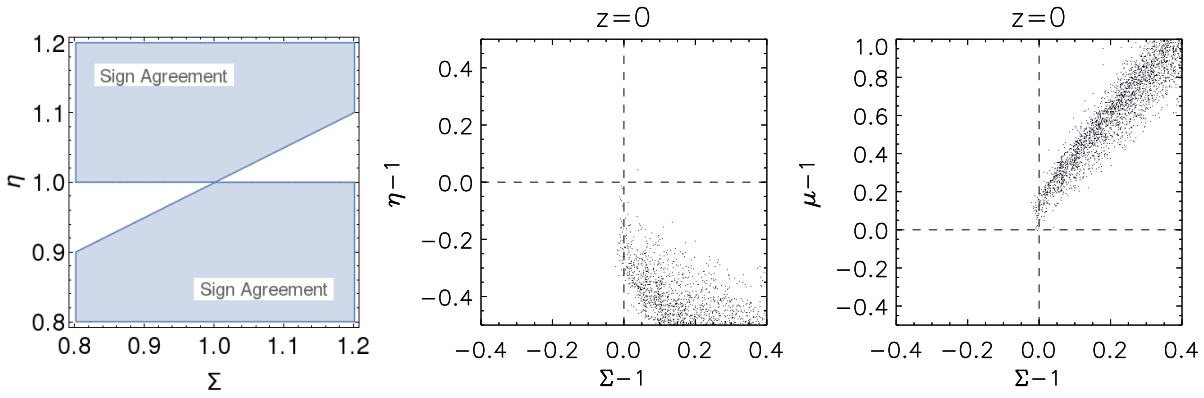

Figure 35: The regions allowing a sign agreement between $\mu-1$ and $\Sigma-1$ in the (η,Σ) plane according to (319) is shown is the *left panel*. In the *middle* and *right* panels, the correlations between the LDE models with $\mu_2^2=0$, $c_s<1$ and $c_T<1$ are shown in the $\mu-1$,$\Sigma-1$ and η planes at $z=0$.

criteria is the scale dependence of the LSS observables μ and Σ (and η). Self accelerating models in the Horndeski class have the Compton wavelength of the scalar field very small, of the order Hubble, so as to drive cosmic acceleration. Therefore, the scale dependence it introduces must bear effects at very large scales, *i.e.* Hubble scales. This begs the conclusions that given surveys of the LSS probe the small scale regime, should any future LSS measurement detect a scale dependence in μ or Σ the self accelerating Horndeski theories would be ruled out. Furthermore, the authors show that the whole Horndeski class would be ruled out if $\mu<\mu_{\rm sc}$ since indeed $\mu_{\rm ff}$ must be positive for a healthy Horndeski theory. Note that the contrary would favour the Kinetic Matter Mixing models we discuss further on.

Authors in [240] also argue that measuring $\mu-1$ and $\Sigma-1$ of opposite signs at any redshift and scale would strongly disfavour all Horndeski models. Given the similarities in the expressions of μ and Σ, producing $\mu-1$ and $\Sigma-1$ of opposite signs could seem as an unlikely tuning of the coupling functions. We find, however, with the correlations of chapter 3 that this statement is progressively weakened at low redshift where a non negligible amount of models display $\mu-1>0$ and $\Sigma-1<0$ at redshift zero for instance. We understand this to originate from a subtle point, and essentially related to the viability conditions. According to (319), one can observe in Figure 35 (left panel) that the region producing a sign disagreement is indeed a small region in the observable space of (η,Σ). Yet we find, within our procedure of chapter 3, this region to become populated when the stability space is broadened either by switching on μ_2^2 or by going to the EDE and EMG scenarios. As a matter of fact, taking the LSS correlations in the LDE case with $\mu_2^2=0$ at all times (see Figure 35 middle and right panel) we observe the sign disagreement region to be depopulated to the benefit of the bottom sign agreement region. The consequence is indeed that $\mu-1$ and $\Sigma-1$ now bears a sign agreement and even the nearly 45 degree correlation obtained previously at higher redshifts is recovered. We also note that when μ_2^2 is switched off the models are pushed further away from their ΛCDM reference values as we had observed in Figure 20. The likeliness of having $\mu-1$ and $\Sigma-1$ displaying a sign agreement should be assessed when higher precision data will be provided in the future.

The authors in [240] give a stringent diagnostic on the Brans-Dicke theories. For instance, the Σ reduces to the inverse of conformal factor relating the Jordan and Einstein frames, $\Sigma=M_{\rm pl}^2/M^2$ in the EFT description. Therefore, detecting any scale dependence in this observable would rule

out these theories. The authors have thoroughly summarised all their findings in a flow chart (see Figure 36); a "must-follow" when exploring Horndeski theories in perspective of higher precision data with future surveys.

Constraints on the EFT parameters taking data into account, both in the α-basis and μ-basis, have been obtained. Authors in [229] made the first constraints ever made on the full Horndeski theories in the EFT. They parametrise the α's at order 0: $\alpha_i = c_i(1-x)/(1-x_0)$ where i stands for $\{M, K, B, T\}$. In this analysis only models unstable in the tensor sector are considered. The constrains they obtain (see Figure 37) show that reasonable values of the c_K parameter virtually do not affect the constraints on the other parameters when considering data. However, one must be cautious since a zero order parametrisation condenses the effects of the coupling at low redshifts. Note that, α_K is the equivalent of the μ_2^2 of the μ-basis. Moreover, the constraints on the parameters exclude their ΛCDM value at more that 2σ, however, the authors show that no evidence against ΛCDM from computing the Bayesian evidence ratio of the MG models with respect to ΛCDM is found.

Authors in [247] parametrise the μ-basis at order zero and consider all the stability priors along with Planck CMB data 2015. They show that the posterior distribution of the EFT parameters are mostly driven by the stability priors. On top of this, asking for sub-luminal propagation of scalar and tensor perturbation are shown to reduce drastically the likelihood contours of the parameters and observables, as shown in Figure 38. Therefore, a model-dependent analysis is optimal if one is to exploit theoretical priors about the physical viability of specific Horndeski models to complement the discriminatory power of data. Also, one can appreciate that our diagnostic fits well with the CMB constraints obtained for a LDE model with $\mu_2^2 = 0$ and order zero expansion of the couplings on the LSS observable displayed Figure 38.

We must emphasize that when taking data into account, two complementary strategies allow to estimate the likelihood of data given MG. One is model dependent and constrains a theory given data. This is what we have discussed up till now. The other, consists in implementing model-independent likelihood analysis and parametrising LSS observables in a purely phenomenological way, blindly of any gravitational theory. The diagnostic developed in chapter 3 is meant to facilitate theoretical interpretation in this case. Interestingly, model-independent analyses have been pursued for example in [205]. More recently, the Planck collaboration [80] have used a simple monotonic redshift evolution for the relevant large-scale structure observable $O(x)$,

$$O(x) = 1 + O_0(1-x)\,, \tag{338}$$

be it μ, Σ or η, so that the MG scenario converges to the standard picture at high redshifts. These observables have thereby been constrained in a fairly model independent way thanks to the cosmological probes as displayed in Figure 39. These results are suggestive of a negative value of $\mu - 1$ at redshift $z = 0$. Should future, higher precision data strengthen the statistical significance of these findings, one can conclude that the Horndeski landscape would face hard times. Moreover, the likelihoods in Figure 39 put the ΛCDM value at the 2σ limit. Therefore, the observables μ, η and Σ given future and more precise constraint could thus be instrumental for a detection of MG.

Hořava Gravity

Hořava gravity was recently suggested as a candidate for an ultra-violet completion of GR [253, 254]. The idea behind this theory is to add higher order spatial derivatives to the action in order to modify the graviton propagator. Authors in [182] give the mapping of this theory into the EFT for-

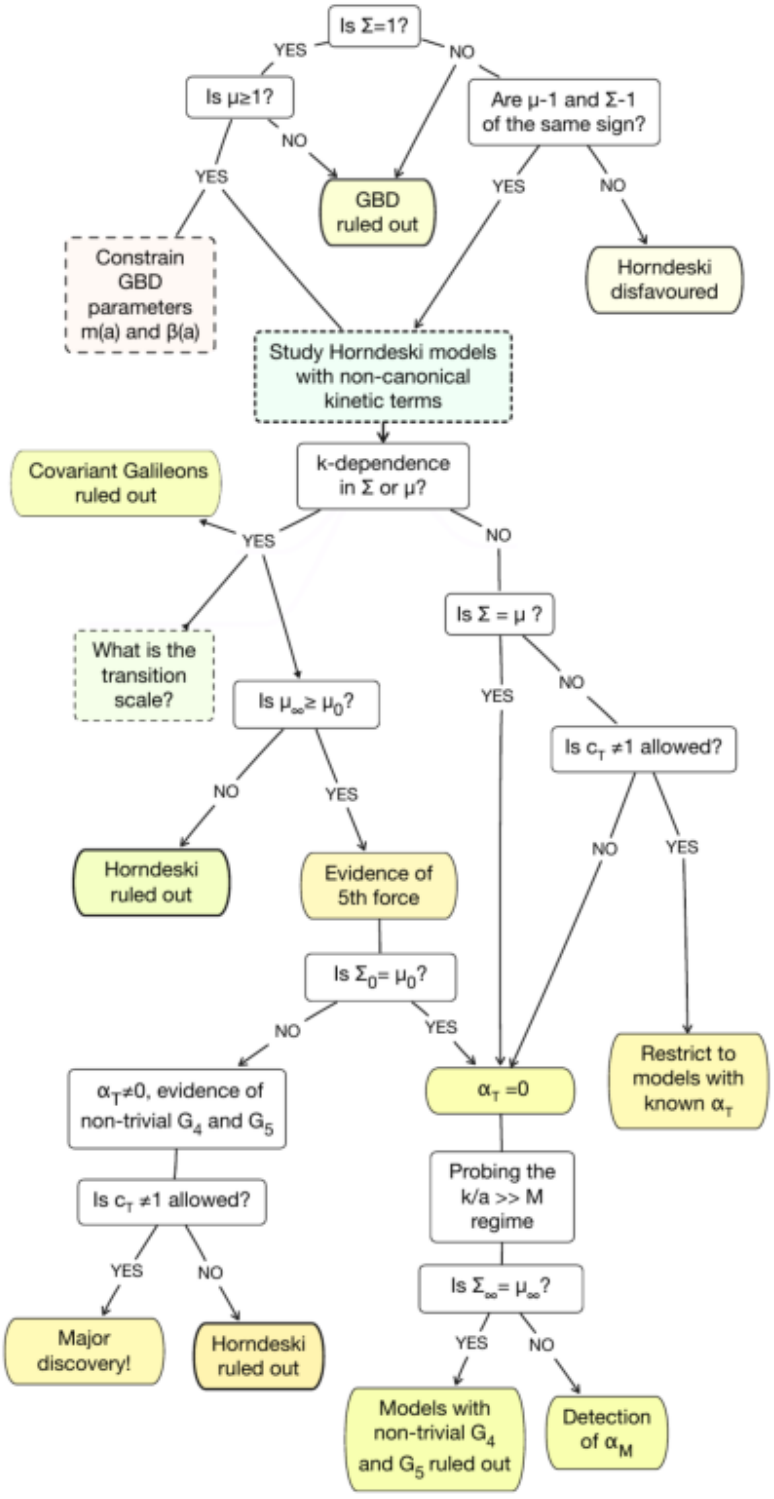

Figure 36: Figure 1 in [240]. Flow chart diagram summarising the possible interpretations once key features of Horndeski theories would been measured or not. In the notations of this diagram the subscript 0 stands for the screened part of the observable, *i.e.* μ_0 is $\mu_{\rm sc}$, and the ∞ subscript stands for the full contribution, *i.e.* μ_∞ is μ.

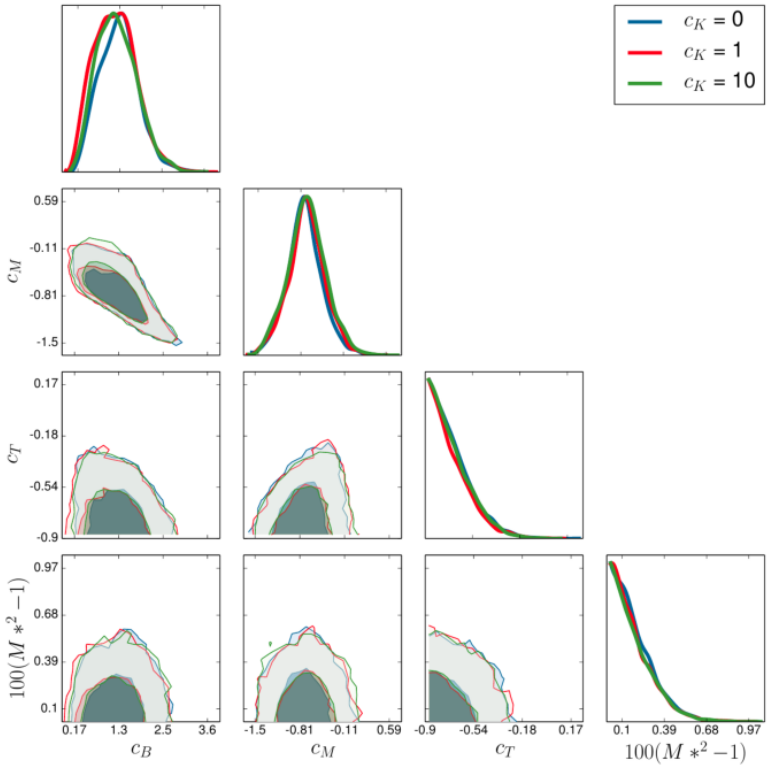

Figure 37: Figure 3 in [229]. Constraints on the parameters of the order zero parametrisation of the α functions from CMB, BAO, RSD and P(k) power spectrum measurements.

malism and study constraints on the low-energy part of the theory. Considering CMB temperature-temperature and lensing power spectra by Planck 2013, WMAP low-polarization spectra, WiggleZ galaxy power spectrum, local Hubble measurements, Supernovae data from SNLS, SDSS and HST and the BAO measurements from BOSS, SDSS and 6dFGS, the authors constrain the background and the perturbations of the low energy theory. Among others, this analysis shows that the quasi-static approximation is not a safe approximation to describe perturbations in Low-energy Hořava gravity. Furthermore, the effects of the modifications induced by the low-energy Hořava gravity action are shown to be quite dramatic and therefore current data places tight bounds on the parameters governing the theory.

Early modified gravity

Early modifications of gravity have been discussed and constrained in the EFT formalism. Authors in [255] embed a hybrid-metric Palatini f(R) gravity with a ΛCDM background into the EFT framework. In this model, the early modifications of gravity can become significant after recombination but then decay towards the present. These decaying early time modifications are tested against geometric probes and Planck measurements. However, no evidence for such effects is found in the observations. Authors find tight constraints for the scalar field value at $|f_R(z = z_{\rm on})| \lesssim 10^{-2}$ for modifications introduced at redshifts $z_{\rm on} \sim (500 - 1000)$ with a present-day value $|f_{R0}| \lesssim 10^{-8}$. It is therefore important to apply such an analysis to our EDE and EMG models. Since they allow for large modifications deep in matter domination, it would be interesting to see if they undergo such tight constraints also.

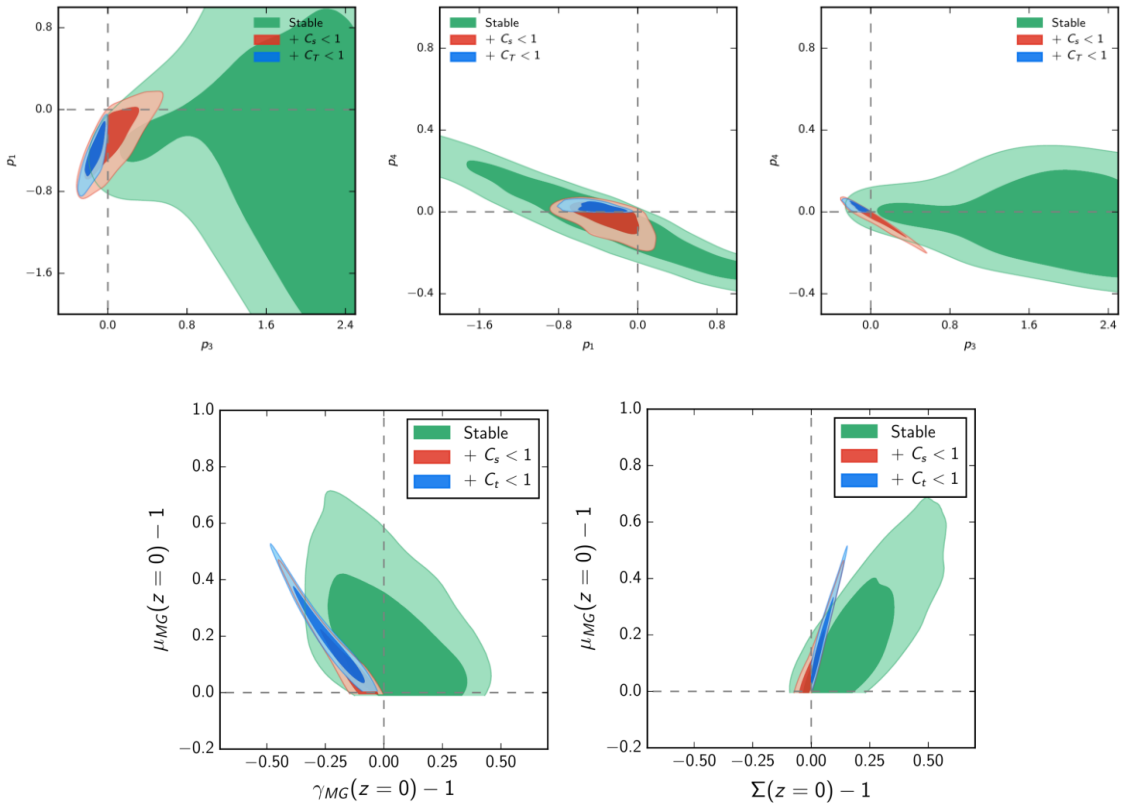

Figure 38: *Top row*: Figure 4 in [247]. The CMB constraints are shown for an order zero expansion of the couplings. *Bottom row*: Figure 7 in [247]. The corresponding CMB constraints shifted to the LSS observables. Several viability conditions are required: stable theories, stable theories and $c_s \leq 1$, stable theories and $c_s \leq 1$ and $c_T \leq 1$. In the models considered here, $\mu_2^2 = 0$ since it would be constrained only from the back-reaction of stability conditions and thus too poorly constrained.

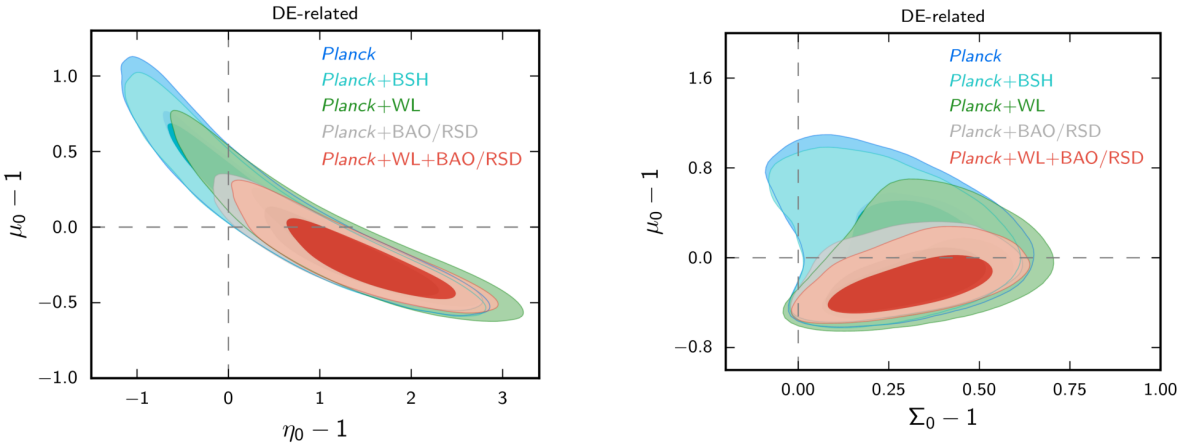

Figure 39: Figures 14 and 15 in [80]. Constraints on the present time value of μ, η and Σ parametrised as (338) based on several combination of cosmological probes is shown.

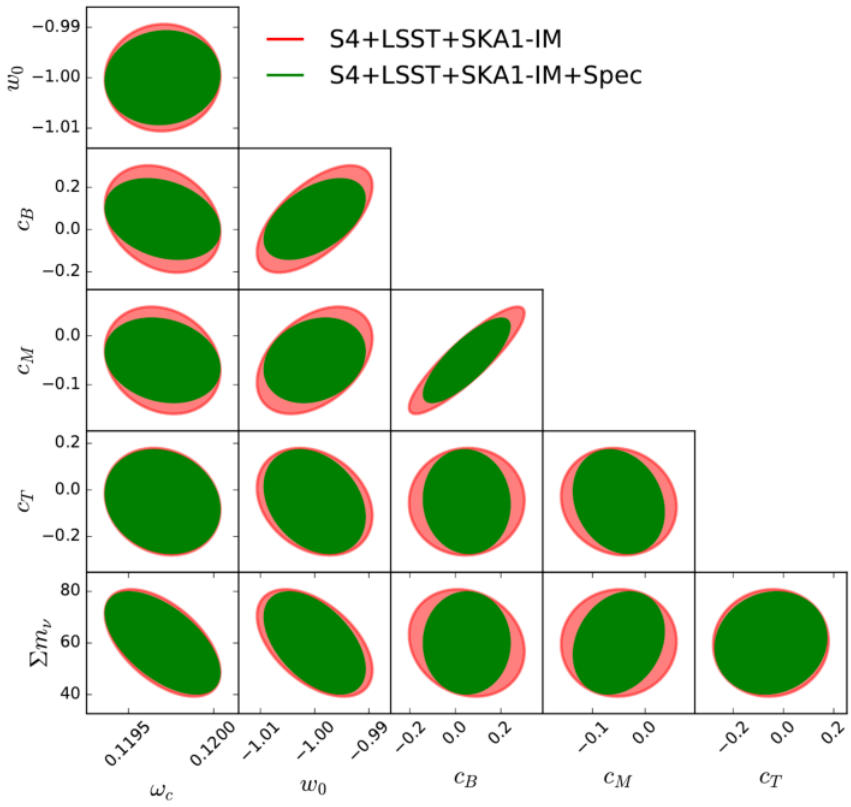

Figure 40: Figure 1 in [11]. The cosmological constraints for the combination of Stage 4 CMB, LSST (galaxy clustering and shear) and an intensity mapping experiment by SKA Stage 1 are shown in pink. Adding to that BAO scale and growth rate measurements from a DESI-like experiment produces the green contours.

Forecasts

The straightforwardness of the computations in the EFT also allows one to make Fisher forecasts for modification of gravity. Authors in [197] give forecasts on the $\gamma_0 - \gamma_1$ parametrisation of the growth rate for a EUCLID-like survey (see Figure 30). Interestingly, authors in [256] have shown the constraints on the dark energy equation of state to be weakly affected from the inclusion of the EFT parameters. Authors in [11] give forecasts on the α-basis considering Stage IV photometric redshift surveys, including weak lensing and multiple tracers of the matter distribution, radio experiments and measurements of the CMB. This analysis is very complete, it includes relativistic effects, it is done without quasi-static approximation and makes conservative assumptions about the effect of screening on small scales. A figure of merit is also computed for cosmological tests of gravity which highlights how the combination of different types of surveys, probing different length scales and redshifts, lead to constraints on MG to better than a few percent. We display some of the constraints obtained in Figure 40 where one can appreciate how using BAO scale and growth rate measurements from a DESI-like experiment on top of CMB Stage 4, LSST and SKA measurements can ameliorate the constraints on the EFT and cosmological parameters. Should the best-fit values obtained in [229] remain, the authors show that a more than 7σ detection of deviations from ΛCDM would be found given the constraints that will be produced the combination of the most efficient probes. The constraints on the Horndeski parameters will greatly improve,

for instance, they estimate in the best combination of probes that $\sigma(c_M) \simeq 0.06$, $\sigma(c_B) \simeq 0.12$ and $\sigma(c_T) \simeq 0.15$. The authors point out also that ultra-large-scale modes will have negligible statistical weight on the constraints on the parameters compared to smaller-scale fluctuations.

ASTROPHYSICAL IMPLICATIONS

The EFT of DE can also allow one to confront MG theories with astrophysics. Notably, an emerging prospects is to use compact systems to constrain modifications of gravity.

GLPV theories

Parameter constraints on GLPV theories have not been released in the literature yet. However, constraints on a set of parameters have been obtained thanks to local objects, based on the findings in [257]. For example, red dwarf stars have been shown to yield the constraint [258, 259]

$$\Upsilon = \frac{\alpha_H^2}{\alpha_H - \alpha_T - \alpha_B(1+\alpha_T)} \lesssim 0.0068\,, \tag{339}$$

where Υ is a free dimensionless parameter characterising the deviations from GR in the hydrostatic equilibrium equation of the stars (see eq.(1) of [258]). This upper bound is obtained thanks to the interplay between plasma physics and the gravitational interaction which sets a minimum mass for the hydrogen burning in stars. This can be compared with observations and thus yield constraints on the underlying theory of gravity. Similarly, galaxy clusters have been used in [260] to constrain the quantities

$$\Upsilon_1 = \frac{4\alpha_H^2}{c_T^2(1+\alpha_B) - \alpha_H - 1} = -0.11^{+0.93}_{-0.67} \qquad \text{and} \qquad \Upsilon_2 = \frac{4\alpha_H(\alpha_H - \alpha_B)}{5(c_T^2(1+\alpha_B) - \alpha_H - 1)} = -0.22^{+1.22}_{-1.19}\,, \tag{340}$$

at 2σ.

Gravitational waves

Horndeski and GLPV theories can produce a propagation speed of gravitational waves (GW) different from that of light. This deviation was constrained thanks to local tests in [232]. An important point shown is why a non standard value of c_T survives the conventional screening even at the linear level in the covariant description of Horndeski and GLPV theories. We see the consequences of this in the EFT of DE through $\mu_{\rm sc}$. It originates from the persistence of the scalar field's gradient inside virialized overdensities. In the authors words: "it effectively *pierces* the Vainshtein screening". This is how the use of the Hulse-Taylor pulsar and the PPN constraint from the Cassini spacecraft experiment $\eta_{\rm PPN} - 1 = \eta_{\rm sc} - 1 = (2.3 \pm 2.1) \times 10^{-5}$ [212] in the analysis carried out in [232] has led to the overall local constraint

$$0.995 \lesssim \mu_{gw} \frac{c}{c_T} \lesssim 1\,, \tag{341}$$

where $\mu_{gw} = G_{\rm N}/c_T^2$. This translates in the constraints on c_T and α_H shown in Figure 41 (left panel). These constraints being local ones, they imply that in Horndeski theories, the value of c_T at present time cannot deviate from that of light by more than 10^{-2}.

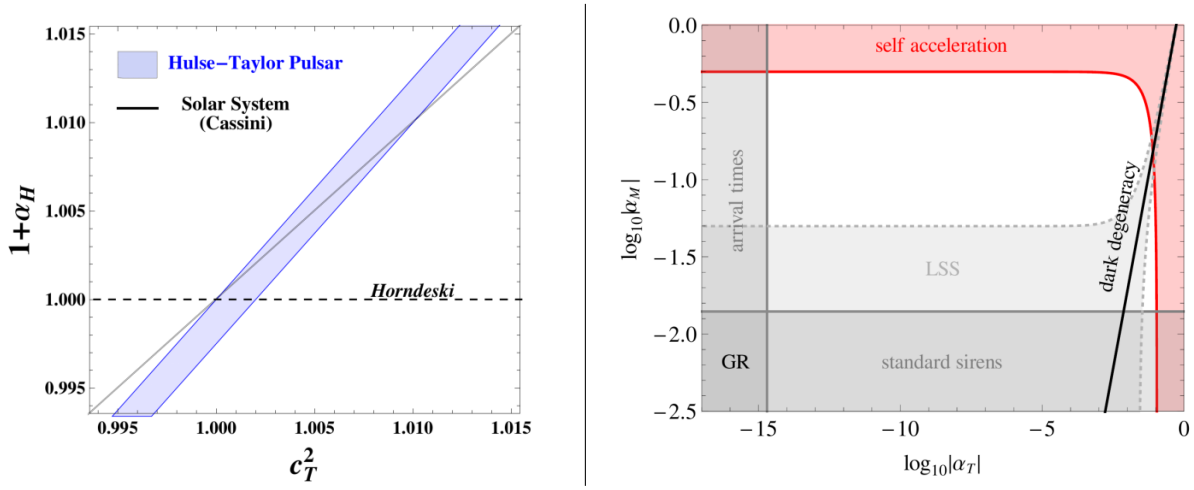

Figure 41: *Left*: Figure in 2 [232]. Hulse-Taylor Pulsar and Cassini constraints on α_H and c_T^2 are shown. *Right*: Figure 4 in [261]. The prospective constraints on α_M and α_T with gravitational wave detectors measuring the decay of the wave amplitude with standard sirens and the arrival time with respect to the electromagnetic emission from a cosmological event. The shaded regions correspond to the allowed regions and the red region corresponds to where self-accelerating models lie.

The anomalous speed of GW has been used in [261] to break the degeneracy between MG and dark energy behaviours within Horndeski theories, *i.e* singling out self-accelerating models. Linear shielded Horndeski models of [185] in the EFT of DE are considered. These models recover the ΛCDM values $\mu(t,k) = \eta(t,k) = 1$ in the quasistatic regime of linear perturbations and are matched with the ΛCDM background expansion history. Therefore, authors identified a stable self-accelerating Horndeski model that is degenerate with ΛCDM at the background and linear level. Some prospective constraints on the couplings α_M and α_T are derived (see Figure 41's right panel). The region that allows for self-acceleration is very narrow. In particular, the self-accelerating degenerate model is shown to induce the present tensor speed to be $< 95\%$ than that of light and a damping of the wave amplitude $> 5\%$ less efficient than in GR. On the contrary, in [238] a minimal modification for self-acceleration within Horndeski theories while bearing $c_T = 1$ is found. However this model is shown to yield a 3σ poorer fit to cosmological observables compared to ΛCDM.

In [262], authors explore up to which extent there is a one-to-one relationship between producing an anomalous speed of GW and a gravitational slip different from unity in MG theories. Bi-metric, Einstein-Aether gravity and Horndeski theories are used as case studies. Horndeski theories are studied in their EFT formulation and they are shown to a have enough freedom to hide its gravitational slip dynamically, but at the cost of making the perturbations evolve towards a divergent kinetic term. The other theories do not offer this possibility.

FURTHER DEVELOPMENTS

Let us now discuss further developments implemented within the EFT of DE.

Neutrinos and modified gravity

The degeneracy between MG and the neutrino mass has been revisited in the EFT framework in [263]. Combinations of the first released data from Planck, BAO measurements, LSS data from WiggleZ and a ΛCDM background are considered. In the case of the designer f(R) model, a lower degeneracy than in the previous literature is found and the data sets the bound $\log_{10} B_0 < -4.1$ at 95% c.l. for $\Sigma m_\nu = 0.06$ eV. On the contrary, no sizable degeneracy is found within the linear EFT model. The bound obtained is $\Omega_0^{\rm EFT} < 0.05$ and $\Sigma m_\nu < 0.26$ at 95% c.l. which is slightly improved with respect to what was obtained in [249].

The neutrino-modified gravity degeneracy has also been explored in the α-basis in [264]. Using forecasted CMB and galaxy power spectrum datasets one observes the parameter c_B, that is the parameter characterising the function α_B, to dominate the correlation with the total neutrino mass. It can cancel the power suppression due to massive neutrinos at a given redshift for certain values. Authors find that future surveys such as EUCLID would limit but not fully break the degeneracy between this parameter and the neutrino mass. In fact, in [11] no apparent degeneracy between MG and the sum of neutrino masses is obtained given the forecasted precision on the α parameters.

Disformal transformations, disformal couplings and non-minimal couplings with matter

The disformal transformations between the Jordan Frame and the Einstein frame within GLPV theories has been explored in [265]. The fact that the matter sector, although being minimally coupled to the metric, feels the modifications of gravity is pointed out. Authors advocate that the disformal transformation is useful for understanding gravitational interactions with matter mediated by the scalar field.

Extensions of the EFT of DE allowing for conformal and disformal couplings of matter species to the gravitational sector have been introduced in [7]. The phenomenological consequences of such inclusion have been explored in [228] where EUCLID-like forecasts are given considering, the galaxy power spectrum in redshift space, tomographic weak-lensing shear power spectrum and the correlation spectrum between the ISW effect and the galaxy distribution. This is done in three fiducial backgrounds, we display the results in the ΛCDM background in Figure 42. In the three fiducial, authors find the 1σ constraints on the MG parameters to be of the order $\sigma \sim 10^{-2}$. One can appreciate how an EUCLID-like survey gives an order of magnitude tighter constraints than CMB Stage IV experiments (see Figure 40). However, we note that in Figure 42 $c_T = 1$ was fixed while in Figure 40 it was not and additional parameters for neutrinos and the background are considered. In [7], the non-minimal coupling of CDM is shown to enhance the effects of MG and to reduce the statistical errors accordingly. In all cases, the parameters are found to be highly degenerate. However, some degeneracies can be broken by combining all three observational probes.

The extension ito disformal couplings has been pushed further with Kinetic Matter Mixing models in [192] where, as the name suggests, kinetic mixing between matter species and the scalar field is considered. In this case, the disformal couplings also depend on the gradient of the scalar field. The effects on the matter power spectrum and the angular spectra of the CMB anisotropies and the CMB lensing potential are displayed. Interestingly, Kinetic Matter Mixing weakens gravity on small scales which leads to lower $\sigma_{8,0}$ predictions with respect to the ΛCDM case. The key

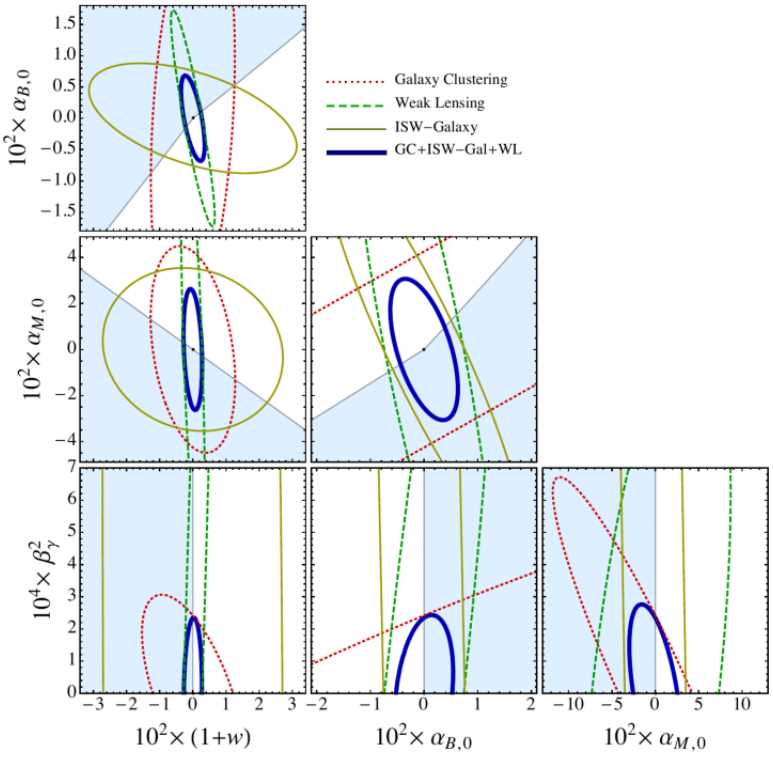

Figure 42: Figure in [228]. The 68% c.l. contours for the Fisher forecasts in the ΛCDM background are shown. The parameters not displayed have been set to their fiducial value. The blue region corresponds to the unstable region.

phenomenon is that this extension allows for the fifth force contribution to the total gravitational interaction to be negative in a healthy way.

Initial conditions and N-body simulations

Initial conditions for cosmological N-body simulations have been discussed within the EFT framework in [266]. The f(R) designer model with wCDM and ΛCDM backgrounds is taken as a case study. The authors first give a description for setting initial particle displacements and field values for simulations of arbitrary metric theories of gravity, fluids (perfect and imperfect) with arbitrary characteristics, which is independent from the EFT of DE. Then, using the designer f(R) model, authors show that initial conditions set at high redshifts are affected up to 5% at Mpc scales. The dynamics of the models are evolved thanks to EFTCAMB. This notably implies that one must go beyond ΛCDM initial conditions if one wants to deal with modifications of gravity outside of the quasi-static approximation. Authors give the initial conditions for a simulation where the modifications of gravity induced by the scalar field is modelled in a Lagrangian particle-like description as well. The contribution of this article paves the way for future simulations and mock galaxy catalogues of MG theories. This is another crucial point for progress towards precise tests of gravity in cosmology.

The study for more precise initial conditions within EFTCAMB has been pushed further in [267]. The authors present a more self-consistent algorithm to set the initial conditions in EFTCAMB.

Some important results are derived from this. For instance, the corrections in the adiabatic initial assumption produced by the linear EFT model and a constant linear EFT model ($\Omega_0^{\rm EFT} = const.$) are found to be negligible with respect to ΛCDM. Indeed, authors highlight that the dominant ingredient is the primordial curvature perturbation from inflation, thus the energy budget of the matter components is not crucial. Also, no iso-curvature mode sourced by the scalar field is found to exist in the two EFT models considered. Lastly, an $\mathcal{O}(1\%)$ and $< \mathcal{O}(1\%)$ difference is found for respectively the constant and linear model when the initial condition is set at $a = 10^{-2}$ and $a = 10^{-7}$.

Semi-dynamical perturbations

Authors in [268] introduce a semi-dynamical treatment extrapolated from the evolution of perturbations at a pivot scale of choice on top of the EFT of DE. This can be useful to keep computations of observables straightforward and more precise on very large scales. For Horndeski theories, this approach has the benefit to recover a quasistatic approximation and to account for corrections near the Hubble scale. For models GLPV theories, authors point out that the velocity field and time derivative of the spatial metric potential should not generally be neglected, even in the small-scale limit. The authors conducts tests in between the semi-dynamical approximation and the linear perturbations for several dark energy and MG models and a good agreement between the two is found.

CONCLUSION AND CAVEATS

The EFT of DE is a linear description of MG theories therefore it cannot capture all the phenomenology of such theories. For example, the dynamics at small scales are not described such as screening mechanisms. However, already at the linear level, a lot has been done and much is still left to be done. We have seen the EFT of DE to be a powerful tool to explore MG scenarios from its straightforwardness to compute observables and to parametrise deviations from standard gravity in terms of coupling functions. This has enabled the findings of universal features and novel observable predictions in the wide class of scalar tensor theories that are Horndeski and GLPV theories. It has also allowed one to constrain deviations from the standard model with data. The EFT framework, does not parametrise a specific theory in terms of variables, letting observations to fix their amplitudes, but, it parametrises theories themselves in terms of structural functions of time. One can thereby interpret observations directly in the space of theories and not within the framework of a single paradigm. However, there is a price to pay. This price is that the functional form of the coupling functions is unknown. Observations generally do not have enough power to fix continuous functions of time, they fix numbers. With future surveys and the growing amounts of data, studies which include principal component analysis, as we have discussed for the background evolution in the EFT of DE, is a promising way to overcoming this issue. Up till now, the apparent intractability of the problem is manoeuvred by phenomenological modelling, that is, by compressing the unknown information contained in the structural functions into a finite set of coefficients thanks to a parametric form. The subtle step then is to engineer a parametrization which is flexible and universal enough to allow exploring most of the phase space of stable theories and yet be effectively constrained by observations. In other words, one faces the dilemma between using a very general parametrisation and not invoking too many free parameters.

The main caveat in the EFT of DE is indeed the parametrisation of the couplings. For instance, as we have discussed in chapter 3, we needed an expansion up to order 3 to capture all the feature in the LSS observables. This implies a Horndeski model in this set-up would have 12 parameters in addition to the cosmological parameters to be constrained in a Monte Carlo Markov chain run. Today, this seems overly CPU greedy to be reasonably feasible. The generality and efficiency of the parametrisations have been explored in the literature in order to find the best middle ground. In [8, 9], the assumption of the couplings evolving as $const. \times (1-x)$ is shown to be a poor fit in general, but one can still derive some general characteristics in early and late time limits. For instance, the authors in [8] prove that the gravitational slip must restore to unity as in GR in the de Sitter limit of Horndeski theories, and why it does not more generally. Interestingly, with a more accurate parametrisation of the α, authors obtained the same trends in the observables we found later in the LDE scenario. That is, the succession of epochs during which μ and η yield larger or lower amplitudes than ΛCDM. In general, authors in [8, 9] argue that the simple parametrisation $const. \times (1-x)$ estimates wrongly the observable and thus, they are unlikely to be successful. Therefore oversimplified approximations of the coupling function could even miss the signature of MG. Thankfully, the author in [10], shows as expected that observables are not extremely sensitive to short time-scale variations. Therefore, smooth parametrizations are in general sufficient to describe the theory space well. Notably, it is shown that using two parameters, an amplitude and a power law index, for each function is preferred over more complex models for 86% of the theory space. Nevertheless, authors in [11], point out that the forecasts on the EFT parameters can be substantially impacted by the model for the time evolution of the coupling functions. Therefore, it seems now crucial to implement forecasts for future measurements in more involved parametrisation of the couplings. The study of the forecasts they would engineer on the LSS observables must also be thoroughly investigated given the status of model dependent and independent analysis we have discussed.

CONCLUSION

Exploring the phenomenology of dark energy models is a vast enterprise. Although this thesis is entitled in this respect, the study it presents is only a grain of sand in a large bucket. We have explored a large class of scalar tensor theories; Horndeski theories themselves but a possibility in a wide range of modified gravity theories. One can look at the summary diagram of Figure 3 in [12] for instance, to appreciate how large the realm of modified gravity theories is. Nonetheless, Horndeski theories are a crucial path to explore. They virtually incorporate all theories that add one scalar degree of freedom in addition to General Relativity. Therefore, by studying these theories one is exploring one of the simplest and physically motivated modification of gravity: one adds a scalar field. Scalar fields have been shown to exist with the Higgs field. One could thus argue why another could not exist and cause cosmic acceleration. Furthermore, adopting a simple modification of gravity is crucial for at least another reason; they provide mathematically sound and physically motivated models for the standard model ΛCDM to be compared to.

The standard model has been shown to have some shortcomings and we have summarised most of them. Whether the latter are theoretical or observational; paths for improvements should be explored. Doing so could very well produce more accurate methods to release precise data and understand it to a greater degree within our gravitational paradigm, or reveal new physics needing to be explained beyond the standard model. Exploring the deviations cosmological probes, and thus specific underlying physical processes, favour is decisive to assess which direction to follow for a completion of the standard model. In this respect, many alternative models explaining cosmic acceleration have been suggested and the task to assess the viability of each theory with observations is an arduous endeavour. Therefore, unifying frameworks have been constructed to yield the possibility of testing several theories at once against observations. We have focused on one of them: the effective field theory of dark energy. This framework grants a parametrisation in terms of couplings functions of its action of virtually all models including an extra scalar degree of freedom to General Relativity, and thus Horndeski theories for example. This framework can only describe modified gravity theories at the linear level and does not allow to describe the screening of modified gravity theories. However, this framework grants a physical motivation for the use of a scalar field; its existence arises naturally as the result of the spontaneously broken time translations of spacetime.

This is the framework that allowed us provided answers to the guiding questions presented in the introduction of this thesis. We have shown that, despite the large functional freedom Horndeski theories exhibit, the application of mathematical and physical viability requirements lead to obtaining bounded predictions on observables of the large-scale structure, and ΛCDM often stands at the border. Notably, we have focused on observables such as: the effective Newton constant, the light deflection parameter and the growth function; all shown to be key for detecting deviations from the standard model. We proceeded thanks to a Monte Carlo approach to generate viable models in the linear Horndeski class, that is the one accessed by the effective field theory of dark energy, and explore the predictions it yields. This approach enabled us to outline an observable diagnostic of Horndeski theories that will be instrumental for ruling out such theories given future measurements. We also granted the possibility for Horndeski theories in the effective field theory of dark energy to account for early modifications of gravity deep in matter domination.

I am now focusing on a study in which we constrain Horndeski and Beyond Horndeski theories within the effective field theory of dark energy with observations where special attention is paid to solar system and astrophysical constraints. We also want to assess the viability of self-accelerating models in this context. However, we have shown that many observational constraints have already been obtained on Horndeski theories and subclasses, thanks to the effective field theory of dark energy. Although these constraints do not particularly favour linear Horndeski theories over ΛCDM at this point, we have shown that the description of these theories must be improved in the effective field theory framework so as to be sure one is capturing all the phenomenology for a thorough assessment in the light of future surveys. We have discussed several paths to follow in the future, notably using the effective field theory of dark energy framework. We are at the beginning of this very exciting era of Precision Cosmology and the next years will give rise to a huge amount of high precision observational data. It is therefore of paramount importance to prepare theoretical, phenomenological and numerical tools to properly analyse all the cosmological information we will be provided with, within pertinently defined paradigms.

LIST OF PUBLICATIONS

PEER-REVIEWED ARTICLES

Diagnostic of Horndeski Theories, L. Perenon, C. Marinoni and F. Piazza, JCAP 1701 (2017) no.01, 035, arXiv:1609.09197

Phenomenology of dark energy: general features of large-scale perturbations, L. Perenon, F. Piazza, C. Marinoni and L. Hui, JCAP 1511 (2015) no.11, arXiv:1506.03047

PROCEEDINGS

General features of single-scalar field dark energy models, L. Perenon, 51st Rencontres de Moriond on Cosmology, 19-26 Mar 2016. La Thuile, Italy, ARISF (2016) – Conference C16-03-19

BIBLIOGRAPHY

[1] Louis Perenon, Federico Piazza, Christian Marinoni, and Lam Hui. "Phenomenology of dark energy: general features of large-scale perturbations." In: *JCAP* 1511.11 (2015), p. 029. DOI: 10.1088/1475-7516/2015/11/029. arXiv: 1506.03047 [astro-ph.CO].

[2] Louis Perenon, Christian Marinoni, and Federico Piazza. "Diagnostic of Horndeski Theories." In: *JCAP* 1701.01 (2017), p. 035. DOI: 10.1088/1475-7516/2017/01/035. arXiv: 1609.09197 [astro-ph.CO].

[3] Eduardo J. Ruiz and Dragan Huterer. "Testing the dark energy consistency with geometry and growth." In: *Phys. Rev.* D91 (2015), p. 063009. DOI: 10.1103/PhysRevD.91.063009. arXiv: 1410.5832 [astro-ph.CO].

[4] Martin Kunz, Savvas Nesseris, and Ignacy Sawicki. "Using dark energy to suppress power at small scales." In: *Phys. Rev.* D92.6 (2015), p. 063006. DOI: 10.1103/PhysRevD.92.063006. arXiv: 1507.01486 [astro-ph.CO].

[5] José Luis Bernal, Licia Verde, and Antonio J. Cuesta. "Parameter splitting in dark energy: is dark energy the same in the background and in the cosmic structures?" In: *JCAP* 1602.02 (2016), p. 059. DOI: 10.1088/1475-7516/2016/02/059. arXiv: 1511.03049 [astro-ph.CO].

[6] Heinrich Steigerwald, Julien Bel, and Christian Marinoni. "Probing non-standard gravity with the growth index: a background independent analysis." In: *JCAP* 1405 (2014), p. 042. DOI: 10.1088/1475-7516/2014/05/042. arXiv: 1403.0898 [astro-ph.CO].

[7] Jérôme Gleyzes, David Langlois, Michele Mancarella, and Filippo Vernizzi. "Effective Theory of Interacting Dark Energy." In: *JCAP* 1508.08 (2015), p. 054. DOI: 10.1088/1475-7516/2015/08/054. arXiv: 1504.05481 [astro-ph.CO].

[8] Eric V. Linder, Gizem Sengör, and Scott Watson. "Is the Effective Field Theory of Dark Energy Effective?" In: *JCAP* 1605.05 (2016), p. 053. DOI: 10.1088/1475-7516/2016/05/053. arXiv: 1512.06180 [astro-ph.CO].

[9] Eric V. Linder. "Challenges in connecting modified gravity theory and observations." In: *Phys. Rev.* D95.2 (2017), p. 023518. DOI: 10.1103/PhysRevD.95.023518. arXiv: 1607.03113 [astro-ph.CO].

[10] Jérôme Gleyzes. "Parametrizing modified gravity for cosmological surveys." In: (2017). arXiv: 1705.04714 [astro-ph.CO].

[11] David Alonso, Emilio Bellini, Pedro G. Ferreira, and Miguel Zumalacárregui. "Observational future of cosmological scalar-tensor theories." In: *Phys. Rev.* D95.6 (2017), p. 063502. DOI: 10.1103/PhysRevD.95.063502. arXiv: 1610.09290 [astro-ph.CO].

[12] Philip Bull et al. "Beyond ΛCDM: Problems, solutions, and the road ahead." In: *Phys. Dark Univ.* 12 (2016), pp. 56–99. DOI: 10.1016/j.dark.2016.02.001. arXiv: 1512.05356 [astro-ph.CO].

[13] Albert Einstein. "Grundgedanken der allgemeinen Relativitätstheorie und Anwendung dieser Theorie in der Astronomie (Fundamental Ideas of the General Theory of Relativity and the Application of this Theory in Astronomy)." In: *Sitzungsber. Preuss. Akad. Wiss. Berlin (Math. Phys.)* 1915 (1915), p. 315.

[14] Albert Einstein. “Zur allgemeinen Relativitätstheorie (On the General Theory of Relativity).” In: *Sitzungsber. Preuss. Akad. Wiss. Berlin (Math. Phys.)* 1915 (1915). [Addendum: Sitzungsber. Preuss. Akad. Wiss. Berlin (Math. Phys.)1915,799(1915)], pp. 778–786.

[15] Albert Einstein. “Erklärung der Perihelbewegung des Merkur aus der allgemeinen Relativitätstheorie (Explanation of the Perihelion Motion of Mercury from the General Theory of Relativity).” In: *Sitzungsber. Preuss. Akad. Wiss. Berlin (Math. Phys.)* 1915 (1915), pp. 831–839.

[16] Albert Einstein. “Feldgleichungen der Gravitation (The Field Equations of Gravitation).” In: *Sitzungsber. Preuss. Akad. Wiss. Berlin (Math. Phys.)* 1915 (1915), pp. 844–847.

[17] Albert Einstein. “Grundlage der allgemeinen Relativitätstheorie (The Foundation of the General Theory of Relativity).” In: *Annalen Phys.* 49 (1916). [Annalen Phys.14,517(2005)], pp. 769–822. DOI: 10.1002/andp.200590044,10.1002/andp.19163540702.

[18] Albert Einstein. “Zur Elektrodynamik bewegter Körper (On the electrodynamics of moving bodies).” In: *Annalen Phys.* 17 (1905). [Annalen Phys.14,194(2005)], pp. 891–921. DOI: 10.1002/andp.200590006.

[19] P. G. Roll, R. Krotkov, and R. H. Dicke. “The equivalence of inertial and passive gravitational mass.” In: *Annals of Physics* 26 (Feb. 1964), pp. 442–517. DOI: 10.1016/0003-4916(64)90259-3.

[20] T. A. Wagner, S. Schlamminger, J. H. Gundlach, and E. G. Adelberger. “Torsion-balance tests of the weak equivalence principle.” In: *Class. Quant. Grav.* 29 (2012), p. 184002. DOI: 10.1088/0264-9381/29/18/184002. arXiv: 1207.2442 [gr-qc].

[21] https://microscope.cnes.fr/en/MICROSCOPE/index.htm.

[22] C.M. Will. *Theory and Experiment in Gravitational Physics*. Cambridge, UK: 2nd ed. Cambridge University Press, 1993.

[23] Timothy Clifton, Pedro G. Ferreira, Antonio Padilla, and Constantinos Skordis. “Modified Gravity and Cosmology.” In: *Phys. Rept.* 513 (2012), pp. 1–189. DOI: 10.1016/j.physrep.2012.01.001. arXiv: 1106.2476 [astro-ph.CO].

[24] Salvatore Capozziello and Mariafelicia De Laurentis. “Extended Theories of Gravity.” In: *Phys. Rept.* 509 (2011), pp. 167–321. DOI: 10.1016/j.physrep.2011.09.003. arXiv: 1108.6266 [gr-qc].

[25] D. Lovelock. “The Einstein tensor and its generalizations.” In: *J. Math. Phys.* 12 (1971), pp. 498–501. DOI: 10.1063/1.1665613.

[26] Clifford M. Will. “The Confrontation between General Relativity and Experiment.” In: *Living Rev. Rel.* 17 (2014), p. 4. DOI: 10.12942/lrr-2014-4. arXiv: 1403.7377 [gr-qc].

[27] F. W. Dyson, A. S. Eddington, and C. Davidson. “A Determination of the Deflection of Light by the Sun’s Gravitational Field, from Observations Made at the Total Eclipse of May 29, 1919.” In: *Phil. Trans. Roy. Soc. Lond.* A220 (1920), pp. 291–333. DOI: 10.1098/rsta.1920.0009.

[28] Albert Einstein. “Kosmologische Betrachtungen zur allgemeinen Relativitätstheorie (Cosmological Considerations in the General Theory of Relativity).” In: *Sitzungsber. Preuss. Akad. Wiss. Berlin (Math. Phys.)* 1917 (1917), pp. 142–152.

[29] W. de Sitter. “On the relativity of inertia. Remarks concerning Einstein’s latest hypothesis.” In: *Koninklijke Nederlandse Akademie van Wetenschappen Proceedings Series B Physical Sciences* 19 (1917), pp. 1217–1225.

[30] A. Friedman. “Über die Krümmung des Raumes (On the Curvature of space).” In: *Z. Phys.* 10 (1922). [Gen. Rel. Grav.31,1991(1999)], pp. 377–386. DOI: 10.1007/BF01332580.

[31] A. Friedmann. “ Über die Möglichkeit einer Welt mit konstanter negativer Krümmung des Raumes (On the Possibility of a world with constant negative curvature of space).” In: *Z. Phys.* 21 (1924). [Gen. Rel. Grav.31,2001(1999)], pp. 326–332. DOI: 10.1007/BF01328280.

[32] G. Lemaître. “Un Univers homogène de masse constante et de rayon croissant rendant compte de la vitesse radiale des nébuleuses extra-galactiques.” In: *Annales de la Société Scientifique de Bruxelles* 47 (1927), pp. 49–59.

[33] Edwin Hubble. “A relation between distance and radial velocity among extra-galactic nebulae.” In: *Proceedings of the National Academy of Sciences* 15.3 (1929), pp. 168–173. DOI: 10.1073/pnas.15.3.168. eprint: http://www.pnas.org/content/15/3/168.full.pdf. URL: http://www.pnas.org/content/15/3/168.short.

[34] V.M. Slipher. “Nebulae.” In: *Proc. Am. Philos. Soc. 56, 403-409 ADS* (1917).

[35] J. Richard Gott III, Mario Juric, David Schlegel, Fiona Hoyle, Michael Vogeley, Max Tegmark, Neta A. Bahcall, and Jon Brinkmann. “A map of the universe.” In: *Astrophys. J.* 624 (2005), p. 463. DOI: 10.1086/428890. arXiv: astro-ph/0310571 [astro-ph].

[36] I. Horvath, J. Hakkila, and Z. Bagoly. “The largest structure of the Universe, defined by Gamma-Ray Bursts.” In: 2013. arXiv: 1311.1104 [astro-ph.CO]. URL: https://inspirehep.net/record/1263350/files/arXiv:1311.1104.pdf.

[37] Daniela Saadeh, Stephen M. Feeney, Andrew Pontzen, Hiranya V. Peiris, and Jason D. McEwen. “How isotropic is the Universe?” In: *Phys. Rev. Lett.* 117.13 (2016), p. 131302. DOI: 10.1103/PhysRevLett.117.131302. arXiv: 1605.07178 [astro-ph.CO].

[38] Arno A. Penzias and Robert Woodrow Wilson. “A Measurement of excess antenna temperature at 4080-Mc/s.” In: *Astrophys. J.* 142 (1965), pp. 419–421. DOI: 10.1086/148307.

[39] Ralph A. Alpher and Robert C. Herman. “On the Relative Abundance of the Elements.” In: *Phys. Rev.* 74 (12 1948), pp. 1737–1742. DOI: 10.1103/PhysRev.74.1737. URL: https://link.aps.org/doi/10.1103/PhysRev.74.1737.

[40] C. Marinoni, J. Bel, and A. Buzzi. “The Scale of Cosmic Isotropy.” In: *JCAP* 1210 (2012), p. 036. DOI: 10.1088/1475-7516/2012/10/036. arXiv: 1205.3309 [astro-ph.CO].

[41] Volker Springel et al. “Simulating the joint evolution of quasars, galaxies and their large-scale distribution.” In: *Nature* 435 (2005), pp. 629–636. DOI: 10.1038/nature03597. arXiv: astro-ph/0504097 [astro-ph].

[42] Viatcheslav F. Mukhanov, H. A. Feldman, and Robert H. Brandenberger. “Theory of cosmological perturbations. Part 1. Classical perturbations. Part 2. Quantum theory of perturbations. Part 3. Extensions.” In: *Phys. Rept.* 215 (1992), pp. 203–333. DOI: 10.1016/0370-1573(92)90044-Z.

[43] Chung-Pei Ma and Edmund Bertschinger. “Cosmological perturbation theory in the synchronous and conformal Newtonian gauges.” In: *Astrophys. J.* 455 (1995), pp. 7–25. DOI: 10.1086/176550. arXiv: astro-ph/9506072 [astro-ph].

[44] Antony Lewis and Sarah Bridle. “Cosmological parameters from CMB and other data: A Monte Carlo approach.” In: *Phys. Rev.* D66 (2002), p. 103511. DOI: 10.1103/PhysRevD.66.103511. arXiv: astro-ph/0205436 [astro-ph].

[45] D. Blas, J. Lesgourgues, and T. Tram. “The Cosmic Linear Anisotropy Solving System (CLASS). Part II: Approximation schemes.” In: *JCAP* 7, 034 (July 2011), p. 034. DOI: 10.1088/1475-7516/2011/07/034. arXiv: 1104.2933.

[46] Marc Davis and P. J. E. Peebles. “A Survey of galaxy redshifts. 5. The Two point position and velocity correlations.” In: *Astrophys. J.* 267 (1982), pp. 465–482. DOI: 10.1086/160884.

[47] S. Chandrasekhar and E. A. Milne. “The Highly Collapsed Configurations of a Stellar Mass.” In: *Mon. Not. Roy. Astron. Soc.* 91.5 (1931), pp. 456–466. DOI: 10.1093/mnras/91.5.456.

[48] S. A. Colgate. “Supernovae as a standard candle for cosmology.” In: *Astrophys. J.* 232 (Sept. 1979), pp. 404–408. DOI: 10.1086/157300.

[49] M. M. Phillips. “The absolute magnitudes of Type IA supernovae.” In: *Astrophys. J.* 413 (1993), pp. L105–L108. DOI: 10.1086/186970.

[50] S. Perlmutter et al. “Measurements of Omega and Lambda from 42 high redshift supernovae.” In: *Astrophys. J.* 517 (1999), pp. 565–586. DOI: 10.1086/307221. arXiv: astro-ph/9812133 [astro-ph].

[51] Adam G. Riess et al. “Observational evidence from supernovae for an accelerating universe and a cosmological constant.” In: *Astron. J.* 116 (1998), pp. 1009–1038. DOI: 10.1086/300499. arXiv: astro-ph/9805201 [astro-ph].

[52] Adam G. Riess. “The case for an accelerating universe from supernovae.” In: *Publ. Astron. Soc. Pac.* 112 (2000), p. 1284. DOI: 10.1086/316624. arXiv: astro-ph/0005229 [astro-ph].

[53] Saul Perlmutter and Brian P. Schmidt. “Measuring cosmology with supernovae.” In: *Lect. Notes Phys.* 598 (2003), pp. 195–217. DOI: 10.1007/3-540-45863-8_11. arXiv: astro-ph/0303428 [astro-ph].

[54] P. A. R. Ade et al. “Planck 2015 results. XIII. Cosmological parameters.” In: (2015). arXiv: 1502.01589 [astro-ph.CO].

[55] N. Suzuki et al. “The Hubble Space Telescope Cluster Supernova Survey. V. Improving the Dark-energy Constraints above z > 1 and Building an Early-type-hosted Supernova Sample.” In: *Astrophys. J.* 746, 85 (Feb. 2012), p. 85. DOI: 10.1088/0004-637X/746/1/85. arXiv: 1105.3470 [astro-ph.CO].

[56] William H. Press and Paul Schechter. “Formation of galaxies and clusters of galaxies by selfsimilar gravitational condensation.” In: *Astrophys. J.* 187 (1974), pp. 425–438. DOI: 10.1086/152650.

[57] Alice Pisani, P. M. Sutter, Nico Hamaus, Esfandiar Alizadeh, Rahul Biswas, Benjamin D. Wandelt, and Christopher M. Hirata. “Counting voids to probe dark energy.” In: *Phys. Rev.* D92.8 (2015), p. 083531. DOI: 10.1103/PhysRevD.92.083531. arXiv: 1503.07690 [astro-ph.CO].

[58] J. A. Tyson, R. A. Wenk, and F. Valdes. “Detection of systematic gravitational lens galaxy image alignments - Mapping dark matter in galaxy clusters.” In: *Astrophys. J.* 349 (1990), pp. L1–L4. DOI: 10.1086/185636.

[59] Henk Hoekstra and Bhuvnesh Jain. "Weak Gravitational Lensing and its Cosmological Applications." In: *Ann. Rev. Nucl. Part. Sci.* 58 (2008), pp. 99–123. DOI: 10.1146/annurev.nucl.58.110707.171151. arXiv: 0805.0139 [astro-ph].

[60] Matthias Bartelmann and Matteo Maturi. "Weak gravitational lensing." In: 2016. arXiv: 1612.06535 [astro-ph.CO]. URL: https://inspirehep.net/record/1505136/files/arXiv:1612.06535.pdf.

[61] Tereasa G. Brainerd, Roger D. Blandford, and Ian Smail. "Measuring galaxy masses using galaxy - galaxy gravitational lensing." In: *Astrophys. J.* 466 (1996), p. 623. DOI: 10.1086/177537. arXiv: astro-ph/9503073 [astro-ph].

[62] Martin Kilbinger. "Cosmology with cosmic shear observations: a review." In: *Rept. Prog. Phys.* 78 (2015), p. 086901. DOI: 10.1088/0034-4885/78/8/086901. arXiv: 1411.0115 [astro-ph.CO].

[63] N. Kaiser. "Clustering in real space and in redshift space." In: *Mon. Not. Roy. Astron. Soc.* 227 (1987), pp. 1–27.

[64] J. C. Jackson. "A Critique of Rees's Theory of Primordial Gravitational Radiation." In: *Monthly Notices of the Royal Astronomical Society* 156.1 (1972), 1P. DOI: 10.1093/mnras/156.1.1P.

[65] P. J. E. Peebles. *Principles of Physical Cosmology*. 1993.

[66] R. Laureijs et al. "Euclid Definition Study Report." In: *ArXiv e-prints* (Oct. 2011). arXiv: 1110.3193 [astro-ph.CO].

[67] J. Amiaux et al. "Euclid Mission: building of a Reference Survey." In: *Proc. SPIE Int. Soc. Opt. Eng.* 8442 (2012), 84420Z. DOI: 10.1117/12.926513. arXiv: 1209.2228 [astro-ph.IM].

[68] Luca Amendola et al. "Cosmology and fundamental physics with the Euclid satellite." In: *Living Rev. Rel.* 16 (2013), p. 6. DOI: 10.12942/lrr-2013-6. arXiv: 1206.1225 [astro-ph.CO].

[69] Philip Bull, Stefano Camera, Alvise Raccanelli, Chris Blake, Pedro G. Ferreira, Mario G. Santos, and Dominik J. Schwarz. "Measuring baryon acoustic oscillations with future SKA surveys." In: *PoS AASKA14 (2015) 024*. 2015. arXiv: 1501.04088 [astro-ph.CO]. URL: https://inspirehep.net/record/1339611/files/arXiv:1501.04088.pdf.

[70] Alvise Raccanelli et al. "Measuring redshift-space distortions with future SKA surveys." In: (2015). arXiv: 1501.03821 [astro-ph.CO].

[71] S. Camera et al. "Cosmology on the Largest Scales with the SKA." In: (2015). arXiv: 1501.03851 [astro-ph.CO].

[72] Roy Maartens, Filipe B. Abdalla, Matt Jarvis, and Mario G. Santos. "Overview of Cosmology with the SKA." In: *PoS* AASKA14 (2015), p. 016. arXiv: 1501.04076 [astro-ph.CO].

[73] https://wfirst.gsfc.nasa.gov/.

[74] Amir Aghamousa et al. "The DESI Experiment Part I: Science,Targeting, and Survey Design." In: (2016). arXiv: 1611.00036 [astro-ph.IM].

[75] Jacob D. Bekenstein. "Black holes and entropy." In: *Phys. Rev.* D7 (1973), pp. 2333–2346. DOI: 10.1103/PhysRevD.7.2333.

[76] Leonard Susskind. "The World as a hologram." In: *J. Math. Phys.* 36 (1995), pp. 6377–6396. DOI: 10.1063/1.531249. arXiv: hep-th/9409089 [hep-th].

[77] Raphael Bousso. “The Holographic principle.” In: *Rev. Mod. Phys.* 74 (2002), pp. 825–874. DOI: 10.1103/RevModPhys.74.825. arXiv: hep-th/0203101 [hep-th].

[78] N. Aghanim et al. “Planck intermediate results. XLVI. Reduction of large-scale systematic effects in HFI polarization maps and estimation of the reionization optical depth.” In: *Astron. Astrophys.* 596 (2016), A107. DOI: 10.1051/0004-6361/201628890. arXiv: 1605.02985 [astro-ph.CO].

[79] Marco Raveri. “Are cosmological data sets consistent with each other within the Λ cold dark matter model?” In: *Phys. Rev.* D93.4 (2016), p. 043522. DOI: 10.1103/PhysRevD.93.043522. arXiv: 1510.00688 [astro-ph.CO].

[80] P. A. R. Ade et al. “Planck 2015 results. XIV. Dark energy and modified gravity.” In: (2015). arXiv: 1502.01590 [astro-ph.CO].

[81] Michel Chevallier and David Polarski. “Accelerating universes with scaling dark matter.” In: *Int. J. Mod. Phys.* D10 (2001), pp. 213–224. DOI: 10.1142/S0218271801000822. arXiv: gr-qc/0009008 [gr-qc].

[82] Eric V. Linder. “Exploring the expansion history of the universe.” In: *Phys. Rev. Lett.* 90 (2003), p. 091301. DOI: 10.1103/PhysRevLett.90.091301. arXiv: astro-ph/0208512 [astro-ph].

[83] Adam G. Riess et al. “A 2.4% Determination of the Local Value of the Hubble Constant.” In: *Astrophys. J.* 826.1 (2016), p. 56. DOI: 10.3847/0004-637X/826/1/56. arXiv: 1604.01424 [astro-ph.CO].

[84] V. Bonvin et al. “H0LiCOW V. New COSMOGRAIL time delays of HE0435-1223: H_0 to 3.8% precision from strong lensing in a flat ΛCDM model.” In: *Mon. Not. Roy. Astron. Soc.* 465.4 (2017), pp. 4914–4930. DOI: 10.1093/mnras/stw3006. arXiv: 1607.01790 [astro-ph.CO].

[85] C. Rodrigues Filho and Edésio M. Barboza. “Constraints on kinematic parameters at $z \neq 0$.” In: (2017). arXiv: 1704.08089 [astro-ph.CO].

[86] N. Suzuki et al. “The Hubble Space Telescope Cluster Supernova Survey: V. Improving the Dark Energy Constraints Above z>1 and Building an Early-Type-Hosted Supernova Sample.” In: *Astrophys. J.* 746 (2012), p. 85. DOI: 10.1088/0004-637X/746/1/85. arXiv: 1105.3470 [astro-ph.CO].

[87] Michele Moresco, Lucia Pozzetti, Andrea Cimatti, Raul Jimenez, Claudia Maraston, Licia Verde, Daniel Thomas, Annalisa Citro, Rita Tojeiro, and David Wilkinson. “A 6% measurement of the Hubble parameter at $z \sim 0.45$: direct evidence of the epoch of cosmic reacceleration.” In: *JCAP* 1605.05 (2016), p. 014. DOI: 10.1088/1475-7516/2016/05/014. arXiv: 1601.01701 [astro-ph.CO].

[88] Catherine Heymans et al. “CFHTLenS: The Canada-France-Hawaii Telescope Lensing Survey.” In: *Mon. Not. Roy. Astron. Soc.* 427 (2012), p. 146. DOI: 10.1111/j.1365-2966.2012.21952.x. arXiv: 1210.0032 [astro-ph.CO].

[89] H. Hildebrandt et al. “KiDS-450: Cosmological parameter constraints from tomographic weak gravitational lensing.” In: *Mon. Not. Roy. Astron. Soc.* 465 (2017), p. 1454. DOI: 10.1093/mnras/stw2805. arXiv: 1606.05338 [astro-ph.CO].

[90] Erminia Calabrese, Anze Slosar, Alessandro Melchiorri, George F. Smoot, and Oliver Zahn. “Cosmic Microwave Weak lensing data as a test for the dark universe.” In: *Phys. Rev.* D77 (2008), p. 123531. DOI: 10.1103/PhysRevD.77.123531. arXiv: 0803.2309 [astro-ph].

[91] N. Aghanim et al. “Planck 2015 results. XI. CMB power spectra, likelihoods, and robustness of parameters.” In: *Astron. Astrophys.* 594 (2016), A11. DOI: 10.1051/0004-6361/201526926. arXiv: 1507.02704 [astro-ph.CO].

[92] G. E. Addison, Y. Huang, D. J. Watts, C. L. Bennett, M. Halpern, G. Hinshaw, and J. L. Weiland. “Quantifying discordance in the 2015 Planck CMB spectrum.” In: *Astrophys. J.* 818.2 (2016), p. 132. DOI: 10.3847/0004-637X/818/2/132. arXiv: 1511.00055 [astro-ph.CO].

[93] Adam G. Riess, Lucas Macri, Stefano Casertano, Hubert Lampeitl, Henry C. Ferguson, Alexei V. Filippenko, Saurabh W. Jha, Weidong Li, and Ryan Chornock. “A 3% Solution: Determination of the Hubble Constant with the Hubble Space Telescope and Wide Field Camera 3.” In: *Astrophys. J.* 730 (2011). [Erratum: Astrophys. J.732,129(2011)], p. 119. DOI: 10.1088/0004-637X/732/2/129,10.1088/0004-637X/730/2/119. arXiv: 1103.2976 [astro-ph.CO].

[94] Charles W. Misner. “The Isotropy of the universe.” In: *Astrophys. J.* 151 (1968), pp. 431–457. DOI: 10.1086/149448.

[95] Alan H. Guth. “The Inflationary Universe: A Possible Solution to the Horizon and Flatness Problems.” In: *Phys. Rev.* D23 (1981), pp. 347–356. DOI: 10.1103/PhysRevD.23.347.

[96] Daniel Baumann. “Inflation.” In: *Physics of the large and the small, TASI 09, proceedings of the Theoretical Advanced Study Institute in Elementary Particle Physics, Boulder, Colorado, USA, 1-26 June 2009*. 2011, pp. 523–686. DOI: 10.1142/9789814327183_0010. arXiv: 0907.5424 [hep-th]. URL: http://inspirehep.net/record/827549/files/arXiv:0907.5424.pdf.

[97] Shinji Tsujikawa. “Introductory review of cosmic inflation.” In: *2nd Tah Poe School on Cosmology: Modern Cosmology Phitsanulok, Thailand, April 17-25, 2003*. 2003. arXiv: hep-ph/0304257 [hep-ph].

[98] Leonardo Senatore and Matias Zaldarriaga. “The Effective Field Theory of Multifield Inflation.” In: *JHEP* 04 (2012), p. 024. DOI: 10.1007/JHEP04(2012)024. arXiv: 1009.2093 [hep-th].

[99] Robert Brandenberger and Patrick Peter. “Bouncing Cosmologies: Progress and Problems.” In: (2016). DOI: 10.1007/s10701-016-0057-0. arXiv: 1603.05834 [hep-th].

[100] D. Battefeld and Patrick Peter. “A Critical Review of Classical Bouncing Cosmologies.” In: *Phys. Rept.* 571 (2015), pp. 1–66. DOI: 10.1016/j.physrep.2014.12.004. arXiv: 1406.2790 [astro-ph.CO].

[101] Kurt Hinterbichler and Justin Khoury. “The Pseudo-Conformal Universe: Scale Invariance from Spontaneous Breaking of Conformal Symmetry.” In: *JCAP* 1204 (2012), p. 023. DOI: 10.1088/1475-7516/2012/04/023. arXiv: 1106.1428 [hep-th].

[102] F. Zwicky. “On the Masses of Nebulae and of Clusters of Nebulae.” In: *APJ* 86 (Oct. 1937), p. 217. DOI: 10.1086/143864.

[103] Gianfranco Bertone, Dan Hooper, and Joseph Silk. “Particle dark matter: Evidence, candidates and constraints.” In: *Phys. Rept.* 405 (2005), pp. 279–390. DOI: 10.1016/j.physrep.2004.08.031. arXiv: hep-ph/0404175 [hep-ph].

[104] Anatoly A. Klypin, Andrey V. Kravtsov, Octavio Valenzuela, and Francisco Prada. “Where are the missing Galactic satellites?” In: *Astrophys. J.* 522 (1999), pp. 82–92. DOI: 10.1086/307643. arXiv: astro-ph/9901240 [astro-ph].

[105] Gianfranco Gentile, P. Salucci, U. Klein, D. Vergani, and P. Kalberla. "The Cored distribution of dark matter in spiral galaxies." In: *Mon. Not. Roy. Astron. Soc.* 351 (2004), p. 903. DOI: 10.1111/j.1365-2966.2004.07836.x. arXiv: astro-ph/0403154 [astro-ph].

[106] Jerome Martin. "Everything You Always Wanted To Know About The Cosmological Constant Problem (But Were Afraid To Ask)." In: *Comptes Rendus Physique* 13 (2012), pp. 566–665. DOI: 10.1016/j.crhy.2012.04.008. arXiv: 1205.3365 [astro-ph.CO].

[107] R. L. Jaffe. "The Casimir effect and the quantum vacuum." In: *Phys. Rev.* D72 (2005), p. 021301. DOI: 10.1103/PhysRevD.72.021301. arXiv: hep-th/0503158 [hep-th].

[108] Navin Sivanandam. "Is the Cosmological Coincidence a Problem?" In: *Phys. Rev.* D87.8 (2013), p. 083514. DOI: 10.1103/PhysRevD.87.083514. arXiv: 1203.4197 [astro-ph.CO].

[109] F. Bernardeau, S. Colombi, E. Gaztanaga, and R. Scoccimarro. "Large scale structure of the universe and cosmological perturbation theory." In: *Phys. Rept.* 367 (2002), pp. 1–248. DOI: 10.1016/S0370-1573(02)00135-7. arXiv: astro-ph/0112551 [astro-ph].

[110] John Joseph M. Carrasco, Mark P. Hertzberg, and Leonardo Senatore. "The Effective Field Theory of Cosmological Large Scale Structures." In: *JHEP* 09 (2012), p. 082. DOI: 10.1007/JHEP09(2012)082. arXiv: 1206.2926 [astro-ph.CO].

[111] R. E. Smith, J. A. Peacock, A. Jenkins, S. D. M. White, C. S. Frenk, F. R. Pearce, P. A. Thomas, G. Efstathiou, and H. M. P. Couchman. "Stable clustering, the halo model and non-linear cosmological power spectra." In: *MNRAS* 341 (June 2003), pp. 1311–1332. DOI: 10.1046/j.1365-8711.2003.06503.x. eprint: astro-ph/0207664.

[112] R. Takahashi, M. Sato, T. Nishimichi, A. Taruya, and M. Oguri. "Revising the Halofit Model for the Nonlinear Matter Power Spectrum." In: *APJ* 761, 152 (Dec. 2012), p. 152. DOI: 10.1088/0004-637X/761/2/152. arXiv: 1208.2701 [astro-ph.CO].

[113] C. Wetterich. "Cosmology and the Fate of Dilatation Symmetry." In: *Nucl. Phys.* B302 (1988), pp. 668–696. DOI: 10.1016/0550-3213(88)90193-9.

[114] Bharat Ratra and P. J. E. Peebles. "Cosmological Consequences of a Rolling Homogeneous Scalar Field." In: *Phys. Rev.* D37 (1988), p. 3406. DOI: 10.1103/PhysRevD.37.3406.

[115] R. R. Caldwell, Rahul Dave, and Paul J. Steinhardt. "Cosmological imprint of an energy component with general equation of state." In: *Phys. Rev. Lett.* 80 (1998), pp. 1582–1585. DOI: 10.1103/PhysRevLett.80.1582. arXiv: astro-ph/9708069 [astro-ph].

[116] Edmund J. Copeland, Andrew R Liddle, and David Wands. "Exponential potentials and cosmological scaling solutions." In: *Phys. Rev.* D57 (1998), pp. 4686–4690. DOI: 10.1103/PhysRevD.57.4686. arXiv: gr-qc/9711068 [gr-qc].

[117] Ivaylo Zlatev, Li-Min Wang, and Paul J. Steinhardt. "Quintessence, cosmic coincidence, and the cosmological constant." In: *Phys. Rev. Lett.* 82 (1999), pp. 896–899. DOI: 10.1103/PhysRevLett.82.896. arXiv: astro-ph/9807002 [astro-ph].

[118] Shinji Tsujikawa. "Quintessence: A Review." In: *Class. Quant. Grav.* 30 (2013), p. 214003. DOI: 10.1088/0264-9381/30/21/214003. arXiv: 1304.1961 [gr-qc].

[119] R. R. Caldwell and Eric V. Linder. "The Limits of quintessence." In: *Phys. Rev. Lett.* 95 (2005), p. 141301. DOI: 10.1103/PhysRevLett.95.141301. arXiv: astro-ph/0505494 [astro-ph].

[120] Paul J. Steinhardt, Li-Min Wang, and Ivaylo Zlatev. "Cosmological tracking solutions." In: *Phys. Rev.* D59 (1999), p. 123504. DOI: 10.1103/PhysRevD.59.123504. arXiv: astro-ph/9812313 [astro-ph].

[121] Arthur Hebecker and C. Wetterich. "Natural quintessence?" In: *Phys. Lett.* B497 (2001), pp. 281–288. DOI: 10.1016/S0370-2693(00)01339-3. arXiv: hep-ph/0008205 [hep-ph].

[122] C. Armendariz-Picon, Viatcheslav F. Mukhanov, and Paul J. Steinhardt. "A Dynamical solution to the problem of a small cosmological constant and late time cosmic acceleration." In: *Phys. Rev. Lett.* 85 (2000), pp. 4438–4441. DOI: 10.1103/PhysRevLett.85.4438. arXiv: astro-ph/0004134 [astro-ph].

[123] C. Armendariz-Picon, Viatcheslav F. Mukhanov, and Paul J. Steinhardt. "Essentials of k essence." In: *Phys. Rev.* D63 (2001), p. 103510. DOI: 10.1103/PhysRevD.63.103510. arXiv: astro-ph/0006373 [astro-ph].

[124] Eric V. Linder. "The paths of quintessence." In: *Phys. Rev.* D73 (2006), p. 063010. DOI: 10.1103/PhysRevD.73.063010. arXiv: astro-ph/0601052 [astro-ph].

[125] Takeshi Chiba, Takahiro Okabe, and Masahide Yamaguchi. "Kinetically driven quintessence." In: *Phys. Rev.* D62 (2000), p. 023511. DOI: 10.1103/PhysRevD.62.023511. arXiv: astro-ph/9912463 [astro-ph].

[126] Nima Arkani-Hamed, Hsin-Chia Cheng, Markus A. Luty, and Shinji Mukohyama. "Ghost condensation and a consistent infrared modification of gravity." In: *JHEP* 05 (2004), p. 074. DOI: 10.1088/1126-6708/2004/05/074. arXiv: hep-th/0312099 [hep-th].

[127] Ashoke Sen. "Supersymmetric world volume action for nonBPS D-branes." In: *JHEP* 10 (1999), p. 008. DOI: 10.1088/1126-6708/1999/10/008. arXiv: hep-th/9909062 [hep-th].

[128] Eva Silverstein and David Tong. "Scalar speed limits and cosmology: Acceleration from D-cceleration." In: *Phys. Rev.* D70 (2004), p. 103505. DOI: 10.1103/PhysRevD.70.103505. arXiv: hep-th/0310221 [hep-th].

[129] Alexei A. Starobinsky. "A New Type of Isotropic Cosmological Models Without Singularity." In: *Phys. Lett.* B91 (1980), pp. 99–102. DOI: 10.1016/0370-2693(80)90670-X.

[130] Antonio De Felice and Shinji Tsujikawa. "f(R) theories." In: *Living Rev. Rel.* 13 (2010), p. 3. DOI: 10.12942/lrr-2010-3. arXiv: 1002.4928 [gr-qc].

[131] Francesco Nitti and Federico Piazza. "Scalar-tensor theories, trace anomalies and the QCD-frame." In: *Phys. Rev.* D86 (2012), p. 122002. DOI: 10.1103/PhysRevD.86.122002. arXiv: 1202.2105 [hep-th].

[132] L. Amendola and S. Tsujikawa. *Dark Energy: Theory and Observations*. 2010.

[133] Wayne Hu and Ignacy Sawicki. "Models of f(R) Cosmic Acceleration that Evade Solar-System Tests." In: *Phys. Rev.* D76 (2007), p. 064004. DOI: 10.1103/PhysRevD.76.064004. arXiv: 0705.1158 [astro-ph].

[134] Alexei A. Starobinsky. "Disappearing cosmological constant in f(R) gravity." In: *JETP Lett.* 86 (2007), pp. 157–163. DOI: 10.1134/S0021364007150027. arXiv: 0706.2041 [astro-ph].

[135] Julien Bel, Philippe Brax, Christian Marinoni, and Patrick Valageas. "Cosmological tests of modified gravity: constraints on $F(R)$ theories from the galaxy clustering ratio." In: *Phys. Rev.* D91.10 (2015), p. 103503. DOI: 10.1103/PhysRevD.91.103503. arXiv: 1406.3347 [astro-ph.CO].

[136] Santiago Esteban Perez Bergliaffa. "Constraining f(R) theories with the energy conditions." In: *Phys. Lett.* B642 (2006), pp. 311–314. DOI: 10.1016/j.physletb.2006.10.003. arXiv: gr-qc/0608072 [gr-qc].

[137] Thomas Faulkner, Max Tegmark, Emory F. Bunn, and Yi Mao. "Constraining f(R) Gravity as a Scalar Tensor Theory." In: *Phys. Rev.* D76 (2007), p. 063505. DOI: 10.1103/PhysRevD.76.063505. arXiv: astro-ph/0612569 [astro-ph].

[138] Philippe Brax, Carsten van de Bruck, Anne-Christine Davis, and Douglas J. Shaw. "f(R) Gravity and Chameleon Theories." In: *Phys. Rev.* D78 (2008), p. 104021. DOI: 10.1103/PhysRevD.78.104021. arXiv: 0806.3415 [astro-ph].

[139] Álvaro de la Cruz-Dombriz, Peter K. S. Dunsby, Sulona Kandhai, and Diego Sáez-Gómez. "Theoretical and observational constraints of viable f(R) theories of gravity." In: *Phys. Rev.* D93.8 (2016), p. 084016. DOI: 10.1103/PhysRevD.93.084016. arXiv: 1511.00102 [gr-qc].

[140] Christof Wetterich. "The Cosmon model for an asymptotically vanishing time dependent cosmological 'constant'." In: *Astron. Astrophys.* 301 (1995), pp. 321–328. arXiv: hep-th/9408025 [hep-th].

[141] Glennys R. Farrar and P. James E. Peebles. "Interacting dark matter and dark energy." In: *Astrophys. J.* 604 (2004), pp. 1–11. DOI: 10.1086/381728. arXiv: astro-ph/0307316 [astro-ph].

[142] W. Zimdahl. "Models of Interacting Dark Energy." In: *AIP Conf. Proc.* 1471 (2012), pp. 51–56. DOI: 10.1063/1.4756811. arXiv: 1204.5892 [astro-ph.CO].

[143] Valentina Salvatelli, Andrea Marchini, Laura Lopez-Honorez, and Olga Mena. "New constraints on Coupled Dark Energy from the Planck satellite experiment." In: *Phys. Rev.* D88.2 (2013), p. 023531. DOI: 10.1103/PhysRevD.88.023531. arXiv: 1304.7119 [astro-ph.CO].

[144] Luca Amendola and Claudia Quercellini. "Tracking and coupled dark energy as seen by WMAP." In: *Phys. Rev.* D68 (2003), p. 023514. DOI: 10.1103/PhysRevD.68.023514. arXiv: astro-ph/0303228 [astro-ph].

[145] G. R. Dvali, Gregory Gabadadze, and Massimo Porrati. "4-D gravity on a brane in 5-D Minkowski space." In: *Phys. Lett.* B485 (2000), pp. 208–214. DOI: 10.1016/S0370-2693(00)00669-9. arXiv: hep-th/0005016 [hep-th].

[146] Arthur Lue. "The phenomenology of dvali-gabadadze-porrati cosmologies." In: *Phys. Rept.* 423 (2006), pp. 1–48. DOI: 10.1016/j.physrep.2005.10.007. arXiv: astro-ph/0510068 [astro-ph].

[147] V. A. Rubakov and M. E. Shaposhnikov. "Extra space-time dimensions: Towards a solution to the cosmological constant problem." In: *Physics Letters B* 125 (May 1983), pp. 139–143. DOI: 10.1016/0370-2693(83)91254-6.

[148] Arthur Lue, Roman Scoccimarro, and Glenn D. Starkman. "Probing Newton's constant on vast scales: DGP gravity, cosmic acceleration and large scale structure." In: *Phys. Rev.* D69 (2004), p. 124015. DOI: 10.1103/PhysRevD.69.124015. arXiv: astro-ph/0401515 [astro-ph].

[149] C. Brans and R. H. Dicke. "Mach's principle and a relativistic theory of gravitation." In: *Phys. Rev.* 124 (1961), pp. 925–935. DOI: 10.1103/PhysRev.124.925.

[150] O. Bertolami and P. J. Martins. "Nonminimal coupling and quintessence." In: *Phys. Rev.* D61 (2000), p. 064007. DOI: 10.1103/PhysRevD.61.064007. arXiv: gr-qc/9910056 [gr-qc].

[151] Clifford M. Will. "The Confrontation between general relativity and experiment." In: *Living Rev. Rel.* 9 (2006), p. 3. DOI: 10.12942/lrr-2006-3. arXiv: gr-qc/0510072 [gr-qc].

[152] Alberto Nicolis, Riccardo Rattazzi, and Enrico Trincherini. "The Galileon as a local modification of gravity." In: *Phys. Rev.* D79 (2009), p. 064036. DOI: 10.1103/PhysRevD.79.064036. arXiv: 0811.2197 [hep-th].

[153] Claudia de Rham and Andrew J. Tolley. "DBI and the Galileon reunited." In: *JCAP* 1005 (2010), p. 015. DOI: 10.1088/1475-7516/2010/05/015. arXiv: 1003.5917 [hep-th].

[154] Savvas Nesseris, Antonio De Felice, and Shinji Tsujikawa. "Observational constraints on Galileon cosmology." In: *Phys. Rev.* D82 (2010), p. 124054. DOI: 10.1103/PhysRevD.82.124054. arXiv: 1010.0407 [astro-ph.CO].

[155] Richard P. Woodard. "Avoiding dark energy with 1/r modifications of gravity." In: *Lect. Notes Phys.* 720 (2007), pp. 403–433. DOI: 10.1007/978-3-540-71013-4_14. arXiv: astro-ph/0601672 [astro-ph].

[156] Hayato Motohashi and Teruaki Suyama. "Third order equations of motion and the Ostrogradsky instability." In: *Phys. Rev.* D91.8 (2015), p. 085009. DOI: 10.1103/PhysRevD.91.085009. arXiv: 1411.3721 [physics.class-ph].

[157] Gregory Walter Horndeski. "Second-order scalar-tensor field equations in a four-dimensional space." In: *Int. J. Theor. Phys.* 10 (1974), pp. 363–384. DOI: 10.1007/BF01807638.

[158] C. Deffayet, Xian Gao, D. A. Steer, and G. Zahariade. "From k-essence to generalised Galileons." In: *Phys. Rev.* D84 (2011), p. 064039. DOI: 10.1103/PhysRevD.84.064039. arXiv: 1103.3260 [hep-th].

[159] Cedric Deffayet, Oriol Pujolas, Ignacy Sawicki, and Alexander Vikman. "Imperfect Dark Energy from Kinetic Gravity Braiding." In: *JCAP* 1010 (2010), p. 026. DOI: 10.1088/1475-7516/2010/10/026. arXiv: 1008.0048 [hep-th].

[160] Jérôme Gleyzes, David Langlois, Federico Piazza, and Filippo Vernizzi. "Healthy theories beyond Horndeski." In: *Phys. Rev. Lett.* 114.21 (2015), p. 211101. DOI: 10.1103/PhysRevLett.114.211101. arXiv: 1404.6495 [hep-th].

[161] Miguel Zumalacárregui and Juan García-Bellido. "Transforming gravity: from derivative couplings to matter to second-order scalar-tensor theories beyond the Horndeski Lagrangian." In: *Phys. Rev.* D89 (2014), p. 064046. DOI: 10.1103/PhysRevD.89.064046. arXiv: 1308.4685 [gr-qc].

[162] A. I. Vainshtein. "To the problem of nonvanishing gravitation mass." In: *Phys. Lett.* B39 (1972), pp. 393–394. DOI: 10.1016/0370-2693(72)90147-5.

[163] E. Babichev, C. Deffayet, and R. Ziour. "k-Mouflage gravity." In: *Int. J. Mod. Phys.* D18 (2009), pp. 2147–2154. DOI: 10.1142/S0218271809016107. arXiv: 0905.2943 [hep-th].

[164] Gia Dvali, Gian F. Giudice, Cesar Gomez, and Alex Kehagias. "UV-Completion by Classicalization." In: *JHEP* 08 (2011), p. 108. DOI: 10.1007/JHEP08(2011)108. arXiv: 1010.1415 [hep-ph].

[165] Justin Khoury and Amanda Weltman. "Chameleon fields: Awaiting surprises for tests of gravity in space." In: *Phys. Rev. Lett.* 93 (2004), p. 171104. DOI: 10.1103/PhysRevLett.93.171104. arXiv: astro-ph/0309300 [astro-ph].

[166] Kurt Hinterbichler and Justin Khoury. “Symmetron Fields: Screening Long-Range Forces Through Local Symmetry Restoration.” In: *Phys. Rev. Lett.* 104 (2010), p. 231301. DOI: 10.1103/PhysRevLett.104.231301. arXiv: 1001.4525 [hep-th].

[167] P. Brax, C. van de Bruck, A.-C. Davis, and D. Shaw. “Dilaton and modified gravity.” In: *Phys. Rev.* 6, 063519 (Sept. 2010), p. 063519. DOI: 10.1103/PhysRevD.82.063519. arXiv: 1005.3735.

[168] Claudia de Rham. “Massive Gravity.” In: *Living Rev. Rel.* 17 (2014), p. 7. DOI: 10.12942/lrr-2014-7. arXiv: 1401.4173 [hep-th].

[169] Nima Arkani-Hamed, Savas Dimopoulos, Gia Dvali, and Gregory Gabadadze. “Nonlocal modification of gravity and the cosmological constant problem.” In: (2002). arXiv: hep-th/0209227 [hep-th].

[170] Justin Khoury. “Les Houches Lectures on Physics Beyond the Standard Model of Cosmology.” In: (2013). arXiv: 1312.2006 [astro-ph.CO].

[171] Alberto Nicolis and Riccardo Rattazzi. “Classical and quantum consistency of the DGP model.” In: *JHEP* 06 (2004), p. 059. DOI: 10.1088/1126-6708/2004/06/059. arXiv: hep-th/0404159 [hep-th].

[172] Markus A. Luty, Massimo Porrati, and Riccardo Rattazzi. “Strong interactions and stability in the DGP model.” In: *JHEP* 09 (2003), p. 029. DOI: 10.1088/1126-6708/2003/09/029. arXiv: hep-th/0303116 [hep-th].

[173] Paolo Creminelli, Markus A. Luty, Alberto Nicolis, and Leonardo Senatore. “Starting the Universe: Stable Violation of the Null Energy Condition and Non-standard Cosmologies.” In: *JHEP* 12 (2006), p. 080. DOI: 10.1088/1126-6708/2006/12/080. arXiv: hep-th/0606090 [hep-th].

[174] Clifford Cheung, Paolo Creminelli, A. Liam Fitzpatrick, Jared Kaplan, and Leonardo Senatore. “The Effective Field Theory of Inflation.” In: *JHEP* 03 (2008), p. 014. DOI: 10.1088/1126-6708/2008/03/014. arXiv: 0709.0293 [hep-th].

[175] Paolo Creminelli, Guido D’Amico, Jorge Norena, and Filippo Vernizzi. “The Effective Theory of Quintessence: the $w < -1$ Side Unveiled.” In: *JCAP* 0902 (2009), p. 018. DOI: 10.1088/1475-7516/2009/02/018. arXiv: 0811.0827 [astro-ph].

[176] Giulia Gubitosi, Federico Piazza, and Filippo Vernizzi. “The Effective Field Theory of Dark Energy.” In: *JCAP* 1302 (2013). [JCAP1302,032(2013)], p. 032. DOI: 10.1088/1475-7516/2013/02/032. arXiv: 1210.0201 [hep-th].

[177] Jerome Gleyzes, David Langlois, Federico Piazza, and Filippo Vernizzi. “Essential Building Blocks of Dark Energy.” In: *JCAP* 1308 (2013), p. 025. DOI: 10.1088/1475-7516/2013/08/025. arXiv: 1304.4840 [hep-th].

[178] Federico Piazza and Filippo Vernizzi. “Effective Field Theory of Cosmological Perturbations.” In: *Class. Quant. Grav.* 30 (2013), p. 214007. DOI: 10.1088/0264-9381/30/21/214007. arXiv: 1307.4350 [hep-th].

[179] Jolyon K. Bloomfield, Éanna É. Flanagan, Minjoon Park, and Scott Watson. “Dark energy or modified gravity? An effective field theory approach.” In: *JCAP* 1308 (2013), p. 010. DOI: 10.1088/1475-7516/2013/08/010. arXiv: 1211.7054 [astro-ph.CO].

[180] Jolyon Bloomfield. “A Simplified Approach to General Scalar-Tensor Theories.” In: *JCAP* 1312 (2013), p. 044. DOI: 10.1088/1475-7516/2013/12/044. arXiv: 1304.6712 [astro-ph.CO].

[181] Ryotaro Kase and Shinji Tsujikawa. “Effective field theory approach to modified gravity including Horndeski theory and Hořava–Lifshitz gravity.” In: *Int. J. Mod. Phys.* D23.13 (2015), p. 1443008. DOI: 10.1142/S0218271814430081. arXiv: 1409.1984 [hep-th].

[182] Noemi Frusciante, Marco Raveri, Daniele Vernieri, Bin Hu, and Alessandra Silvestri. “Hořava Gravity in the Effective Field Theory formalism: From cosmology to observational constraints.” In: *Phys. Dark Univ.* 13 (2016), pp. 7–24. DOI: 10.1016/j.dark.2016.03.002. arXiv: 1508.01787 [astro-ph.CO].

[183] Emilio Bellini and Ignacy Sawicki. “Maximal freedom at minimum cost: linear large-scale structure in general modifications of gravity.” In: *JCAP* 1407 (2014), p. 050. DOI: 10.1088/1475-7516/2014/07/050. arXiv: 1404.3713 [astro-ph.CO].

[184] Ryotaro Kase, László Árpád Gergely, and Shinji Tsujikawa. “Effective field theory of modified gravity on the spherically symmetric background: leading order dynamics and the odd-type perturbations.” In: *Phys. Rev.* D90.12 (2014), p. 124019. DOI: 10.1103/PhysRevD.90.124019. arXiv: 1406.2402 [hep-th].

[185] Lucas Lombriser and Andy Taylor. “Classifying Linearly Shielded Modified Gravity Models in Effective Field Theory.” In: *Phys. Rev. Lett.* 114.3 (2015), p. 031101. DOI: 10.1103/PhysRevLett.114.031101. arXiv: 1405.2896 [astro-ph.CO].

[186] Antonio De Felice and Shinji Tsujikawa. “Inflationary gravitational waves in the effective field theory of modified gravity.” In: *Phys. Rev.* D91.10 (2015), p. 103506. DOI: 10.1103/PhysRevD.91.103506. arXiv: 1411.0736 [hep-th].

[187] Shinji Tsujikawa. “Disformal invariance of cosmological perturbations in a generalized class of Horndeski theories.” In: *JCAP* 1504.04 (2015), p. 043. DOI: 10.1088/1475-7516/2015/04/043. arXiv: 1412.6210 [hep-th].

[188] David Pirtskhalava, Luca Santoni, Enrico Trincherini, and Filippo Vernizzi. “Weakly Broken Galileon Symmetry.” In: *JCAP* 1509.09 (2015), p. 007. DOI: 10.1088/1475-7516/2015/09/007. arXiv: 1505.00007 [hep-th].

[189] Marco Crisostomi, Kazuya Koyama, and Gianmassimo Tasinato. “Extended Scalar-Tensor Theories of Gravity.” In: *JCAP* 1604.04 (2016), p. 044. DOI: 10.1088/1475-7516/2016/04/044. arXiv: 1602.03119 [hep-th].

[190] Antonio De Felice, Noemi Frusciante, and Georgios Papadomanolakis. “On the stability conditions for theories of modified gravity in the presence of matter fields.” In: *JCAP* 1703.03 (2017), p. 027. DOI: 10.1088/1475-7516/2017/03/027. arXiv: 1609.03599 [gr-qc].

[191] Antonio De Felice, Noemi Frusciante, and Georgios Papadomanolakis. “A de Sitter limit analysis for dark energy and modified gravity models.” In: (2017). arXiv: 1705.01960 [gr-qc].

[192] Guido D’Amico, Zhiqi Huang, Michele Mancarella, and Filippo Vernizzi. “Weakening Gravity on Redshift-Survey Scales with Kinetic Matter Mixing.” In: (2016). DOI: 10.1088/1475-7516/2017/02/014. arXiv: 1609.01272 [astro-ph.CO].

[193] Noemi Frusciante and Georgios Papadomanolakis. “Tackling non-linearities with the effective field theory of dark energy and modified gravity.” In: (2017). arXiv: 1706.02719 [gr-qc].

[194] László Á. Gergely and Shinji Tsujikawa. “Effective field theory of modified gravity with two scalar fields: dark energy and dark matter.” In: *Phys. Rev.* D89.6 (2014), p. 064059. DOI: 10.1103/PhysRevD.89.064059. arXiv: 1402.0553 [hep-th].

[195] Philippe Brax and Patrick Valageas. "The effective field theory of K-mouflage." In: *JCAP* 1601.01 (2016), p. 020. DOI: 10.1088/1475-7516/2016/01/020. arXiv: 1509.00611 [astro-ph.CO].

[196] David Langlois, Michele Mancarella, Karim Noui, and Filippo Vernizzi. "Effective Description of Higher-Order Scalar-Tensor Theories." In: *JCAP* 1705.05 (2017), p. 033. DOI: 10.1088/1475-7516/2017/05/033. arXiv: 1703.03797 [hep-th].

[197] Federico Piazza, Heinrich Steigerwald, and Christian Marinoni. "Phenomenology of dark energy: exploring the space of theories with future redshift surveys." In: *JCAP* 1405 (2014), p. 043. DOI: 10.1088/1475-7516/2014/05/043. arXiv: 1312.6111 [astro-ph.CO].

[198] Steven Weinberg. "Physical Processes in a Convergent Theory of the Weak and Electromagnetic Interactions." In: *Phys. Rev. Lett.* 27 (1971), pp. 1688–1691. DOI: 10.1103/PhysRevLett.27.1688.

[199] Hideo Kodama and Misao Sasaki. "Cosmological Perturbation Theory." In: *Prog. Theor. Phys. Suppl.* 78 (1984), pp. 1–166. DOI: 10.1143/PTPS.78.1.

[200] Shin'ichi Nojiri and Sergei D. Odintsov. "Modified Gauss-Bonnet theory as gravitational alternative for dark energy." In: *Phys. Lett.* B631 (2005), pp. 1–6. DOI: 10.1016/j.physletb.2005.10.010. arXiv: hep-th/0508049 [hep-th].

[201] Tessa Baker, Pedro G. Ferreira, Constantinos Skordis, and Joe Zuntz. "Towards a fully consistent parameterization of modified gravity." In: *Phys. Rev.* D84 (2011), p. 124018. DOI: 10.1103/PhysRevD.84.124018. arXiv: 1107.0491 [astro-ph.CO].

[202] Alberto Nicolis, Riccardo Penco, Federico Piazza, and Riccardo Rattazzi. "Zoology of condensed matter: Framids, ordinary stuff, extra-ordinary stuff." In: *JHEP* 06 (2015), p. 155. DOI: 10.1007/JHEP06(2015)155. arXiv: 1501.03845 [hep-th].

[203] Levon Pogosian, Alessandra Silvestri, Kazuya Koyama, and Gong-Bo Zhao. "How to optimally parametrize deviations from General Relativity in the evolution of cosmological perturbations?" In: *Phys. Rev.* D81 (2010), p. 104023. DOI: 10.1103/PhysRevD.81.104023. arXiv: 1002.2382 [astro-ph.CO].

[204] Yong-Seon Song, Gong-Bo Zhao, David Bacon, Kazuya Koyama, Robert C. Nichol, and Levon Pogosian. "Complementarity of Weak Lensing and Peculiar Velocity Measurements in Testing General Relativity." In: *Phys. Rev.* D84 (2011), p. 083523. DOI: 10.1103/PhysRevD.84.083523. arXiv: 1011.2106 [astro-ph.CO].

[205] Fergus Simpson et al. "CFHTLenS: Testing the Laws of Gravity with Tomographic Weak Lensing and Redshift Space Distortions." In: *Mon. Not. Roy. Astron. Soc.* 429 (2013), p. 2249. DOI: 10.1093/mnras/sts493. arXiv: 1212.3339 [astro-ph.CO].

[206] Bin Hu, Marco Raveri, Noemi Frusciante, and Alessandra Silvestri. "Effective Field Theory of Cosmic Acceleration: an implementation in CAMB." In: *Phys. Rev.* D89.10 (2014), p. 103530. DOI: 10.1103/PhysRevD.89.103530. arXiv: 1312.5742 [astro-ph.CO].

[207] Miguel Zumalacárregui, Emilio Bellini, Ignacy Sawicki, and Julien Lesgourgues. "hi_class: Horndeski in the Cosmic Linear Anisotropy Solving System." In: (2016). arXiv: 1605.06102 [astro-ph.CO].

[208] Johannes Noller, Francesca von Braun-Bates, and Pedro G. Ferreira. "Relativistic scalar fields and the quasistatic approximation in theories of modified gravity." In: *Phys. Rev.* D89.2 (2014), p. 023521. DOI: 10.1103/PhysRevD.89.023521. arXiv: 1310.3266 [astro-ph.CO].

[209] Ignacy Sawicki and Emilio Bellini. "Limits of quasistatic approximation in modified-gravity cosmologies." In: *Phys. Rev.* D92.8 (2015), p. 084061. DOI: 10.1103/PhysRevD.92.084061. arXiv: 1503.06831 [astro-ph.CO].

[210] Junpu Wang, Lam Hui, and Justin Khoury. "No-Go Theorems for Generalized Chameleon Field Theories." In: *Phys. Rev. Lett.* 109 (2012), p. 241301. DOI: 10.1103/PhysRevLett.109.241301. arXiv: 1208.4612 [astro-ph.CO].

[211] James G. Williams, Slava G. Turyshev, and Dale Boggs. "Lunar Laser Ranging Tests of the Equivalence Principle." In: *Class. Quant. Grav.* 29 (2012), p. 184004. DOI: 10.1088/0264-9381/29/18/184004. arXiv: 1203.2150 [gr-qc].

[212] B. Bertotti, L. Iess, and P. Tortora. "A test of general relativity using radio links with the Cassini spacecraft." In: *Nature* 425 (2003), pp. 374–376. DOI: 10.1038/nature01997.

[213] Bhuvnesh Jain, Vinu Vikram, and Jeremy Sakstein. "Astrophysical Tests of Modified Gravity: Constraints from Distance Indicators in the Nearby Universe." In: *Astrophys. J.* 779 (2013), p. 39. DOI: 10.1088/0004-637X/779/1/39. arXiv: 1204.6044 [astro-ph.CO].

[214] Vinu Vikram, Anna Cabré, Bhuvnesh Jain, and J. T. VanderPlas. "Astrophysical Tests of Modified Gravity: the Morphology and Kinematics of Dwarf Galaxies." In: *JCAP* 1308 (2013), p. 020. DOI: 10.1088/1475-7516/2013/08/020. arXiv: 1303.0295 [astro-ph.CO].

[215] Nathan Chow and Justin Khoury. "Galileon Cosmology." In: *Phys. Rev.* D80 (2009), p. 024037. DOI: 10.1103/PhysRevD.80.024037. arXiv: 0905.1325 [hep-th].

[216] C. Wetterich. "Quintessence: The Dark energy in the universe?" In: *Space Sci. Rev.* 100 (2002), pp. 195–206. DOI: 10.1023/A:1015878430289. arXiv: astro-ph/0110211 [astro-ph].

[217] Rachel Bean, Steen H. Hansen, and Alessandro Melchiorri. "Early universe constraints on a primordial scaling field." In: *Phys. Rev.* D64 (2001), p. 103508. DOI: 10.1103/PhysRevD.64.103508. arXiv: astro-ph/0104162 [astro-ph].

[218] Michael Doran and Georg Robbers. "Early dark energy cosmologies." In: *JCAP* 0606 (2006), p. 026. DOI: 10.1088/1475-7516/2006/06/026. arXiv: astro-ph/0601544 [astro-ph].

[219] Christof Wetterich. "Phenomenological parameterization of quintessence." In: *Phys. Lett.* B594 (2004), pp. 17–22. DOI: 10.1016/j.physletb.2004.05.008. arXiv: astro-ph/0403289 [astro-ph].

[220] Erminia Calabrese, Dragan Huterer, Eric V. Linder, Alessandro Melchiorri, and Luca Pagano. "Limits on dark radiation, early dark energy, and relativistic degrees of freedom." In: *Phys. Rev. D* 83 (12 2011), p. 123504. DOI: 10.1103/PhysRevD.83.123504. URL: http://link.aps.org/doi/10.1103/PhysRevD.83.123504.

[221] Christian L Reichardt, Roland de Putter, Oliver Zahn, and Zhen Hou. "New limits on Early Dark Energy from the South Pole Telescope." In: *Astrophys. J.* 749 (2012), p. L9. DOI: 10.1088/2041-8205/749/1/L9. arXiv: 1110.5328 [astro-ph.CO].

[222] Jonathan L. Sievers et al. "The Atacama Cosmology Telescope: Cosmological parameters from three seasons of data." In: *JCAP* 1310 (2013), p. 060. DOI: 10.1088/1475-7516/2013/10/060. arXiv: 1301.0824 [astro-ph.CO].

[223] Maria Archidiacono, Laura Lopez-Honorez, and Olga Mena. "Current constraints on early and stressed dark energy models and future 21 cm perspectives." In: *Phys. Rev.* D90.12 (2014), p. 123016. DOI: 10.1103/PhysRevD.90.123016. arXiv: 1409.1802 [astro-ph.CO].

[224] Valeria Pettorino, Luca Amendola, and Christof Wetterich. "How early is early dark energy?" In: *Phys. Rev.* D87 (2013), p. 083009. DOI: 10.1103/PhysRevD.87.083009. arXiv: 1301.5279 [astro-ph.CO].

[225] Difu Shi and Carlton M. Baugh. "Can we distinguish early dark energy from a cosmological constant?" In: (2015). arXiv: 1511.00692 [astro-ph.CO].

[226] Bo-Yu Pu, Xiao-Dong Xu, Bin Wang, and Elcio Abdalla. "Early dark energy and its interaction with dark matter." In: *Phys. Rev.* D92.12 (2015), p. 123537. DOI: 10.1103/PhysRevD.92.123537. arXiv: 1412.4091 [astro-ph.CO].

[227] Philippe Brax, Carsten van de Bruck, Sebastien Clesse, Anne-Christine Davis, and Gregory Sculthorpe. "Early Modified Gravity: Implications for Cosmology." In: *Phys. Rev.* D89.12 (2014), p. 123507. DOI: 10.1103/PhysRevD.89.123507. arXiv: 1312.3361 [astro-ph.CO].

[228] Jérôme Gleyzes, David Langlois, Michele Mancarella, and Filippo Vernizzi. "Effective Theory of Dark Energy at Redshift Survey Scales." In: *JCAP* 1602.02 (2016), p. 056. DOI: 10.1088/1475-7516/2016/02/056. arXiv: 1509.02191 [astro-ph.CO].

[229] Emilio Bellini, Antonio J. Cuesta, Raul Jimenez, and Licia Verde. "Constraints on deviations from ΛCDM within Horndeski gravity." In: *JCAP* 1602.02 (2016). [Erratum: JCAP1606,no.06,E01(2016], p. 053. DOI: 10.1088/1475-7516/2016/06/E01,10.1088/1475-7516/2016/02/053. arXiv: 1509.07816 [astro-ph.CO].

[230] Emilio Bellini, Raul Jimenez, and Licia Verde. "Signatures of Horndeski gravity on the Dark Matter Bispectrum." In: *JCAP* 1505.05 (2015), p. 057. DOI: 10.1088/1475-7516/2015/05/057. arXiv: 1504.04341 [astro-ph.CO].

[231] Allan Adams, Nima Arkani-Hamed, Sergei Dubovsky, Alberto Nicolis, and Riccardo Rattazzi. "Causality, analyticity and an IR obstruction to UV completion." In: *JHEP* 10 (2006), p. 014. DOI: 10.1088/1126-6708/2006/10/014. arXiv: hep-th/0602178 [hep-th].

[232] Jose Beltran Jimenez, Federico Piazza, and Hermano Velten. "Evading the Vainshtein Mechanism with Anomalous Gravitational Wave Speed: Constraints on Modified Gravity from Binary Pulsars." In: *Phys. Rev. Lett.* 116.6 (2016), p. 061101. DOI: 10.1103/PhysRevLett.116.061101. arXiv: 1507.05047 [gr-qc].

[233] Guy D. Moore and Ann E. Nelson. "Lower bound on the propagation speed of gravity from gravitational Cherenkov radiation." In: *JHEP* 09 (2001), p. 023. DOI: 10.1088/1126-6708/2001/09/023. arXiv: hep-ph/0106220 [hep-ph].

[234] Jean-Philippe Uzan. "Varying Constants, Gravitation and Cosmology." In: *Living Rev. Rel.* 14 (2011), p. 2. DOI: 10.12942/lrr-2011-2. arXiv: 1009.5514 [astro-ph.CO].

[235] J. Neveu, V. Ruhlmann-Kleider, A. Conley, N. Palanque-Delabrouille, P. Astier, J. Guy, and E. Babichev. "Experimental constraints on the uncoupled Galileon model from SNLS3 data and other cosmological probes." In: *Astron. Astrophys.* 555 (2013), A53. DOI: 10.1051/0004-6361/201321256. arXiv: 1302.2786 [gr-qc].

[236] Alexandre Barreira, Baojiu Li, Carlton M. Baugh, and Silvia Pascoli. "Spherical collapse in Galileon gravity: fifth force solutions, halo mass function and halo bias." In: *JCAP* 1311 (2013), p. 056. DOI: 10.1088/1475-7516/2013/11/056. arXiv: 1308.3699 [astro-ph.CO].

[237] Shinji Tsujikawa. "Possibility of realizing weak gravity in redshift space distortion measurements." In: *Phys. Rev.* D92.4 (2015), p. 044029. DOI: 10.1103/PhysRevD.92.044029. arXiv: 1505.02459 [astro-ph.CO].

[238] Lucas Lombriser and Nelson A. Lima. "Challenges to Self-Acceleration in Modified Gravity from Gravitational Waves and Large-Scale Structure." In: *Phys. Lett.* B765 (2017), pp. 382–385. DOI: 10.1016/j.physletb.2016.12.048. arXiv: 1602.07670 [astro-ph.CO].

[239] Teppei Okumura et al. "The Subaru FMOS galaxy redshift survey (FastSound). IV. New constraint on gravity theory from redshift space distortions at $z \sim 1.4$." In: *Publ. Astron. Soc. Jap.* 68.3, id. 38 (2016), p. 24. DOI: 10.1093/pasj/psw029. arXiv: 1511.08083 [astro-ph.CO].

[240] Levon Pogosian and Alessandra Silvestri. "What can cosmology tell us about gravity? Constraining Horndeski gravity with Σ and μ." In: *Phys. Rev.* D94.10 (2016), p. 104014. DOI: 10.1103/PhysRevD.94.104014. arXiv: 1606.05339 [astro-ph.CO].

[241] Atsushi Nishizawa and Takashi Nakamura. "Measuring Speed of Gravitational Waves by Observations of Photons and Neutrinos from Compact Binary Mergers and Supernovae." In: *Phys. Rev.* D90.4 (2014), p. 044048. DOI: 10.1103/PhysRevD.90.044048. arXiv: 1406.5544 [gr-qc].

[242] Dario Bettoni, Jose María Ezquiaga, Kurt Hinterbichler, and Miguel Zumalacárregui. "Gravitational Waves and the Fate of Scalar-Tensor Gravity." In: (2016). arXiv: 1608.01982 [gr-qc].

[243] Zhiqi Huang. "Observational effects of a running Planck mass." In: *Phys. Rev.* D93.4 (2016), p. 043538. DOI: 10.1103/PhysRevD.93.043538. arXiv: 1511.02808 [astro-ph.CO].

[244] Jérôme Gleyzes, David Langlois, Federico Piazza, and Filippo Vernizzi. "Exploring gravitational theories beyond Horndeski." In: *JCAP* 1502 (2015), p. 018. DOI: 10.1088/1475-7516/2015/02/018. arXiv: 1408.1952 [astro-ph.CO].

[245] Jérôme Gleyzes, David Langlois, and Filippo Vernizzi. "A unifying description of dark energy." In: *Int. J. Mod. Phys.* D23.13 (2015), p. 1443010. DOI: 10.1142/S021827181443010X. arXiv: 1411.3712 [hep-th].

[246] Janina Renk, Miguel Zumalacarregui, and Francesco Montanari. "Gravity at the horizon: on relativistic effects, CMB-LSS correlations and ultra-large scales in Horndeski's theory." In: *JCAP* 1607.07 (2016), p. 040. DOI: 10.1088/1475-7516/2016/07/040. arXiv: 1604.03487 [astro-ph.CO].

[247] Valentina Salvatelli, Federico Piazza, and Christian Marinoni. "Constraints on modified gravity from Planck 2015: when the health of your theory makes the difference." In: *JCAP* 1609.09 (2016), p. 027. DOI: 10.1088/1475-7516/2016/09/027. arXiv: 1602.08283 [astro-ph.CO].

[248] Marco Raveri, Philip Bull, Alessandra Silvestri, and Levon Pogosian. "Priors on the effective Dark Energy equation of state in scalar-tensor theories." In: (2017). arXiv: 1703.05297 [astro-ph.CO].

[249] Marco Raveri, Bin Hu, Noemi Frusciante, and Alessandra Silvestri. "Effective Field Theory of Cosmic Acceleration: constraining dark energy with CMB data." In: *Phys. Rev.* D90.4 (2014), p. 043513. DOI: 10.1103/PhysRevD.90.043513. arXiv: 1405.1022 [astro-ph.CO].

[250] Bin Hu and Marco Raveri. "Can modified gravity models reconcile the tension between the CMB anisotropy and lensing maps in Planck-like observations?" In: *Phys. Rev.* D91.12 (2015), p. 123515. DOI: 10.1103/PhysRevD.91.123515. arXiv: 1502.06599 [astro-ph.CO].

[251] Bin Hu, Marco Raveri, Matteo Rizzato, and Alessandra Silvestri. "Testing Hu–Sawicki f(R) gravity with the effective field theory approach." In: *Mon. Not. Roy. Astron. Soc.* 459.4 (2016), pp. 3880–3889. DOI: 10.1093/mnras/stw775. arXiv: 1601.07536 [astro-ph.CO].

[252] Pengjie Zhang, Michele Liguori, Rachel Bean, and Scott Dodelson. "Probing Gravity at Cosmological Scales by Measurements which Test the Relationship between Gravitational Lensing and Matter Overdensity." In: *Phys. Rev. Lett.* 99 (2007), p. 141302. DOI: 10.1103/PhysRevLett.99.141302. arXiv: 0704.1932 [astro-ph].

[253] Petr Horava. "Membranes at Quantum Criticality." In: *JHEP* 03 (2009), p. 020. DOI: 10.1088/1126-6708/2009/03/020. arXiv: 0812.4287 [hep-th].

[254] Petr Horava. "Quantum Gravity at a Lifshitz Point." In: *Phys. Rev.* D79 (2009), p. 084008. DOI: 10.1103/PhysRevD.79.084008. arXiv: 0901.3775 [hep-th].

[255] Nelson A. Lima, Vanessa Smer-Barreto, and Lucas Lombriser. "Constraints on decaying early modified gravity from cosmological observations." In: *Phys. Rev.* D94.8 (2016), p. 083507. DOI: 10.1103/PhysRevD.94.083507. arXiv: 1603.05239 [astro-ph.CO].

[256] Jason S. Y. Leung and Zhiqi Huang. "Marginalized Fisher Forecast for Horndeski Dark Energy Models." In: *Int. J. Mod. Phys.* D0 (2017), p. 1750070. DOI: 10.1142/S0218271817500705. arXiv: 1604.07330 [astro-ph.CO].

[257] Ryo Saito, Daisuke Yamauchi, Shuntaro Mizuno, Jérôme Gleyzes, and David Langlois. "Modified gravity inside astrophysical bodies." In: *JCAP* 1506 (2015), p. 008. DOI: 10.1088/1475-7516/2015/06/008. arXiv: 1503.01448 [gr-qc].

[258] Jeremy Sakstein. "Hydrogen Burning in Low Mass Stars Constrains Scalar-Tensor Theories of Gravity." In: *Phys. Rev. Lett.* 115 (2015), p. 201101. DOI: 10.1103/PhysRevLett.115.201101. arXiv: 1510.05964 [astro-ph.CO].

[259] Jeremy Sakstein. "Testing Gravity Using Dwarf Stars." In: *Phys. Rev.* D92 (2015), p. 124045. DOI: 10.1103/PhysRevD.92.124045. arXiv: 1511.01685 [astro-ph.CO].

[260] Jeremy Sakstein, Harry Wilcox, David Bacon, Kazuya Koyama, and Robert C. Nichol. "Testing Gravity Using Galaxy Clusters: New Constraints on Beyond Horndeski Theories." In: *JCAP* 1607.07 (2016), p. 019. DOI: 10.1088/1475-7516/2016/07/019. arXiv: 1603.06368 [astro-ph.CO].

[261] Lucas Lombriser and Andy Taylor. "Breaking a Dark Degeneracy with Gravitational Waves." In: *JCAP* 1603.03 (2016), p. 031. DOI: 10.1088/1475-7516/2016/03/031. arXiv: 1509.08458 [astro-ph.CO].

[262] Ignacy Sawicki, Ippocratis D. Saltas, Mariele Motta, Luca Amendola, and Martin Kunz. "Nonstandard gravitational waves imply gravitational slip: On the difficulty of partially hiding new gravitational degrees of freedom." In: *Phys. Rev.* D95.8 (2017), p. 083520. DOI: 10.1103/PhysRevD.95.083520. arXiv: 1612.02002 [astro-ph.CO].

[263] Bin Hu, Marco Raveri, Alessandra Silvestri, and Noemi Frusciante. "Exploring massive neutrinos in dark cosmologies with *EFTCAMB*/ EFTCosmoMC." In: *Phys. Rev.* D91.6 (2015), p. 063524. DOI: 10.1103/PhysRevD.91.063524. arXiv: 1410.5807 [astro-ph.CO].

[264] Nicola Bellomo, Emilio Bellini, Bin Hu, Raul Jimenez, Carlos Pena-Garay, and Licia Verde. "Hiding neutrino mass in modified gravity cosmologies." In: *JCAP* 1702.02 (2017), p. 043. DOI: 10.1088/1475-7516/2017/02/043. arXiv: 1612.02598 [astro-ph.CO].

[265] Shinji Tsujikawa. “Cosmological disformal transformations to the Einstein frame and gravitational couplings with matter perturbations.” In: *Phys. Rev.* D92.6 (2015), p. 064047. DOI: 10.1103/PhysRevD.92.064047. arXiv: 1506.08561 [gr-qc].

[266] Wessel Valkenburg and Bin Hu. “Initial conditions for cosmological N-body simulations of the scalar sector of theories of Newtonian, Relativistic and Modified Gravity.” In: *JCAP* 1509.09 (2015), p. 054. DOI: 10.1088/1475-7516/2015/09/054. arXiv: 1505.05865 [astro-ph.CO].

[267] Xue-Wen Liu, Bin Hu, and Yi Zhang. “A note on the initial conditions within the effective field theory approach of cosmic acceleration.” In: (2017). arXiv: 1705.00502 [astro-ph.CO].

[268] Lucas Lombriser and Andy Taylor. “Semi-dynamical perturbations of unified dark energy.” In: *JCAP* 1511.11 (2015), p. 040. DOI: 10.1088/1475-7516/2015/11/040. arXiv: 1505.05915 [astro-ph.CO].